Canterbury Earthquakes 2010/11 Port Hills Slope Stability: Pilot study for assessing life-safety risk from cliff collapse

C.I. Massey
M.D. Yetton
B. Lukovic
M.J. McSaveney
D. Heron
Z.R.V. Bruce

GNS Science Consultancy Report 2012/57
March 2012 FINAL

GNS SCIENCE
TE PŪ AO

DISCLAIMER

This report has been prepared by the Institute of Geological and Nuclear Sciences Limited (GNS Science) exclusively for and under contract to Christchurch City Council. The report considers the risk associated with geological hazards. As there is always uncertainty inherent within the nature of natural events GNS Science gives no warranties of any kind concerning its assessment and estimates, including accuracy, completeness, timelines or fitness for purpose and accepts no responsibility for any actions taken based on, or reliance placed on them by any person or organisation other than Christchurch City Council. GNS Science excludes to the full extent permitted by law any liability to any person or organisation other than Christchurch City Council for any loss, damage or expense, direct or indirect, and however caused, whether through negligence or otherwise, resulting from any person or organisation's use of, or reliance on this report.

The data presented in this Report are available to GNS Science for other use after the public release of this document.

BIBLIOGRAPHIC REFERENCE

Massey, C.I.; McSaveney, M.J.; Yetton, M.D.; Heron, D.; Lukovic, B and Bruce, Z.R.V. 2012. Canterbury Earthquakes 2010/11 Port Hills Slope Stability: Pilot study for assessing life-safety risk from cliff collapse, GNS Science Consultancy Report 2012/57.

REVIEW DETAILS

This report in draft form was independently reviewed by T. Taig, TTAC Limited and F.J. Baynes of Baynes Geologic Pty. Ltd. Internal GNS Science reviews of drafts were provided by N. Litchfield and G. Dellow.

Risk calculations were independently checked by TTAC Limited.

This report was completed March 2012 with corrections of minor typographical errors September 2012

CONTENTS

FIGURES

TABLES

APPENDICES

EXECUTIVE SUMMARY

ES.1 Scope and purpose

GNS Science has been commissioned by Christchurch City Council to assess and report on slope-instability risk in the Port Hills following the deaths of three people from cliff collapse in the earthquakes of 22nd February 2011. This report is one of a series of reports on selected areas where much damage occurred from boulders moved during earthquakes. It specifically presents assessments of the risk to life (death) faced by an individual living above or below some of the major cliffs between Redcliffs and Scarborough. The risk is expressed as the annual individual fatality risk.

A pilot study has been carried out to assess the annual individual fatality risks in the main areas where cliffs collapsed during the 2010/2011 Canterbury earthquakes. Cliffs also collapsed outside of these areas, but they were more localised and affected only a few dwellings; these are not included in this report.

The quantitative risk assessment uses risk-estimation methods that follow appropriate parts of the Australian Geomechanics Society framework for landslide risk management (Australian Geomechanics Society, 2007). It provides risk estimates suitable for use under SA/SNZ ISO31000: 2009.

The report considers cliff collapses triggered by both earthquakes and by other causes such as rainfall and spontaneous collapse. It includes expected effects of anticipated decrease in seismic activity in the Port Hills region over time. The report presents an analysis of the cliff-collapse hazard in those Port Hills areas that were most affected by collapsing cliffs in 2011. It estimates the annual individual fatality risk (death of an individual) in the analysed areas specifically from the hazard of cliff collapse.

The areas included in this report are those areas immediately above or below the cliffs at parts of Redcliffs, Shag Rock Reserve (Kinsey Terrace, and the non-residential Shag Rock Reserve), Sumner (Wakefield Avenue, Nayland Street and Richmond Hill Road) and Whitewash Head (Scarborough). In these areas, lives are threatened by the hazards of cliff-top recession (loss of land from the cliff top and consequent shift in the cliff edge), and debris avalanche (falling debris from the cliff face).

ES.2 Context and terminology

This report uses the terms: “cliff-top recession” to describe the result of landslides from the top and face of cliffs, and “debris avalanche” to describe the landslide process that inundates land at the cliff foot (referred to as “toe”) with countless boulders. The two are collectively referred to as cliff collapse.

Debris avalanche refers to a type of landslide comprising many boulders falling simultaneously from a slope. The avalanching mass starts by sliding, toppling or falling before descending the slope rapidly (> 5 m/sec) (following Cruden and Varnes, 1996) by any combination of falling, bouncing and rolling.

Cliff collapses have been considered separately from the failure and runout of individual boulders, referred to as “boulder rolls” (addressed in Massey et al., 2012). Although cliff

collapses and boulder rolls both can be classified as rockfalls (Cruden and Varnes, 1996), the risk analysis for boulder rolls uses information on the location of each fallen boulder. Mapping individual boulder locations in a cliff collapse is impractical due to the large number of boulders involved.

Three of the five people killed by falling rock on 22nd February 2011 died when inundated by avalanching debris from the collapse of cliffs on residential properties considered in this report.

Annual individual fatality risk is the probability (likelihood) that a particular individual will be killed by a cliff collapse in any year at their place of residence. For most localities this probability is an imprecisely determined, very small number. The report makes extensive use of the scientific number format of expressing risk in terms of powers of ten. For example, the number 10^{-4} ("10 to the power of minus 4") is the fraction 1/10,000, and the decimal number 0.0001; it may also be expressed as 0.01%. The units of risk are dimensionless probability per unit of time and the units of annual fatality risk are probability of fatality (death or loss of life, but in this report also including life-threatening injury) per year.

ES.3 Conclusions

1) Following the 4th September 2010 Darfield Earthquake, seismic activity in the Christchurch region has been considerably higher than the previous, and the expected future, long-term average, and is likely to remain higher for several decades. A seismicity model that takes into account the recent data indicates that the long- term estimates now are about an order of magnitude higher than they were before 4th September 2010. As a result, cliff-collapse fatality risk in the Port Hills is considerably higher now than it was before 4th September 2010. However, this fatality risk is expected to decrease over decades in direct proportion to any decrease in the seismic hazard.

2) The risks presented in this pilot study relate to the annual individual fatality risk from debris avalanches and cliff-top recession triggered by earthquakes or by any other causes.

3) Structurally controlled deformation of the cliffs within and between geological layers and defects and other large landslides at the cliff tops have been recognised and mapped. Any annual individual fatality risk from these features remains to be estimated when they are more fully investigated. They are not believed to pose an immediate fatality risk at their current rates and amounts of movement.

4) Precise measurements made of seismic shaking and associated volumes of cliff collapse in the assessment area resulting from aftershocks in 2011 provide very high quality data for calibration of the risk model.

5) The number of dwellings where the individual fatality risk exceeds 10^{-4} per year is similar for each of the scenarios considered. This means that the numbers are insensitive to model uncertainty and the choice of risk scenario.

6) The annual individual fatality risk decreases rapidly with distance back from the cliff edge, or distance outward from the bottom of the cliff, so that the overall numbers of dwellings affected are smaller than the numbers of dwellings at risk from boulder fall (falls of individual boulders).

7) The time-varying nature of the seismic hazard has been considered by comparing the differences in risk associated with the next 1- and 50-year composite seismic hazard model results (50-years being consistent with the design life used in typical seismic hazard analysis for residential building construction).

8) Over the next 10 years, the annual individual fatality risk of a person residing in at-risk dwelling is significantly higher (by a factor of about 3 to 5) when compared with the average over the next 50-years.

9) Using the revised "field verified" risk maps there are about 42 dwellings (including those classified as "unknown") located in the debris avalanche annual individual fatality risk zones. On the final field verified maps (shown in Appendix D), 22 dwellings expose people to annual individual fatality risks estimated to be greater than 10^{-2}/year, 12 expose people to risks between 10^{-2} and 10^{-3}/year, three expose people to risks between 10^{-3} and 10^{-4}/year, one exposes people to risks between 10^{-4} and 10^{-5}/year and four expose people to risks less than 10^{-5}/year.

10) The risk outside of the 31° fly rock angle are assessed as being less than 10^{-6}/year.

11) Using the revised "field verified" risk maps there are 33 dwellings (including those classified as "unknown") located in the cliff recession annual individual fatality risk zones. On the final field verified maps (shown in Appendix D), 25 dwellings expose people to annual individual fatality risks estimated to be greater than 10^{-3}/year and eight expose people to risks between 10^{-3} and 10^{-4}/year. There are 15 dwellings located between earthquake event lines 1 and 2, and 25 dwellings between earthquake event lines 2 and 3.

12) Within the analysed cliff-top recession areas, annual individual fatality risks are greater than 10^{-4}/year.

13) Cliff-top recession mainly occurs during earthquakes as witnessed during the 2010/2011 Canterbury earthquakes. It is likely that in the next decade further recession of the cliff edge will also occur during earthquakes. Each time the cliff top moves so too will the risk zones by an equal amount.

14) To take account of cliff-top recession and to make the risk assessment robust to further large earthquakes, "earthquake event" lines have been included on the maps. These lines represent the likely maximum loss of the cliff edge in future earthquakes with associated peak ground accelerations of about twice the gravitational acceleration (2 g), which is similar to those in the 22nd February and 13th June 2011 earthquakes.

15) These earthquake event lines do not mean that the entire cliff between that line and the cliff edge will recede in a single event; they mean that any given part of the cliff in this area could recede back to this line in another event of this magnitude. The distance between each earthquake event line is set equal to the width of the maximum cliff-top recession measured at each cliff after the 2010/2011 Canterbury earthquakes.

16) An additional 40 properties are, in part, within areas that could be affected in the next three earthquakes that are associated with peak ground accelerations of about two times the gravitational acceleration (2 g).

17) The annual individual fatality risk from falling into a crack near the cliff edge has been

assessed using a similar analysis method to that adopted for cliff-top recession.

18) The annual individual fatality risk from falling into a crack formed in an earthquake with peak ground acceleration between one and two times gravity is about 10^{-7}. This is significantly lower than the nearby annual individual fatality risk from falling over the cliff as the cliff edge falls away, or from being hit by a debris avalanche triggered in a comparable event, both of which are higher than 10^{-4}. The estimation of individual fatality risk from falling into a crack does not take into account that differential movement across a crack could possibly cause a building to collapse. Building damage, and risk to people from collapsing buildings are not addressed in the report.

19) The report recognises that the cracks at the cliff top might evolve into cliff collapses at a later date, and that associated landslides might become more mobile. If these were to occur in some locations, such cracking could lead to failure of large areas of the cliff top and cause large debris avalanches to fall. It is not possible at present to determine the likelihood of such failures, or indeed that they can occur.

ES.4 Recommendations

1) Christchurch City Council decide what levels of life risk will be regarded as tolerable and how Council will manage risk on land where life risk is assessed to be at various levels of intolerability.

2) Christchurch City Council adopts the next 1-year seismicity model used in the analysis, as the number of dwellings exposing residents to particular levels of annual individual fatality risk are not expected to change significantly as the seismic hazard declines over time.

3) Given the time-varying nature of the seismic hazard, the assessed individual fatality risks should be re-evaluated after a period of about 10 years to incorporate a seismic hazard model appropriate to the knowledge of that time. This also would allow data collected on the stability of the now seismically disturbed cliffs of the Port Hills to be considered in the risk.

4) It is recommended that dwellings within areas showing evidences of large-scale rock-mass deformation and/or deep-seated landsliding not be occupied before these areas have been more rigorously investigated and the annual individual fatality risk within them determined.

5) Christchurch City Council, in the short term (over the next few years), should continue to monitor the movement of the land in the deformation areas and set in place emergency management plans that take account of any potentially life-threatening changes in the displacement patterns.

6) The areas of ongoing ground deformation and their surroundings need further subsurface investigation and in-situ deformation monitoring before analysis of the annual individual fatality risk from these features can be undertaken.

ES.5 Methodology

The risk assessment comprised the following steps (Figure ES.1) based on the Australian Geomechanics Society landslide risk management framework (Australian Geomechanics Society, 2007):

1. Consideration of possible range of cliff-collapse triggering events (e.g., earthquakes, rain) (following the method of Moon et al., 2005) in terms of a set of earthquake triggers and a set of other non-seismic triggers
2. Selection of a small set of representative events for each type of trigger spanning the range of severity of events from the smallest to the largest
3. For each representative event, estimate:

For debris avalanche:

   a) the annual frequency of the event and the volume of material produced;
   b) the proportion of debris reaching/passing a given distance out from the cliff toe and the probability of at least one of the boulders in the debris hitting a person at that location;
   c) the probability that a person is present when the debris moves past;
   d) the probability that a person will be killed if hit by at least one boulder as the debris passes

For cliff-top recession:

   a) the annual frequency of the event causing a given area of cliff top to be lost;
   b) the proportion of cliff top lost at a given distance back from the cliff edge if *a given amount of area* of cliff top is lost at that location;
   c) the probability that a person is present on the material when it falls;
   d) the probability that a person will be killed, if they fall;

4. 3(a) – (d) are combined for each of debris avalanche and cliff-top recession to estimate the annual individual fatality risk at different locations above or below the cliff contributed by each representative event, and
5. Summation of the risks from all events to obtain the overall risk.
6. Enter the risk values at each toe and slope-edge zone into a Geographic Information System and interpolate between the risks estimated for each zone to provide a map with contours of equal annual individual fatality risk.

ES.5.1 Range of triggering events

Studies of the cliff collapses from the 2010/2011 Canterbury earthquakes in the Port Hills area have yielded much high quality evidence about the generation of cliff collapses from different amounts of ground shaking. GNS Science, the Earthquake Commission and various geotechnical consultants in the Port Hills area hold substantial historical data on previous cliff collapses (mostly triggered by rainfall, but some falls have been spontaneous with no known trigger). Archaeological and geomorphological studies indicate that there have been past large events similar in magnitude to the events of 2011. The risk assessment model represents all earthquake triggers of cliff collapse by considering a representative event from each of four bands of maximum ground-shaking intensity with peak ground accelerations (measured as a proportion of the gravitational acceleration g) in the ranges less than 0.4 g, 0.4–1 g, 1–2 g and more than 2 g. The model represents all non-seismic cliff collapse triggers by considering events of progressively increasing return period: 0–15 years, 15–100 years, 100–1000 years and greater than 1000 years.

ES.5.2 Collapse frequencies and volumes

The frequency of occurrence of earthquake peak ground accelerations in the chosen bands was obtained from the GNS Science composite seismic hazard model (a modified version of the national seismic hazard model; Stirling et al., in press) which includes the increased level of seismicity following the 4th September 2010 Darfield Earthquake. This composite model was used to estimate the likelihood of a given earthquake peak ground acceleration occurring within the next 1-year and within the next 50-years to illustrate and provide information on the effect of the currently rapidly changing seismic hazard. The volume of debris estimated to be produced from each cliff collapse at these accelerations was estimated from the precisely surveyed volumes of debris that fell during the Darfield 2010 and 22nd February, 16th April and 13th June 2011 earthquakes. Volumes of storm-induced collapses were estimated with much lesser precision from data on historical and pre-historical rockfalls. The 23rd December 2011 earthquakes occurred subsequent to the reported analysis, but served to verify the predicted outcome.

At Redcliffs, two fatalities occurred on residential properties where the dwellings had been built, in part, on accumulations of debris that has fallen from the cliffs before the 2010/2011 Canterbury earthquakes. At these locations and elsewhere, pre-4th September 2010 rockfall debris had been removed in creating the building platforms. Earthquake Commission claims and local geotechnical consultant reports provide evidence that dwellings in Wakefield Avenue and at Redcliffs had been damaged by debris avalanches triggered by non-seismic events prior to 4th September 2010.

ES.5.3 Consequences of cliff collapse

The volume of debris falling from a cliff, the associated area of cliff top lost, and the runout of the avalanching debris were estimated based on field mapping and surveying of the cliff collapses triggered by the 2010/2011 Canterbury earthquake sequence. The probability of debris reaching a given downslope location and the probability of a particular location at the cliff edge receding were calculated for each site, using site-specific data.

The probability of a person being killed from cliff-top recession or debris avalanches was determined by:

- Estimation of the probability that they will be occupy on an area of ground that slips or be in the path of debris that falls in a given event, at a given distance either back from the cliff edge (cliff top recession), or downslope (debris avalanche), using the approximation that debris and area slipping can occur with equal probability anywhere along the cliff in question
- Estimation of the proportion of time a person spends on their property (occupancy) in proximity to the cliff, and
- Estimation of the probability of the person being fatally injured if they fall or are hit by debris (vulnerability).

For cliff-top recession and debris avalanche respectively, 90% and 100% dwelling occupancies were assumed. 90% has been used for cliff-top recession because a person present on an area of cliff top that is showing signs that it will fall, momentarily has a brief chance of getting off this area onto stable ground. Escaping from an area that is about to fall does not affect the person's vulnerability in a fall, but it affects the probability of the person being present on falling ground.

These values ensure that the estimated annual individual fatality risks are robust to any reasonable use people make of their property, as is standard practice based on individual risk to people living near significant hazards. 100% vulnerability for both cliff top recession and debris avalanche has been assumed as people are unlikely to survive either a fall from a high cliff onto rocky debris, or burial under by boulders.

ES.6 Uncertainties

Significant uncertainties have been noted and their likely implications to fatality risk have been investigated. The greatest uncertainties in the absolute values of risk come from the composite seismic hazard model and the natural variability in the volumes of debris generated by events of known peak ground acceleration. Overall, the uncertainties in the estimated absolute fatality risks presented in this report are less than a factor of 3 up or down. These uncertainties affect all of the assessed areas.

ES.7 Acknowledgment

This work was funded by the New Zealand Natural Hazards Platform and Christchurch City Council, and carried out by GNS Science, assisted by the Port Hills Geotechnical Group.

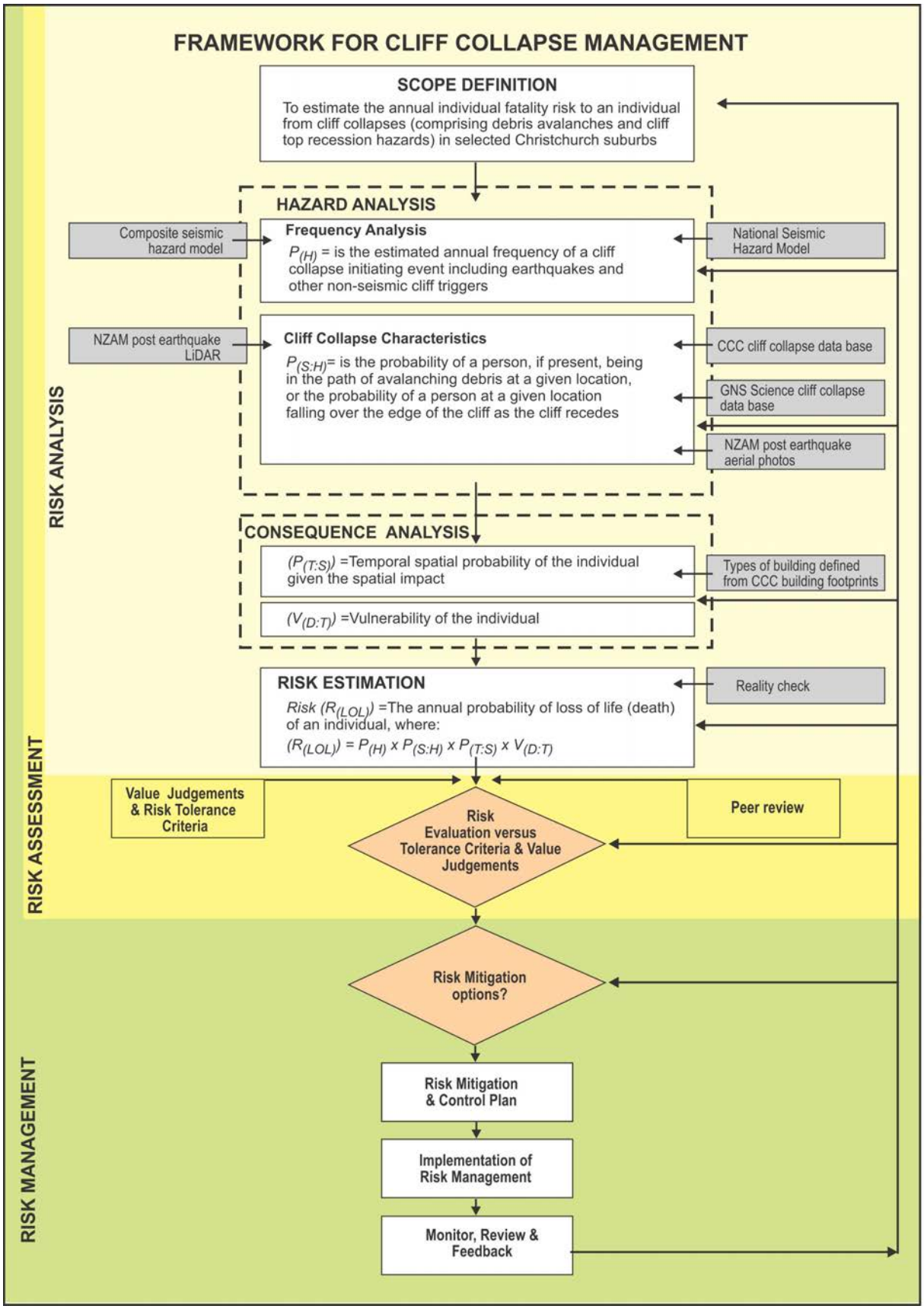

Figure ES.1 Framework used to assess the annual probability of loss of life (death) of an individual from cliff collapses in the Port Hills. Modified after the Australian Geomechanics Society Guidelines for landslide risk management (Australian Geomechanics Society, 2007).

1.0 INTRODUCTION

GNS Science has been commissioned by Christchurch City Council to assess and report on slope-instability risk in the Port Hills following the deaths of five people (two from rockfalls and three from cliff collapse) in the earthquakes of 22nd February 2011. This report is one of a series of reports on selected areas where much damage occurred. It specifically presents quantitative assessments of the risk to life (death) faced by an individual living above or below cliffs. This risk is expressed as the annual individual fatality risk.

A pilot study has been carried out to assess the annual individual fatality risks in the main areas where cliffs collapsed during the 2010/2011 Canterbury earthquakes. Cliffs also collapsed outside of these areas, but they were more localised and only affected a few dwellings and have therefore not been included in this study.

The risk assessment method follows appropriate parts of the Australian Geomechanics Society framework for landslide risk management (Australian Geomechanics Society, 2007). It provides risk estimates suitable for use under SA/SNZ ISO31000: 2009.

The report considers cliff collapses, a type of landslide involving many boulders, triggered by earthquakes (taking into account expected changes in seismic activity in the Port Hills region over time) (Figure 1) and by other non-seismic triggering events such as rainfall and spontaneous collapse. The report:

1) presents an analysis of the cliff collapse hazard in those Port Hills suburban areas that were most affected in 2011; and

2) estimates the annual individual fatality risk (the risk of death) from cliff collapses in these areas.

This report presents the risk to life (death) to an individual living above or below parts of the cliffs at Redcliffs, Shag Rock Reserve (Kinsey Terrace, and the non-residential Shag Rock Reserve), Sumner (Wakefield Street, Nayland Street and Richmond Hill Road) and Whitewash Head (Scarborough).

Five deaths from rockfalls and cliff collapses occurred as a result of the 22nd February 2011 earthquakes. The main M_w6.2 earthquake occurred on Tuesday 22nd February at 12:51 pm New Zealand Daylight Time, when many people were not at home. Of the three people killed by cliff collapse, one died in their home, one died in their garden, and the other died at a construction site. It is uncertain how many of these people died from rockfalls and cliff collapses triggered by the main earthquake, but one of the five is known to have died in a later earthquake on the same day.

Many features of the 2010/2011 Canterbury earthquakes have not been seen in previous New Zealand earthquakes, and are rare internationally. The exceptionally high peak ground accelerations, and particularly the high vertical peak ground accelerations, may be responsible for the abundance of rockfalls and cliff collapses in the Port Hills. Both internationally and in New Zealand, vertical peak ground accelerations are not usually factored into seismic hazard models.

This report provides estimates of the annual individual fatality risk to individuals living in residential dwellings in the areas analysed from cliff collapse. It does not assess the risk to critical infrastructure. This report deals specifically with cliff collapse. An analysis of the annual individual fatality risk to individuals living in areas affected by rockfalls is reported in Massey et al. (2012).

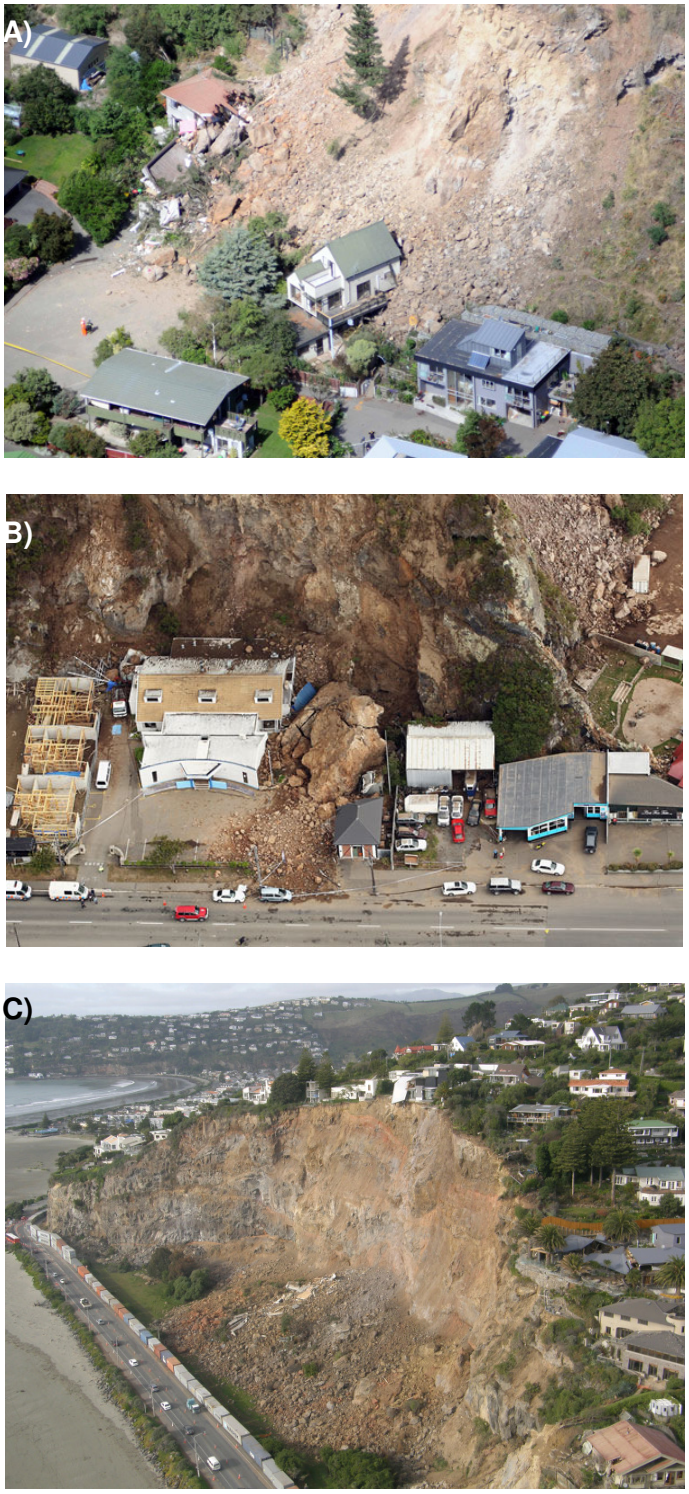

Figure 1 Examples of cliff collapses triggered by the 2010/2011 Canterbury earthquakes, A) Raekura Place, Redcliffs (location of two fatalities), B) Wakefield Avenue, Sumner (location of one fatality) and C) Shag Rock Reserve, Clifton Hill, Sumner. Photographs by G. Hancox and C. Massey, GNS Science.

1.1 Aims and objectives

The objectives of this work are to:

1. Undertake a life-safety risk assessment pilot study of some parts of the Port Hills where residential properties were affected by cliff collapses; and

2. Estimate the annual individual fatality risk to an individual living in these areas from cliff collapses triggered by earthquakes and other non-seismic triggers such as rainfall.

This work is based on surveyed cliff collapses triggered by the 22nd February, 16th April, 13th June and 23rd December 2011 earthquakes, in areas where cliff collapse is the dominant slope stability hazard. The assessed areas are: 1) Redcliffs, 2) Shag Rock Reserve (Kinsey Terrace, and the non-residential Shag Rock Reserve), 3) Sumner (Wakefield Street, and Nayland Street) and 4) Whitewash Head (Scarborough).

1.2 Cliff collapse

In this report, GNS Science uses the terms: “cliff top recession” to describe the result of landslides from the top and face of cliffs, and “debris avalanche” to describe the landslide process that inundates land at the cliff foot (referred to as “toe”) with countless boulders. Collectively the two are referred to as cliff collapse.

Debris avalanche refers to a type of landslide comprising many boulders falling simultaneously from a slope. The rocks start by sliding, toppling or falling before descending the slope rapidly (> 5 m/sec) (following Cruden and Varnes, 1996) by any combination of falling, bouncing and rolling.

Cliff collapses are here considered separately from the failure and runout of individual boulders, referred to as “boulder rolls” (addressed by Massey et al., 2012). Although both cliff collapses and boulder rolls are classified as rockfalls (Cruden and Varnes, 1996), the risk analysis for boulder rolls utilises information on the location of each fallen boulder. Mapping individual boulder locations in a cliff collapse is impractical due to the large number of boulders involved (Figure 2).

Figure 2 Illustration of the difference between *cliff collapse* with countless boulders (left, Raekura Place, Redcliffs) and *rockfall* where the location of each boulder can be precisely located (right, Rapaki Bay). Differences in what data can be collected about the two types lead to differences in how they are analysed to determine life-safety risk. The illustrated rockfalls occurred in the 22nd February 2011 earthquakes. Photographs by G. Hancox (left); D. Barrell (right), GNS Science.

1.3 Geology and slopes in the affected areas

An area of about 65 km^2 extending from Mount Pleasant in the north to Lyttelton in the south, and from Godley Head in the east to Governors Bay in the west was affected by rockfalls and cliff collapses on 22nd February 2011 (Hancox et al., 2011) (Figure 3). This area is referred to as the Port Hills. Most, but not all of the rockfalls and cliff collapses were triggered by the main M_w6.2 earthquake.

The Port Hills are the northern sector of the eroded extinct Lyttelton basalt volcano, comprising five overlapping volcanic cones (Hampton, 2010). The rocks forming the 400-500 m high ridge, slopes, and sea cliffs of the Port Hills (Summit Road, Sumner and Redcliffs areas) belong to the Lyttelton Volcanics Group rocks of late Tertiary (Miocene) age, and are about 10–12 million years old (Forsyth et al., 2008). These volcanic rocks comprise layers of hard, jointed, basaltic and trachytic lava flows cut by numerous intruded dykes, and interbedded with breccia (scoria), agglomerate (coarse angular gravel), compact sandy tuff (ash) beds, and ancient buried soils. The volcanic rocks are mantled by soils derived from wind-blown sand and silt (loess) typically about 1 m thick and locally more than 5 m thick. The lava flows and dykes in the Lyttelton area generally are strong, and the interbedded scoria, tuff and ancient soils are softer but compact. Lava flows in the Lyttelton area are closely and irregularly cracked by cooling joints, forming blocky rock masses that episodically release one to many blocks of rock to roll downhill and accumulate as talus (scree) at the base of slopes. Many natural slopes around Lyttelton Harbour are formed on strong interbedded lava flows and stand at steep angles, forming cliffs on many coastal slopes (such as those around Diamond Harbour and Quail Island). The principle sea cliff failures in Sumner-Redcliffs are developed in rocks of the Lyttelton 2 and Mount Pleasant Formations of the Lyttelton volcano (Sewell, 1988; Sewell et al., 1992), which have been more recently termed the Whakaraupo Cone, with failure occurring in rocks derived from eruptive phases VIII, IX, X and XI of that cone (Hampton, 2010). In the intervening 10 million years to the present, those rocks more susceptible to chemical weathering have been deeply weathered and now consist largely of clay minerals.

Steep coastal cliffs occur around Lyttelton Harbour and the outer coast, and continue inland into the suburban areas from Sumner to Redcliffs. In these suburbs the cliffs are no longer being actively cut by the sea, and the cliffs furthest inland may not have been affected by wave action for the past ~9,000 years. These steep (65–85°) cliffs are typically 15 to 30 m high and locally up to about 100 m high, and their height and slope angle makes them susceptible to cliff collapse. Where they have not been removed for use in roading fill or to create level building sites, small sloping aprons of rockfall talus (scree) occur at the base of the cliffs. Beyond the short talus aprons, there is flat or gently sloping land, mostly artificially flattened from coastal sand dunes and swampland. The life-safety risks resulting from the collapse of these cliffs, and the runout of the debris onto the talus and flat land at their toe are the subject of this report.

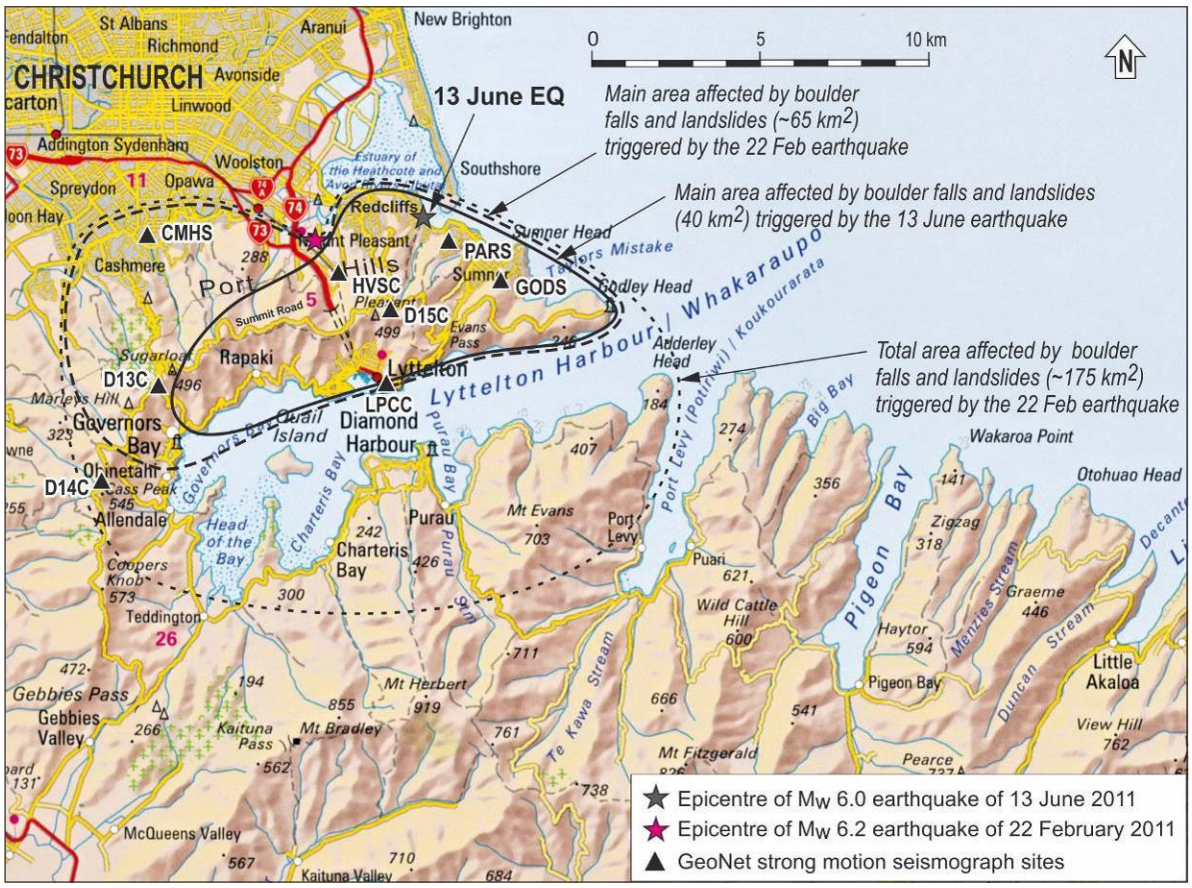

Figure 3 Location map showing the area affected by rockfalls triggered by the 2010/2011 Canterbury earthquakes (modified after Hancox et al., 2011).

1.4 The 2010/2011 Canterbury earthquakes

The 2010/2011 Canterbury earthquakes that have affected the Port Hills and their consequences with regards to rockfalls and cliff collapses are summarised in Table 1. Of these, the 22nd February and 13th June 2011 earthquakes caused the most rockfalls and cliff collapses, and affected the widest areas. A detailed description of the 2010/2011 Cantebrury earthquakes can be found in Webb et al. (2011). The size of an earthquake is generally reported in terms of a magnitude relating to the total energy released in the event. However, of much greater importance in relation to damage caused by an earthquake is the force exerted on surface structures.

A commonly measured surface parameter in earthquakes is the peak horizontal ground acceleration, commonly referred to simply as peak ground acceleration, measured by strong motion instruments. However, many of the 2010/2011 Canterbury earthquakes have been characterised by their unusually high peak vertical ground accelerations, which have in the past received less attention in earthquake engineering than horizontal accelerations (Kramer, 1996). Ground accelerations are commonly expressed in units of either metres per second per second (m/s/s) or as a percentage of gravity (%g), where gravity is equal to 9.81 m/s/s (therefore 3.4 m/s/s is about 35 %g or 0.35 g).

In this study, peak horizontal ground acceleration has been used to characterise ground shaking based on the assumption that cliff collapses are triggered mostly by an instantaneous force exceeding a critical value to trigger them, rather than the multiple accelerations associated with longer duration shaking.

Table 1 Summary of the 2010/2011 Canterbury earthquakes and their measured peak ground acceleration (PGA) records from accelerometers located in the Port Hills, for the main earthquakes that have triggered rockfalls, cliff collapses and landslides. The listed stations are GeoNet Strong-motion recording sites: CMHS - Cashmere High School; GODS - Godley Drive; HVSC - Heathcote Valley Primary School; LPCC - Lyttelton Port Company; PARS - Panorama Road.

Date (NZ time)	Moment magnitude (M_w)	PGA horizontal[1] (g)	PGA vertical (g)	Strong motion station	Consequences in Port Hills
4/09/2010 Darfield Earthquake	7.1 (M_W)	0.3	0.3	CMHS	A few localised rockfalls and cliff collapses
		0.6	0.0	HVSC	
22/02/2011 Christchurch Earthquake	6.2 (M_W)	0.5	0.9	CMHS	Many widespread rockfalls, cliff collapses and landslides occurred over all of the Port Hills
		2.1	2.2	HVSC	
		1.3	0.5	LPCC	
16/04/2011	5.3 (M_L)	0.2	0.1	CMHS	Some localised rockfalls and cliff collapses
		0.8	0.4	PARS	
		0.2	0.1	LPCC	
13/06/2011	6.2 (M_W)	2.2	1.1	GODS	Many widespread rockfalls, cliff collapses and landslides occurred in the epicentral region
		1.0	0.7	PARS	
		0.4	0.1	LPCC	
23/12/2011	5.8 (M_W)	0.4	0.3	HVSC	Some localised rockfalls and cliff collapses
		0.3	0.2	PARS	
		0.4*	0.3*	LPCC	
23/12/2011	6.0 (M_W)	0.7	0.2	HVSC	Some localised rockfalls and cliff collapses
		0.3	0.2	PARS	
		0.6	0.2	LPCC	

[1]Calculated from the maximum vector of both horizontal components
* Recorded by adjacent station Lyttelton Port, Cashin Quay (LPQC)

1.4.1 22nd February 2011 earthquakes

The 22nd February 2011 M_w[1]6.2 Christchurch Earthquake was part of the aftershock sequence of the 4th September 2010 M_w7.1 Darfield Earthquake (Berryman, 2011) (Figure 4). The M_w6.2 earthquake occurred at 12:51 pm when about 50,000 people were in the inner city area, where building failures resulted in 176 fatalities. Rockfalls and cliff collapses in the Port Hills area caused an additional five fatalities. Other earthquake-related deaths around the city related to falls of frail people around their homes during the strong shaking. In all, there have been 186 acknowledged earthquake fatalities.

The 22nd February 2011 Christchurch Earthquake was by far the most destructive of the 2010/2011 Canterbury earthquakes, with severe ground shaking occurring over much of the city. The earthquake occurred on a northeast-southwest oriented fault at shallow depth. Slip along the fault reached within ~1 km of the surface but did not break the surface. This fault was unknown prior to the 4th September 2010 Darfield Earthquake, but had experienced aftershock activity in the months prior to the Christchurch Earthquake. The faulting movement for this earthquake is technically described as oblique-reverse (a combination of right-lateral strike-slip and thrust faulting) (Webb et al., 2011).

The main M_w6.2 22nd February 2011 Christchurch Earthquake was followed within the hour by a large aftershock that also triggered rockfalls. Rockfalls from events on 22nd and 23rd February 2011 have not been able to be separately identified, and have been treated in this report as if they all fell in the main M_w6.2 Christchurch Earthquake.

[1] Moment magnitude (M_w) is a measure of the final displacement of a fault after an earthquake. It is proportional to the average slip on the fault times the fault area. M_w is more complicated to determine than M_L (Richter magnitude), but is much more accurate, although the standard methods used to determine it are valid only for larger earthquakes (~M_w>4.0). M_w is a rough proxy for the amount of low-frequency energy radiated by an earthquake and is commonly used worldwide to characterise large earthquakes.

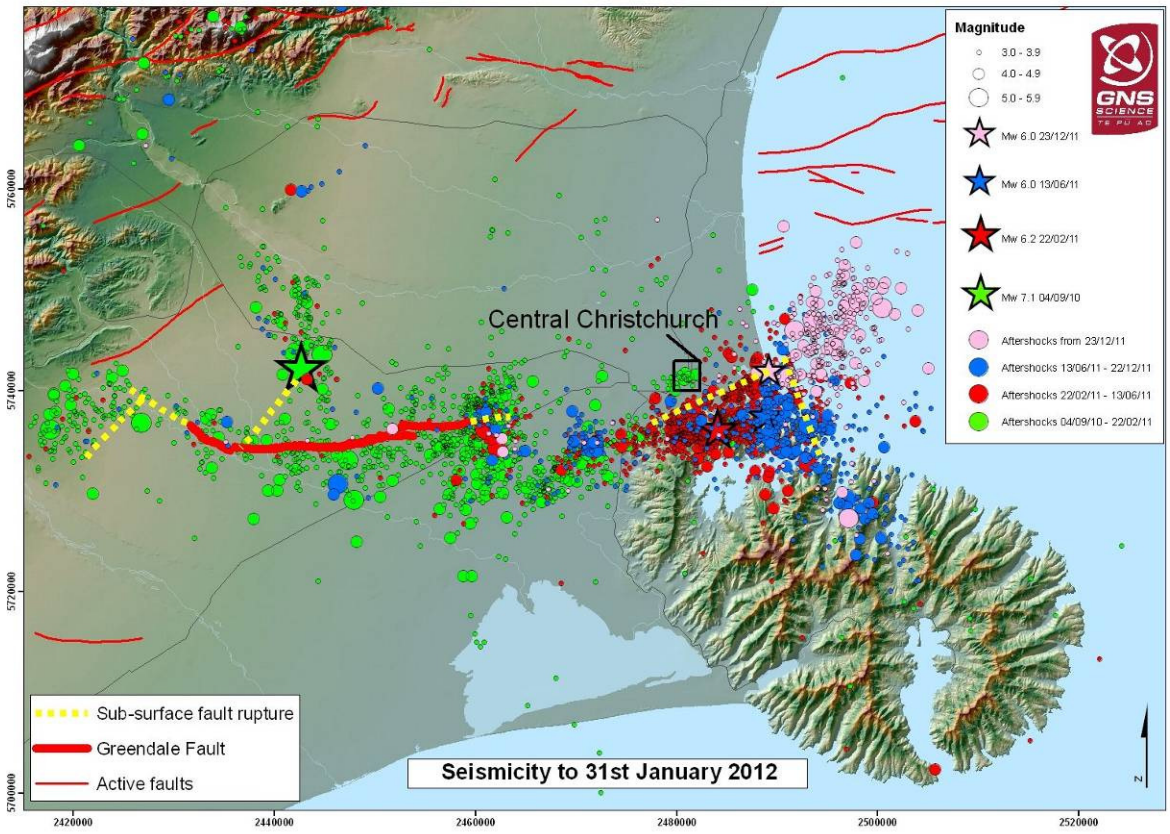

Figure 4 Epicentres of the 4th September 2010 Darfield Earthquake and aftershocks, to the end of January 2012.

Peak ground accelerations in the 22nd February 2011 Christchurch Earthquake were well recorded at many sites throughout Christchurch. Three of these strong-motion sites in the GeoNet monitoring network were in the Port Hills (Figure 3). Peak (horizontal) ground accelerations recorded at these strong-motion recording sites (Cashmere High School (CMHS); Lyttelton Port Company (LPCC) and Heathcote Valley Primary School (HVSC), Figure 3) range from 0.5 g to 2.1 g (Table 2). Following the 22nd February 2011 earthquakes, further strong motion recorders were installed in the Port Hills area.

The Christchurch earthquake and many of its aftershocks are notable in having unusually high peak vertical ground accelerations (Table 2 and Figure 5).

Table 2 Summary of Peak Ground Acceleration (PGA) strong motion records from GeoNet accelerometers located in the Port Hills for the 12:51pm, 22nd February 2011 Christchurch Earthquake.

Station	PGA horizontal (maximum vector of both horizontal components) (g)	PGA vertical (g)	Site Class (NZS1170)
Cashmere High School (CMHS)	0.5	0.9	D (deep soil)
Heathcote Valley Primary School (HVSC)	2.1	2.2	C (shallow soil)
Lyttelton Port Company (LPCC)	1.3	0.5	B (weak rock)

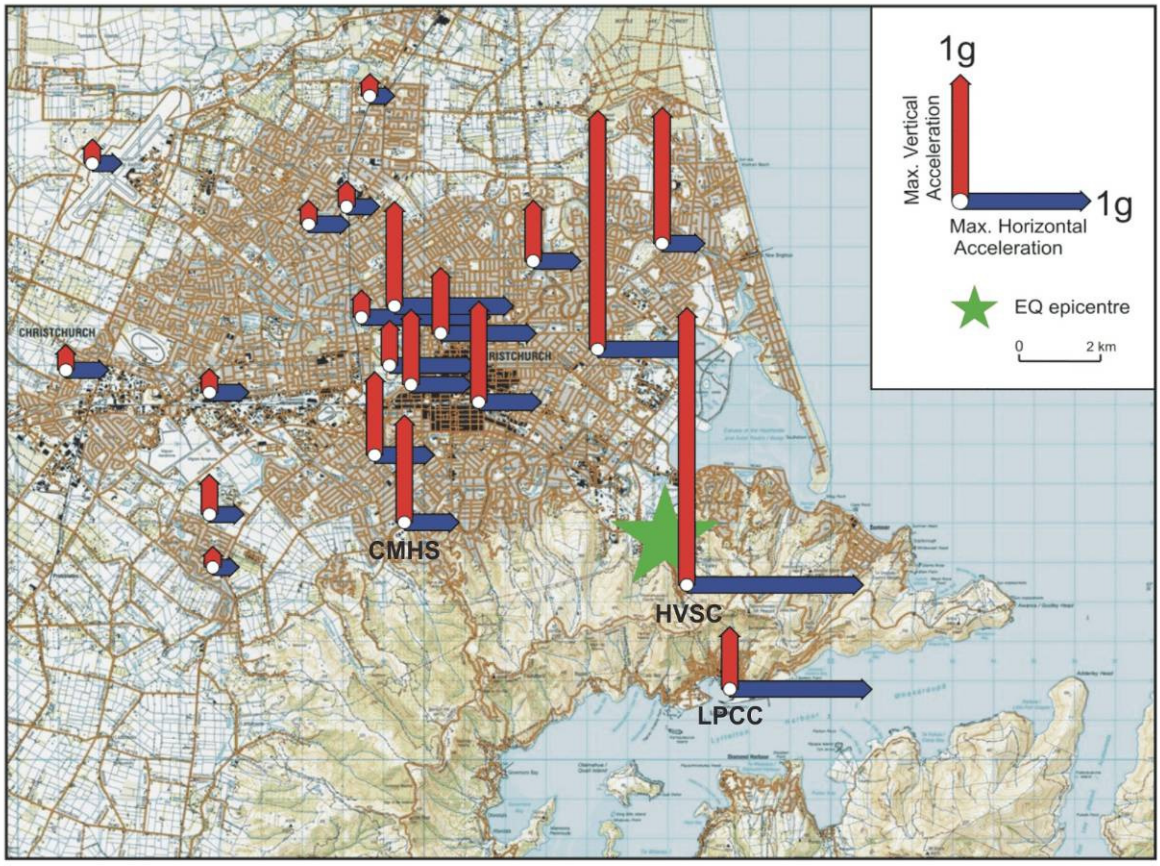

Figure 5 Maximum horizontal (single component only) and vertical peak ground accelerations recorded during the 22nd February 2011 Christchurch Earthquake at GeoNet stations and using temporary low-cost accelerometers (Quake-Catcher Network) (Kaiser et al., 2011). Note that the arrows indicate only the magnitudes and not the directions of the vector components.

A number of factors are believed to have contributed to the high peak ground accelerations experienced in Christchurch City during the 22nd February 2011 Christchurch Earthquake (Fry et al., 2011; Reyners, 2011). Firstly, because the earthquake was close to the city and at a shallow depth, ground shaking was high compared to the more distant 4th September 2010 Darfield Earthquake, as the energy of seismic waves reduces very rapidly away from where the fault rupture occurred. Secondly, the energy magnitude (M_e)[2] of the 22nd February 2011 Christchurch Earthquake was 6.75 (compared to the moment magnitude (M_L)[3] of 6.2), indicating that, like the 4th September 2010 Darfield Earthquake, this was a high stress-drop earthquake. Stress drop is the sudden reduction of stress across a fault during rupture, and a measure of the energy released in relation to the size of the rupture. High stress-drop earthquakes radiate more energy than average for an earthquake of this size. Thirdly, seismological and geodetic modelling shows that the maximum fault displacement in the 22nd February 2011 Christchurch Earthquake was shallow and the direction of rupture was in a north-westward direction and upwards towards Christchurch city. Therefore stacking of energy in the direction of earthquake rupture (a directivity effect) is likely to have further enhanced peak ground acceleration within 10 km of the fault (Webb et al., 2011).

Other site, basin and topographical effects also contributed to the strong ground shaking in Christchurch. Of particular significance was that vertical peak ground accelerations were greater than horizontal peak ground accelerations near to the fault source (Figure 5). This can be partly attributed to the rupture directivity, but local site conditions are also thought to have contributed. Striking differences in the frequency characteristics of seismic waves in the horizontal and vertical directions were observed at many Christchurch GeoNET stations. Vertical peak ground accelerations near the fault were higher in high-frequency (short period) energy, in marked contrast to the dominant lower frequency energy (longer period) measured in the horizontal component. In addition, a 'trampoline' effect involving complex behaviour of near-surface unconsolidated soil may have increased accelerations in the 'upwards' direction at stations near the fault source (Fry et al., 2011). This effect has previously been observed only in a small number of earthquakes worldwide with very large accelerations (e.g., Aoi et al., 2008; Yamada et al., 2009; Webb et al., 2011)

1.4.2 13th June 2011 earthquakes

The epicentre of the M_W6.0 earthquake on 13th June 2011 was located close to the eastern suburb of Sumner (Figure 4). The June 13th earthquake was preceded about an hour before by a significant foreshock of M_L5.7 in a similar location.

[2] Energy magnitude (M_e) is a measure of the amount of energy released in an earthquake so it is very useful for determining an earthquake's potential for damage. M_e is determined from the amplitude of all frequencies of seismic waves as measured on seismographs (as opposed to just the peak amplitude for M_L) and thus contains more information about the overall energy released in an earthquake and hence its destructive power.

[3] Richter magnitude (M_L) is the initial magnitude assigned to an earthquake with routine GeoNet processing. The GeoNet M_L is a modification of the original magnitude scale defined by C.F. Richter in 1935. M_L is derived from measurements of the peak amplitude on seismographs and is thus a preliminary estimate of the amount of energy released by the earthquake. It is measured on a logarithmic scale, so each magnitude increment of 1 represents an order of magnitude increase in the measured amplitude or about 30 times more energy released.

The ground-damaging effects of the 13th June 2011 M_W6.0 earthquake were most strongly felt in the southern and eastern suburbs. Further damage to vulnerable already damaged structures occurred in the Central Business District and there were more extensive triggered rockfalls on slopes in the southern Port Hills. As in the 22nd February 2011 Christchurch Earthquake, peak ground accelerations in Christchurch were again very high during the 13th June 2011 earthquake (Table 3), reaching 2 g in Sumner and 0.4 g in the Central Business District (Figure 6). The energy magnitude (M_e) of 6.7 indicates that energy released during the 13th June 2011 earthquake was again high, as in the 4th September 2010 and 22nd February 2011 earthquakes, indicating a large stress drop and radiation of higher-than-average levels of seismic energy. In contrast to the high vertical peak ground accelerations during the 22nd February 2011 Christchurch Earthquake, horizontal peak ground accelerations dominated the 13th June 2011 earthquake, particularly near the source fault in the Port Hills (Figure 6). It is likely that the different fault movement of the two earthquakes (strike-slip in 13th June; oblique-reverse in 22nd February 2011) contributed to the differences in the dominant acceleration directions. The extremely high peak accelerations at the Sumner station (GODS, which is on rock at Godley Drive) may also have been influenced by amplification of seismic waves due to the surface topography at the site (Webb et al., 2011).

Table 3 Summary of strong motion records from GeoNet accelerometers located in the Port Hills for the 13th June 2011 earthquake. PGA is Peak Ground Acceleration, here listed as a proportion of the gravitational acceleration (g is 9.81 m per sec per sec). GeoNet Station codes are: CMHS - Cashmere High School; GODS - Godley Drive; HVSC - Heathcote Valley Primary School; LPCC - Lyttelton Port Company; PARS - Panorama Road, D15C is a temporary station located on the Summit Road. See Figure 6 for site locations.

GeoNet Station	PGA horizontal (vector of both horizontal components) (g)	PGA vertical (g)	Site Class (NZS1170)
CMHS	0.3	0.2	D (deep soil)
HVSC	0.6	0.2	C (shallow soil)
LPCC	0.4	0.1	B (weak rock)
PARS	1.0	0.7	B (weak rock)
GODS	2.2	1.1	B (weak rock)
D15C	0.9	0.6	B (weak rock)

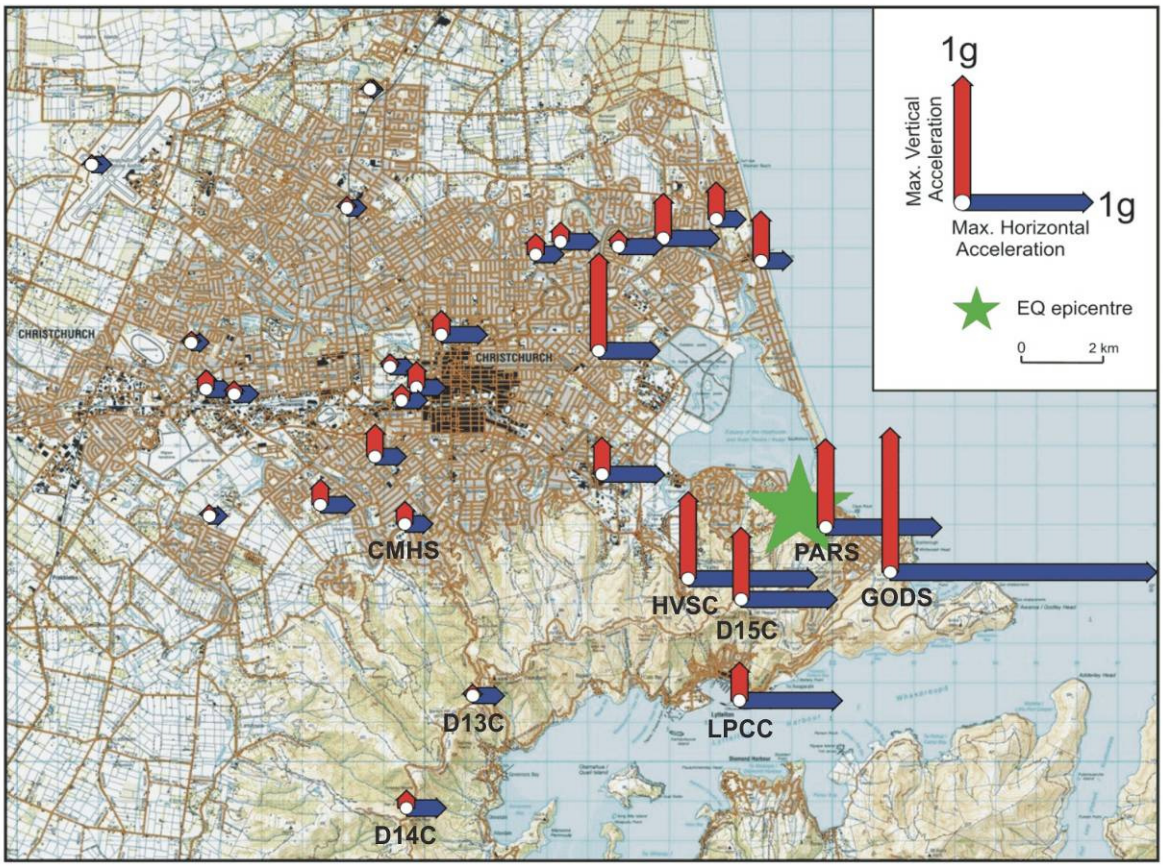

Figure 6 Maximum horizontal (single component) and vertical peak ground accelerations recorded during the 13th June 2011 earthquake at GeoNet stations and using temporary low-cost accelerometers (Quake-Catcher Network) (Kaiser et al., 2011).

1.4.3 23rd December 2011 earthquakes

Two notable earthquakes occurred on the 23rd December 2011. The first occurred at 13:58 in the afternoon and had a magnitude M_w5.8 and the second at 15:18 with a magnitude M_w6.0. The epicentres of both earthquakes were located offshore, but close to the eastern suburb of New Brighton (Figure 4).

The effects of these earthquakes were most strongly felt in the eastern suburbs. Further damage to vulnerable structures occurred in the Central Business District, and there were minor cliff collapses and boulder rolls on slopes in the Port Hills. Peak ground accelerations in Christchurch were moderately high during the December events (Table 4)—0.7 g was recorded at Heathcote Valley Primary School (station HVSC) (Figures 7 and 8). In contrast to the high vertical peak ground accelerations during the 22nd February 2011 Christchurch Earthquake, peak horizontal accelerations were dominant in the December 2011 earthquakes.

Table 4 Summary of strong motion records from GeoNet accelerometers located in the Port Hills for the 23rd December 2011 earthquakes. PGA is Peak Ground Acceleration, here listed as a proportion of the gravitational acceleration (g = 9.81 m per sec per sec). GeoNet Station codes are: CMHS - Cashmere High School; GODS - Godley Drive; HVSC - Heathcote Valley Primary School; LPCC - Lyttelton Port Company; PARS - Panorama Road, D15C and D14C are temporary stations located along the Summit Road. See Figure 6 for site locations.

GeoNet Station	PGA horizontal (vector of both horizontal components) (g)		PGA vertical (g)		Site Class (NZS1170)
	M_w5.8	M_w6.0	M_w5.8	M_w6.0	
CMHS	0.2	0.3	0.1	0.1	D (deep soil)
HVSC	0.4	0.7	0.3	0.2	C (shallow soil)
LPCC	0.4*	0.6	0.3*	0.2	B (weak rock)
PARS	0.3	0.3	0.2	0.2	B (weak rock)
GODS	0.3	0.3	0.1	0.1	B (weak rock)
D15C	0.3	0.3	0.2	0.1	B (weak rock)
D14C	0.1	0.2	0.1	0.1	B (weak rock)

*Recorded by adjacent station Lyttelton Port Cashin Quay (LPQC)

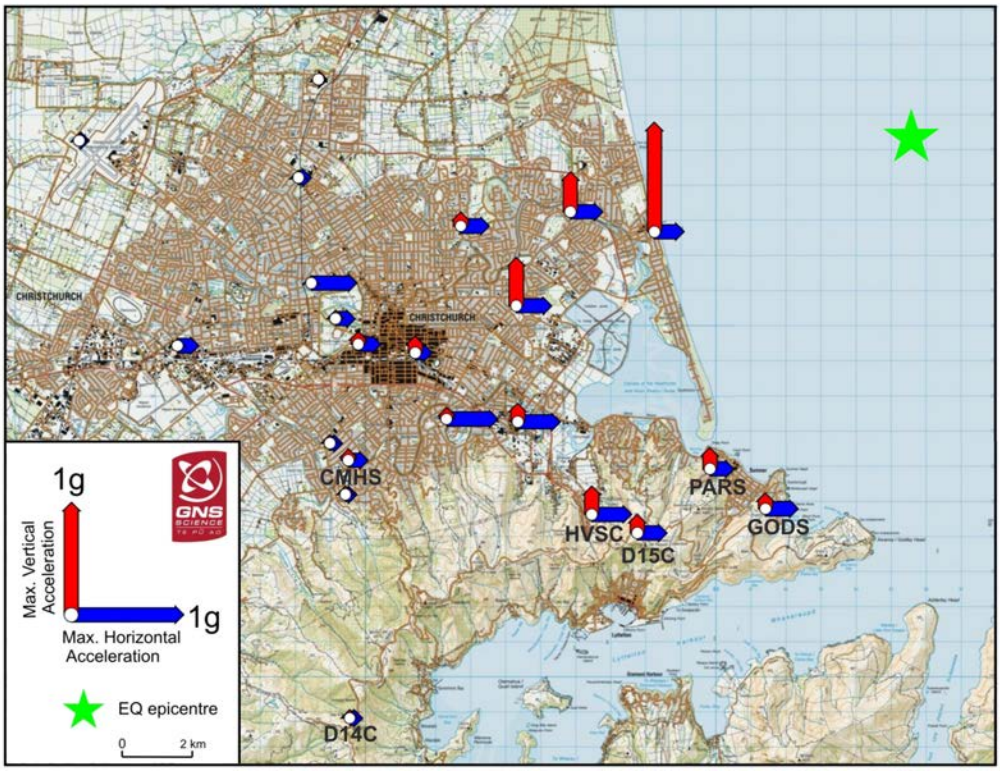

Figure 7 Maximum horizontal (single component) and vertical peak ground accelerations recorded during the M_w5.8 23rd December 2011 earthquake at GeoNet stations and using temporary low-cost accelerometers (Quake-Catcher Network) (Kaiser et al., 2011).

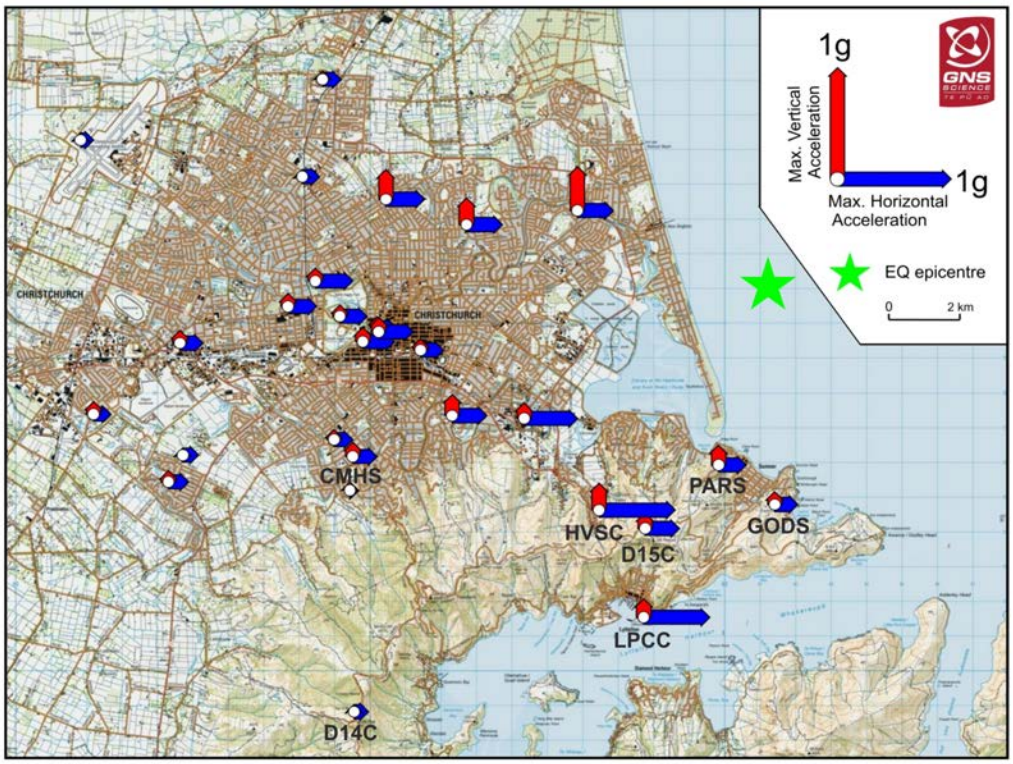

Figure 8 Maximum horizontal (single component) and vertical peak ground accelerations recorded during the M_w6.0 23rd December 2011 earthquake at GeoNet stations and using temporary low-cost accelerometers (Quake-Catcher Network) (Kaiser et al., 2011).

1.4.4 Topographic amplification

Inspections of damaged homes after the earthquakes indicate that geological and topographical site effects caused localized higher levels of house damage. For example, at Redcliffs during the 22nd February and 13th June 2011 earthquakes, the row of homes located nearest to the sharp break in slope at the cliff top were destroyed by a combination of structural damage caused by shaking, and cliff top recession as the outside edge of the slope fell away. Those homes located further back from the sharp break in slope suffered much less shaking damage. Similar patterns of building damage were also observed elsewhere, e.g., more damage at the tops of steep slopes formed in rock and less damage on lower angled slopes formed on loess overlying basalt.

Amplified ground motions can result from near-surface impedance contrasts due to variations in material properties (e.g., a loess mantle or highly fractured rock/scoria overlying bedrock), as well as focussing of seismic waves by surface topography, as in the recent case of the 2010 Haiti earthquake (Hough et al., 2010). Additionally, seismic waves can constructively interfere with one another. All of these collectively cause complex patterns of ground accelerations within quite small areas. Such complex patterns are seen widely within affected areas of the Port Hills.

1.4.5 Evidence of pre-historical earthquake-triggered cliff collapses

Historical and pre-historical collapses of the steep coastal cliffs, that are now inland and no longer being actively eroded by waves, have accumulated as talus on top of relict coastal marine surfaces. At Redcliffs, for example, about 60,000 m^3 of talus mixed with dune sand had accumulated at the toe of the slope prior to the 2010/2011 Canterbury earthquakes. The

age of the coastal beach surface at Redcliffs is about 3,500 to 3,700 calibrated radiocarbon years before present (McFadgen and Goff, 2005).

There is archaeological evidence of some substantial individual rockfalls from the cliffs in the Sumner-Redcliffs area about 500 years ago (e.g., Trotter, 1975). At Moncks Cave, a substantial fall of rocky debris completely blocked the cave entrance and prevented access until workmen removed the debris for road fill in the 1880s. Rocks fell from the roof in Moa Bone Cave around the same time, leading to a change in how the cave was used (Waka were subsequently stored under robust wooden structures to protect them from falling rocks). In addition, middens have been excavated by archaeologists from beneath a cover of rockfall debris beneath the cliff at Redcliffs. The precise triggers and timing of these rockfalls are unknown, but their size and similar ages suggest that they were triggered by strong earthquake ground shaking.

Newspaper accounts report a substantial cliff collapse into the harbour near Lyttelton during the Ellesmere earthquake of 1870, and the fall of several 10-ton boulders onto the Lyttelton to Sumner road near to Lyttelton in the 1888 Cheviot (Amuri) earthquake which shook the spire off of the Christchurch Anglican Cathedral.

At Redcliffs, the two fatalities occurred on residential properties where the dwellings had been constructed, in part, on talus that pre dates the 2010/2011 Canterbury earthquakes. In these locations and elsewhere, pre-4th September 2010 talus has been removed to provide building platforms for houses.

2.0 DATA USED

Table 5 Summary of the main data used in the analysis. LiDAR is Light Detecting and Ranging.

Data	Description	Source	Date	Where used in the analysis
Post 22nd February 2011 earthquake digital aerial photographs	Aerial photographs were taken on 24th February 2011 by NZ Aerial Mapping and were orthorectified by GNS Science (10 cm ground resolution).	NZ Aerial Mapping	Last updated 24th February 2011	Used for base maps and to map extents of cliff collapses triggered by the 22nd February 2011 earthquakes.
LiDAR digital elevation model (2003)	Digital Elevation Model derived from LiDAR survey carried out in 2003; resampled to a 1 m ground resolution.	AAM Hatch	2003	Used as the pre 22nd February 2011 ground model
LiDAR digital elevation model (2011a)	Digital Elevation Model derived from post 22nd February 2011 earthquake LiDAR survey; re-sampled to 1 m ground resolution.	NZ Aerial Mapping	8th to 10th March 2011	To generate change models (between the 2003 and 2011a surveys) to determine the locations, extents and volumes of material leaving the cliffs and where it was deposited.
LiDAR digital elevation model (2011b)	Digital Elevation Model derived from LiDAR survey; resampled to a 1 m ground resolution.	AAM Hatch	May 2011	To generate a model of changes (between the 2011a and 2011b surveys) to determine the locations, extents and volumes of the material leaving the cliffs and where it was deposited.
LiDAR digital elevation model (2011c)	Digital Elevation Model derived from post 13th June 2011 earthquake LiDAR survey; re-sampled to 1 m ground resolution.	NZ Aerial Mapping	18th July to 26th August 2011	To generate a model of changes (between the 2011b and 2011c, and the 2011a and 2011c surveys) to determine the locations, extents and volumes of the material leaving the cliffs and where it was deposited.
Terrestrial laser scan (TLS) surveys	Multiple Digital Elevation Model's derived from surveys following the 22nd February, 16th April and 13th June 2011 earthquakes.	GNS Science	Last survey carried out January 2012	To generate models of changes (between surveys) to determine the distribution and volume of material leaving the cliffs in some limited areas.
Christchurch building footprints	Footprints are derived from aerial photographs. The data originate from 2006 but have been updated in the cliff collapse zones by CCC using the post-earthquake aerial photos.	Christchurch City Council (CCC)	Unknown	Used to identify the locations of residential buildings in the cliff collapse zones and to distribute the population (from the 2006 census data).
Christchurch City Council (CCC) cliff collapse database	The location, date and size of debris associated with cliff collapses mapped in the field from 22nd February and 13th June 2011 earthquakes	Engineering consultants working for CCC. Data compiled by CCC	Last updated 11th October 2011	Used to estimate the travel distance of debris from the cliffs.
GNS Science cliff collapse database	Location, date and size of debris associated with cliff collapses mapped from aerial photographs (utilising the NZAM 26th February	GNS Science and University of	Last updated 8th May 2011	

Data	Description	Source	Date	Where used in the analysis
	2011 10 cm ground resolution), and from field mapping.	Canterbury		
Christchurch City Council recorded house hits	Data on the numbers of houses hit and penetrated by debris from cliff collapses triggered during the 2010/2011 earthquakes	Engineering consultants working for CCC.	Received 22nd November 2011	Used to assess the vulnerability of people in the homes affected by cliff collapse
GNS Science landslide database	Approximate location, date, and probably trigger of newsworthy landslides	GNS Science	Updated monthly	Used to estimate the likely numbers and volumes of pre earthquake cliff collapses in the areas of interest.
Earthquake Commission claims database	Location, date and brief cause of claims made in the Port Hills of Christchurch since 1993.	Earthquake Commission (EQC)	1993 to August 2010	Used to estimate the likely numbers and volumes of pre earthquake cliff collapses in the areas of interest.
Ground-acceleration records for the 2010/2011 Canterbury earthquakes	Ground accelerations recorded at the GeoNet strong motion sites located in the Port Hills.	GeoNet	From 22nd February 2011	Used to correlate with the estimated volumes of material leaving the cliffs in response to the 2010/2011 Canterbury earthquakes.
Composite seismic hazard model	The increased level of seismicity in the Canterbury region since 4th September 2010 has been quantified using a modified form of the national seismic hazard model.	GNS Science	Updated 1st January 2012	Used to estimate the frequency of occurrence of a given peak ground acceleration.
Drillhole logs	The logs from cores extracted from holes bored into the cliff top areas covered by this report.	Tonkin and Taylor on behalf of EQC	February 2012	Used in generating the engineering geological models of the cliff interiors.
Field work	Field mapping of cliff collapses and ground truthing of the risk analyses.	GNS Science and the Port Hills Geotechnical group	22nd February 2011 to March 2012	Used in generating the engineering geological models of the cliffs. Results from field checks used to update risk maps.

3.0 METHODS

Using the Australian Geomechanics Society guidelines for landslide risk management (Australian Geomechanics Society, 2007), the risk of loss of life to an individual is calculated from:

$$R_{(LOL)} = P_{(H)} \times P_{(S:H)} \times P_{(T:S)} \times V_{(D:T)} \quad [1]$$

where:

- $R_{(LoL)}$ is the risk (annual probability of loss of life (death) of a person) from debris avalanches or cliff top recession;
- $P_{(H)}$ is the annual probability of an initiating event;
- $P_{(S:H)}$ is the probability of a person, if present, being in the path of avalanching debris at a given location, or the probability of a person at a given location falling over the edge of the cliff as the cliff recedes;
- $P_{(T:S)}$ is the probability that a person is present at that location;
- $V_{(D:T)}$ is the vulnerability, or probability of a person being killed if present and hit by debris or from falling over the edge of the cliff top as it recedes.

The steps in the cliff collapse risk analysis are laid out in Figure 9, and include the following key steps:

1. Risk analysis carried out as per the Australian Geomechanics Society (2007) method;

2. Field verification of the analysis results by the Port Hills Geotechnical Group; and

3. Updating of the fatality risk maps with the results from field verification.

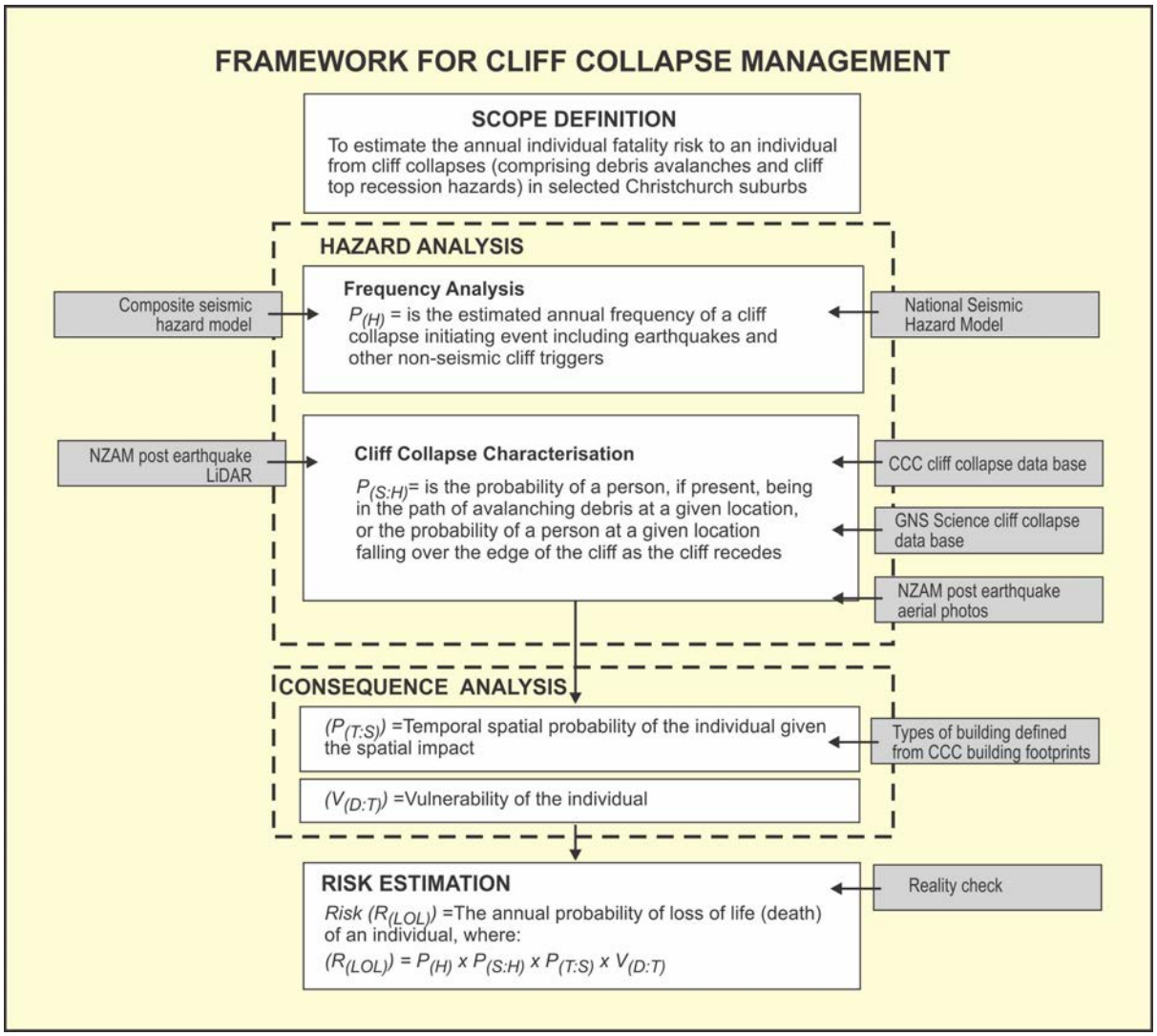

Figure 9 Framework used to assess the annual probability of loss of life (death) of an individual from cliff collapses in the Port Hills. Modified after the Australian Geomechanics Society Guidelines for landslide risk management (Australian Geomechanics Society, 2007).

4.0 CHARACTERISING CLIFF COLLAPSE

4.1 Description of the cliffs

The slopes at Redcliffs (Figure 10), Shag Rock Reserve (Figure 11), Wakefield Avenue and Nayland Street (Figure 12) are former sea cliffs (no longer subjected to marine erosion), while Whitewash Head (Figure 13A, B) is being actively eroded by the sea (Appendix A). The slopes at Redcliffs, Wakefield Avenue and Nayland Street were abandoned by the sea about 3,600 years ago (McFadgen and Goff, 2005). Erosion of the cliff toe at Shag Rock Reserve stopped when the road to Sumner was formed in the latter half of the 19th Century. The cliffs at Redcliffs and Wakefield Avenue have been analysed in several sections. A summary of the main attributes of the slopes is contained in Table 6.

Table 6 Main details of the cliffs included in this assessment.

Site	Height (m)	Length (m)	Aspect (°)	Slope angle (°)
Redcliffs Road	40	120	060	50 to 70
Redcliffs Northwest	40	170	140	50 to 80
Redcliffs Southwest	70	280	065	50 to 90
Shag Rock Reserve	80	400	020	50 to 80
Nayland Street	50	80	360	60 to 80
Wakefield Avenue North	70	260	110	50 to 90
Wakefield Avenue South	70	260	080	50 to 90
Whitewash Head North	80	110	045	60 to 90
Whitewash Head Central	110	370	090	60 to 90
Whitewash Head South	100	160	065	60 to 90

The following information was acquired by GNS Science for each site:

1. Crack maps – mapping traces of ground cracks behind the slope edge formed in the post-22nd February 2011 earthquakes. Carried out by the Port Hills Geotechnical Group of consultants for Christchurch City Council.

2. Crack displacements along transects – at selected locations along the cliff edge, to record horizontal and vertical offsets across post-22nd February 2011 ground cracks. Carried out by Geotechnical Consulting Ltd for Christchurch City Council.

3. Drillholes – at selected locations, to assess the thickness and geotechnical properties of the materials forming the slopes. Carried out by Tonkin and Taylor Ltd, for the Earthquake Commission. Supplementary logging of selected drillcores carried out by GNS Science.

4. Photogrammetry – to remotely assess the orientation and spacing of discontinuities (e.g., joints, fractures and other defects) within the materials forming the slopes. Carried out by University of Auckland for the New Zealand Natural Hazards Research Platform.

5. 2011 talus and rockfall (individual boulder rolls) limits – delimiting of the furthest extent of debris from the foot of the cliffs. Carried out by GNS Science and Geotechnical Consulting Ltd.

6. Repeat terrestrial laser scan surveys of the cliff faces – to quantify the changes of the cliff face (erosion and deposition on the cliff faces) between terrestrial laser scan surveys. Carried out by GNS Science for the New Zealand Natural Hazards Research Platform.

7. Repeat airborne Light Detecting and Ranging (LiDAR) surveys of the cliffs – to quantify the changes of the cliff edge (cliff edge) and the volumes of material deposited at the toe of the cliffs between subsequent surveys.

The exposed cliff faces are currently very disturbed and fragmented, with many areas of loose rock apparent. At the cliff top, there are many tens of houses that are in part overhanging the cliff edge, where their foundations and structure have fallen away. Many cracks have been mapped at the cliff top, with some showing displacements towards the cliff edge of up to 0.5 m. At the cliff bottom, many tens of houses have been inundated (partially buried and covered) with debris that has fallen from the cliffs. Shipping containers have been placed at the bottom of the cliffs to help contain any future debris avalanches. The containers are a temporary measure. Those residential properties affected have been issued with notices under section 124 of the Building Act preventing access to the building until it is no longer unsafe. Anecdotal evidence from residents living near the affected areas suggests that rock continues to fall from the cliffs between earthquakes.

Quarrying of the cliffs for construction materials has occurred in the past in the Port Hills. The causeway between Sumner and Mount Pleasant (McCormick's Bay) and the sea wall at Sumner were quarried from a site in McCormacks Valley, the nearest site where the rock was of suitable durability. GNS Science found no evidence to support the view that the cliffs at Redcliffs, Shag Rock Reserve, Nayland Street and Wakefield Avenue were modified by quarrying. Talus was taken from the toes of some cliffs for use as fill in local road construction, and has been excavated locally to create space for residential building sites, but the cliff faces themselves do not contain rock material of adequate quality to support a quarrying operation. At Redcliffs, a Maori settlement was located at the toe of the cliff (Jacomb, 2008); some middens excavated from beneath rockfall talus at "Redcliffs Flat" indicate significant rockfall activity since Maōri occupation of the area.

Figure 10 Redcliffs following the 22nd February 2011 Christchurch Earthquake. Photograph taken by G. Hancox, GNS Science.

Figure 11 Shag Rock Reserve following the 13th June 2011 earthquake. Photograph taken by C. Gibbons.

Figure 12 Nayland Street (foreground) and Wakefield Avenue (left) following the 13th June 2011 earthquake. Photograph taken by C. Massey, GNS Science.

Figure 13A Whitewash Head following the 22nd February 2011 earthquakes but before the 13th June 2011 earthquake. Photograph taken by M. Yetton.

Figure 13B Whitewash Head following the 13th June 2011 earthquake. Photograph taken by C. Massey, GNS Science.

4.2 Engineering geology and geomorphology of the cliffs

The cliffs of Redcliffs and have formed within lavas of the Mt Pleasant Formation, while the eastern cliffs above Wakefield Avenue, Nayland Street and Whitewash Head have formed within older Lyttelton Volcanic Group rocks. Both Mt Pleasant Formation and Lyttelton Volcanic Group range in age from 11 to 9.7 million years old (Sewell et al., 1988).

GNS Science and Geotech Consulting Ltd. carried out engineering geological mapping of all four areas (Appendices B and C). For Redcliffs, Shag Rock Reserve, Wakefield Avenue and Nayland Street, mapping of the main lithologies and rock-mass conditions was done in the field on orthorectified aerial photographs, and slope-face maps were derived from terrestrial laser scan surveys of the cliffs. For Whitewash Head, where field access was limited to the cliff top, mapping was done using oblique aerial photographs onto slope-face maps derived from LiDAR surveys (the 2011a LiDAR survey, Section 2). Mapping was carried out following the 22nd February and 13th June 2011 earthquakes. Therefore the slope-face logs represent the materials exposed on the cliff faces after the 13th June earthquakes, but before the 23rd December 2011 earthquakes. Locally, substantial lateral variations in geological structure have been revealed in the newly created cliff faces.

All cliff faces comprise near horizontal (but can be locally steep) interlayered variations of the following main rock types: 1) Blocky columnar-jointed lava (typically basalt and trachyte lavas); 2) Lava breccia; 3) Lahar deposits; 4) Pyroclastic deposits (palaeosol/ash layers); and 5) Recent debris (mainly talus from the 2010/2011 Canterbury earthquake sequence). In some locations, pre-earthquake debris (and talus) is present at the toe of the slopes. Descriptions of the main units are given in Table 7.

Table 7 Engineering geological descriptions of the main geological units forming the cliffs (descriptions as per New Zealand Geotechnical Society, 2005).

Unit name	Description	Location
Basalt Lava	Dark greenish grey to black, unweathered to moderately weathered, sometimes vesicular, Basalt, very strong with variably developed columnar joints, widely to very widely spaced (1.5 to 25 m), typically giving large to very large block sizes that are columnar in shape. Columnar joints are often radial to flow margins, and lavas have gradational contacts with lava breccia at their upper and side margins. Joint faces are generally rough to very rough, stepped or irregular, commonly manganese oxide or calcite coated, and only rarely have clay or silt fill. Individual flows form lensoidal bodies throughout the cliffs, ranging from 0.5 to 2-4 m thick. Columnar jointing is well expressed where flows are thick, and gives way to thin, platy flow orientated jointing where flows are thin.	All sites
Trachyte Lava	Unweathered to moderately weathered, pinkish brown to grey brown when fresh, flow-banded Trachyte, very strong, with pronounced anastomosing flow parallel banding and joints that are closely spaced (approximately 0.1 to 0.25 m spacing), typically giving large to very large block sizes that are tabular shaped. Columnar joints are either very poorly developed or absent. Lower contact with its own breccia is often sharp, upper contact is gradational into autobreccia.	Nayland Street and Wakefield Avenue
	Slightly weathered to highly weathered, light grey to dark grey when slightly weathered to orange or red-brown when highly weathered, massive, brecciated Basaltic Lava Fragments, moderately strong to strong (but varies to weak or very weak when highly or completely weathered), with very widely spaced irregular discontinuities.	
Basaltic Lava Breccia	At all sites basaltic lavas have flowed within thick carapaces of brecciated lava, with the breccia often exceeding the thickness of its source lava (brecciated units may be 2 to >10 m thick.). Breccias are poorly graded, angular lava fragments with a fine to coarse matrix supporting unsorted cobbles, blocks and often 1-5 m diameter megablocks of broken lava. Breccia fragments are often more vesicular and scoriaceous than the source lava, and prone to weathering due to high porosity. Bedding is massive, poorly jointed, with lower boundaries gradational with the source lava and upper boundaries roughly planar. Weathering expression is cavernous and spheroidal, of fine and coarse blocks respectively, and in some cases development of cliff parallel exfoliation joints/cracks. Freshly exposed breccia faces show extensive interstitial clay weathering and deposition of clay within vesicles and between clasts.	All sites
Trachytic Lava Breccia	Slightly weathered to highly weathered, dark grey when fresh, weathering to pale tan, yellow or mauve patches with spheroidal and cavernous weathering structures; massive and unsorted brecciated Trachytic Lava Fragments, moderately strong when fresh but weak to extremely weak when highly weathered. The Trachytic Lava on Wakefield Avenue has flowed within a thick upper and lower carapace of autobrecciated lava, up to 4-5 m thick below the main lava, and up to 10 m thick above it, with gradational contacts between the lava and its breccia. Massive and poorly jointed, but with extensive leaching and clayey alteration present in upper parts below top contact with overlying tuffs and	Nayland Street and Wakefield Avenue

Unit name	Description	Location
	basalt lavas, and at lower contact below the lava at South Wakefield Avenue. Weathering expression is cavernous and spheroidal, with extensive clayey alteration and oxidation of clasts in some locations (South Wakefield Avenue). Freshly exposed faces by Wakefield Avenue Croquet Club show interstitial clay deposition and shrinkage cracks on exposure, and examples of polished slickensides (Iron and manganese oxide stained slickensides have been observed in blocks of lava breccia that have fallen from the Wakefield Avenue slope face during the 2010/2011 Canterbury earthquakes).	
Pyroclastic Deposits	Moderately to highly weathered or oxidised brown to red-brown or yellow-brown thinly bedded Tuff or Tuffaceous Sandstone, intercalated with or grading into fine to coarse pebbly Lapilli Tuffs or Gravelly Sandstone, with occasional cobble-sized blocks and bombs of basalt, moderately strong to weak, very weak to extremely weak when highly weathered. Rarely jointed, prone to cracking on exposed surfaces and easily eroded (One clean, undulating slickensided joint was observed in tuffaceous material in the Tonkin and Taylor Borehole at 8d Balmoral Lane, at 23.1 m depth.). Bedding is thin (0.1 to 2 m) and discontinuous, disrupted by overlying lavas. In all sites, these layers of red-oxidised pyroclastic and epiclastic paleosol material are found between lava flows and breccias, usually at the top of the preceeding lava breccia, and oxidised/baked by the overlying lava flow. The thinly bedded ash and lapilli, with occasional blocks and bombs, is discontinuous due to re-working by water-driven epiclastic processes or re-working by overlying lava flows. The pyroclastic material exposed in the cliffs is often vegetated or a focus for fluid flow, being relatively impermeable compared to the overlying jointed lavas and porous breccias. Contacts are often gradational into lava breccia or lahar/debris flow material.	All sites
Lahar Deposits	Moderately weathered or oxidised in most exposures, thickly to massively bedded (0.25 m to 2+ m thick beds), red to red brown, Lahar Deposits, comprising fine-grained poorly sorted coarse sandy matrix with occasional pebbly layers with matrix support, and 0.3 to 1 m diameter rounded cobbles of both basaltic and trachytic material, moderately strong, weak where highly weathered, unjointed or poorly jointed, occasionally fractured. Lahar deposits were mapped at the western end of the Redcliffs face below Balmoral Lane. Smaller debris-flow structures have been observed in borehole examples in all sites, usually intercalated with or in gradational contact with tuffaceous layers or the upper parts of lava breccias.	Northwest Redcliffs, and in small exposures in borehole and seacliffs throughout the area.
Recent Debris	Massive, unconsolidated debris aprons of recent material from the 22nd February, 13th June and 23rd December 2011 aftershocks have built up at the base of all cliffs mapped. These are unsorted fall deposits of cobble through to megablocks of all lithologies described above, lying at repose angles of 25-35º in fans at the base of the cliffs, extending from a few metres to several tens of metres from the cliff base, and in excess of 10 to 15 m thick in some cases. Talus cones of finer material, gravity sorted from dust through fine pebbles to cobbles and small boulders, are building above the massive debris fans from constant small erosive events, both aeolian and water driven.	All Sites.

For each slope, the proportion of slope face (area) exposing a particular geological unit was estimated from slope-face geological mapping and slope-face topography. These data show that the slopes are formed dominantly in lava breccia (Figure 14).

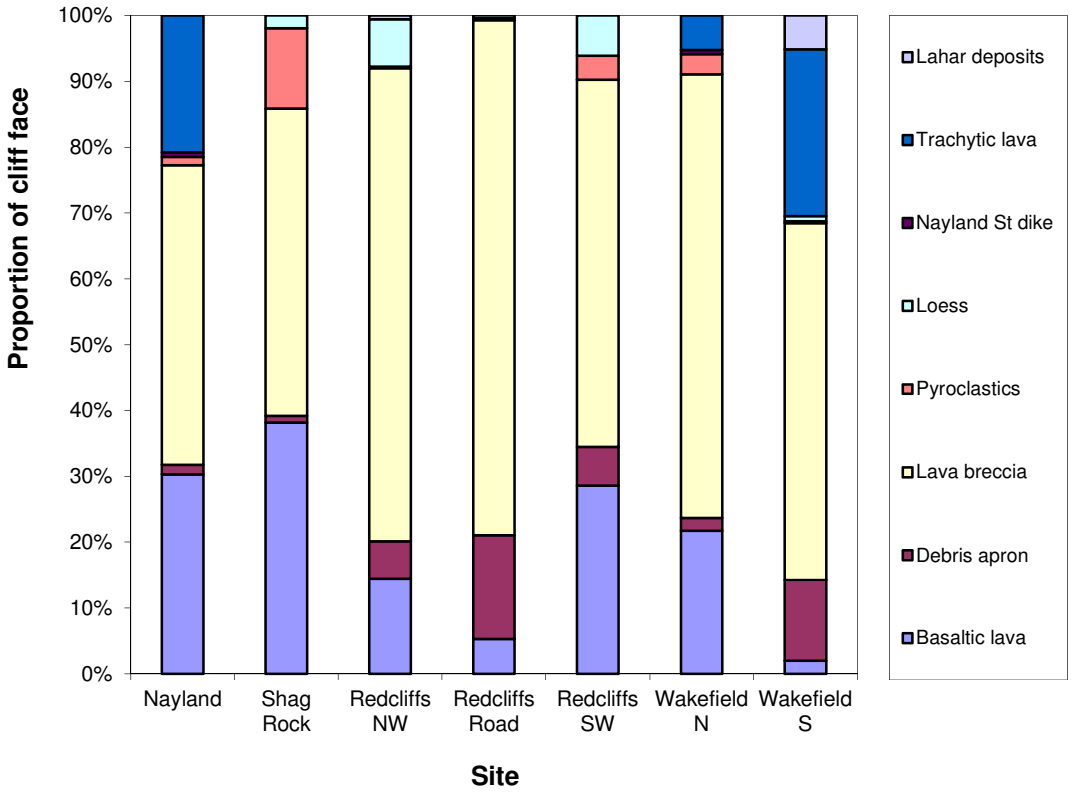

Figure 14 Proportion of cliff face formed within a given material type per location.

Estimation of the rock-mass strength properties of the different geological rock units using the Geological Strength Index (Hoek, 1999; Marinos and Hoek, 2000) was carried out on field exposures and cores from drillholes. The range of strength indices for the different units is shown in Figure 15.

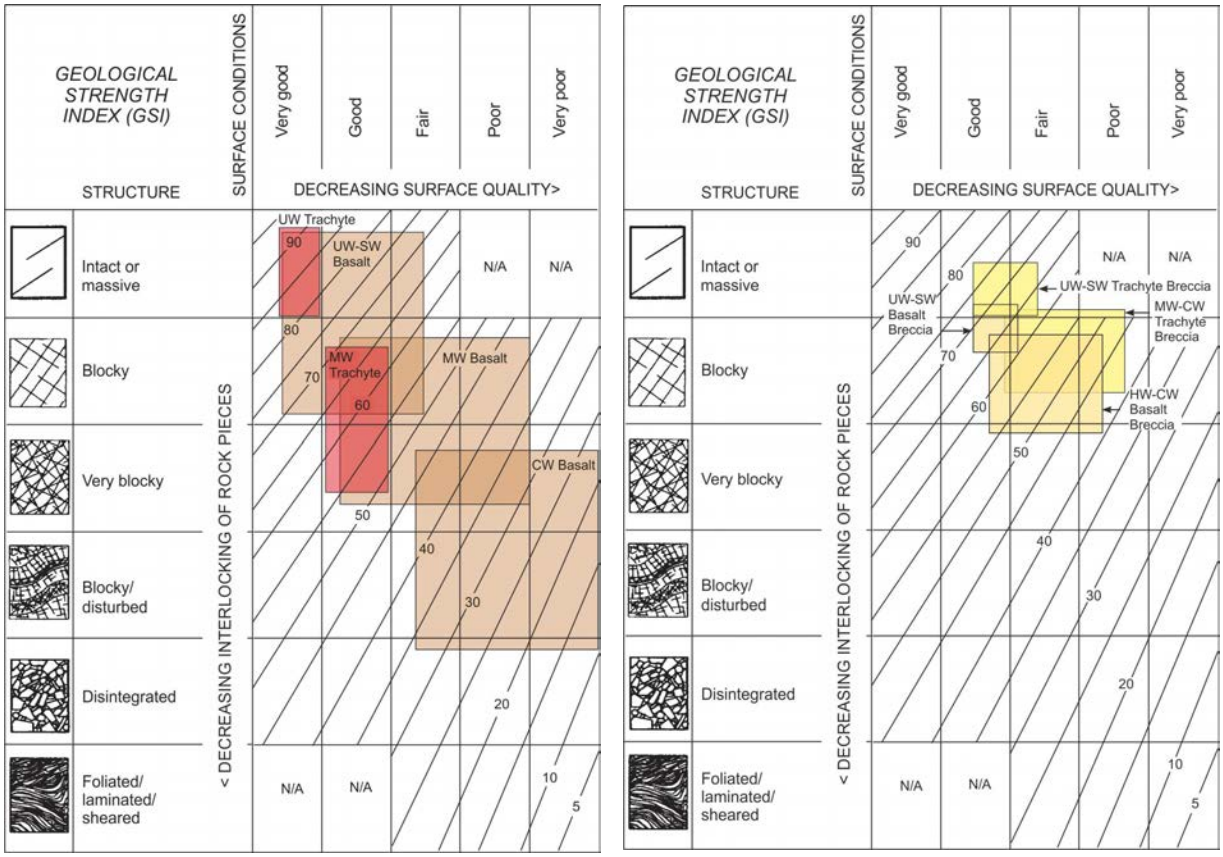

Figure 15 Geological strength index plot for Basalt and Trachyte lavas and Basaltic and Trachytic lava breccias exposed on the cliffs at Redcliffs, Shag Rock Reserve, Nayland Street and Wakefield Avenue.

4.2.1 Geomorphology of the cliffs

Many of the abandoned costal cliffs in the northern Port Hills from Mount Pleasant through to Sumner are typically <30 m in height and formed predominantly in basalt and trachytic lava. These cliffs are believed to have been abandoned by the sea between about 2,000 to 4,000 years before present (Brown and Weeber, 1992; McFadgen and Goff, 2005). Out of a sample of 74 of the cliffs that did not fail during the 2010/2011 Canterbury earthquakes (Appendix A), mean slope angles are 59° (±9° at one standard deviation) with minimum and maximum recorded angles of 40° and 74° respectively, with slope heights (of the rock-face portion only) of <30 m.

The cliffs that failed during the 2010/2011 Canterbury earthquakes at Redcliffs, Shag Rock Reserve, Nayland Street, Wakefield Avenue and Whitewash Head form the most prominent cliffs in the area, ranging from 30 to 110 m in height. With the exception of Whitewash Head, all of the other cliffs are now abandoned coastal sea cliffs. Mean slope angles are 68° (±8° at one standard deviation) with minimum and maximum recorded angles of 45° and 82° respectively, indicating that the slope angles of the cliffs that failed are slightly steeper than those that did not fail. Locally, the stronger lava units form steeper slopes and the lava breccias and thin layers of pyroclastics form the weaker and lower angle intervening slopes (Figures 16 and 17), reflecting the differing rock mass conditions (Figure 15).

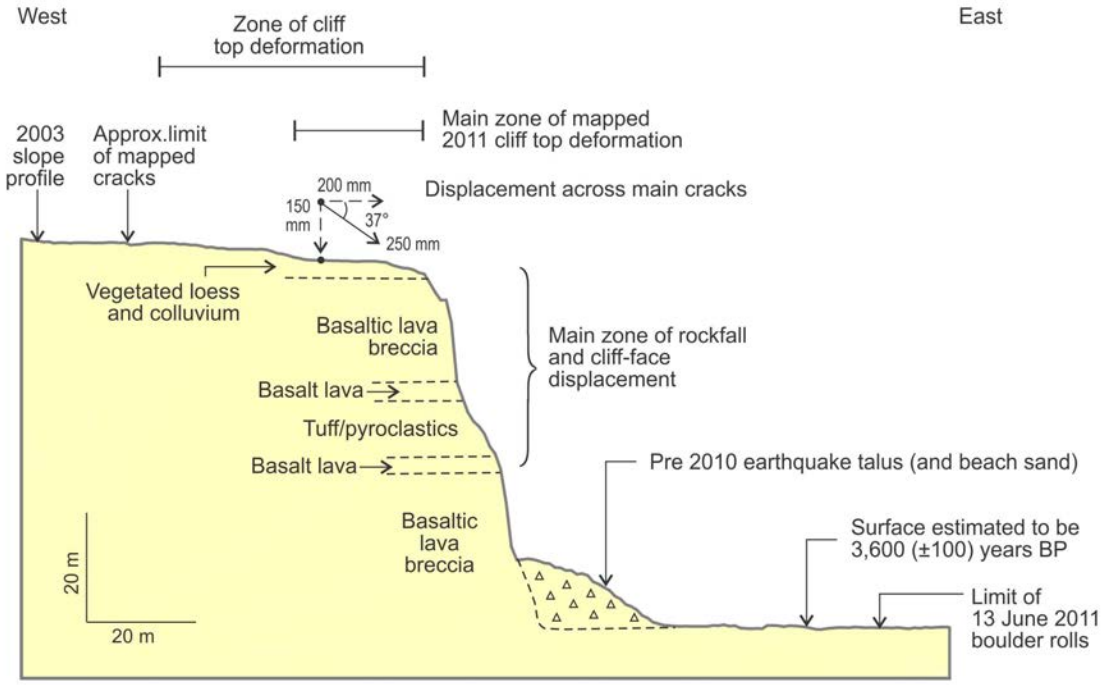

Figure 16 Engineering geological cross section No. 1 at Redcliffs.

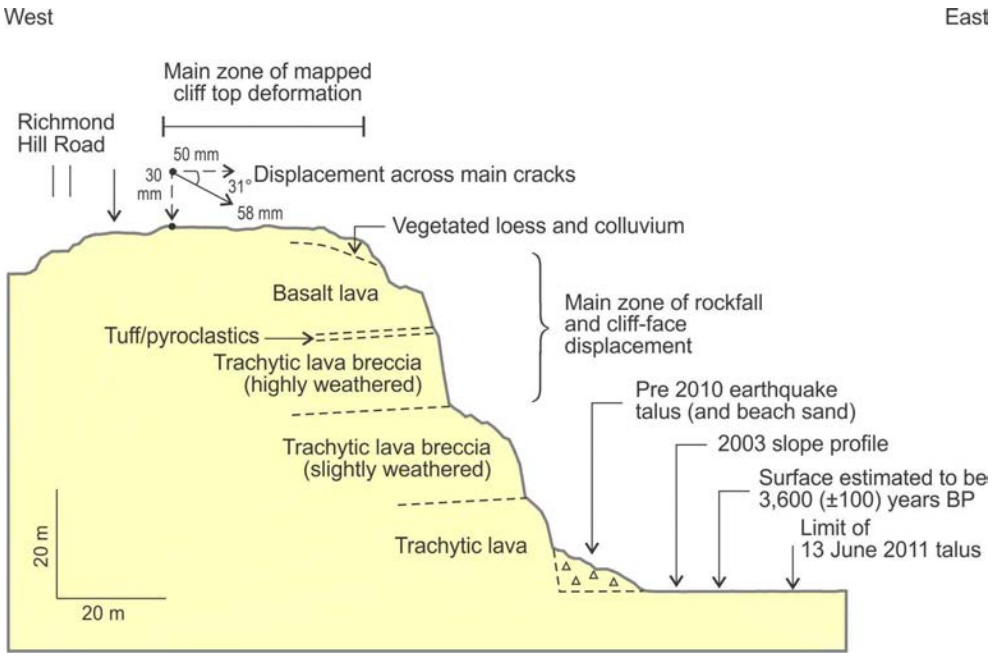

Figure 17 Engineering geological cross section No. 2 at Wakefield Avenue.

The slope aspect of these cliffs range from 360° (north) to 090° (east) with a mean of about 045° (northeast), which is towards the coast. However, many of the cliffs that did not fail have similar aspects to those that did. Therefore it is likely that the formation of these steeper and taller cliffs is a function of both pre-historical coastal erosion, and the presence of weaker and erodible materials, such as the lava breccias at the bases of the cliffs.

4.3 Assessment of 2011 cliff collapses

4.3.1 Assessment method

Changes of the cliffs in the pilot study areas in response to the 2011 earthquakes have been quantified using repeat terrestrial laser scan surveys and LiDAR surveys (Table 8) with field mapping.

Table 8 Summary of terrestrial laser scan (TLS) and airbone Light Detecting and Ranging (LiDAR) surveys in chronological order

Name	Type of survey	Date	Site
2003 (reprocessed)	LiDAR	2003	All cliff areas
2011a	LiDAR	8th to 10th March 2011	All cliff areas
TLSa	TLS	8th to 9th March 2011	All cliff areas – but limited by access conditions
TLSb	TLS	5th April 2011	Shag Rock Reserve – but limited by access conditions
TLSc	TLS	3rd to 6th May 2011	Redcliffs, Wakefield Avenue and Nayland Street – but limited by access conditions
2011b	LiDAR	May 2003	All cliff areas
TLSd	TLS	15th to 16th June 2011	All cliff areas – but limited by access conditions
2011c	LiDAR	18th July to 26th August 2011	All cliff areas

Digital elevation models representing the ground surface at a given time were generated for each data set. For the LiDAR surveys, a 1-m grid (ground resolution) of elevations was generated from filtered scan data points supplied by the contractor. For each of the terrestrial laser scan surveys a 0.1-m grid was generated from the filtered point data. Filtering comprised removal of points representing vegetation and buildings from the supplied point data, thereby creating a “bare earth” or “filtered” point elevation data set. This was undertaken by GNS Science for the terrestrial laser scan survey data, and by the consultants AAM Hatch and New Zealand Aerial Mapping for the LiDAR datasets (these companies were commissioned by other parties, mainly the Earthquake Commission and the Christchurch City Council, to carry out the surveys).

The grid resolution generated from the terrestrial laser scan survey data (0.1-m ground resolution) is higher than that generated for the LiDAR surveys (1-m ground resolution) to take into account the original point spacing of the survey data. For LiDAR, the steep angle of the cliffs relative to the line of sight of the survey instrument makes it difficult to precisely survey very steeply sloping ground, while for the terrestrial laser scan surveys the instrument faces directly onto the cliff face and can therefore capture much more cliff face topographic

data. However, the terrestrial laser scan surveys cover only limited portions of the sites, a function of site access, whilst the LiDAR surveys cover all of the sites, but at a reduced resolution.

Errors are assessed for each digital elevation model by comparing the modelled surface with the filtered point data used to generate it in a few sample areas of the digital elevation model. Errors in the terrestrial laser scan survey data are generally ±0.02 m at one standard deviation and for the LiDAR data generally ±0.1 m (in height) for the New Zealand Aerial Mapping data sets (LiDAR surveys 2011a and 2011c), and ±0.2 m (in height) for the AAM Hatch data sets.

Change models were generated by subtracting successive digital elevation models, e.g., subtracting 2011a from 2003. Volumes were calculated as the difference between the two surfaces. A simple digital elevation model subtraction gave the change and hence volume for each grid cell. The volume of change for each cliff (including the material lost from the cliff (erosion) and material deposited either on or at the toe of the cliff) was then calculated by adding the individual change volumes for each grid cell. The relative accuracy between any two modelled surfaces was assessed following the "modelled surface error" method outlined by G. Archibald (personal communication 2011) to derive the estimated statistical error associated with the volume calculation. For the terrestrial laser scan surveys this error was about 3%, and for the LiDAR surveys between 14 to 22%, depending upon which change models were being compared.

Large errors can be introduced in the assessments due to the positional accuracy of the original point data and derived digital elevation model generated from it. These errors can be compounded between different surveys and the resultant volume-change models. The positional errors between the terrestrial laser scan digital elevation models are estimated to be about ±0.05 m (estimated from field targets and expressed as one standard deviation), as repeated surveys were carried out from the same setup positions. The positional errors between the LiDAR digital elevation models are larger, about ±1.0 m (at one standard deviation) in some instances. This precision has been estimated using indicators on the ground comprising hard edges such as roads and walls. This has been undertaken by GNS Science because positional metadata was not available for the 2003 and 2011b surveys, and there appear to be alignment issues between the two surveys. The selected features were mapped from the March 2011, orthorectifed aerial photographs and compared to their corresponding positions shown on the different LiDAR digital elevation models. Although a ±1.0-m error may have little consequence on estimated volumes calculated for relatively flat areas, it has a larger impact on steeper slopes such as the cliffs assessed here. The largest positional errors appear to be associated with the 2011b survey and as a result the 2011b digital elevation model has not been used in analysis.

In the volume-change models, zones with changes greater than ±0.1 m for the terrestrial laser scan surveys and ±1.0 m for the LiDAR 2003 survey and ±0.5 m for the 2011a and 2011c surveys were assessed as real and not the result of positional or measurement error.

The times of the 2011 LiDAR and terrestrial laser scan surveys were chosen (by the funding agencies) to assess changes caused by larger events in the earthquake sequence. By comparing surveys before and after the main earthquakes, changes caused by the earthquake(s) can be assessed. For example, the change model from subtracting the 2011a digital elevation model from the 2003 model quantifies changes caused mainly by the 22nd

February 2011 earthquakes, when most of the change occurred.

The digital elevation models and surface-change models have been used to quantify:

1. Cliff top recession – changes in the cliff edge between surveys

2. Volume lost from the cliffs – the volume of debris lost from the cliffs between successive surveys and the distribution of where the debris fell from

3. Runout of debris avalanches – where the debris that fell from the cliff went to, i.e., the volumes of deposition at the cliff toe.

In addition to the change models derived from the terrestrial laser scanning and LiDAR surveys, the runout of debris falling from the cliffs as a result of the 22nd February and 13th June 2011 earthquakes was mapped in the field and has been used to verify remotely sensed data.

As well as material falling from cliff faces during the 2010/2011 Canterbury earthquakes, cracks also developed behind the cliff tops. These cracks were mapped in the field by the Port Hills Geotechnical Group. In several locations, close inspection and measurements along transect lines were used to quantify horizontal and vertical displacements across cracks. Where possible, the material in which the cracks had formed (e.g., loess, fill and rock) was determined and the likely crack-formation mechanisms (e.g., localised retaining wall failure, settlement and landslides) estimated. However, in many instances it was not possible to determine what mechanisms formed them.

4.3.2 Cliff top recession

For each site, the location of the cliff edge was estimated from the LiDAR digital elevation models with a resolution of 1-m. The position of the cliff edge was defined using the 2003, 2011a and 2011c LiDAR surveys. The cliff edge is defined as the line of intersection between the steeper slope (greater than 45º slope angle), forming the cliff face (typically formed of rock) and the shallower slope above the cliff face.

Cliff edges derived from the 2003, 2011a and 2011c surveys are shown on the maps in Appendix B. The location of the cliff edge in the 2011a LiDAR model was verified against the cliff edge location in the orthorectified aerial photographs relating to the same time. It was not possible to verify cliff edges at other times. The cliff edge defined from the 2003 LiDAR survey was the most problematic because the original survey point spacing resulted in a lower resolution than that of the 2011a and 2011c surveys.

The area of cliff top lost from each site between surveys, mainly between the 2003 and 2011a, and the 2011a and 2011c surveys, was quantified by counting the number of 1-m grid squares between successive cliff edges (Figure 18). The area lost represents the area of the cliff top that has fallen away between any given surveys.

Figure 18 Example of how the area lost at the top of the cliff between the LiDAR surveys has been estimated. The solid red line represents the 2003 cliff edge and the dashed red line represents the 2011a cliff edge. The black lines with numbers (see inset) represent 1 metre zones (back from the 2003 cliff edge) that run parallel to the 2003 cliff edge. Area shown is on Whitewash Head.

The total area lost at a given cliff top between surveys is summarised in Table 9. The loss of cliff tops between the 2003 and 2011a surveys are shown in Figure 19. The interval between the 2003 and 2011a surveys is about 8 years. Although minor loss from cliff edge may have occurred during this period from other triggers, the majority of the loss is due to the 22nd February 2011 earthquakes, particularly the 22nd February M_W6.2 earthquake, which was associated with peak ground accelerations exceeding 1.0 g in the Port Hills.

Table 9 Summary of the area lost at the top of the cliffs between LiDAR surveys

Site	Area lost (m^2) between LiDAR surveys (errors at one standard deviation)	
	2003 to 2011a	2011a to 2011c
Redcliffs	480 (± 22%)	489 (± 14%)
Shag Rock Reserve	327 (± 22%)	1047 (± 14%)
Nayland Street	10 (± 22%)	16 (± 14%)
Wakefield Avenue	27 (± 22%)	265 (± 14%)
Whitewash Head	334 (± 22%)	2466 (± 14%)

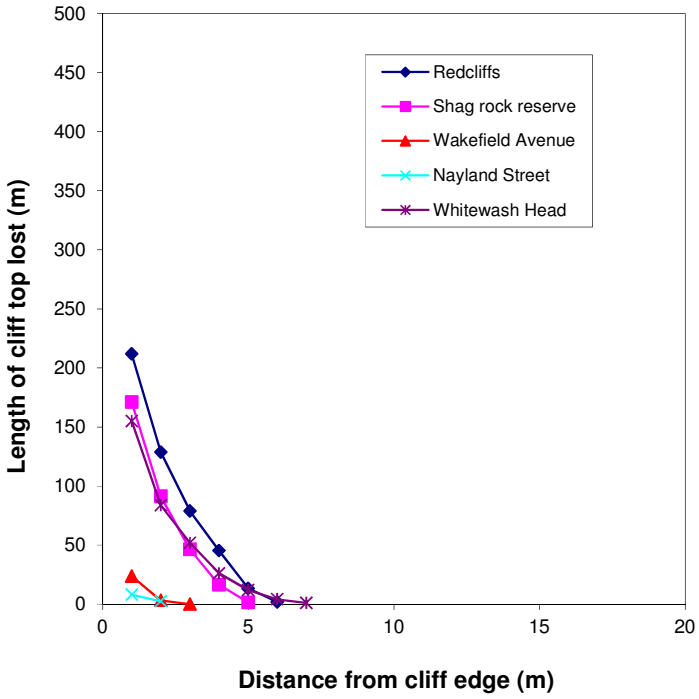

Figure 19 Length of cliff top lost per metre distance back from the cliff edge. Length lost is calculated as the change between cliff edges identified using the LiDAR surveys 2003 and 2011a (assumed to be caused by the 22nd February 2011 earthquakes).

For all cliffs, the largest calculated losses were between the 2011a and 2011c surveys (Figure 20). During this period, two large earthquakes occurred that were greater than M_W5. These were on 16th April 2011, $M_W5.2$; and on 13th June 2011, $M_W6.2$. Peak ground accelerations in the Port Hills in the 13th June 2011 earthquake were greater than 2.0 g, while those in the 16th April 2011 earthquake were below 1.0 g. Terrestrial laser scan surveys of the cliffs carried out before and after the 16th April 2011 earthquake (TLSa and TLSb before, and TLSc after) indicate little change in the cliff edge as a result of that earthquake. Therefore the majority of the change recorded between the 2011a and 2011c LiDAR survey is attributed to the 13th June 2011 $M_W6.2$ earthquake.

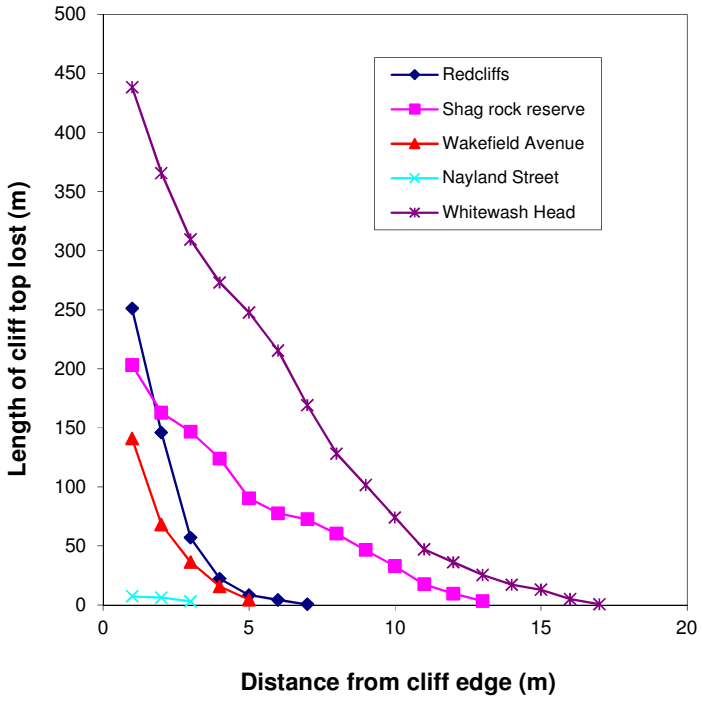

Figure 20 Length of cliff top lost per metre distance back from the cliff edge. Length lost is calculated as the change between cliff edges identified using the LiDAR surveys 2011a and 2011b (reasoned to be caused by the 13th June 2011 earthquakes).

The cliffs at Whitewash Head and Shag Rock Reserve show the most change in response to the 13th June 2011 earthquake, with loss extending up to 17 m back from the initial cliff edge (Whitewash Head). Cliff top loss at Wakefield Avenue is anomalous when compared to similarly high and long cliffs at Redcliffs and Shag Rock Reserve. This may be due to a thick layer of basaltic lava which forms the upper part of the slope at Wakefield Avenue but which is absent at the other cliffs (Appendix C).

The areas of cliff top lost can be expressed as a proportion of the total area of cliff top that failed at given distances back from the cliff edge. These proportions are shown in Table 10.

Table 10 Summary of the area lost at the top of the cliffs as a proportion (percentage) of the total area lost per metre back from the cliff edge, between LiDAR surveys 2011a and 2011c.

Distance back from cliff edge (m)	Area lost as a proportion of the total area lost between LiDAR surveys 2011a and 2011c				
	Redcliffs	Shag Rock Reserve	Nayland Street	Wakefield Ave	Whitewash Head
1	51.3%	19.4%	44.1%	53.1%	17.8%
2	29.8%	15.5%	37.7%	25.6%	14.8%
3	11.6%	14.0%	18.2%	13.7%	12.5%
4	4.5%	11.8%	0.0%	5.9%	11.1%
5	1.7%	8.6%	0.0%	1.7%	10.0%
6	0.9%	7.4%	0.0%	0.0%	8.7%
7	0.1%	6.9%	0.0%	0.0%	6.9%
8	0.0%	5.8%	0.0%	0.0%	5.2%
9	0.0%	4.4%	0.0%	0.0%	4.1%
10	0.0%	3.1%	0.0%	0.0%	3.0%
11	0.0%	1.7%	0.0%	0.0%	1.9%
12	0.0%	0.9%	0.0%	0.0%	1.5%
13	0.0%	0.3%	0.0%	0.0%	1.0%
14	0.0%	0.0%	0.0%	0.0%	0.7%
15	0.0%	0.0%	0.0%	0.0%	0.5%
16	0.0%	0.0%	0.0%	0.0%	0.2%
17	0.0%	0.0%	0.0%	0.0%	0.0%
18	0.0%	0.0%	0.0%	0.0%	0.0%
19	0.0%	0.0%	0.0%	0.0%	0.0%
20	0.0%	0.0%	0.0%	0.0%	0.0%

4.3.3 Cliff top cracks and ground displacement

In addition to the loss of material fallen from the cliff edge, there was also displacement of ground behind the cliff edge. For example, the maximum recorded recession of the cliff edge was about 17 m (at Whitewash Head), while cracks in the ground showing movement towards the cliff edge extend about 40 m back from the post-failure cliff edge (Figure 21).

Transects of crack-displacement measurements were used to assess the amount of displacement towards the cliff edges in response to the 2010/2011 Canterbury earthquakes. Transect measurements were taken at all of the sites in September 2011. In some locations the lines of measurement extended over 50 m back from the cliff edge, with lengths determined from the observed crack distribution (Appendix B).

At most sites, the predominantly rocky cliffs are topped by a relatively thin (1 to 5 m) cover of non-volcanic material, typically loess, colluvial (remoulded) loess and placed fill. Much of the land in these cliff top areas comprises landscaped and heavily vegetated gardens in which it is difficult to detect or follow cracks. In areas where the ground surface was relatively brittle and not obscured by vegetation, such as driveways and paths, the numbers of observed cracks were greater than in heavily vegetated or landscaped areas, indicating sample bias.

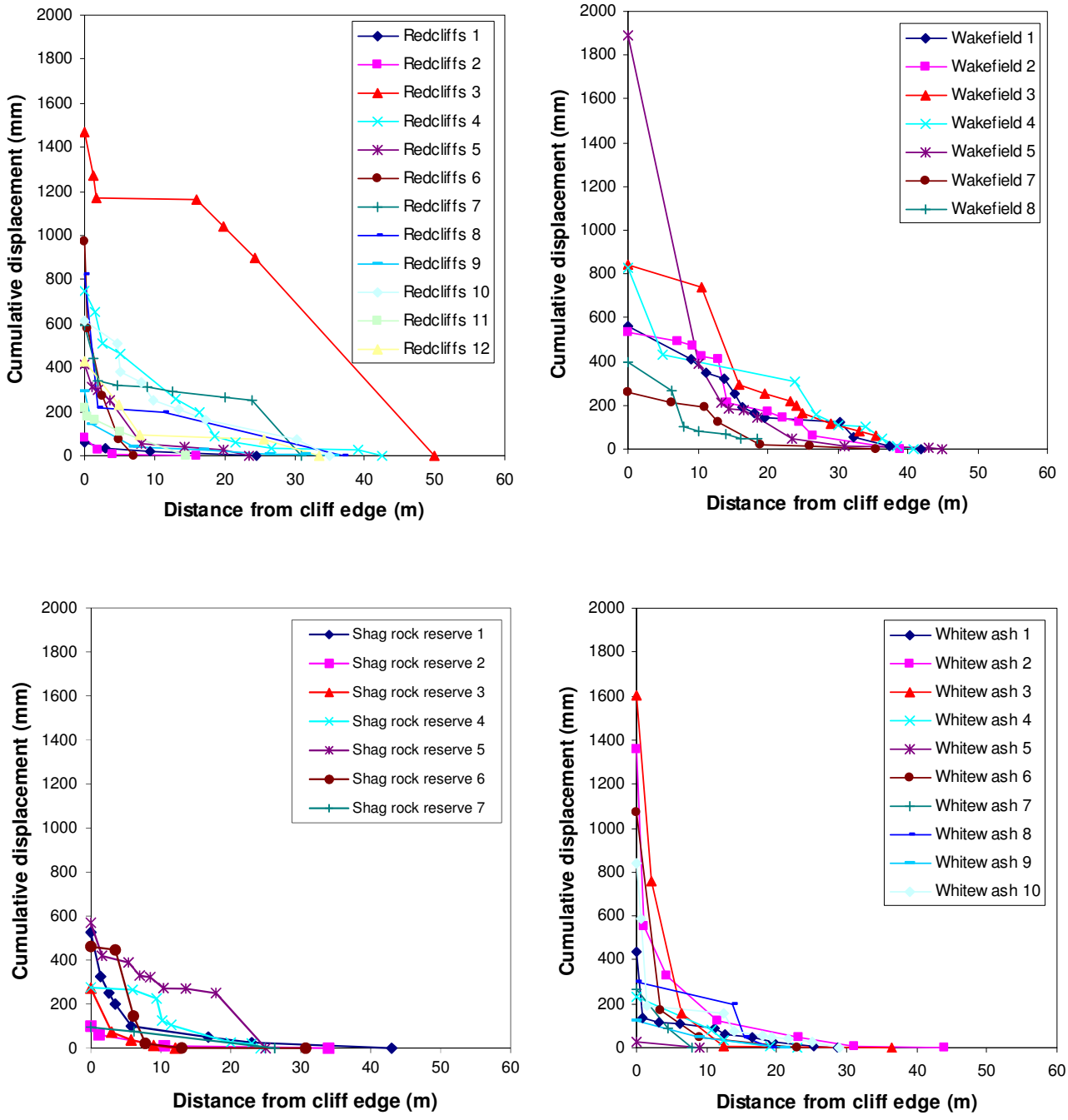

Figure 21 Cumulative horizontal displacements recorded from cracks along transects mapped at the edges of the cliffs in September 2011.

Only transect number 10 at Whitewash Head was predominantly in rock. At this location the extent of cliff top cracking extended much further back from the cliff edge than cracks in

adjacent areas where the rock was deeply mantled by surficial material, indicating displacement of the rock mass may be obscured by the surficial materials. Where possible, the date of the earthquake that generated the cracks was recorded, however in many locations this was unknown.

The change models generated from the terrestrial laser scan surveys also helped to define areas of cliff face that deformed during the earthquakes. These change models show areas of cliff face that had moved towards the scanning instrument's line-of-site (downslope towards the cliff toe), but without the material falling off the cliff face (Appendix C). At Redcliffs and Wakefield Avenue these changes are below areas of cliff top where there are cracks and recroded surface deformation towards the cliff.

4.3.4 Volumes lost from the cliffs

Volumes of material lost from cliffs (Table 11 and Figure 22) were estimated using change models generated from the terrestrial laser scan and LiDAR surveys.

Table 11 Estimated volumes lost from the cliffs calculated from the terrestrial laser scan and LiDAR surveys.

Site	Change model	Volume leaving slope (m^3)*	Area of slope face (m^2)	Volume per unit area (m^3/m^2)	Probable trigger (all earthquakes were in 2011)
Redcliffs	2003 to 2011a	15,065 (±22%)	25,094	0.60	22nd February earthquake
	TLSa to TLSc	2,181 (±3%)	20,506	0.11	16th April earthquake
	TLSc to TLSd	10,336 (±3%)	20,506	0.50	13th June earthquake
	2011a to 2011c	10,182 (±14%)	25,094	0.41	13th June earthquake
Shag Rock Reserve	2003 to 2011a	27,983 (±22%)	20,212	1.39	22nd February earthquake
	TLSa to TLSb	589 (±3%)	15,782	0.04	No obvious trigger
	TLSb to TLSd	35,034 (±3%)	15,782	2.22	13th June earthquake
	2011a to 2011c	34,282 (±14%)	20,212	1.70	13th June earthquake
Nayland Street	2003 to 2011a	1,660 (±22%)	2,881	0.58	22nd February earthquake
	TLSa to TLSc	71 (±3%)	2,413	0.03	16th April earthquake
	TLSc to TLSd	601 (±3%)	2,413	0.25	13th June earthquake
	2011a to 2011c	910 (±14%)	2,881	0.32	13th June earthquake
Wakefield Avenue	2003 to 2011a	7,734	28,192	0.27	22nd February earthquake
	TLSa to TLSc	4,125 (±3%)	22,137	0.19	16th April earthquake
	TLSc to TLSd	11,162 (±3%)	22,137	0.50	13th June earthquake

Site	Change model	Volume leaving slope (m^3)*	Area of slope face (m^2)	Volume per unit area (m^3/m^2)	Probable trigger (all earthquakes were in 2011)
Whitewash Head	2011a to 2011c	6,164 (±14%)	28,192	0.22	13th June earthquake
	2003 to 2011a	42,279 (±14%)	124,484	0.34	22nd February earthquake
	2011a to 2011c	151,379 (±22%)	124,484	1.22	13th June earthquake

*errors expressed as one standard deviation

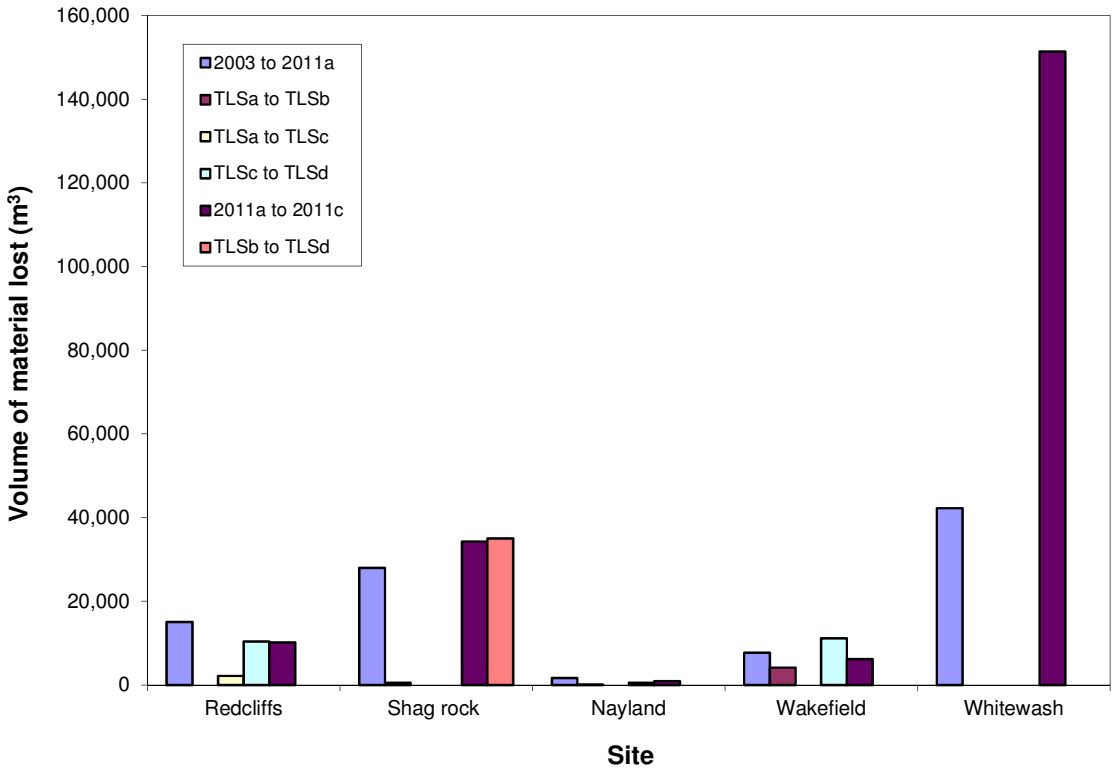

Figure 22 Volumes of material lost from cliffs between listed surveys, using all data.

In most cases, the cliff changes occurred during earthquakes, the exception being at Shag Rock Reserve where 589 m^3 (±3%) of material fell from the cliff between surveys TLSa and TLSb, when no notable earthquakes (>M_W5) occurred within this period. The largest volumes lost were from Whitewash Head. This cliff is the longest and highest of those analysed and its base is being continually eroded by the sea.

The volume, frequency and magnitude of material falling from the cliffs has been assessed from the change models generated from the TLSb to TLSc and TLSc to TLSd surveys (Figure 23). These change models are assumed to represent cliff collapses triggered by the 13th June 2011 earthquake. The different source areas imaged on the slope-face logs were outlined as polygons grouping contiguous areas of negative change. The volume of loss within each polygon was then calculated.

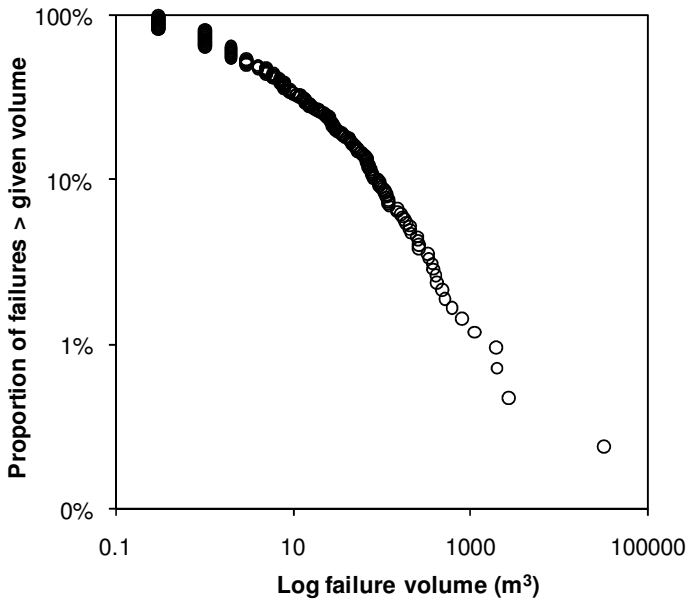

Figure 23 Volume magnitude frequency distribution of material leaving the cliffs between terrestrial laser scan (TLS) surveys. Plot is generated from change models between TLS surveys TLSb to TLSc and TLSc to TLSd, assuming the change to be caused by the 13th June 2011 earthquake.

The cliff gradient, height and in-situ rock strength are thought to be the main factors controlling the seismic response of slopes (e.g., Muhammad et al., 2011). In the main cliff collapse areas (those included in this study) the cliffs have predominantly formed in lava breccia, which is weaker than the basalt lava sequences (Figure 15). Of the sample of cliffs that did not fail during the 2010/2011 Canterbury earthquakes the majority were predominantly formed in basalt lava (with thinner lava breccia units), which is typically stronger than the lava breccia.

Change models generated from the surveys were overlain on the geological face logs to assess the role of geology and slope height (Appendix C) by comparing the volumes of material that were lost from the cliffs and the locations from where material fell. This was done for Redcliffs, Shag Rock Reserve, Nayland Street and Wakefield Avenue. Whitewash Head could not be included, as the data available for this slope are too imprecise.

For each cliff, the proportion of face backed by a given material type was estimated by comparing the geological cliff-face logs with the surveyed cliff face outline (Figure 24). Areas of slope face were calculated from the outlines shown in Appendix C. For each cliff, the volume lost between surveys was estimated for each material type. These data were compared to the area of the cliff formed in the material.

If geology were an important control on the location of cliff collapses, the data would be expected to show bias, where for example a certain material type may have yielded a disproportionately large volume of debris with respect to the area of slope-face formed in it. For example, the proportion of cliff faces (all cliffs) formed in lava breccia is between 40 and 70%, indicating that the majority of the cliffs are formed in this material. Of the total volume of material leaving the cliffs, about 40-70% has fallen from lava breccia sources, indicating that for this material, the volume leaving the cliff is proportional to the area of cliff face formed in it. This is also the case for the other material types (Figure 24), where the ratio between volume of debris, and slope-face area formed in a given geological rock type is

1.06 (±0.07 at one standard deviation), and therefore not significantly different from 1.0. Therefore on a small scale geology does not appear to be an important factor on cliff collapse, but at a larger scale the main cliffs that failed were formed in weaker materials than those that didn't, indicating that geology is an important controlling factor on cliff formation.

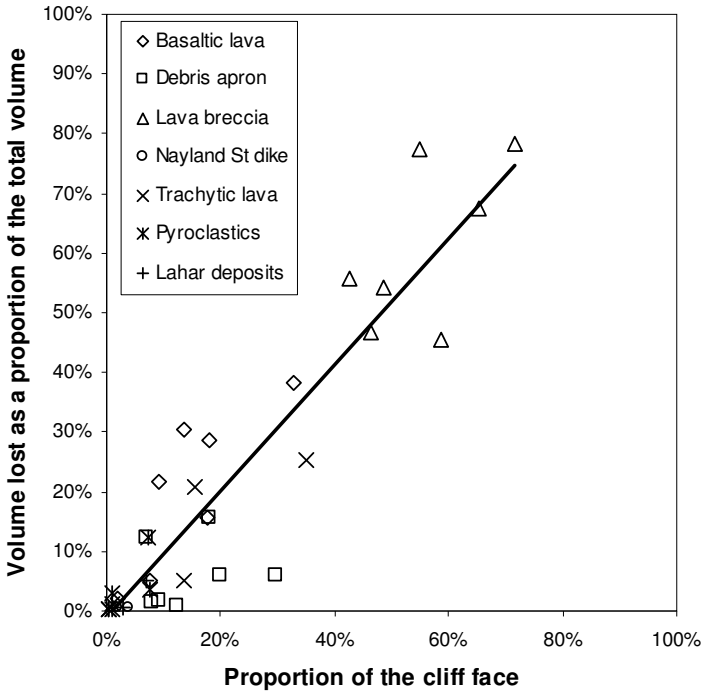

Figure 24 Volume lost, per material type, as a proportion of the total volume (of that material leaving the cliffs) plotted against the proportion of the cliff face formed in that material. Data are for the TLSb to TLSc and TLSc to TLSd change models. Changes are assumed to be due to the 13th June 2011 earthquake. The linear trend line is fitted to all data.

The role of source height on the distribution of rock source volumes from cliffs was assessed by dividing the slope faces (as shown in Appendix C) into 10 m elevation zones, starting from the toe of the slope, and calculating the volume of material leaving each zone. The volume of material lost per unit area of cliff face, per zone was then calculated by dividing the volume lost in each elevation zone by the area of cliff face within that zone (Figure 25).

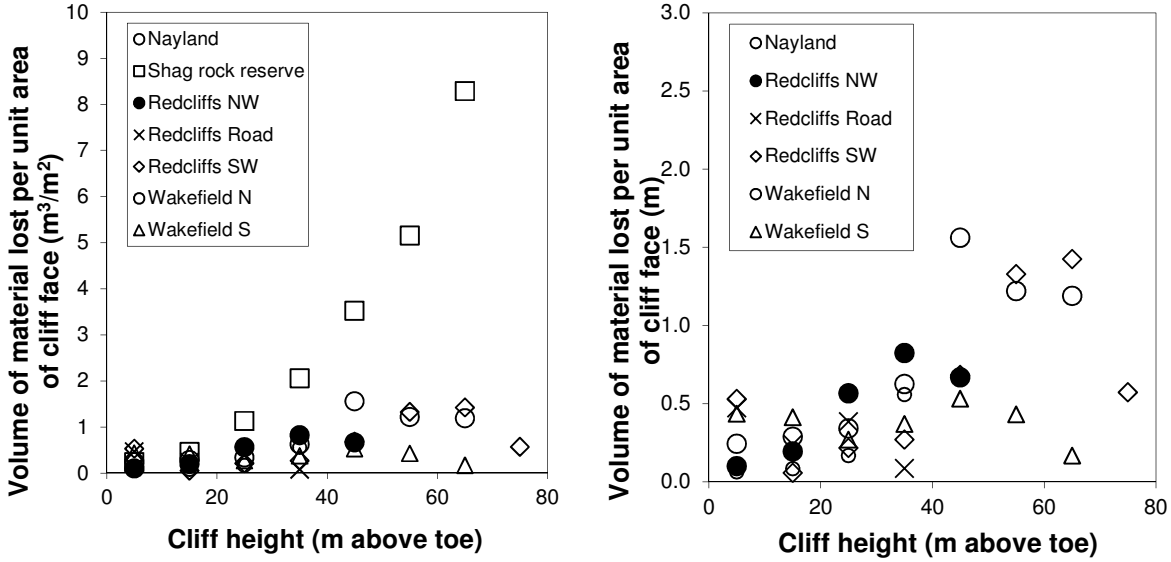

Figure 25 The volume of material leaving each cliff per unit area of cliff face plotted against the source height on the cliff face within 10 m elevation zones. Data are for the TLSb to TLSc and TLSc to TLSd change models. The changes are assumed to be due to the 13th June 2011 earthquakes.

Results show that cliff height appears to be an important control on cliff failure, whereby the areas of cliff typically >20 m in elevation (above the cliff toe) lost more material per unit area than those areas at lower elevations, and that in most cases the volume of material lost per unit area increases with increasing elevation.

4.3.5 Runout of debris avalanches

The runout of the debris avalanches derived from the cliffs has been assessed using the LiDAR survey change models and field mapping of the debris that fell in the earthquakes.

The 2011a to 2011c LiDAR survey change model was used to estimate the volume of material deposited beyond the toe of each cliff, assuming a ±0.5 m neutral zone (a zone where the change is assessed as being error) to take into account positional or measurement errors between the two surveys. Whitewash Head was not included as there debris fell into the sea. The 2011a to 2011c change model was used because it presented the largest measured cliff losses (attributable to the 13th June 2011 earthquakes). The volume of debris deposited at the toe of each cliff is summarised in Table 12. In most cases, the volume deposited is larger than the volume leaving the cliffs, which is a function of the debris bulking (bulking factor of about 20 to 25%) as it breaks into fragments. For Nayland Street, the volume deposited is less than the volume leaving the cliff, this is because much of the debris untypically stayed on the rockslope portion of the cliff.

Table 12 Estimated volume of materials deposited at the toe of the cliffs, using the 2011a to 2011c change model.

Site	Volume deposited (2011a to 2011c change model) (m^3)
Redcliffs	13,677 (±14%)
Shag Rock Reserve	38,607 (±14%)
Nayland Street	419 (±14%)
Wakefield Avenue	7,663 (±14%)

The distribution of debris fallen from the cliffs was assessed by calculating the volume of debris deposited in 10 m wide zones extending from the toe of the rock slope portion of the cliffs (Figure 26). These data show that the debris from Shag Rock Reserve travelled the furthest from the cliff toe. Shag Rock Reserve also had the largest volume of material deposited.

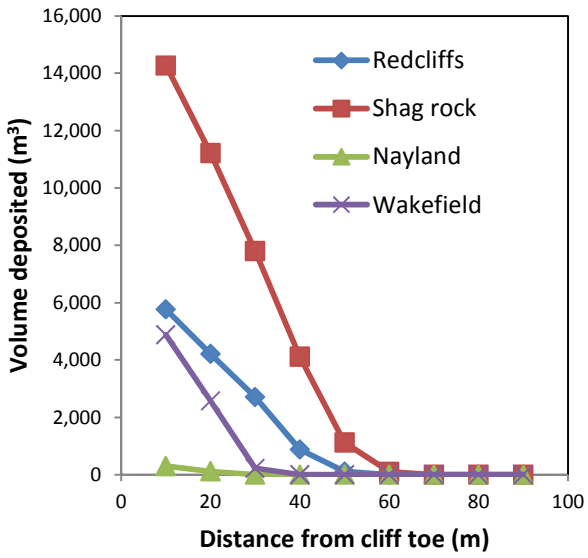

Figure 26 Distribution of deposited debris volume with distance from the toe of the rock slope portion of the cliff. Volumes were calculated from the 2011a to 2011c LiDAR survey change model.

Polygons were drawn around the main areas of cliff that failed (based on the cliff top recession and volume-change models, 2003 to 2011a and 2011a to 2011c). It was assumed that the 2003 to 2011a models present changes caused by the 22nd February 2011 earthquakes and the 2011a to 2011c models present changes caused by the 13th June earthquakes. The polygons show the main source areas for the failures. Section lines were drawn though each of these source areas and the following information was recorded along each section:

1. Elevation of the source area crown – In all cases this was the top of the cliff as determined in the cliff edge analysis. For 22nd February 2011 failures, the 2003 cliff edge was used, and for the 13th June 2011 failures the 2011a cliff edge was used.

2. Elevation of, and distance from the crown (cliff edge) to:

    a. the toe of the rockslope portion of the cliff;

    b. the outer limit of talus delimited by the downslope limit of the area covered by debris from the cliffs, where the original ground surface cannot be seen through it (this was easily identified in the LiDAR survey change models and easily verified in the field);

    c. the outer limit of boulder rolls – delimited by individual boulders that had been either thrown out beyond the debris as it fell, or that fell from the cliff and rolled down the talus onto the original ground surface beyond the limit of continuous debris (this was mapped in the field because the resolution of the LiDAR survey change models was not sufficient to identify isolated small boulders);

    d. the outer limit of fly rock – fly rocks are shards of broken rock released as high-velocity projectiles, created by impacts between boulders and other hard objects. Fly rocks have only been mapped in the field using evidence of their impact marks. Volumes of fly rock shards were not possible to estimate as the dataset was incomplete (e.g., many were inside houses and buildings and could not be mapped).

The relationship between source volume (of the main failures) and runout (along the section lines) was assessed (e.g. Corominas, 1996) for each of the main cliff collapse source areas triggered during the 22nd February and 13th June 2011 earthquakes. However, no such relationship could be established, possibly because the debris was essentially dry or the volumes of failed material too small.

The runout of debris triggered by the 22nd February and 13th June 2011 earthquakes were assessed using the empirical Fahrboeschung model, based on a relationship between topographical factors and the lengths of runout of the debris (Dorren, 2003). These models are sometimes referred to as statistical models (Keylock and Domaas, 1999).

The Fahrboeschung[4] (often referred to as the “travel angle”) method (Keylock and Domaas, 1999), uses the slope of a straight line between the top of the source area (the crown) and the furthest point of travel of: 1) talus; 2) boulders; and 3) fly rock (Figures 27 and 28). For the analysis presented here, the starting point of the failure is assumed to be the cliff top edge (the source area crown).

[4] Fahrboeschung is a German word meaning ”travel angle” adopted in 1884 by a pioneer in landslide runout studies, Albert Heim. It is still used in its original definition.

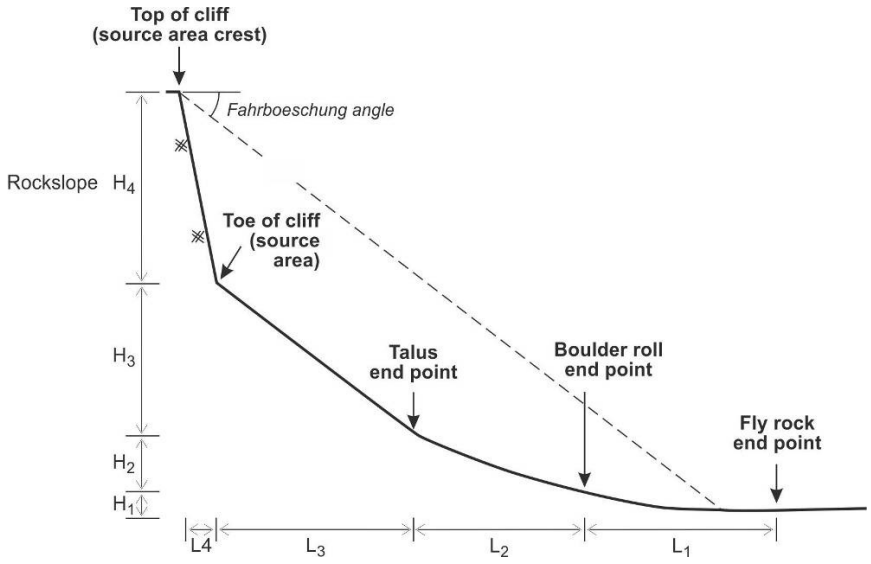

Figure 27 Schematic diagram illustrating the terrain parameters used in this study to assess the runout of debris avalanches. The section is shown in map view in Figure 28.

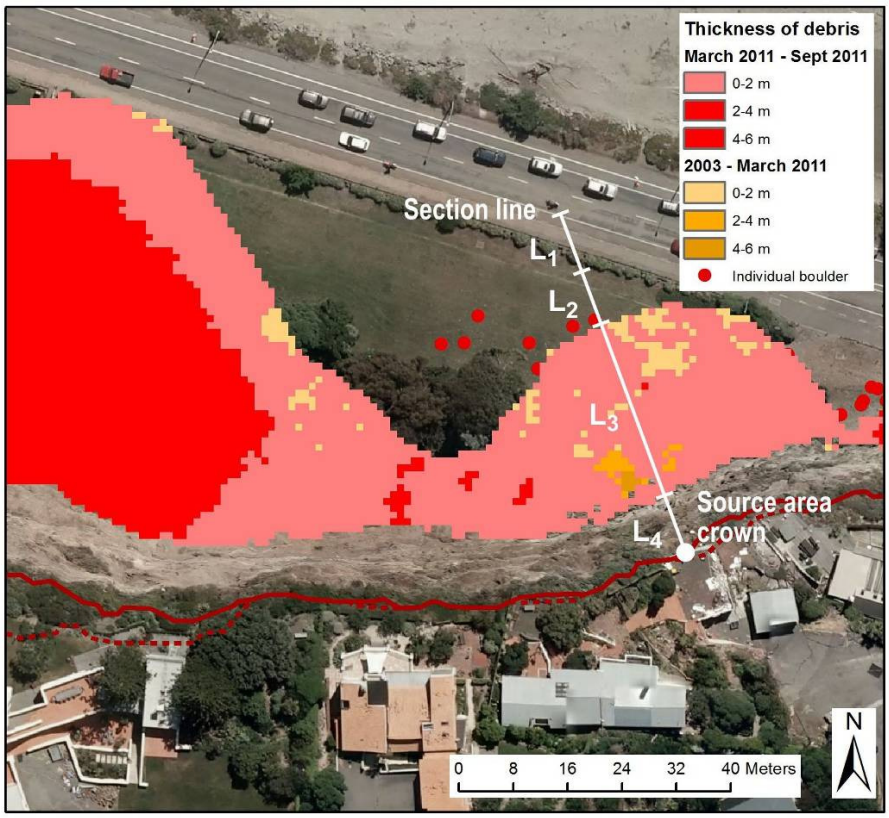

Figure 28 Example of the parameters used in this study in assessing expected debris runout. Refer to Figure 27. The red solid line represents the cliff edge from the 2003 LiDAR survey, and the red dashed line the position of the cliff edge from the 2011c LiDAR survey.

The Fahrboeschung models performed well statistically (Table 13) indicating a good relationship between the height of a cliff and runout of debris falling from it. Note that the debris derived from these cliffs is predominantly unconfined by topography below the source area, indicating no channelling effects. Channelling by topography (e.g., along gullies) can cause debris to travel further.

Table 13 Statistical results from the Fahrboeschung model

Assumed date of rockfalls	Type	Gradient (ratio of slope height to runout length in metres)[1]	Error on the gradient[2]	Number of sections analysed
22nd February 2011	Debris avalanche	0.92	±0.07	30
22nd February 2011	Boulder roll	0.81	±0.07	30
13th June 2011	Debris avalanche	0.74	±0.16	19
13th June 2011	Boulder roll	0.66	±0.19	18

[1]Calculated using the least-squares method
[2]Standard error on the gradient

Data from cliff collapses initiated by the 22nd February and 13th June 2011 earthquakes were compiled and the Fahrboeschung angles were determined for talus, boulder roll and fly rock (Table 14).

Table 14 Summary of Fahrboeschung angles for talus, boulder roll and fly rock for collapses triggered in the 22nd February and 13th June 2011 earthquakes.

	Debris avalanche angle (°)	Boulder roll angle (°)	Fly rock angle (°)
Mean	47	41	41
Minimum	33	33	31
Standard deviation	±6.6	±6.0	±6.4
Standard deviation (±) of mean	±0.9	±0.8	±1.6
95% confidence limit	±1.7	±1.6	±2.9
95% limit	46	40	38
Degrees of freedom	49	48	17

The risk to an individual at a particular location from debris avalanches is not only from boulders stopping at that location, but also from those passing the location to stop further down slope (Evans and Hungr, 1993). The volume of debris reaching or passing a given distance on a slope within a runout zone was estimated for each cliff using the 22nd February and 13th June 2011 cliff collapses. Fahrboeschung angles were used to provide a consistent measure of map distance out from the cliff edges, while talking into account the height of the cliff as a runout-controlling factor. The volume of material from these events passing a given Fahrboeschung was then estimated per site (Figure 29), with the results expressed as the proportion of the total debris (both events) passing a given Fahrboeschung (Table 15 and Figure 30). Volumes were estimated using the 2003 to 2011a and 2011a to 2011c LiDAR survey change models, and data from the field mapping of individual boulders. To individual boulders, an average boulder volume of 1 m^3 was assigned. Ten degree Fahrboeschung

angle divisions were generally used, however, the 30° to 40° zone was further subdivided into 3° subdivisions to give a finer resolution in this distal part of the runout zone. One degree subdivisions were initially assessed but not used as their resolution was too high with respect to the area occupied by the dwellings.

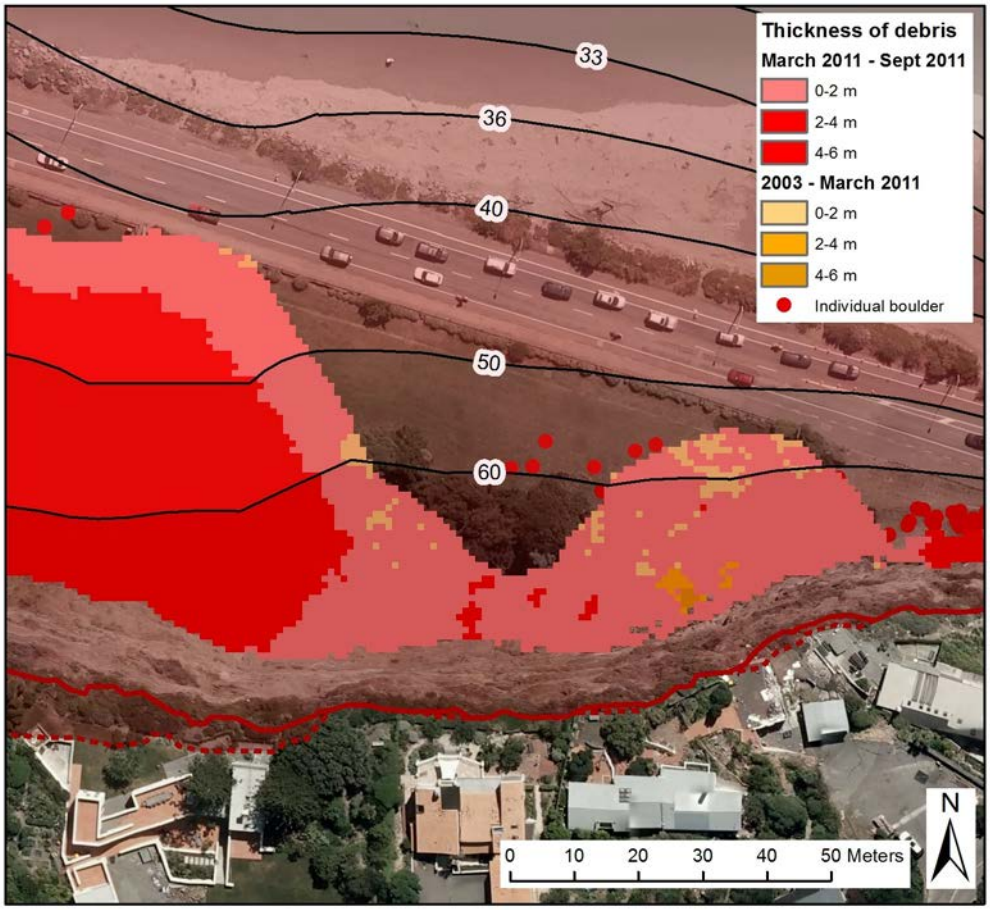

Figure 29 Illustrative map (Shag Rock Reserve) showing the debris deposited by cliff collapses triggered by the 22nd February and 13th June 2011 earthquakes, relative to various Fahrboeschung angles (black lines with numbers representing the angle in degrees) projected from the cliff top obtained from the 2011c LiDAR survey. The red solid line represents the cliff edge from the 2003 LiDAR survey, and the red dashed line the position of the cliff edge from the 2011c LiDAR survey.

Table 15 Proportion of debris passing a given Fahrboeschung angle at named sites.

Site	Proportion of debris passing a given Fahrboeschung angle*						
	20°	30°	33°	36°	40°	50°	60°
Redcliffs	0	0	0	0.0003	0.002	0.16	0.80
Shag Rock Reserve	0	0	0	0.00004	0.0001	0.07	0.47
Nayland St	0	0	0	0	0.02	0.04	0.08
Wakefield Ave	0	0	0	0.002	0.008	0.19	0.40
Whitewash Head	N/A – Debris travelled into the sea						

*Excludes fly rock because it was not possible to estimate the volumes of fly rock as the dataset was incomplete (e.g., many were inside houses and buildings and could not be mapped).

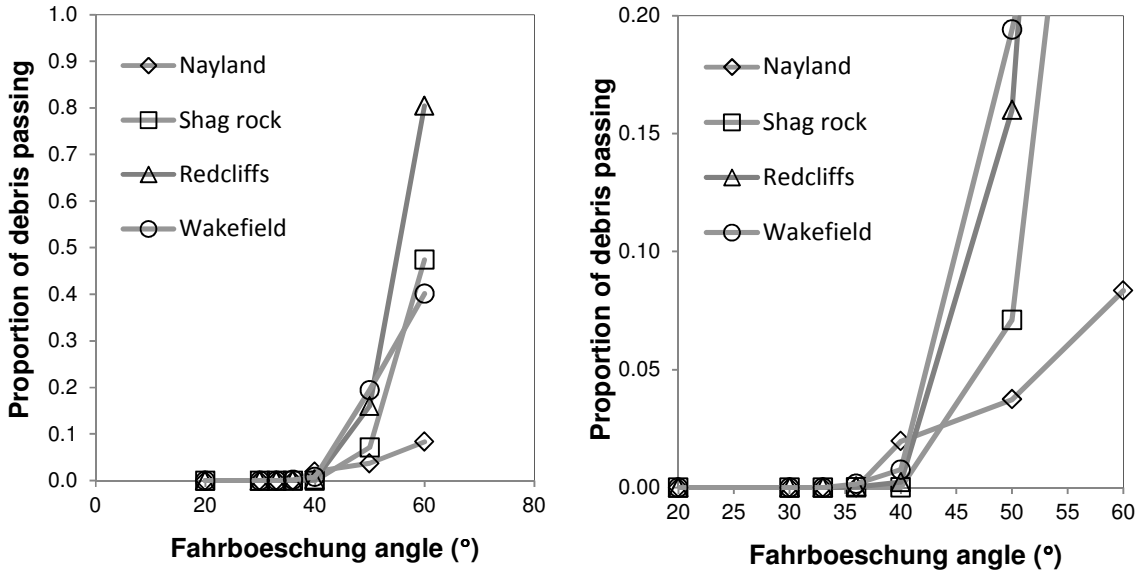

Figure 30 Proportion of debris passing a given Fahrboeschung angle per site. Calculated as the proportion of the total volume of debris passing each zone, combining the debris from collapses triggered by the 22nd February and 13th June 2011 earthquake events, and using both the aerial survey and field mapped data.

The proportions of debris passing given Fahrboeschung angles at Redcliffs and Wakefield Avenue are similar, while those at Shag Rock Reserve are lower. The cliff at Nayland Street cannot be compared as it is low in comparison to the other cliffs. However the data for Nayland Street shows that the majority of the recent debris avalanche deposits did not make it past the toe of the pre-existing talus at the bottom of the cliff. The cliffs at Redcliffs and Wakefield Avenue had substantial pre-existing talus deposits at their bases, while only minor amounts of pre-existing talus were present at the toe of the cliff at Shag Rock Reserve. Therefore the presence of talus at the base of cliffs appears to increase the runout distance of debris avalanches.

4.3.6 Other cliffs in the area

Other former sea cliffs (outside of the pilot-study areas) in the northern Port Hills (Appendix A) were identified and assessed as to whether they had failed or not failed during the 2010/2011 Canterbury earthquakes. These cliffs were identified with a numerical Geographic Information System slope-angle function using the 2011a LiDAR survey digital elevation model. Slopes (cliffs) with 1-m grids (pixels) steeper than 35° were identified and sections were drawn at locations that characterised these slopes. Along each section the height and length of the rocky portion of the slope were measured. The slope was classified as having not failed if no evidence of multiple boulders could be observed as falling from it. This was undertaken using the post-22nd February 2011 orthophotographs with field checking. In many locations it was found that these slopes had shed only a few localised boulders. The slope was removed from the analysis where evidence of more than a few rockfalls was found; in these instances the slope was assessed as having failed. The data are plotted in Figure 31, along with data from those slopes which did fail (Appendix A), using only measurements from the rocky portion of the slope.

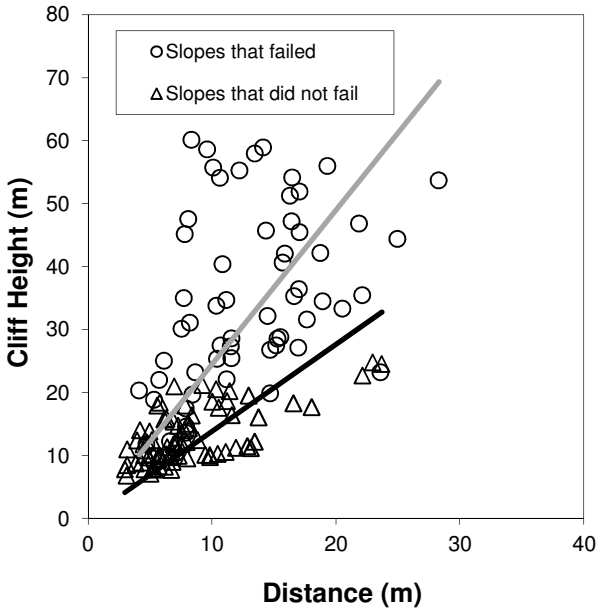

Figure 31 Geometrical relationships between those slopes that did fail and those that did not fail during the 2011 earthquakes. Slopes that did fail are from the slope sections discussed in Section 4.3.5 (n = 48) and the slopes that did not fail are from measurements of slopes in the same area of the Port Hills (n = 72). Linear trend lines are fitted to the data, the grey line represents slopes that failed and the black line slopes that did not fail.

The results show that: 1) the geology of the slope; 2) height of the slope; and 3) angle of the slope appears to control whether or not a given slope failed during the 2010/2011 Canterbury earthquakes. There does not appear to be any correlation between slope orientation and the location of the earthquake epicentres. The majority of slopes that produced no multiple rockfalls were typically less than 20 m in height and at mean angles of 58° (±9 at one standard deviation). By comparison, those that were assessed as failing (multiple boulders) were typically greater than 20 m high and standing at mean angles of 68° (±8), indicating they were slightly steeper.

4.4 Historical and pre-historical cliff collapse rate

Historical and pre-historical talus, formed of rockfall deposits from the collapse of cliffs, has accumulated on top of ancient former beaches at Redcliffs and Wakefield Avenue. Using the 2003 LiDAR survey digital elevation model of these slopes, and by projecting the rockslope face at the toe of the slope through the talus to intersect an assumed pre-talus ground surface, it was possible to estimate likely volumes of talus present before the 2010/2011 Canterbury earthquakes. At Redcliffs, about 66,000 m^3 of talus mixed with an unknown proportion of dune sand had accumulated at the toe of the slope prior to 4th September 2010, and at Wakefield Avenue, about 55,000 m^3 had accumulated. The age of the coastal beach surfaces on which this material was deposited is about 3,500 to 3,700 calibrated radiocarbon years (McFadgen and Goff, 2005), indicating accumulation rates averaging 15 to 20 m^3/year. If it is assumed that dune sand is only filling interstices between fallen boulders, the proportion of dune sand may be ignored.

These accumulation rates would suggest that the annual volumes of material leaving the cliffs, assuming a 20% bulking factor from source to debris would be about 16 and 12 m^3/year at Redcliffs and Wakefield Avenue respectively. Therefore the cliff top recession

rate at Redcliffs would be about 0.6 m per 1000 years (assuming a slope face area of 25,094 m^2) and at Wakefield about 0.4 m per 1000 years (assuming a slope face area of 28,192 m^2). However, the majority of cliff top recession occurs during discrete events, as shown by the 2010/2011 Canterbury earthquakes. It is therefore possible that the pre-2003 talus accumulated in response to past earthquakes.

Other earthquake-triggered cliff collapses have been recorded in the Port Hills. On 1st September 1888, an earthquake with an estimated magnitude of 7.0–7.3 struck the Amuri district of North Canterbury, about 100 km northwest of Christchurch (Cowan, 1991). The shaking lasted 40-50 seconds in Christchurch and Lyttelton, and was followed by several aftershocks (McSaveney, 2009). Damage occurred to several buildings in Christchurch (most notably the Christ Church Cathedral, which lost its spire), with more damage in the northern and north-western suburbs, probably due to the peaty subsoils underlying the buildings there (McSaveney, 2009). Cliff collapses appear to have occurred near Lyttelton, with The Press (Volume XLV, Issue 7143, 3 September 1888) reporting: "*About a quarter of a mile from Lyttelton, on the Sumner road, a few boulders, weighing about ten tons each, were shaken from the land on the high side of the road. They bounded with great speed into the harbor, and carried fences and everything before them."* The earthquake also caused landslides in loose sediment, and fissures up to 30 cm wide appeared along terraces of the Percival River and in the Hanmer Plains (McSaveney, 2009). A rockfall/cliff collapse was also reported as being triggered by the 3rd September 1877 earthquake near Lake Ellesmere. The rockfall/cliff collapse occurred somewhere on the Pilot station in Lyttelton Harbour and involved several tons of loose rock that fell into the sea (Star Newspaper, Issue 712, 3rd September 1870, page 2).

4.5 Cliff collapse mechanisms

Three possible failure mechanisms have been identified to account for the observed responses of cliffs in the 2010/2011 Canterbury earthquakes. These are:

1. Debris avalanche – falls of individual or many tens of thousands of rocks from the face of the cliffs;

2. Surficial cracking – of covering materials mantling the bedrock above the cliff edge (e.g., loess and fill); and

3. Rockslope deformation – structurally controlled displacement and/or deformation of weaker materials forming the slope

The majority of the assessment has been to characterise the material that fell from the cliffs in response to the 2010/2011 Canterbury earthquakes. These have primarily comprised the falling of rock from the cliffs. In areas where basalt and trachytic lavas are present, failure of the fallen blocks tend to have been kinematically controlled by discontinuities within the rock mass or by the boundaries between contrasting materials. However, the spacing and persistence of these predominantly cooling joints are almost random (M. Brideau, personal communication 2011) and the terrestrial laser scan survey change models suggest that the distribution of debris falling from these materials is also random. For material falling from the lava breccia there is little kinematic control, as the material tends to be massive, with few, very widely spaced discontinuities present. However, at the northern end of Wakefield Avenue, localised kinematically-controlled failure occurred, which was controlled by the

"Nayland Street dyke"; therefore kinematically-controlled failures do occur, but they tend to be local and isolated. The failures appear to be breaking out on defects and especially at boundaries between materials with very different seismic parameters, e.g., basalt versus pyroclastics (Figures 32 and 33). However, due to the heterogenic nature of the rock masses, there are so many lithological and other defects present that the failures can effectively occur on any boundary.

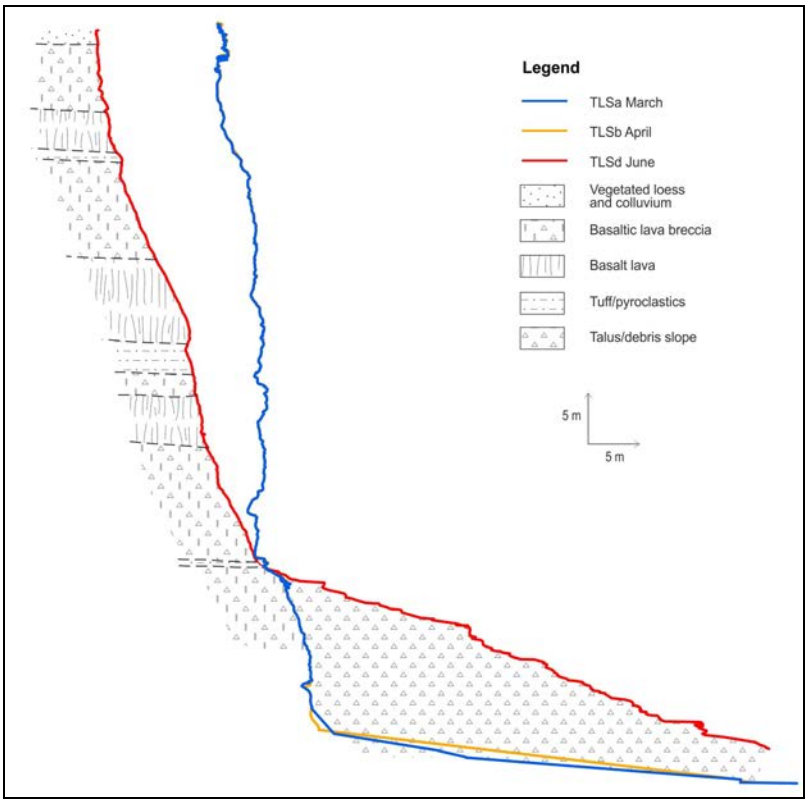

Figure 32 Shag Rock Reserve section (located at chainage 180 m on maps in Appendix B). The blue profile represents the slope face generated from the TLSa survey, the yellow profile from TLSb and the red profile from TLSd.

The main factors controlling the susceptibility of the cliffs to earthquake-generated failures are assessed as: 1) the height of the cliff, where cliffs higher than 20 m are more susceptible to failure; 2) the angle of the cliff, where cliffs steeper than 58° are more susceptible to failure; and 3) amplified peak ground motions, which can result from near-surface impedance contrasts due to variations in material properties (e.g., a highly fractured basalt overlying lava breccia). In addition, focussing of seismic waves by surface topography may result in topographic amplification, as occurred in the 2010 Haiti earthquake (Hough et al., 2010). However, it should also be noted that some cliffs >30 m in height at angles of >60° did not fail in the 2010/2011 Canterbury earthquakes, i.e., they did not produce debris avalanches although localised boulders did fall from them.

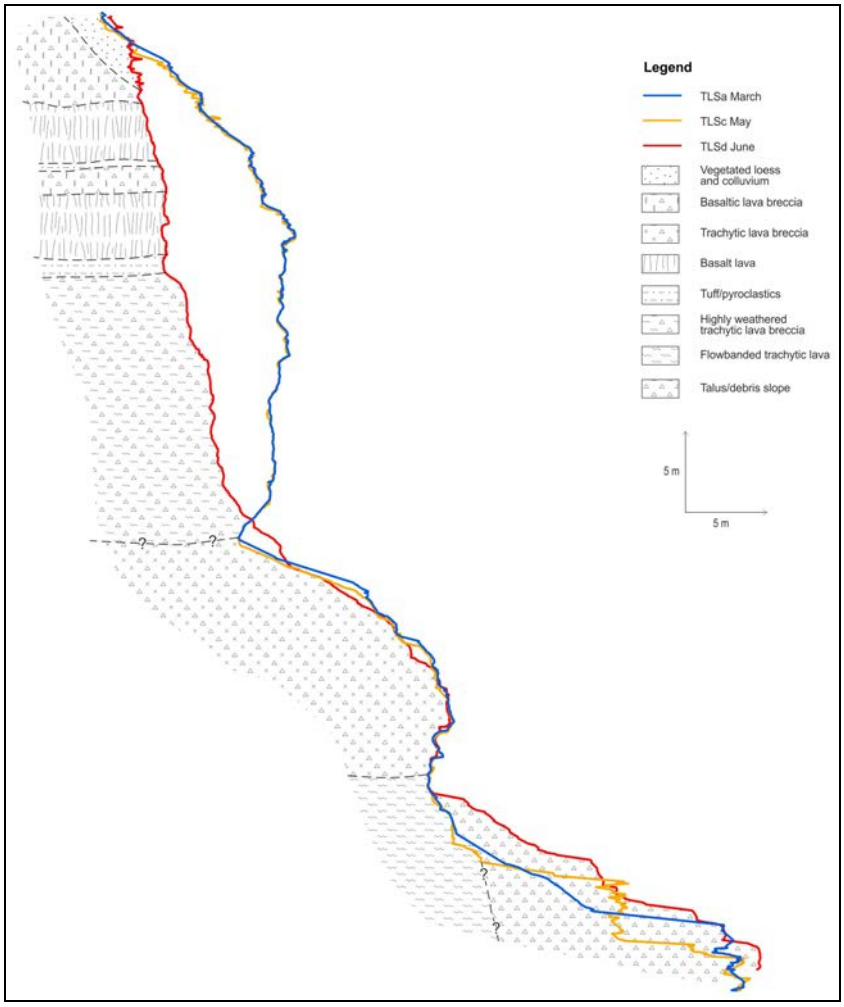

Figure 33 Wakefield Avenue section (located at chainage 100 m on map shown in Appendix B). The blue profile represents the slope face generated from the TLSa survey, the yellow profile from TLSc and the red profile from TLSd.

The rockslope deformation failure mechanism is harder to characterise because it is internal. Evidence from the field suggests there are three types of cracks at the cliff edge: 1) surficial cracking in the loess, fill, road and curb edges and around retaining walls; 2) cracking around house foundations caused by the movement of the house in response to the earthquakes; and 3) cracks relating to displacement and deformation of the underlying rock mass, which could be related to sliding, e.g., formation of a failure mechanism giving rise to the development of possible rockslides, or to general deformation of the cliff with no obvious developing failure mechanism.

Cracks associated with displacement and deformation of the rock mass are believed to have displayed the largest horizontal and vertical displacements, as well as being the most laterally persistent of the cracks recorded. At Wakefield Avenue, cracks along Richmond Hill Road on the opposite side of the hill crest indicate displacement towards Wakefield Avenue, which is in the opposite direction to the local dip of the slope. This indicates that they probably relate to deformation of the underlying rock mass (Figure 17). At Redcliffs, the cracking in the area near the end of Glendevere Road and at the end of Balmoral Lane indicate cliff top displacements of 0.7 m to more than 1.0 m towards the cliff edges. The crack frequency, persistence and distance back from the cliff edge indicate a larger contiguous area of displacement than those areas elsewhere along the cliff top (Figure 16).

At Redcliffs and Wakefield Avenue the areas of more pronounced cliff top displacement correspond to areas of cliff face deformation recognised in the terrestrial laser scan survey change models as areas of positive changes, indicating outward displacement of the face. These areas also coincide with significant cliff face cracks. At Wakefield Avenue, several pre-earthquake (pre-4th September 2010) landslide scarp features were identified with corresponding debris piles. These appeared to have fallen primarily from the trachytic lava breccia. Abundant slickensides were found among the debris from the recent failures within this material and the terrestrial laser scan survey change models show that this material has displaced (but not detached) outwards from the slope. These data indicate that the upper part of the rockslope is deforming and this could be the mechanism by which the cracks in Richmond Hill Road have formed.

Although these locations can be described as areas of cliff deformation, it is not yet known whether the displacements are associated with formation of a failure surface along which sliding could occur or whether the displacements relate to distributed deformation within a larger portion of the rock mass. At present no obvious slide surface can be seen day lighting in the cliff face. Therefor it is not possible to assess, with any certainty, the annual individual fatality risk these features might pose.

Trial pits have been excavated by Tonkin and Taylor Ltd. to inspect some of the cracks. However, in many instances the pits failed to reach bedrock underlying the surficial materials, and therefore the results are inconclusive. Further subsurface investigations, such as cored boreholes and in situ inclinometer and groundwater monitoring are required to assess the likely crack formation mechanisms at the cliff tops.

At Shag Rock Reserve, a large landslide (the Clifton Terrace Landslide) has developed on the eastern flank of the cliff. This landslide displaces parts of Kinsey Terrace and Clifton Hill Road. Although the landslide does not yet appear to daylight in the cliff face, its northern flank is very close to the current edge of the cliff top. The landslide has been investigated by Tonkin and Taylor Ltd. on behalf of the Earthquake Commission and by the Port Hills Geotechnical Group and GNS Science. At present there is insufficient information to determine whether the landslide is a shallow failure confined to the loess cover, or a deeper, structurally controlled failure within the underlying rock mass akin to the deformation above Wakefield Avenue, or a combination of both.

On the western flank of Shag Rock Reserve a landslide (the Dean's Head Landslide) has developed in what appears to be loess. The movement appears to be confined predominantly within the loess cover, which is quite thick (>10 m in parts), although some parts appear to be related to movement within the underlying rock, especially near the edge of the cliff above Main Road. There are also a few older and now vacated landslide scarps (i.e., the debris has now gone) visible on the flanks of this area, suggesting that the landslide material could be quite mobile, especially during heavy or prolonged rainfall.

Further investigation and ongoing monitoring of these landslides and areas of cliff deformation will be needed in order to analyse their likely failure mechanisms and therefore assess whether they pose a risk to life.

5.0 CLIFF COLLAPSE TRIGGERING MECHANISMS

In the literature, a wide range of rockfall (both individual boulders and debris avalanches) trigger mechanisms and conditions have been described. These trigger mechanisms can be divided into initiation factors (i.e., factors that prepare the slope for failure) and triggering events. However, in reality it is difficult to make a distinction between the two, since often one process both promotes weathering and causes failure, e.g., frost shattering (Dorren, 2003).

Events that trigger rockfalls are typically, in no particular order: 1) rainfall; 2) earthquake-induced peak ground accelerations; 3) frost shattering; 4) anthropogenic activities, e.g., modification of slopes; 5) activity of animals; 6) vegetation changes; and 7) time, i.e., no obvious trigger. In a review, Dorren (2003) found that various factors are often reported as triggers of rockfall but, in most cases, a combination of topographical, geological and climatological factors and time determine whether a rockfall occurs.

5.1 Earthquake triggers

Kanari (2008) reports that a sequence of earthquakes is required to trigger rockfalls and debris avalanches, rather than an isolated earthquake, suggesting that it takes time for rock masses to become ready or “ripe” for failure. Kanari (2008) suggests that strong peak ground acceleration is not the only variable in triggering, but a certain stage of maturity of fracture weakening (and/or deformation) of the rock mass must be reached. Analysis of the 1987 South California earthquakes (Harp and Wilson, 1995) indicates two shaking velocity thresholds for the limits of rockfalls and slides (debris avalanches). The sites with the lower velocity thresholds were those with large-aperture (wide open) fractures and loose rock (as could be caused by repeated earthquake shaking) and were therefore easier to dislodge at lower accelerations. Conversely earthquakes may remove those rocks more susceptible to failure, but in turn may reduce the stability of other rocks (through earthquake-induced fracture weakening and deformation of the rock mass), making them susceptible to failure during a subsequent earthquake. In the Port Hills the frequency (number) and magnitude (volume) of cliff collapses triggered during the 2010/2011 Canterbury earthquakes appears to be a function of the peak ground acceleration. However, at higher peak ground accelerations the number and magnitude of cliff collapses does vary. This may be due to localised conditions giving rise to topographic amplification. Studies reported by Harp and Jibson (2002), and Sepulveda et al. (2005) have shown that higher concentrations of rockfalls occur in areas where shaking is amplified by local topography, complicating the relationship between measured ground accelerations and the volumes of rock produced.

In this study, peak ground acceleration has been used to characterise ground shaking, as it is assumed cliff collapses require an instantaneous force exceeding a critical value to trigger them, rather than the multiple accelerations associated with longer duration shaking. Observations on the ground suggest many boulders and large plant pots were thrown upwards and outwards in a single motion, as no evidence of “scuff” marks were apparent around such displaced objects. An additional reason for using the measured peak ground acceleration value at a fixed instrumental site is that that value is used only to estimate the probability of occurrence of the earthquake trigger; it is not used in any dynamic analysis of cliff collapse triggering.

Earthquake magnitude and distance relationships have been developed for landslides and rockfalls. Wieczorek and Jager (1996) use the procedure of Keefer (1984), who developed curves representing the upper bound of the maximum distance from an earthquake epicentre for different types of landslides, to assess historical global earthquakes of different magnitudes. These relationships were summarised by Hancox et al. (2002) (Figure 34), who also assessed the relationship of the area affected by landslides during historical New Zealand earthquakes. The distribution of mapped rockfalls and cliff collapses for the five main 2010/2011 Canterbury earthquakes have been added to this dataset in Figure 34. The new Canterbury data plot below equivalent data from international events, but are consistent with the relationship reported by Hancox et al. (2002). Much of the scatter is believed to reflect the different depths of earthquakes, which is not taken into account, along with changes in geology, and slope angle of the sources. The main reason why the New Zealand data plot below the international data is because of topographic constraints. Much of the area affected by the strong ground shaking in the 2010/2011 Canterbury earthquakes was flat land and sea, where rockfalls or landslides do not occur.

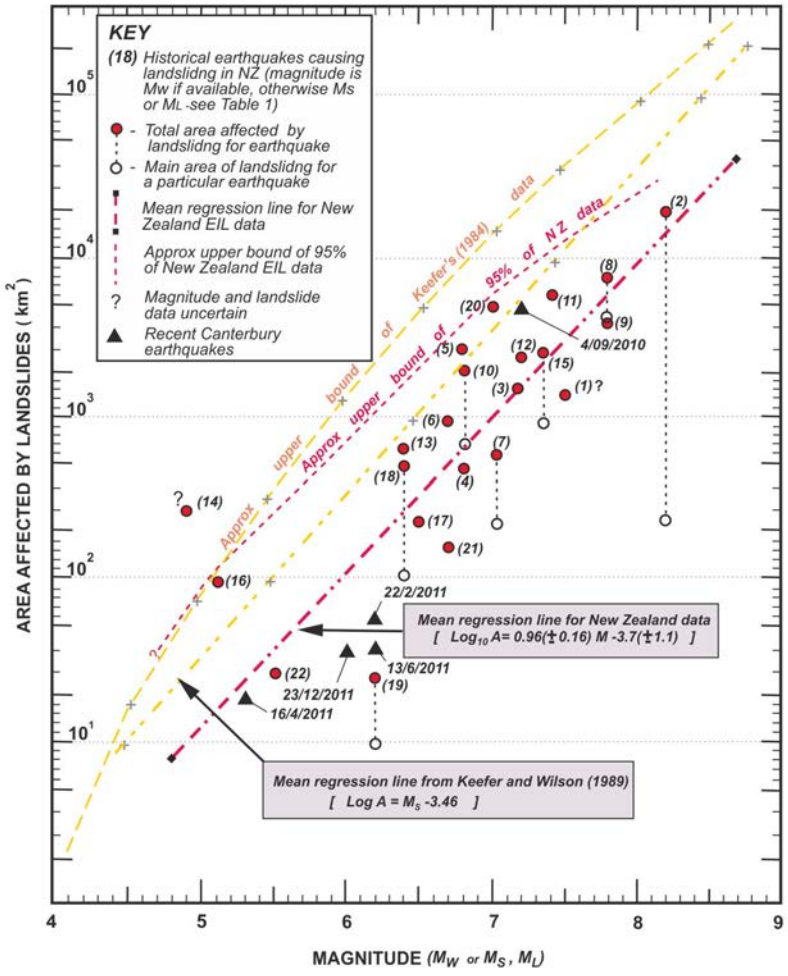

Figure 34 Relationship of the area affected by landslides during historical earthquakes of different magnitude in New Zealand and worldwide. The black triangles represent the main areas affected by the 2010/2011 Canterbury earthquakes. Modified from Hancox et al. (2002).

5.1.1 Estimating earthquake-trigger frequency

The volume of material leaving the cliffs, mostly in the 22nd February and 13th June 2011 earthquakes, and the peak ground accelerations that triggered them have been used to assess the probability ($P_{(H:PGA)}$) of collapse given a range of peak ground acceleration values. The overall spectrum of earthquakes has been divided into four peak ground acceleration bands that provide an integrated assessment across all earthquakes likely to trigger collapse (Table 16). The average consequences of the representative event in each band were then estimated in terms of the volume produced or area of cliff top lost due to recession.

Table 16 Likely cliff collapses and the volumes of material leaving the cliffs in the Port Hills at different bands of peak ground acceleration (PGA), determined using the 2010/2011 Canterbury earthquakes. Volumes are estimated from terrestrial laser scan and LiDAR surveys carried out between earthquakes.

PGA band (g)	Description of the frequency (number) and magnitude (size) of cliff collapses in the Port Hills
0.1 - 0.4	The number of cliff collapses tend to be minimal and isolated within this range of peak ground accelerations and their volumes are relatively small, e.g., 1 to 10 m^3. Many earthquakes have been recorded in the Port Hills at this range, with only minor cliff collapses reported.
0.4 – 1.0	Cliff collapses occur at this range but they tend to be isolated, with volumes of around 10 to 1,000 m^3. This is the PGA range of the earthquakes on 16th April 2011 (PGA's at the upper end of the band) and 23rd December 2011 (PGA's at the lower end of the band).
1.0 – 2.0	Cliff collapses are widespread, with volumes of about 10,000 to 100,000 m^3. This is the peak ground acceleration range of the 22nd February and 13th June 2011 earthquakes.
2.0 – 5.0	Expected to trigger more cliff collapses of larger volume than those triggered by the 22nd February and 13th June 2011 events.

The frequency of a given peak ground acceleration band occurring is based on the national seismic hazard model. In general, the hazard calculations within this model are based on time-independent (Poissonian) earthquake probabilities, which is standard practice for probabilistic hazard analysis for engineering design applications (G. McVerry, personal communication 2011). Time-independent earthquake probabilities are based on the average rate of occurrence of earthquakes on a source, but do not take account of the elapsed time since the last event or enhanced activity associated with earthquake sequences following major events. As a result of the 4th September 2010 Darfield Earthquake and its associated aftershocks, the current level of seismic activity in the Christchurch region is considerably higher than the long-term average, and is likely to remain enhanced for several decades (Webb et al., 2011). Given this current enhancement of seismicity, it is necessary to develop earthquake probabilities that vary over time to represent the on-going earthquake sequence in the region.

This increased level of seismicity has been quantified using a modified form of the 2010 version of the national seismic hazard model (Stirling et al., in press), which incorporates the now-increased probabilities for major faults in the region (Gerstenberger, 2011). This is hereafter referred to as the composite seismic hazard model and is the same model used in the liquefaction susceptibility assessments for Christchurch (Webb et al., 2011;

Gerstenberger, 2011).

The time-varying nature of the hazard has been accommodated by estimating, for each location on a geographical grid, the earthquakes expected in a series of 0.2 magnitude intervals over each of the next 50 years, and then finding the average rates over the 50-year period. As the model incorporates seismic activity that decreases with time, the annual probability of exceeding any ground-motion level is highest in the first year, gradually decreasing with time after that. Using the information in Webb et al. (2011), which predates the 13th June 2011 earthquake, the annual probability of earthquakes is higher than the 50-year average in the first few years but drops below the 50-year average after about 9 to 10 years (illustrated for an earthquake of M_W 6 to 7 in Figure 35).

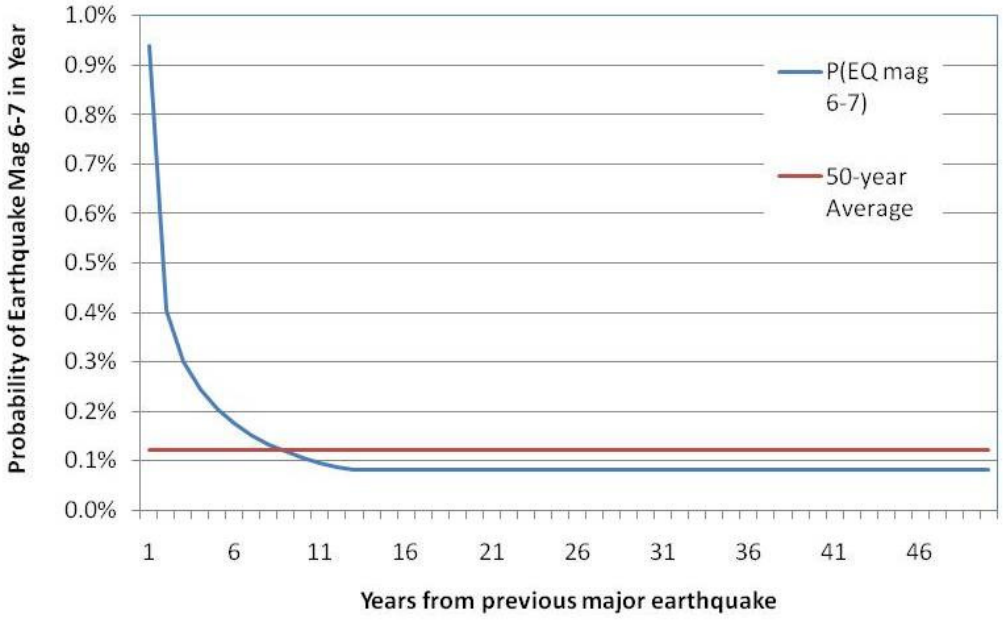

Figure 35 Estimated probability of an earthquake of M_W6-7 occurring in the next 50-year period. Data contained in Webb et al. (2011) (which predates the 13th June 2011 earthquake model).

For the seismic model used for this work, GNS Science considers that the most realistic representations of current seismicity and of longer term seismicity are provided by the 1-year average (starting 1st January 2012) and 50-year average, respectively.

The peak ground acceleration (horizontal) hazard curves for the site at Heathcote Valley Primary School, calculated using the composite seismic hazard model, show that the frequency of a given peak ground acceleration within the next 1-year period is higher when compared to those over a 50-year period (Figure 36). As a result, there are two possible target periods for the risk calculation. One is the next 50 years, which is consistent with the design life used in typical seismic hazard analysis for building construction. However, unlike the usual national seismic hazard model calculations, these forecasts are specific to the next 50 years, rather than any 50-year period. The other is the immediate (and short-term) risk associated with the recognised higher earthquake frequency over the next year.

The composite seismic hazard model site records have been used to estimate the likelihood of a given peak ground acceleration occurring in the future. Values are calculated for the Heathcote Valley Primary School site, as the values for this site are representative of those

estimated for other sites in the Port Hills (e.g., Lyttelton Port Company and Cashmere High School).

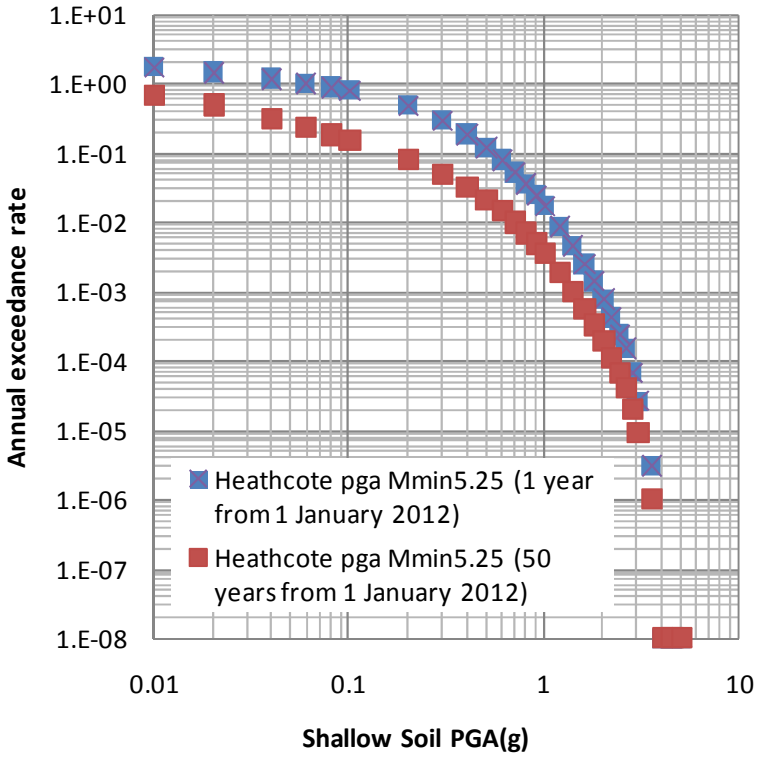

Figure 36 Peak ground acceleration (PGA) hazard curves for the Heathcote Valley Primary School site in the Port Hills, using the composite seismic hazard model results for the next 1-year and 50-year periods, using a minimum earthquake magnitude (M_{min}) of M_W5.25. The Heathcote Valley Primary School site is classed as a shallow soil site (NZS 1170 site class C). These values do not include amplification effects induced in the source areas, or any magnitude weighting.

The model estimates the frequency with which a given peak ground acceleration will be exceeded at a point in the Port Hills by summing the contributions from a large catalogue of likely future earthquakes of different magnitudes both close to the area and further from it. This catalogue is developed from known historical earthquakes, expected rates of aftershocks and other triggered earthquakes, and known active faults in the area. Thus the contributions from modest energy earthquakes close to the area and from higher energy earthquakes further away are both included. A minimum earthquake magnitude of M_W 5.25 has been used in the model, as the composite seismic hazard model provides overly conservative values at magnitudes <M5, leading to large overestimates of the exceedance values (T. Webb and G. McVerry, personal communications 2011).

For the assessments given in this report, the next 1- and 50-year frequencies from the 1st January 2012 at the Heathcote Valley Primary School site are used to estimate the likelihood of a given peak ground acceleration band occurring in the Port Hills (Table 17).

The Heathcote Valley Primary School peak ground acceleration hazard curves were used for all suburbs in the analyses, as this site is located in the central part of the Port Hills and there is little difference between the peak ground acceleration hazard curves for the Heathcote Valley Primary School and the other curves generated for the Lyttelton Port Company and Cashmere High School sites. Heathcote Valley Primary School is located on gently sloping ground in shallow soil (NZS 1170 Site Class C) and does not include amplification effects induced in the source areas. It should be noted that the frequencies of seismic events used throughout these assessments are the frequencies of events at a particular point – the frequency of an event somewhere within the area being considered will be somewhat higher than that at any individual point within it.

Table 17 Peak ground acceleration (PGA) bands and their annual frequency of occurrence estimated using the next 1-year and 50-year peak ground acceleration hazard model results for the Heathcote Valley Primary School site, using median values.

PGA band (g)	Frequency – events per year		Description
	Current – within the next 1-year period	Over the next 50 years*	
0.1 - 0.4	0.6	0.12	Cliff collapses tend to be minimal at this range of accelerations
0.4 – 1.0	0.17	0.03	Cliff collapses occur at this range but their numbers tend to be limited and localised
1.0 – 2.0	0.016	0.003	This is the acceleration range of the 22nd February and 13th June 2011 earthquakes
2.0 – 5.0	0.0008	0.0002	Could trigger more (in number) and larger (in volume) cliff collapses than the 22nd February and 13th June 2011 earthquakes

*Average frequency per year over the next 50 years

5.1.2 Estimating volumes of earthquake-triggered cliff collapses

Cliff collapse volumes likely to be generated by an earthquake representative of each peak ground acceleration band were determined for each suburb. For each site, the volumes of material leaving the cliffs per square metre of cliff face, assumed to be triggered by the 4th September 2010 Darfield Earthquake and its aftershocks, were plotted against the associated index peak ground acceleration recorded at the nearest strong motion station to that suburb; a total of eight strong motion sites are currently located in the Port Hills (Table 18).

These measurements were from three of the strong motion stations in the Port Hills that are typically sited on class B (rock) and C (shallow soil) (NZS1170.5:2004). The recorded values do not represent the actual peak ground accelerations recorded at the rockfall source areas, which are likely to have been higher as a result of localised site effects.

The measured peak ground accelerations are used as an index of what the range of peak ground accelerations were that triggered a particular number of recorded boulders.

Table 18 Debris avalanche volumes per site triggered by the 2010/2011 Canterbury earthquakes and the maximum horizontal vector (both components) of peak ground acceleration (PGA) recorded at the nearest strong motion station to the site. Note that the number of stations in the Port Hills was increased following the 22nd February 2011 earthquakes. Zero observations are not shown. LPCC - Lyttelton Port Company; PARS - Panorama Road; GODS - Godley Drive. See Figure 6 for site locations.

Site	Earthquake date	PGA (g)	Strong motion site	Volume leaving cliff (m^3)	Area of cliff face (m^2)	Comments
Redcliffs	3/09/10	0.4	LPCC	60	20,506	Estimated by consultants
	22/02/11	1.3	LPCC	15,065	25,094	2003 to 2011a LiDAR change
	16/04/11	0.8	PARS	2,181	20,506	TLSa to TLSc change
	13/06/11	1.0	PARS	10,336	20,506	TLSc to TLSd change
	15/06/11	0.1	PARS	0.1	20,506	Estimate
Shag Rock Reserve	3/09/10	0.4	LPCC	30	20,212	Estimated by consultants
	22/02/11	1.3	LPCC	27,983	20,212	2003 to 2011a LiDAR change
	16/04/11	0.8	PARS	No data	20,212	No data
	13/06/11	1.0	PARS	34,282	20,212	TLSb to TLSd change
	15/06/11	0.1	PARS	0.1	20,212	Estimate
Nayland Street	3/09/10	0.4	LPCC	5	2,413	Estimated by consultants
	22/02/11	1.3	LPCC	1,660	2,881	2003 to 2011a LiDAR change
	16/04/11	0.8	PARS	71	2,413	TLSa to TLSc change
	13/06/11	2.2	GODS	601	2,413	TLSc to TLSd change
	15/06/11	0.2	GODS	0	2,413	Estimate
Wakefield Avenue	3/09/10	0.4	LPCC	40	22,137	Estimated by consultants
	22/02/11	1.3	LPCC	7,734	28,192	2003 to 2011a LiDAR change
	16/04/11	0.8	PARS	4,125	22,137	TLSa to TLSc change
	13/06/11	2.2	GODS	11,162	22,137	TLSc to TLSd change
	15/06/11	0.2	GODS	1	22,137	Estimate
Whitewash Head	3/09/10	0.4	LPCC	100	124,484	Estimated by consultants
	22/02/11	1.3	LPCC	42,279	124,484	2003 to 2011a LiDAR change
	16/04/11	0.4	GODS	No data	124,484	No Data
	13/06/11	2.2	GODS	151,379	124,484	2011a to 2011c change
	15/06/11	0.2	GODS	10	124,484	Estimate

A linearized power-law was fitted to the data in Table 18, of the form:

$$\log VPA = a + b \log PGA \qquad [2]$$

where *VPA* is the expected volume of material leaving the cliff per square metre of cliff, and is measured in metres and represents the average thickness of cliff face lost, *a* and *b* are constants and *PGA* is peak ground acceleration (m/sec/sec) (Figure 37). Details of the fitted parameters and their uncertainties are given in Table 19. The relation is a moderately good fit to the data (R^2 = 0.91), but there is large spread of *VPA* values at high peak ground accelerations. This variation could be due to poor estimation of peak ground accelerations at some sites, or to other unknown local variables such as topographic amplification influencing the volume of material leaving the cliff (D. Rhoades, personal communication 2011).

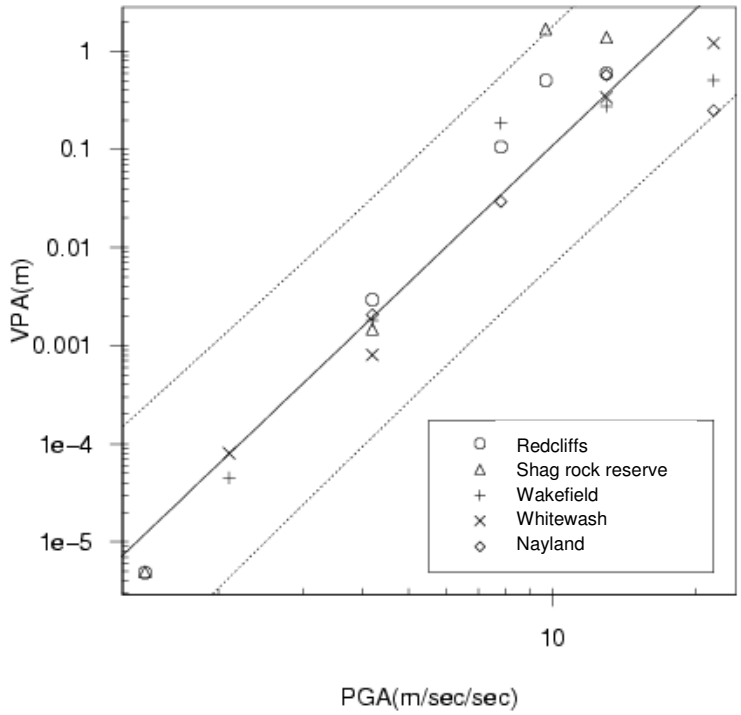

Figure 37 Fitted relation of volume of material leaving slope per square metre of cliff face (VPA) against peak ground acceleration (PGA) as fitted by a generalized linear model [Eq. 2] to the data of Table 18. Dotted lines are 95% tolerance limits.

Table 19 Statistics of linear regression as fitted by a generalized linear model [Eq. 2] to the data of Table 18

Parameter	Value	Standard error
a	-12.8887	0.6945
b	4.6334	0.3325
Residual standard error: 1.305 on 20 degrees of freedom		
Correlation of Coefficients *a* and *b*: -0.91		

The results (Table 20) suggest that a lower-bound peak ground acceleration threshold for triggering 1 m^3 of debris from the cliffs is about 0.1 to 0.2 g (for the sites analysed). The above analysis treats each triggering earthquake as independent of other earthquakes and takes no account of conditional probability. The available data do not allow us to investigate the possibility that the thresholds of triggering may change as a result of the earthquake sequence.

Table 20 Expected volume of material leaving the cliff per square metre of cliff (VPA) and 95% tolerance limits for the actual VPA, in a future occurrence of peak ground accelerations (PGA) of 0.7 g and 1.5 g at any site.

PGA(g)	Expected VPA (m)	95% tolerance limits
0.7	0.019	0.0012 to 0.306
1.5	0.647	0.038 to 11.01

5.1.3 Expected volume of rock triggered in each peak ground acceleration band

The expected volume of material to leave a slope triggered by an earthquake within the 0.4 – 1.0 g and the 1.0 – 2.0 g peak ground acceleration bands have been estimated from Figure 35 using Eq. 2 (Tables 21 and 22), using the slope-face areas in Table 18.

Table 21 Expected volumes of rock leaving the cliffs and uncertainties from an event within the 0.4 – 1.0 g peak ground acceleration band. The tolerance limits are the uncertainties on the actual volumes of rock leaving the cliffs in a future occurrence of accelerations of 0.7 g.

Suburb	Expected volume (m^3)*	95% tolerance limits (m^3)	
		From	To
Redcliffs	477	30	7,679
Shag Rock Reserve	384	24	6,185
Nayland Street	55	3	882
Wakefield Avenue	536	34	8,627
Whitewash Head	2,365	149	38,092

*Note that only the first digit in the number is significant

Table 22 Expected volumes of rock leaving the cliffs and uncertainties from an earthquake within the 1.0 – 2.0 g acceleration band. The tolerance limits are the uncertainties on the expected volumes of rock leaving the cliffs in a future occurrence of accelerations of 1.5 g.

Suburb	Expected volume (m^3)*	95% tolerance limits (m^3)	
		From	To
Redcliffs	16,236	954	276,285
Shag Rock Reserve	13,077	768	222,534
Nayland Street	1,864	109	31,720
Wakefield Avenue	18,240	1,071	310,394
Whitewash Head	80,541	4,730	1,370,569

*Note that only the first digit in the number is significant

For the 0.1 – 0.4 peak ground acceleration band a small non-zero estimate of the expected volume of rock leaving a cliff from a representative earthquake has been assumed (10 m^3 per cliff). This is consistent with the results from the 2010/2011 Canterbury earthquakes. For the highest peak ground acceleration band of 2.0 – 5.0 g, the volumes of rock leaving the cliffs triggered by a representative event were estimated, using the upper 95% error limit of the event within the 1.0 – 2.0 g peak ground acceleration band. These volumes are summarised in Table 23.

Table 23 The estimated volume of cliff collapses triggered by a representative event within each peak ground acceleration (PGA) band for all suburbs included in the assessment. These represent the estimated volume of debris leaving a source area (rock slope) for a particular event (values in the table have been rounded to whole numbers).

Site	Estimated volumes of material leaving cliffs per PGA band[1] (m^3)			
	0.1 – 0.4 g	0.4 – 1.0[2] g	1.0 – 2.0[2] g	2.0 – 5.0[2] g
Redcliffs	10	477	16,236	276,285
Shag Rock Reserve	10	384	13,077	222,534
Nayland Street	10	55	1,864	31,720
Wakefield Avenue	10	536	18,240	310,394
Whitewash Head	10	2,365	80,541	1,370,569

[1]Note that only the first digit in the number is significant
[2]Estimated from Figure 35.

5.1.4 Estimating the annual probability of cliff collapse initiating events

In the Australian Geomechanics Society guidelines for landslide risk management (Australian Geomechanics Society, 2007) $P_{(H)}$ is the annual probability of an initiating event. For this study, the annual frequency, rather than probability (with corresponding units of "per year" as opposed to "dimensionless probability of occurrence in one year"), has been used. This is because the term "probability" invites confusion when events can occur several or more times in a year (Taig et al., 2012).

For this study $P_{(H)}$ is the annual frequency of a given volume of material being triggered over a given period of time.

For seismic triggers $P_{(H)}$ is estimated using the composite seismic hazard model, where $P_{(H)}$ is the range of each peak ground acceleration band. For the 0.4 – 1.0 g peak ground acceleration band, the annual frequency of exceedence of these accelerations (estimated from the 1-year composite seismic hazard model results) are 0.185 and 0.017 respectively (Table 24), therefore the width of the band (the frequency of events within the band) is:

$$P_{(H)} = 0.185 - 0.017 = 0.168 \quad [3]$$

Table 24 Annual frequency of a given volume of earthquake-triggered debris occurring within a given time. This has been calculated for all assessed areas using the next median 1-year seismic hazard model results.

Peak ground acceleration band	$P_{(H}$ Frequency – events per year*	Estimated volume of debris from band (all areas) (m^3)**	Collapse process rate# (Volume/year)
0.1 – 0.4 g	0.60	50	30.0
0.4 – 1.0 g	0.168	3,816	642.1
1.0 – 2.0 g	0.0164	129,958	2,129.5
2.0 – 5.0 g	0.00076	2,211,502	1,687.4
	Total annual cliff collapse process rate		**4,488.9**

*Derived from the composite seismic hazard model results for Christchurch over the next 1-year.
**Note that only the first digit in the number is significant
#Calculated by multiplying the estimated volumes of debris per band by the annual frequency of the band occurring.

If the next 50-year seismicity results are used (median values), the total annual process rate is about 980 m^3 per year, compared to the 4,489 m^3/year estimated using the next 1-year model results. This consequence is not because there is more risk per expected earthquake, but because there is more risk of earthquakes in the first year, and so there is an increased annual process rate.

5.2 Other cliff collapse triggers

To compare the risk from collapses triggered by the 2010/2011 Canterbury earthquakes with the risk from other triggering events, and to develop a full risk profile for the area, requires quantitative information on collapses triggered by other (non-seismic) events (mainly high-intensity or long-duration rainfall). For most locations on the Port Hills, quantitative data for

other events is sparse. However, some sources of information were available for this report. The risk from cliff collapse from causes other than earthquakes has been addressed by the use of fences, and gabion and earth bunds, in Redcliffs and Wakefield Avenue. These structures provide protection to houses located below cliffs.

5.2.1 Estimating other non-seismic triggers – cliff collapse frequencies and volumes

There are four main sources of information on historical rockfalls for the Port Hills: 1) archive newspaper reports between 1870 and 1938; 2) GNS Science landslide database, which is "complete" only since 1996; 3) insurance claims made to the Earthquake Commission for landslip which is "complete" only since 1996; and 4) information from local consultants (M. Yetton, Geotechnical Consulting Ltd and D. Bell, University of Canterbury) which covers the period from 1968 to present.

Archive newspapers report several rockfall events over the past about 100 years. One event occurred in 1907 at Shag Rock Reserve and involved the failure of about 1,500 to 2,000 m^3 of rock from the northern part of the cliff opposite Shag Rock (Star newspaper issue 8891). A further failure from the same slope but at the southern end was also reported in 1912, involving about 150 m^3 of rock (Brown and Weeber, 1992). These can be associated with rainfall but they were not reported to have fallen during rain. Earthquake triggering can be ruled out as none were reported at these times.

The Star on 30 March 1907, in reporting on the "Great landslip" of the night before which blocked the Sumner Road and tramline at Clifton, remarked that "The cliffs on the Sumner Road have been a source of anxiety to the authorities and the public ever since the road was first opened by the Provincial Engineer, and periodically there have been falls of rock, more or less serious. The cliff, of course, is constantly "tailing" [ravelling]."

The GNS Science catalogue records six landslides that mainly affected roads in the region between 1996 and 2011, about 0.4 events per year. These are all recorded as being small (<10 m^3) and mainly initiated by rainfall. The GNS Science database records a home in Heberden Avenue destroyed by rockfall during rain on 24th October 2000, and two homes hit by rockfall in Wakefield Avenue (at the toe towards the southern end of the cliff) during rain on 13-14th August 2006, which involved several hundred cubic metres of rock. These are the only rockfall-related events in the Port Hills in the GNS Science landslide database before 2010.

A total of about 14 claims were made for what is assessed to be cliff collapses in the Redcliffs to Sumner area, about 1.1 claims per year. These claims include the three events recorded in the GNS Science catalogue. Claims assessments carried out on behalf of the Earthquake Comission by local consultants Geotechnical Consulting Ltd. report the volumes of rock that fell from the Wakefield Cliff in August 2006 were about 300 m^3 (N. Traylen, personal communication 2011). The reported volumes of the other rockfalls are estimated to be in the range of 1 – 10 m^3.

Other information that may contain records of rockfalls in the Port Hills, e.g., Christchurch City Council files and reports, were not investigated in the time allowed. Knowledge held by other local geotechnical consultants indicate that rockfalls have occurred in the Port Hills over the past 30 years or more. Information contained in Bell (1992), reports two failures of the rock slope at Redcliffs, the first in 1968 and the second in 1992; both are estimated to be about 50 m^3 in volume and rainfall is reported as the trigger.

The pre-4th September 2010 earthquake talus identified at the toe of Redcliffs and Wakefield Avenue indicates accumulation rates of about 15 – 20 m^3/year, assuming the surface on which it rests is about 3,600 (±100) years old (McFadgen and Goff, 2005). However, this material may not all be attributed to non-seismic events, as it may include previous earthquake-triggered material. Work is currently on going to quantify the likely origin of this material.

In view of the lack of detailed records, rockfall rates triggered by non-seismic events were estimated based on the above limited available data, discussion with local consultants, anecdotal evidence from residents, and judgement. These have been used to estimate the total risk contribution from non-seismic rockfall triggering events (Table 25).

Four representative time periods (in terms of resolution in time) have been used and the volumes of the rockfalls triggered within these time periods have been estimated using a series of steps:

Step 1 – Estimate the number of events that have occurred over a given time period for all sites using the available data. Four time-period bands have been used: 1) 1 – 15 years; 2) 15 – 100 years; 3) 100 – 1,000 years; and 4) >1,000 (nominally 1,000 – 10,000 years) (Table 23).

Step 2 – Assume a conservative volume of N m^3 per "typical" event in each band, assuming the same volumes per event for all cliffs.

Step 3 – Estimate the frequency (annual frequency) of a given event occurring in each band. Scale the frequency up or down depending on the area of each cliff face, assuming the event frequency is greater for larger slopes than those on smaller slopes.

Table 25 Information used to estimate event volumes contributing to the total risk from non-seismic rockfall triggering events, all sites.

Time period (years)	Type of events	Description
<1 – 15	Rainstorms/frosts that occur frequently	Cliff collapses tend to be small and localised from events with this high frequency of occurrence. Estimated volumes of events derived using Earthquake Commission claims, local consultant files and the GNS Science database
15 – 100	Rainstorms with larger intensities and durations that occur once every 15 – 100 years on average	Cliff collapses occur but their volumes tend to be limited and localised. Estimated volumes of events derived using historical newspapers and consultant reports.
100 – 1,000	Rainstorms with very large intensities and durations that occur once every 100 – 1,000 years on average	Cliff collapses will be widespread. Estimated volumes of events derived using old newspaper reports.
1,000 – 10,000	Rainstorms with extreme intensities and durations exceeding Cyclone Bola (1988) and the Manawatu storm (2004) that occur once every >1,000 years on average	These events might trigger a large number of cliff collapses over a wide area and may be large in volume. However, cliff collapse risk would be low compared with risk from flooding or debris flows

It is unlikely that a rainstorm will trigger a comparable number and volume of cliff collapses over an area similar to a large magnitude earthquake (typically > M_W6). This is because as earthquake loading can "throw" debris from slopes and generate cracks, while intense rain can only erode material from around rock blocks (making them unstable), and increase water pressures acting within joints.

The number of events in each band and the representative volume per event were estimated using the historical information per site. For Redcliffs, Shag Rock Reserve and Wakefield, in the 1 – 15 year period, using the Earthquake Commission claims data, there has been a total of about 1.1 claims per year, which is equivalent to about 1.1 events per year (or 0.4 events per year per site), with the average volume of material per event estimated to be about 5 m^3. In the 15 – 100 year period there have been four recorded events (about 1.3 per site), with the average volume of material per event estimated to be about 170 m^3. In the 100 – 1,000 period there has been one recorded event of about 1,500 m^3; if it is assumed that two of these events occurred (where one has not been recorded), the number of events per site would be about 0.7. For the 1,000 – 10,000 year period it is estimated that there has been one event (about 0.3 per site), of about 10,000 m^3, an order of magnitude greater than the 1,500 m^3 event that occurred in the 100 – 1,000 year period. For these three sites the geometry of the cliffs are similar and so it is reasonable to assume a similar magnitude and frequency distribution of events. For Nayland Street, where the cliff is about a third of the area, the event frequencies have been reduced by a third. In contrast, for Whitewash Head, where the cliff area is typically about 1.5 times larger than the area of Redcliffs, Shag Rock Reserve and Wakefield Avenue (and is being actively eroded by the sea), the event frequencies have been increased by about one and a half times. In contrast to the

earthquake-triggering events, the representative events for non-seismic triggers have been kept the same, with only the annual frequencies of the event changing from site to site (Table 26).

Table 26 Estimated annual event frequency of a cliff collapse event occurring and the representative volume of the event, for each time-period band. These represent the estimated volumes of the material leaving the cliffs per site over a given time period, for non-seismic triggers.

Location	Time period (years)	Number of events in band	Annual frequency of events	Mean event volume (m^3)	Annual accumulation rate (m^3/year)
Redcliffs, Shag Rock Reserve and Wakefield Avenue	1 – 15	5.5	0.37	5	1.8
	15 – 100	1.3	0.0133	170	2.3
	100 – 1,000	0.7	0.0007	1500	1.0
	1,000 – 10,000	0.3	0.00003	10000	0.3
Nayland Street	1 – 15	1.8	0.12	5	0.6
	15 – 100	0.4	0.0044	170	0.8
	100 – 1,000	0.2	0.0002	1500	0.3
	1,000 – 10,000	0.1	0.00001	10000	0.1
Whitewash Head	1 – 15	8.3	0.55	5	2.8
	15 – 100	2.0	0.02	170	3.4
	100 – 1,000	1.0	0.001	1500	1.5
	1,000 – 10,000	0.5	0.00005	10000	0.5
			Summary process rate (all slopes)		**26.3**

The estimated volumes of debris accumulated per band are thought to reasonably represent the overall non-seismic cliff collapse rates determined from all available data sources prior to the 2010/2011 Canterbury earthquakes.

5.3 Cliff-top recession rates

The annual frequency of a given cliff collapse event occurring in each band for both seismic (using the next 1-year model results) and non-seismic triggers can be summed for each site. The results, when plotted as a histogram, give an indication of the likely total number and magnitude (volume) of cliff collapses triggered over the considered period of time (Figure 38). The average volume of material leaving the cliffs per year (or cliff collapse process rate) can be estimated as the area under the log-log histogram (Moon et al., 2005). This allows the relative importance of the different triggers to be assessed over time. For seismic triggers the mean process rate for all cliffs is about 4,489 m^3/year (assuming the 1-year seismic model), and for non-seismic events about 26 m^3/year. These data show that:

1. Earthquakes contribute more to the overall risk than non-seismic triggering events;
2. Frequently occurring non-seismic events contribute more risk than do frequently occurring earthquakes, but
3. Earthquakes dominate the risk for rare events that occur every few hundred years.

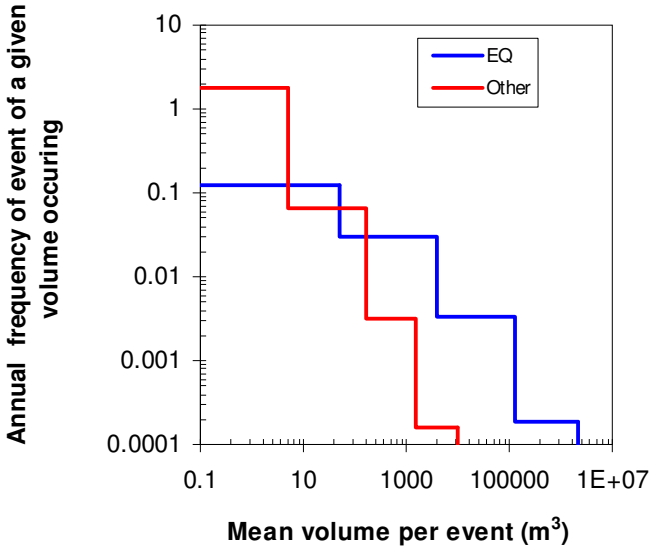

Figure 38 The cliff collapse frequency magnitude model developed for this study incorporating earthquake and non-seismic triggers. The frequency and magnitude of earthquake-triggered cliff collapses are shown using the next 1-year median composite seismic hazard model results. Plot is for all sites.

The effects of using the next 50-year composite seismic hazard model results instead of the next 1-year results are compared in Figure 39. The effect of using the next 50-year results is a lower calculated risk of a cliff collapse triggering earthquake, and thereby a lower risk of a given volume of material leaving the cliffs and therefore a lower cliff top recession rate.

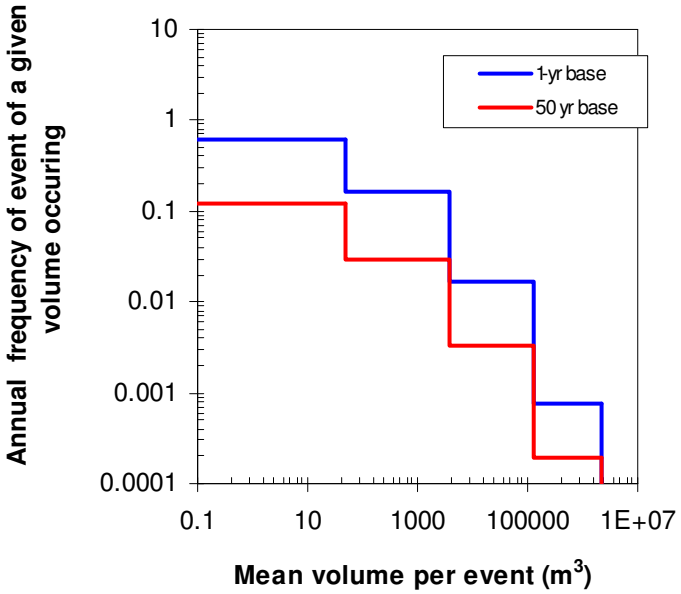

Figure 39 The cliff collapse frequency magnitude model developed for this study comparing results using the next 1-year with the next 50-year composite seismic hazard models. Plot is for all sites.

The annual volumes of debris leaving the cliffs at Redcliffs and Wakefield Avenue from seismic events only and using the 50-year seismic model are 123 and 138 m^3/year respectively. Therefore the cliff top recession rate at Redcliffs and Wakefield would be about 5 m per 1,000 years (assuming a slope face area of 25,094 m^2 at Redcliffs and 28,192 m^2 at Wakefield Avenue), and assuming the entire slope erodes at the same rate. In comparison, the longer-term rates (over the last 3,600 years) estimated from the accumulated talus at the toe of these cliffs are 0.6 m per 1,000 years at Redcliffs about 0.4 m per 1,000 years at Wakefield Avenue. These large differences in the recession rates are a function of the currently increased seismicity of the region following the 2010/2011 Canterbury earthquakes.

However, the cliffs do not solely recess by gradual erosion. Instead, cliff top recession mainly occurs in events, as shown by the 2010/2011 Canterbury earthquakes. Therefore longer-term cliff top recession rates should not be used for the risk assessment, as in reality they vary over time, resulting in short periods of rapid recession interspersed with long periods of negligible recession.

6.0 RISK ASSESSMENT

6.1 Risk analysis steps

The analyses includes the assessment of the risk to an individual from: 1) debris avalanches (derived from the cliffs); and 2) cliff top recession, at Redcliffs, Shag Rock Reserve, Nayland Street, Wakefield Avenue and Whitewash Head. It also assesses the risk from large, rockmass controlled cliff deformation or landslides, albeit in a simplistic way.

The risk is expressed as the annual individual fatality risk, which is the probability (likelihood) that a particular individual will be killed by a cliff collapse in any year at their place of residence. For most localities this probability is an imprecisely determined, very small number and the report makes extensive use of the scientific number format of expressing risk in terms of powers of ten. For example the number 10^{-4} ("10 to the power of minus 4") is the fraction 1/10,000, and the decimal number 0.0001; it may also be expressed as 0.01%. The units of risk are dimensionless probability per unit of time and the units of annual fatality risk are probability of fatality (death or loss of life) per year.

For debris avalanches and cliff top recession the risk analysis comprises the following steps:

1. Consider the full possible range of triggering events, e.g., earthquakes, rain (following the method of Moon et al., 2005) in terms of a set of earthquake triggers and a set of non-seismic triggers
2. Choose a small set of representative events for each type of trigger spanning the range of severity of events from the smallest to the largest
3. For each representative event, estimate:

For debris avalanches:

   a) the frequency of the event and the volume of material produced ($P_{(H)}$)
   b) the proportion of debris reaching/passing a given Fahrboeschung angle (distance) down the slope and the probability of one of *N* boulders (in the debris) hitting a person at that location on the slope ($P_{(S:H)}$)

c) the probability that a person is present on the slope as the debris moves through it ($P_{(T:S)}$)

d) the probability that a person will be killed if present and hit by one or more boulders within the debris ($V_{(D:T)}$)

For cliff top recession:

a) the frequency of the event and the area of cliff top lost ($P_{(H)}$)

b) the proportion of cliff top lost at a given distance back from the cliff edge and the probability of a person falling if one of *N* square metres of cliff top is lost at that location ($P_{(S:H)}$)

c) the probability that a person is present at the cliff top as the material falls ($P_{(T:S)}$)

d) the probability that a person will fall and is killed, if present at the cliff edge ($V_{(D:T)}$)

4. Combine 3(a) – (d) for debris avalanche and cliff top recession to estimate the annual individual fatality risk for individuals at different locations below the cliff or at the cliff edge contributed by each representative event
5. Sum the risks from all events to estimate the overall risk
6. Enter the risk values at each fahrboeschung and slope-edge zone into a Geographical Information System programme and interpolate between the risks estimated for each zone to produce contours of equal risk on a map.

6.2 Event frequency magnitude

The magnitude (volume) and frequency (annual frequency of occurrence) of the representative events for seismic and non-seismic sources, per cliff are taken from section 5, Tables 23 and 26 respectively. For cliff top recession, the loss of material at the cliff edge is proportional to the volume of material lost from the cliff face. The relationship between the volume lost from the cliff face and the corresponding area of cliff top lost during the 2010/2011 Canterbury earthquakes has been analysed. From these data the gradient (or ratio) of area lost to volume leaving the cliff face is about of 0.016 ±0.001 at one standard deviation. Therefore the area lost is 0.016 multiplied by the volume leaving the cliff, i.e., for every 100 m^3 of cliff face lost you would expect about 1.6 m^2 (±6%) of cliff top area to be lost. For this assessment a ratio of 0.019 has been adopted, which is the ratio plus two standard deviations (95% error limit) (Tables 27 and 28).

Table 27 Relationship between the volume leaving the cliff and the area of cliff top lost for seismic triggers.

Site	Volume (m^3) of cliff face lost (per peak ground acceleration band (g))[1]				Corresponding area (m^2) of cliff top lost (per peak ground acceleration band (g))[1]			
	0.1 – 0.4	0.4 – 1.0	1.0 – 2.0	2.0 – 5.0	0.1 – 0.4	0.4 – 1.0	1.0 – 2.0	2.0 – 5.0
Redcliffs	10	477	16,236	276,285	0.2	9	308	5,249
Shag Rock Reserve	10	384	13,077	222,534	0.2	7	248	4228
Nayland	10	55	1,864	31,720	0.2	1	35	603
Wakefield	10	536	18,240	310,394	0.2	10	347	5,897
Whitewash	10	2,365	80,541	1,370,569	0.2	45	1,530	26,041

[1]Note only the first digit of the number is significant

Table 28 Relationship between the volume leaving the cliff and the area of cliff top lost for non-seismic triggers.

Site	Volume (m^3) of cliff face lost (per time period band (years))[1]				Corresponding area (m^2) of cliff top lost (per time period band (years))[1]			
	1 – 15	15 – 100	100 – 1,000	>1,000	1 – 15	15 – 100	100 – 1,000	>1,000
Redcliffs	5	170	1,500	10,000	0.1	3	29	190
Shag Rock Reserve	5	170	1,500	10,000	0.1	3	29	190
Nayland	5	170	1,500	10,000	0.1	3	29	190
Wakefield	5	170	1,500	10,000	0.1	3	29	190
Whitewash	5	170	1,500	10,000	0.1	3	29	190

[1]Note only the first digit of the number is significant

6.3 Impact from debris avalanches

$P_{F(S:H)}$ is the probability of the debris hitting a portion of slope as it travels downhill from the source area. The probability of one boulder hitting an object when passing through a particular portion of the slope, perpendicular to the boulder path, is expressed as:

$$P_{F1(S:H)} = \frac{(2D+d)}{L} \quad [4a]$$

where D is the diameter of the design boulder (assumed to be 1.0 m) that travels along a path either side of d, within which the boulder cannot miss, d is the diameter of an object such as a person or width of a building, and L is the unit length of slope perpendicular to the runout path.

However, the debris leaving the cliffs during the 2010/2011 Canterbury earthquakes predominantly consisted of a mass of boulder- and cobble-sized blocks that were not all equal in volume. The distribution of block sizes within the debris has not yet been quantified (for Health and Safety reasons), however, using the data set for fallen boulder-roll (Massey et al., 2012), the 50th percentile of the fallen boulder volumes was about 0.5 m^3. If it is assumed that each cubic metre of debris comprises two blocks of 0.5 m^3 in volume, then the probability of one cubic metre of debris hitting an object when passing through a particular portion of the slope is expressed as.

$$P_{F2(S:H)} = 1 - \left(1 - \frac{(2D+d)}{L}\right)^2 \quad [4b]$$

The probability of one cubic metre of debris formed of two boulders hitting the same portion of slope increases as a function of the volume of debris travelling down the slope. The probability of one cubic metre of N cubic metres of debris hitting an object when passing through that same portion of slope is then given, if the debris is randomly distributed across the slope, by:

$$P_{FN(S:H)} = 1 - (1 - P_{2(S:H)})^N \quad [4c]$$

For the purposes of risk estimation, it is necessary to have a quantitative measure of the size of a person. In this report, a "person" is assumed to be a cylinder of 1 m diameter and unspecified height (no specification of height was required in the model). The assumed value covers the order-of-magnitude range from about 0.3 m to about 3 m.

6.4 Falling due to cliff top recession

$P_{R(S:H)}$ is the probability of a particular location at the cliff top recessing and a person falling should the person be present. The probability of a person or object at the cliff top falling, given one metre of cliff top recessing, perpendicular to cliff edge, is expressed as.

$$P_{R1(S:H)} = \frac{(2D)}{L} \quad [5a]$$

where D is the approximate area occupied by a person at the cliff edge, assumed to be 1 m^3, and L is the unit length of cliff parallel to the cliff edge.

The probability of a person or object falling is dependent upon the total area of cliff edge that collapses during a given event, and how close the person or object is to the cliff edge, as the proportion of cliff top that collapses in any event decreases away from the cliff edge. Therefore the probability of a person falling if one square metre of *N* square metres of cliff top were to collapse, if the area collapsing is randomly distributed across the cliff edge, is given by:

$$P_{RN(S:H)} = 1 - (1 - P_{R1(S:H)})^N \quad [5b]$$

6.5 Probability a person is present

$P_{(T:S)}$ is the probability an individual is present in the portion of the slope when either the debris moves through it or when it falls away, and is a function of the proportion of time spent by a person at a particular location each day. A recent study carried out for the UK Health & Safety Executive (Hunt et al., 2010), identified several types of people – including the elderly, parents with young children, very young, disabled or other vulnerable people – who may spend a very high proportion of their lives at home. The assumption used in the risk assessment for judging whether risk controls should be applied at individual homes was thus that a most-exposed individual at risk could spend 100% of their time at home.

It is standard practice in risk assessments for the purpose of assessing tolerability of risk in support of planning issues to assume 100% occupancy for domestic properties, so as to ensure that decisions are robust to any reasonable future use of the homes in question (GEO Report No. 75, 1999).

Three people were killed in the residential areas (included in this risk assessment) by debris avalanches triggered by the 22nd February 2011 Christchurch Earthquake. This earthquake occurred during the day, when most, but not all people were out. There might have been very substantial household fatalities had the earthquake occurred at night when most people would have been at home. The actual occupancy of homes thus varies widely, leaving open a question as to what occupancy should be assumed for the purposes of risk assessment.

Nobody was killed as a result of the cliff tops recessing during the 2010/2011 Canterbury earthquakes, although there has been at least one very near miss. However, now that much of the cliff tops have migrated backwards, many homes and gardens extend up to, and in some places overhang, the current cliff edge. Any future cliff top recession could therefore cause these houses to fall and so the current situation is very different to the pre-earthquake one.

A person standing on an area of cliff top that is showing signs that it will fall, momentarily has a brief chance of getting off this area and onto stable ground. Getting off the area that is about to fall does not affect the vulnerability of the person to falling, but it affects the probability of the person being present when it falls. For a person standing at the cliff top the probability of being present on an area of ground as it falls is a number <1.0. Hence in this report $P_{(T:S)}$ is within the range of 0.9 and 1.0, to allow for the possibility of escape.

6.6 Probability of the person being killed if hit or falling

$V_{(D:T)}$ is the probability of a person being killed (or receiving injuries which prove fatal in the near aftermath of the event) if present on the slope and either in the path of debris, or falling from the cliff top. It is expressed as a vulnerability, which is the term used to describe the

amount of damage that results from a particular degree of hazard. Vulnerabilities range between 0 (no damage) and 1 (total loss, i.e. death) and represent the severity of injury sustained by the individual when in the path of debris – they take into account both the possibility of getting out of the way to avoid being struck, and the likelihood of fatality if struck.

Observations of homes in the cliff collapse areas indicate they were struck by many boulders, and in some cases the building collapsed. At Redcliffs one person was killed in their home as it was struck by many hundreds of boulders, which caused it to collapse. Another person was buried and killed by many boulders while in their garden. Finlay et al. (1999) recommend using a vulnerability value of 1.0 if a person is in a building and if the building is hit by debris and collapses, or is inundated with debris. Taking all these considerations into account, for this study $V_{(D:T)}$, the probability of a person being killed or receiving fatal injuries, is assumed to be 1.0. That is, the lack of ability for pre-warning and evasive action for a person in a home, in combination with the many number of boulders, and that New Zealand houses are typically made of wood, are considered broadly to negate the protective effect provided by the house. Therefore, on this basis it is reasonable to adopt values at the upper end of those identified in research elsewhere.

For a person falling from a cliff top the severity of injury increases with the height of the fall, but it also depends on the age of the person, nature of the impact surface and how the body impacts on to the surface. The chance of surviving increases if landing on a surface that can deform, such as snow or water. In a study by Barlow et al. (1983), the height at which 50% of children die from a fall is between 12 to 15 m. The cliffs in this study range from 40 to 110 m in height and the nature of the surface onto which a person would fall is assumed to be debris formed of rock. Taking all these considerations into account, for this study, $V_{(D:T)}$, the probability of being killed or receiving fatal injuries for a person falling from a cliff, is assumed to be 1.0.

6.7 Illustrative example – debris avalanche

An example from Redcliffs can be used to step through the debris avalanche risk analysis process. Consider the risk of debris hitting and killing a person located on the 50° Fahrboeschung line from an event occurring within the 1.0 – 2.0 g peak ground acceleration band. The estimated volume of the representative event in this band is about 16,236 m^3 (Table 27). About 16% of this debris (about 2,596 m^3) would pass the 50° Fahrboeschung angle.

Step 3a: Estimate the annual frequency of the event occurring within the 1.0 – 2.0 g peak ground acceleration band, using the composite seismic hazard model, where $P_{(H)}$ = 0.016 (about 1/60 years using the next 1-year composite seismic hazard model results).

Step 3b: Estimate the probability of one cubic metre of debris hitting an individual (if present) in the portion of the slope when the debris moves through it ($P_{F1(S:H)}$) using Eqs. [3a and 3b], where each cubic metre of debris comprises two boulders, and where D = 1.0 m, the diameter of a person d = 1.0 m and the length of the 50° Fahrboeschung angle (L) = 836 m.

$$P_{F1(S:H)} = 1 - \left(1 - \frac{(2 \times 1.0 + 1.0)}{836}\right)^2 = 7.2 \times 10^{-3} \qquad \text{[from Eqs. 4a and 4b]}$$

Estimate the probability of *N* cubic metres of debris hitting an individual (if present) in the portion of slope (the 50° Fahrboeschung angle) when the boulders move through it, using Eq. [4c], where:

$$P_{FN(S:H)} = 1-(1-7.2\times10^{-3})^{2596} = 1.0 \qquad \text{[from Eq. 4c]}$$

Step 3c: Estimate the probability that the person is present and hit, considering the time spent at home ($P_{(T:S)}$ = 1).

Step 3d: Estimate the probability of the person being killed if present and hit by debris ($V_{(D:T)}$ = 1.0).

Step 4: Multiply steps 3a, 3b, 3c and 3d to calculate the annual individual fatality risk. Therefore the annual individual fatality risk ($R_{(BAND)}$) to a person on/around the 50° Fahrboeschung angle from avalanching debris triggered by an earthquake in the 1.0 – 2.0 g peak ground acceleration band is:

$$\mathrm{R}_{\text{(1-2g PGA BAND)}} = 0.016\times1.0\times1.0\times1.0 = 1.6\times10^{-2} \qquad \text{[from Eq. 1]}$$

Step 5: Repeat Steps 3 to 4 for each Fahrboeschung angle for each of the considered bands, and sum the results for each Fahrboeschung angle to estimate the total risk to the life of an individual on a given fahrboeschung angle-line (Table 29).

The annual individual fatality risk from fly rock is estimated to be $<10^{-5}$ to an individual occupying a dwelling located between the debris avalanche risk zones and the fly rock Fahrboeschung angle line (31°). The annual individual fatality risk in this area has been estimated by taking the estimated mean volumes of material passing the lowest Fahrboeschung angles per earthquake and non-seismic triggering band (for all sites), and by reducing the volume of the blocks (used in the model) that could hit a person from 0.5 m^3 to 0.1 m^3. The vulnerability of a person if present and hit, has also been reduced from 0.5 to 0.05 to take into account the reduced size of the blocks and the relative protection a house may give from such small flying blocks.

Table 29 The debris avalanche annual individual fatality risk analysis method results for the 50° Fahrboeschung angle at Redcliffs

	Parameter estimated	EARTHQUAKES (1-year model results) Peak ground acceleration band					NON-SEISMIC EVENTS Time periods				
		0.1-0.4 g	0.4-1 g	1-2 g	>2 g	ALL earthquakes	1 - 15 years	15 - 100 years	100 - 1000 years	>1000 years	ALL non-seismic events
A	**$P_{(H)}$** Annual frequency of number of boulders leaving source (years)	0.60	0.17	0.02	0.001		0.37	0.01	0.0007	$3x10^{-5}$	
B	Expected volume of debris leaving source for representative event in band (m^3)	10	477	16,236	276,285		5	170	1,500	10,000	
C	Relative proportion of debris passing 50º Fahrboeschung angle	0.16	0.16	0.16	0.16		0.16	0.16	0.16	0.16	
D	Expected volume passing 50º Fahrboeschung angle for representative event in band (BxC)	1.6	76	2596	44182		1	27	240	1599	
E	Probability a person is within path of one m^3 of debris GIVEN each 1 m^3 comprises two blocks	$7x10^{-3}$	$7x10^{-3}$	$7x10^{-3}$	$7.2x10^{-3}$		$7x10^{-3}$	$7x10^{-3}$	$7x10^{-3}$	$7x10^{-3}$	
F	**$P_{(S:H)}$** Probability person is within path of N m3 of debris GIVEN volume of debris passing F-angle for this event	$1x10^{-2}$	$4x10^{-1}$	1.0	1.0		$6x10^{-3}$	$2x10^{-1}$	$8x10^{-1}$	1.0	
G	**$P_{(T:S)}$** Probability of a person being present	1	1	1	1		1	1	1	1	
H	**$V_{(D:T)}$** Probability of a person being killed by a debris if present and hit	1	1	1	1		1	1	1	1	
R	**$R_{(LOL)}$** Annual risk (death) all bands for Fahrboeschung angle (AxFxGxH)	$7x10^{-3}$	$7x10^{-2}$	$2x10^{-2}$	$8x10^{-4}$	**$1x10^{-1}$**	$2x10^{-3}$	$2x10^{-3}$	$6x10^{-4}$	$3x10^{-5}$	**$5x10^{-3}$**
	GRAND TOTAL RISK (ALL EVENTS)					**$1x10^{-1}$**					

Step 6: The annual individual fatality risk considering all events was calculated for each Fahrboeschung angle for each site, following the steps outlined in the example. These values were then modelled using ArcGIS®. ArcGIS is used to interpolate between the risks calculated at given Fahrboeschung angles so as to produce contours of equal risk (Figure 40). Contours were developed for logarithmic classes, e.g., 10^{-2} to 10^{-3}, 10^{-3} to 10^{-4} of individual risk values. The Christchurch City Council building footprints were then overlain on the risk model and the centroids of the dwellings, within each property, were used to assign the risk value.

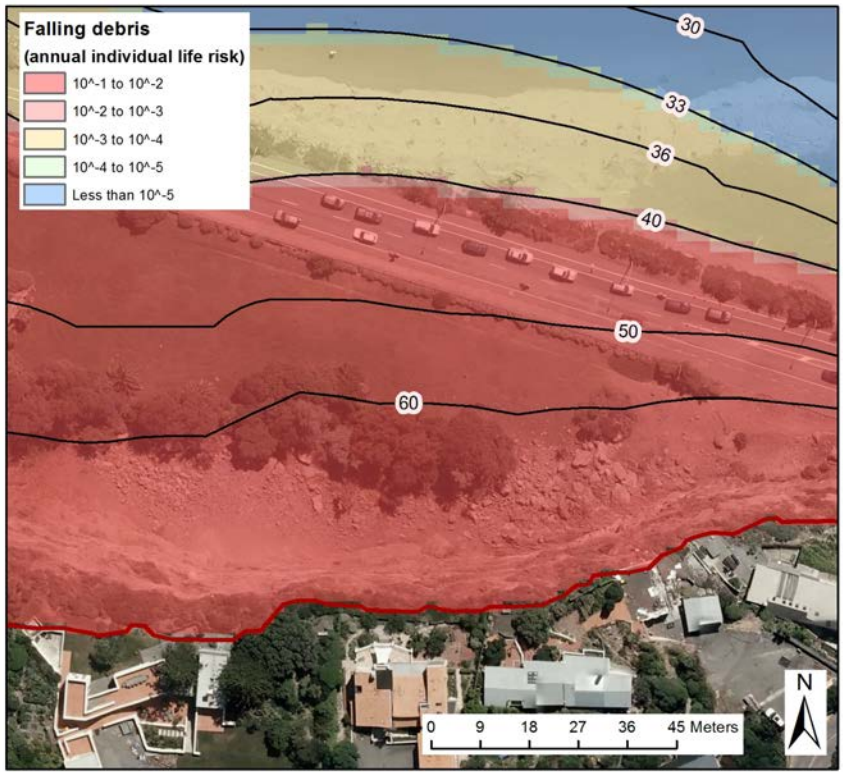

Figure 40 Example of the annual individual fatality risk zones (considering all earthquake and non-seismic events) calculated for debris avalanches. The black lines are the Fahrboeschung angles with the numbers shown in degrees.

6.8 Illustrative example – cliff top recession

An example from Whitewash Head can be used to explain the cliff top recession risk analysis process. Consider the risk to a person falling from the top of the cliff as the ground collapses beneath them. The risk to the person decreases with distance away from the cliff edge. This is because the proportion of cliff top that collapses in any event decreases away from the cliff edge (Figure 16), i.e., the worst place to stand on the cliff top during an earthquake is at the cliff edge.

What is the risk to life of a person falling who happens to be standing within the 2 m cliff top recession zone (i.e., 1 – 2 m back from the cliff edge) at Whitewash Head while the representative event in the 1.0 – 2.0 g peak ground acceleration band occurs?

The estimated volume of the representative event in this band is about 80,541 m^3 (Table 27), which would cause about 1,530 m^2 of the cliff top to fall (assuming a ratio of about 0.02). The proportion of the 2 m wide area that could collapse is estimated to be about 15% of the total collapse area (Table 10), which is estimated from the proportions of cliff top lost during the 13th June 2011 earthquake. This would mean that about 227 m^2 (or a strip 227 m long and 1 m wide) of the 2 m zone would fall away during an event of this size.

Step 3a: Estimate the annual frequency of the event occurring within the 1.0 – 2.0 g peak ground acceleration band, using the composite seismic hazard model, where $P_{(H)}$ = 0.016 (about 1 in 60 years using the next 1-year composite seismic hazard model results).

Step 3b: Estimate the probability of a person falling over the edge of the cliff (if present) given one square metre of cliff top collapsing (A_{CT}) in the 2 m zone ($P_{R1(S:H)}$) using Eq. [4a], where the area of ground occupied by a typical person (A_P) = 2.0 m^2 and the area of the 2 m zone ($A_{(1-2)}$), parallel to the cliff edge, which is 1005 m long, is = 1005 m x 1 m = 1005 m^2 .

$$P_{R1(S:H)} = \frac{A_P}{A_{(1-2)}} \qquad \text{[Eq. 5a]}$$

$$P_{R1(S:H)} = \frac{2}{1005} = 0.002 \qquad \text{[from Eq. 5a]}$$

Estimate the probability of person falling (if present) if *N* square metres of cliff top in the 2 m zone were to collapse, using Eq. [4b], where:

$$P_{RN(S:H)} = 1 - (1 - P_{R1(S:H)})^N \qquad \text{[Eq. 5b]}$$

$$P_{RN(S:H)} = 1 - (1 - 0.002)^{227} = 0.364 \qquad \text{[from Eq. 5b]}$$

Step 3c: Estimate the probability that the person is present and falls considering the time spent at home, assuming there is a slim chance that the person can escape ($P_{(T:S)}$ = 0.9).

Step 3d: Estimate the probability of the person (if present) dying as a result of falling ($V_{(D:T)}$ = 1.0).

Step 4: Multiply steps 3a, 3b, 3c and 3d to calculate the annual individual fatality risk from the representative earthquake in the 1.0 – 2.0 g peak ground acceleration band, to someone who spends the year standing 1 – 2 m back from the cliff edge. Therefore the annual individual fatality risk ($R_{(BAND)}$) to a person is:

$$\mathrm{R}_{(\text{1-2g PGA BAND})} = 0.016 \times 0.364 \times 0.9 \times 1.0 = 5.4 \times 10^{-3} \qquad \text{[from Eq. 1]}$$

Step 5: Repeat Steps 3 to 4 for each 1 m zone back from the cliff edge for each of the considered bands (earthquake and non-seismic), and sum the results for each zone to estimate the total risk to the life of an individual at a given location (Table 30).

Step 6: The annual individual fatality risk considering all events was calculated for each zone back from the cliff edge for each site, following the steps outlined in the example. These values were then modelled using ArcGIS®. ArcGIS is used to interpolate between the risks calculated at given zones back from the cliff edge so as to produce contours of equal risk

(Figure 41). The annual individual fatality risk zones were projected back from the current cliff edge location, as derived from the 2011c LiDAR survey. Contours were developed for logarithmic classes, e.g., 10^{-2} to 10^{-3}, 10^{-3} to 10^{-4} of individual risk values. The Christchurch City Council building footprints were then overlain on the risk model and each dwelling was assigned a risk value, based on the highest risk value that the building intersected.

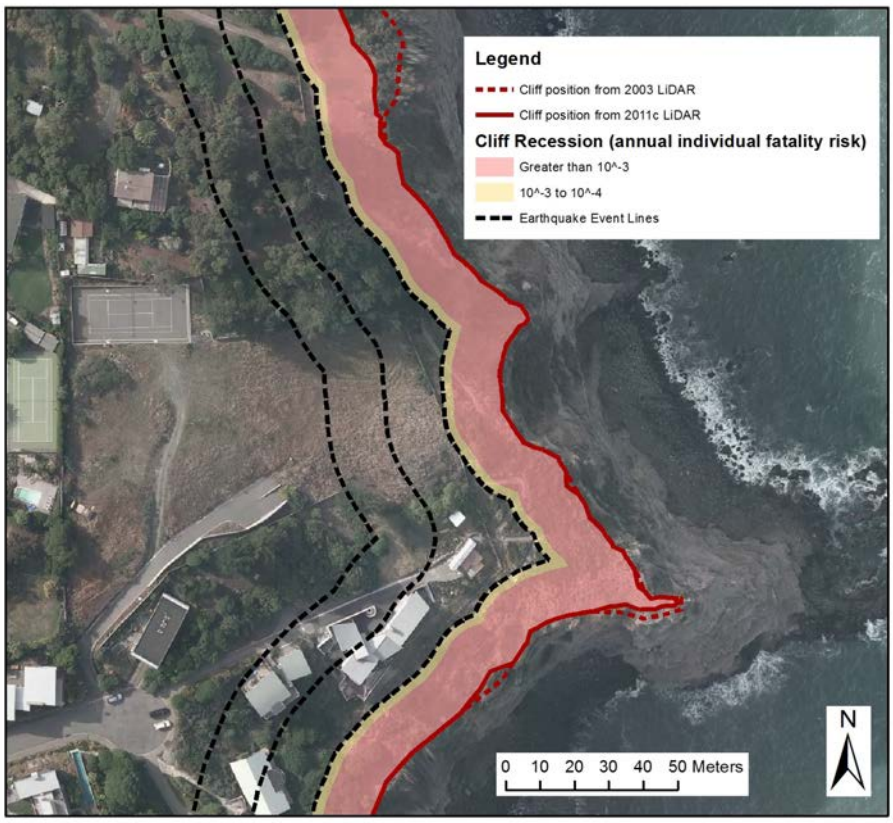

Figure 41 Illustrative example of the estimated annual individual fatality risk (considering all events) zones calculated for cliff top recession.

The above analysis defines *annual* individual fatality risk zones for cliff top recession. However, as discussed in section 4.3, cliff top recession is likely to occur during discrete events. Therefore, if a portion of the cliff top collapses in a future event (e.g., an earthquake), then the annual individual fatality risk zones will accordingly migrate parallel with the new cliff top edge. An example is shown in Figure 42.

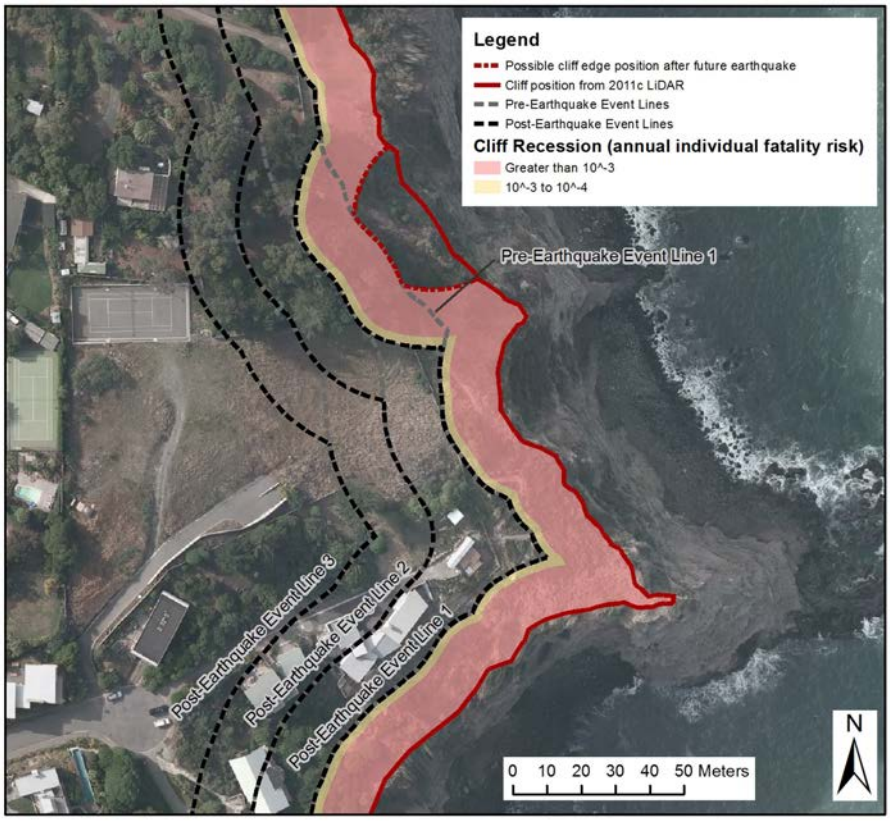

Figure 42 An example of the how the annual individual fatality risk zone may migrate after a future earthquake causes a partial cliff collapse.

To take these issues into account and to make the risk assessment robust to future cliff top recession, "earthquake event" lines have been shown on the maps. These lines represent the possible maximum recession position of the cliff edge given future earthquakes with associated peak ground accelerations in the 2.0 g range, similar to the 22nd February and 13th June 2011 earthquakes. These lines do not mean that the entire cliff in front of them, and extending to the cliff edge, is likely to recess, but that any given part of the cliff in this area could recess back to this line given a future event of this magnitude, such as shown in the example in Figure 42. Thus each line can be considered a worse-case-scenario in an individual earthquake. The width of each earthquake-event zone is equal to the width of the maximum cliff top recession recorded during the 2010/2011 Canterbury earthquakes, per site. As a "rule of thumb" the width (in metres) of the life-risk zone plus one earthquake event line approximates to about one third of the cliff height.

Table 30 The cliff top recession annual individual fatality risk analysis method results for the 2 m cliff top zone at Whitewash Head

	Parameter estimated	EARTHQUAKES (1-year model results) Peak ground acceleration band					NON-SEISMIC EVENTS Time bands				
		0.1 - 0.4 g	0.4 - 1 g	1 - 2 g	>2 g	ALL earthquakes	1 - 15 years	15 - 100 years	100 - 1000 years	>1000 years	ALL non-seismic events
A	**$P_{(H)}$** Annual frequency of event (years)	0.60	0.17	0.02	0.001		0.55	0.02	0.001	0.00005	
B	Expected volume of debris leaving source for representative event in band (m^3)	10	2,365	80,541	1,370,569		5	170	1,500	10,000	
C	Area of cliff top collapsing (m^2)	0.2	45	1,530	26,041		0.1	3	29	190	
D	Relative proportion of cliff top collapsing at a given distance back from cliff edge	0.15	0.15	0.15	0.15		0.15	0.15	0.15	0.15	
E	Expected area (m^2) of cliff top collapsing for representative event in band (CxD)	0.03	7	227	3862		0.01	0	4	28	
F	Probability a person falls given one m^2 of cliff top collapsing	$2x10^{-3}$	$2x10^{-3}$	$2x10^{-3}$	$2x10^{-3}$		$2x10^{-3}$	$2x10^{-3}$	$2x10^{-3}$	$2x10^{-3}$	
G	**$P_{(S:H)}$** Probability of person falling given N m^2 of cliff top collapsing at this location for this event	$6x10^{-5}$	$1x10^{-2}$	$4x10^{-1}$	1.0		$3x10^{-5}$	$1x10^{-3}$	$8x10^{-3}$	$6x10^{-2}$	
H	**$P_{(T:S)}$** Probability of a person being present	0.9	0.9	0.9	0.9		0.9	0.9	0.9	0.9	
I	**$V_{(D:T)}$** Probability of a person dying as a result of falling	1	1	1	1		1	1	1	1	
R	**$R_{(LOL)}$** Annual risk (death) all bands for given location (AxGxHxI)	$3x10^{-5}$	$2x10^{-3}$	$5x10^{-3}$	$7x10^{-4}$	**$8x10^{-3}$**	$1x10^{-5}$	$2x10^{-5}$	$8x10^{-6}$	$3x10^{-6}$	**$4x10^{-5}$**
	GRAND TOTAL RISK (ALL EVENTS)					**$8x10^{-3}$**					

6.9 Cliff top deformation risk

The annual individual fatality risk to a person in an area susceptible to cliff top deformation or landsliding has been simply assessed using a similar analysis method as that adopted for cliff top recession. The probability of a crack developing somewhere at the cliff edge is a function of the annual frequency of the triggering event. As the majority of the main cracks were mapped following the 22nd February 2011 earthquakes the annual individual fatality risk to a person falling into a crack generated by the 22nd February 2011 earthquakes can be assessed. This can then be used to compare against the risk from cliff top recession and debris avalanches, as the risk from these two hazards is dominated by an event within the 1.0 – 2.0 g peak ground acceleration range, which is similar to the accelerations associated with the 22nd February 2011 Christchurch Earthquake.

The annual individual fatality risk to a person falling into a crack, or from a building collapsing in response to cracks formed by the representative event in the 1.0 – 2.0 g peak ground acceleration band is much lower (about 10^{-7}/year for all areas) than to a person falling over the cliff edge as the cliff recesses (greater than 10^{-3} – 10^{-4}/year), or from being hit by debris from a debris avalanche (about 10^{-1} – 10^{-4}/year), triggered by a comparable event. This simple analysis does not take into account the possibly that differential movement across cracks could cause a building to collapse killing the occupant(s).

This analysis does not take into account that the cracks at the cliff top could develop into a cliff collapse scenario or that the landslide areas could become more mobile. In such instances the cracking could be significantly worse, and in some cases involve the entire failure of the cliff top. At present it is not possible to analyse whether these are realistic scenarios.

7.0 RESULTS

The results from the risk analysis for Redcliffs are summarised in Tables 31 to 34. The values of risk are the annual individual fatality risk of an individual located in either the debris avalanche (Fahrboeschung) or cliff top recession zones used in the analyses, adopting the next 1-year (median) composite seismic hazard model results. Redcliffs is representative of the results from the other sites.

Table 31 Contribution to annual individual fatality risk from debris avalanches across each earthquake peak ground acceleration band (Redcliffs), using the median 1-year composite seismic hazard model results, and $P_{(T:S)}$ = 1.0 and $V_{(D:T)}$ = 1.0.

Fahrboeschung angle (º)	Earthquake peak ground acceleration band				Total earthquake annual individual fatality risk
	0.1 – 0.4 g	0.4 – 1 g	1 – 2 g	2 – 5 g	
20	0	0	0	0	0
30	0	0	0	0	0
33	0	0	0	0	0
36	$1x10^{-5}$	$2x10^{-4}$	$6x10^{-4}$	$4x10^{-4}$	$1x10^{-3}$
40	$1x10^{-4}$	$1x10^{-3}$	$4x10^{-3}$	$8x10^{-4}$	$6x10^{-3}$
50	$7x10^{-3}$	$7x10^{-2}$	$2x10^{-2}$	$8x10^{-4}$	$1x10^{-1}$
60	$3x10^{-2}$	$2x10^{-1}$	$2x10^{-2}$	$8x10^{-4}$	$2x10^{-1}$

Table 32 Contribution to annual individual fatality risk from debris avalanches across each non-seismic event band (Redcliffs), adopting $P_{(T:S)}$ = 1.0 and $V_{(D:T)}$ = 1.0.

Fahrboeschung angle (º)	Non-seismic band				Total non-seismic annual individual fatality risk
	1 – 15 years	15 – 100 years	100 – 1,000 years	> 1,000 years	
20	0	0	0	0	0
30	0	0	0	0	0
33	0	0	0	0	0
36	$4x10^{-6}$	$5x10^{-6}$	$2x10^{-6}$	$8x10^{-7}$	$1x10^{-5}$
40	$3x10^{-5}$	$4x10^{-5}$	$2x10^{-5}$	$5x10^{-6}$	$1x10^{-4}$
50	$2x10^{-3}$	$2x10^{-3}$	$6x10^{-4}$	$3x10^{-5}$	$5x10^{-3}$
60	$1x10^{-2}$	$8x10^{-3}$	$7x10^{-4}$	$3x10^{-5}$	$2x10^{-2}$

Table 33 Contribution to annual individual fatality risk from cliff top recession across each earthquake peak ground acceleration (PGA) band (Redcliffs), using the 1-year composite seismic hazard model results and $P_{(T:S)}$ = 0.9 and $V_{(D:T)}$ = 1.0.

Distance from current cliff edge (m)	Earthquake peak ground acceleration band				Total earthquake annual individual fatality risk
	0.1 – 0.4 g	0.4 – 1 g	1 – 2 g	2 – 5 g	
1	$2x10^{-4}$	$2x10^{-3}$	$5x10^{-3}$	$7x10^{-4}$	$8x10^{-3}$
2	$9x10^{-5}$	$1x10^{-3}$	$3x10^{-3}$	$7x10^{-4}$	$5x10^{-3}$
3	$3x10^{-5}$	$5x10^{-4}$	$1x10^{-3}$	$6x10^{-4}$	$3x10^{-3}$
4	$1x10^{-5}$	$2x10^{-4}$	$6x10^{-4}$	$3x10^{-4}$	$1x10^{-3}$
5	$5x10^{-6}$	$7x10^{-5}$	$2x10^{-4}$	$2x10^{-4}$	$4x10^{-4}$
6	$3x10^{-6}$	$3x10^{-5}$	$1x10^{-4}$	$8x10^{-5}$	$2x10^{-4}$
7	$3x10^{-7}$	$4x10^{-6}$	$1x10^{-5}$	$1x10^{-5}$	$3x10^{-5}$
8	0	0	0	0	0

Table 34 Contribution to annual individual fatality risk from cliff top recession across each non-seismic event band (Redcliffs), adopting $P_{(T:S)}$ = 0.9 and $V_{(D:T)}$ = 1.0.

Distance from current cliff edge (m)	Non-seismic band				Total non-seismic annual individual fatality risk
	1 to 15 years	15 to 100 years	100 to 1,000 years	>1,000 years	
1	$5x10^{-5}$	$7x10^{-5}$	$3x10^{-5}$	$8x10^{-6}$	$2x10^{-4}$
2	$3x10^{-5}$	$3x10^{-5}$	$2x10^{-5}$	$5x10^{-6}$	$8x10^{-5}$
3	$1x10^{-5}$	$2x10^{-5}$	$7x10^{-6}$	$2x10^{-6}$	$4x10^{-5}$
4	$6x10^{-6}$	$7x10^{-6}$	$3x10^{-6}$	$1x10^{-6}$	$2x10^{-5}$
5	$2x10^{-6}$	$2x10^{-6}$	$1x10^{-6}$	$3x10^{-7}$	$5x10^{-6}$
6	$5x10^{-7}$	$6x10^{-7}$	$3x10^{-7}$	$9x10^{-8}$	$2x10^{-6}$
7	$4x10^{-8}$	$5x10^{-8}$	$2x10^{-8}$	$7x10^{-9}$	$1x10^{-7}$
8	0	0	0	0	0

The results from the risk analysis for all sites are summarised in Tables 35 to 38, adopting $P_{(T:S)}$ and $V_{(D:T)}$ values of 1.0 and 1.0 respectively for debris avalanche risk and $P_{(T:S)}$ and $V_{(D:T)}$ values of 0.9 and 1.0 respectively for cliff top recession risk. For earthquake events the 1-year median composite seismic hazard model results have been used.

Table 35 Annual individual fatality risk from earthquake-triggered debris avalanches (1-year seismicity, all sites).

Site	Fahrboeschung angle (º)						
	20	**30**	**33**	**36**	**40**	**50**	**60**
Redcliffs	0	0	0	$1x10^{-3}$	$6x10^{-3}$	$1x10^{-1}$	$2x10^{-1}$
Shag Rock Reserve	0	0	0	$2x10^{-4}$	$5x10^{-4}$	$8x10^{-2}$	$2x10^{-1}$
Nayland Street	0	0	0	0	$3x10^{-2}$	$6x10^{-2}$	$1x10^{-1}$
Wakefield Avenue	0	0	0	$3x10^{-3}$	$1x10^{-2}$	$8x10^{-2}$	$2x10^{-1}$

Table 36 Annual individual fatality risk from debris avalanches triggered by non-seismic events.

Site	Fahrboeschung angle (º)						
	20	**30**	**33**	**36**	**40**	**50**	**60**
Redcliffs	0	0	0	$6x10^{-6}$	$5x10^{-5}$	$3x10^{-3}$	$1x10^{-2}$
Shag Rock Reserve	0	0	0	$1x10^{-6}$	$3x10^{-6}$	$2x10^{-3}$	$1x10^{-2}$
Nayland Street	0	0	0	0	$8x10^{-4}$	$2x10^{-3}$	$3x10^{-3}$
Wakefield Avenue	0	0	0	$2x10^{-5}$	$7x10^{-5}$	$2x10^{-3}$	$7x10^{-3}$

Table 37 Annual individual fatality risk from earthquake-triggered cliff top recession (1-year seismicity, all sites).

Site	Recession (m) from current cliff edge																
	1	2	3	4	5	6	7	8	9	10	11	12	13	14	15	16	17
Redcliffs	$8x10^{-3}$	$5x10^{-3}$	$2x10^{-3}$	$1x10^{-3}$	$4.x10^{-4}$	$2x10^{-4}$	$3x10^{-5}$	0	0	0	0	0	0	0	0	0	0
Shag Rock Reserve	$4x10^{-3}$	$4x10^{-3}$	$3x10^{-3}$	$3x10^{-3}$	$2x10^{-3}$	$2x10^{-3}$	$2x10^{-3}$	$2x10^{-3}$	$1x10^{-3}$	$9x10^{-4}$	$5x10^{-4}$	$3x10^{-4}$	$1x10^{-4}$	0	0	0	0
Nayland Street	$8x10^{-3}$	$7x10^{-3}$	$4x10^{-3}$	0	0	0	0	0	0	0	0	0	0	0	0	0	0
Wakefield Avenue	$1x10^{-2}$	$6x10^{-3}$	$4x10^{-3}$	$2x10^{-3}$	$6x10^{-4}$	0	0	0	0	0	0	0	0	0	0	0	0
Whitewash	$9x10^{-3}$	$8x10^{-3}$	$7x10^{-3}$	$6x10^{-3}$	$6x10^{-3}$	$5x10^{-3}$	$4x10^{-3}$	$4x10^{-3}$	$3x10^{-3}$	$2x10^{-3}$	$2x10^{-3}$	$1x10^{-3}$	$9x10^{-4}$	$6x10^{-4}$	$5x10^{-4}$	$2x10^{-4}$	$2x10^{-5}$

Table 38 Annual individual fatality risk from cliff top recession triggered by non-seismic events

Site	Recession (m) from current cliff edge																
	1	2	3	4	5	6	7	8	9	10	11	12	13	14	15	16	17
Redcliffs	$1x10^{-4}$	$8x10^{-5}$	$3x10^{-5}$	$1x10^{-5}$	$5x10^{-6}$	$2x10^{-6}$	$3x10^{-7}$	0	0	0	0	0	0	0	0	0	0
Shag Rock Reserve	$8x10^{-5}$	$6x10^{-5}$	$5x10^{-5}$	$5x10^{-5}$	$3x10^{-5}$	$3x10^{-5}$	$3x10^{-5}$	0	$2x10^{-5}$	$1x10^{-5}$	$7x10^{-6}$	$4x10^{-6}$	$1x10^{-6}$	0	0	0	0
Nayland Street	$2x10^{-4}$	$2x10^{-4}$	$8x10^{-5}$	0	0	0	0	0	0	0	0	0	0	0	0	0	0
Wakefield Avenue	$2x10^{-4}$	$8x10^{-5}$	$4x10^{-5}$	$2x10^{-5}$	$6x10^{-6}$	0	0	0	0	0	0	0	0	0	0	0	0
Whitewash	$5x10^{-5}$	$4x10^{-5}$	$4x10^{-5}$	$3x10^{-5}$	$3x10^{-5}$	$2x10^{-5}$	$2x10^{-5}$	$1x10^{-5}$	$1x10^{-5}$	$8x10^{-6}$	$5x10^{-6}$	$4x10^{-6}$	$3x10^{-6}$	$2x10^{-6}$	$2x10^{-6}$	$6x10^{-7}$	$7x10^{-8}$

7.1 Validation of the model against known fatalities

Three fatalities from debris avalanches were recorded in the areas covered by this assessment, two at Redcliffs and one at Wakefield Avenue. The number of deaths estimated by the model for these areas using the volumes of debris that fell on the 22nd February 2011, and assuming $P_{(T:S)}$ and $V_{(D:T)}$ values of 1.0 and 1.0 respectively, are one at Redcliffs and one at Wakefield, assuming 0.5 people present per dwelling during the earthquake, estimated from the 2006 census data collated by Statistics New Zealand. If night time occupancy rates are used, where the average number of people per dwelling is estimated as 2.5, the number of fatalities would be about 5 at Redcliffs and 5 at Wakefield Avenue.

These are high numbers, considering only about 75 properties are within the areas analysed. In comparison, the number of fatalities predicted by the rockfall (boulder roll model) risk assessments, which includes about 790 dwellings, from the 22nd February 2011 earthquakes is about 1 for day-time occupancy rates and about 20 for night-time.

These comparisons provide a high degree of confidence that the risk analysis methodology can adequately predict the consequences of debris avalanches triggered by the 22nd February 2011 earthquakes.

Nobody died from cliff top recession, however, one of the authors narrowly escaped falling from the cliff top at Whitewash Head, as the cliff edge recessed during the 13th June 2011 earthquake.

7.2 Model sensitivities and uncertainties

In this section the sensitivity of the model to key uncertainties and reliability of the assessments are identified. Four particular sets of assumptions (or "scenarios") are then considered, as in the opinion of GNS Science they span the range of possibilities that Christchurch City Council would wish to consider in addressing this time-varying and uncertain risk.

7.2.1 Sensitivity to key uncertainties

The sensitivity of the estimated risk has been assessed to the following changes:

1) Using the composite seismic hazard model results for the next 50-years instead of the next 1-year

2) Changes to the volumes of debris triggered by the representative events for both seismic and non-seismic triggers (i.e., using scale factors to increase the volume of debris).

    a. For seismically triggered debris avalanches this scale factor takes into account any variation in the relationship between peak ground acceleration and volume leaving the slope.

    b. For non-seismically triggered debris avalanches this scale factor takes into account the likely increased rates of cliff collapses due to the now dilated and highly disturbed nature of the cliffs.

c. The number of boulders making up each cubic metre of debris - increasing from 2 to 4 blocks per m^3.

3) Changes to the area of cliff top recessing as a result of the representative event for both earthquake and non-seismic triggers (i.e., using scale factors to increase the area lost).

   a. For earthquake triggered recession this takes into account any variation in the relationship between peak ground acceleration and volume leaving the slope and the ratio of volume to cliff top area lost.

   b. For non-seismically triggered recession this scale factor takes into account the likely increased rates of cliff collapse due to the now dilated and highly disturbed nature of the cliffs.

   c. The relationship between the volume leaving the cliffs and the area of cliff top lost from a ratio of 0.019 to a ratio of 0.025, i.e., for 100 m^3 of debris leaving the cliff face the area lost would increase from 1. 9 m^2 to 2.5 m^2.

4) The probability of a person being present at the top of the cliff changing from 70% to 100% of the time.

5) For debris avalanches the diameter of a person is increased from 1 m to 2 m, and for cliff top recession the area occupied by a person is increased from 1 m^2 to 2 m^2.

6) The vulnerability of a person if hit changing from 0.5 to 1.0.

The risks have been calculated per Fahrboeschung angle and cliff top recession zone, per site. Details of seven different possible scenarios, their input parameters and the impacts on the estimated risk are shown in Tables 39 and 40. The impact on the risk is calculated by comparing each successive scenario, from an initial base-line scenario.

Table 39 Debris avalanche risk sensitivity analysis and the parameters used. The impact is calculated between successive tests, with test 1 providing the baseline risks. EQ is Earthquake.

Sensitivity test number	Seismic hazard model results[1]	EQ debris scale factor	Non-seismic debris scale factor	Number of blocks per m^3 of debris	Probability person present	Vulnerability of a person if hit	Diameter of a person	Factor by which the risk increases)[2]
1	50-year	1	1	2	70%	50%	1 m	-
2	50-year	1.5	1	2	70%	50%	1 m	1.1
3	50-year	1.5	2	2	70%	50%	1 m	1.2
4	50-year	1.5	2	4	70%	50%	1 m	1.4
5	50-year	1.5	2	4	70%	100%	1 m	2.0
6	1-year	1.5	2	4	70%	100%	1 m	3.4
7	1-year	1.5	2	4	100%	100%	1 m	1.4
8	1-year	1.5	2	4	100%	100%	2 m	1.1

[1]The composite seismic hazard model results used are the medians generated by the model
[2]The factors by which the risks change are calculated successively from the previous test

Table 40 Cliff top recession risk sensitivity analysis and the parameters used. The impact is calculated between successive tests, with test 1 providing the baseline risks. EQ is Earthquake.

Sensitivity test number	Seismic hazard model results[1]	EQ debris scale factor	Non-seismic debris scale factor	Ratio of volume to area	Probability person present	Vulnerability of a person if hit	Area occupied by a person	Factor by which the risk is multiplied)[2]
1	50-year	1	1	0.19	70%	50%	1 m	-
2	50-year	1.5	1	0.19	70%	50%	1 m	1.4
3	50-year	1.5	2	0.19	70%	50%	1 m	1.03
4	50-year	1.5	2	0.25	70%	50%	1 m	1.2
5	50-year	1.5	2	0.25	70%	100%	1 m	2.0
6	1-year	1.5	2	0.25	70%	100%	1 m	5.1
7	1-year	1.5	2	0.25	100%	100%	1 m	1.4
8	1-year	1.5	2	0.25	100%	100%	2 m	1.2

[1]The composite seismic hazard model results used are the medians generated by the model
[2]The factors by which the risks change are calculated successively from the previous test

The results show that the largest impact on the risk is from the composite seismic hazard model. The annual frequency of a cliff collapse-triggering earthquake occurring is much higher in the next few years, and will decrease by about 3 to 5 times over the next decade. All of the other parameters individually cause the risk to change by modest factors of about 1.2 to 1.4. The risk that would be estimated using the parameters in test number 8 is about 15 to 22 times greater (larger than one order of magnitude) than that estimated using the parameters in test number 1.

7.2.2 How reliable are the results?

Potentially significant uncertainties noted and their likely implications for risk are summarised in Table 41.

Table 41 Uncertainties and their implications for risk

Issue	Direction & Scale of Uncertainty	Implications for Risk
a) Under-prediction of annual frequency for a given peak ground acceleration by the composite seismic hazard model.	Upward, potentially considerable – but geomorphological evidence in the Port Hills suggests there is a sensible cap that can be placed on the upward uncertainty, which is about an order of magnitude.	Risk due to earthquakes could be systematically under- or over-estimated.
b) Choice of whether to use average earthquake annual frequencies for next 50-years, or higher frequencies for next 1-year.	Use of 'next 1-years' figure builds in factor of about 3 to 5 pessimism for longer term.	Longer term risk is potentially 3 to 5 times lower.

	Issue	Direction & Scale of Uncertainty	Implications for Risk
c)	Volume of debris produced by the 0.4 – 1.0 g and 1.0 – 2.0 g peak ground acceleration events.	Factor of about 10 times (one order of magnitude) uncertainty in either direction.	c) and d) combine to give a factor of about 3 and 6 uncertainty in the upward direction, but lower in the downward direction, about 0.03 and 0.1 for debris avalanches and cliff top recession respectively.
d)	Volume of debris produced by events in the > 2.0 g peak ground acceleration band.	Factor of about 10 times (one order of magnitude) uncertainty in either direction.	
e)	Volume of debris produced by other (non-seismic) events.	Factors of 2 – 3+ uncertainty either way in the annual frequency, but constrained by the geomorphology suggesting such extreme events (that dominate the risk) are at the medium and low frequency end. However, current frequency of debris production is likely to be higher due to the disturbed nature of the rock masses. It may take many years for the frequency to drop back to pre-earthquake rates	Factor of 1.1 – 1.2 uncertainty in the upward direction, but lower in the downward direction.
f)	Ratio between the volume leaving the face and area of cliff top recessing	Factors of 2 – 3+ uncertainty either way. However, ratios may increase as the rock masses become more disturbed as the earthquakes continue.	Factor of about 1.2 uncertainty in the upward direction, but lower in the downward direction.
g)	Volume of debris travelling downslope and passing a given shadow angle.	Less than a factor of 2 uncertainty either way.	Factor of about 1.4 uncertainty in the upward direction, but lower in the downward direction.
h)	Debris travelling further than observed during the 2010/2011 Canterbury earthquakes	Would push the risk zones further out from the toe of the slope. The observed distances that debris travelled are thought to be representative of the distances debris triggered by future events could travel. However, there is a possibility that future debris could go further as talus is building up at the toe of each cliff which tends to act as a ramp that can increase the runout distance. This assumes that future failures are going to occur in the same locations.	Would push the risk zones further out from the 33° Fahrboeschung zones, which are the current limits of mapped debris.
i)	Local effects on debris runout such as channeling or topographic sheltering	The models are site scale and cannot take into account local small-scale site effects that could either enhance or reduce the estimated risk. Impact not known	Could increase or reduce the risk. Ground truthing results showed this to be of no significance.
j)	Occupancy (proportion of time people are at home)	Assumption of 70% occupancy instead of 100% would modestly decrease estimated risk.	Would decrease by a factor of about 1.4.
k)	Probability person killed	Uncertainty potentially reducible but unlikely	A change in the

Issue	Direction & Scale of Uncertainty	Implications for Risk
if struck by debris	to make large difference – will always be fairly large given the volumes of debris involved or height of fall.	vulnerability from 50 to 100% would increase the risk by a factor of about 2.0.

8.0 DISCUSSION

8.1 Particular risk assessment scenarios

The largest impact on the risk is from the composite seismic hazard model. To take this into account four particular risk assessment scenarios have been developed, using the median base case (50th percentile) and upper case (84th percentile) estimates of seismic risk over the next 1-year and 50-year periods. The other parameters represent GNS Sciences "best" and "reasonable but more cautious" estimates based on the range of uncertainties identified in the available data at the time of writing (Table 39).

The results for each scenario were modelled using the ArcGIS programme as described in Section 6 above to produce the risk contour maps, and the numbers of homes falling into different risk bands were derived from these maps (Table 42). Figures 43 and 44 are graphical representations of the impact of the assessment selection on the risk from debris avalanches and cliff top recession, expressed as the estimated number of residential homes in each risk category, for each assessment scenario.

Table 42 Details of the four risk scenarios developed for this assessment. EQ is Earthquake.

Scenario	Seismic model results	EQ debris volume scale factor	Other debris volume scale factor	Probability person present	Vulnerability of a person if hit
A	50-year base	1	2	90%	100%
B	50-year upper	1	3	100%	100%
C	1-year base	1	2	90%	100%
D	1-year upper	1	3	100%	100%

The scenarios range from Scenario A, the most optimistic with regards to the parameters adopted, to Scenario D, the most pessimistic assessment. Scenario D may be overly pessimistic, but has been included to illustrate the impact that increased levels of seismicity and conservative assumptions could realistically have. Scenario A is at the other end of the spectrum and is not considered reasonable at the current time of writing, considering the current increased level of seismic activity.

The most important uncertainties identified in this assessment are those connected with the

frequency of seismic events, and how the frequency of these events changes over time. The different return periods estimated for earthquakes in the 1 – 2 g peak ground acceleration range (the range experienced by most suburbs in the 2011 events generating cliff collapses), are:

- about 300 years using the median 50-year seismic model results;
- about 200 years using the 84th percentile [5] 50-year seismic model results;
- about 60 years using the median 1-year seismic model results; and
- about 40 years using the 84th percentile 1-year seismic model results.

These return periods show:

a) the increase in expected likelihood of severe earthquakes now that hazard models have been updated to include the 2010/11 Christchurch earthquakes (prior to these events an earthquake ground motion on this scale would have been predicted to be a once in thousands of years event);

b) the substantial current elevation in risk levels compared to the longer-term levels to which they will decay in a few years' time (1-year versus 50-year comparisons); and

c) the importance of uncertainty in the frequency of events predicted using the best available models of seismicity.

The risk model preferred by GNS Science (Scenario C, Table 42) is one which uses the higher risk 1-year base seismic model, and includes allowance for an expected increase in the numbers of boulders generated from "non-seismic" events in the near future because the rockfall-source areas are now in a disturbed state.

This scenario provides a reasonably central estimate of the current, elevated level of risk. As time progresses, any decisions made on the basis of this scenario will become more defensible with respect to the uncertainties inherent in any assessment about future cliff collapse hazard.

[5] The composite seismic hazard model used take account of the variability in ground shaking for different earthquakes and can predict any required percentile of the statistical distribution of shaking expected from all the earthquakes included in the model. In other contexts such as dam safety in New Zealand, a precedent has been established for using the median of these distributions (central estimate) as a basis for economic risk assessment, and using the 84th percentile (to provide a more precautionary, higher estimate of seismic event frequency) for life safety risk assessment.

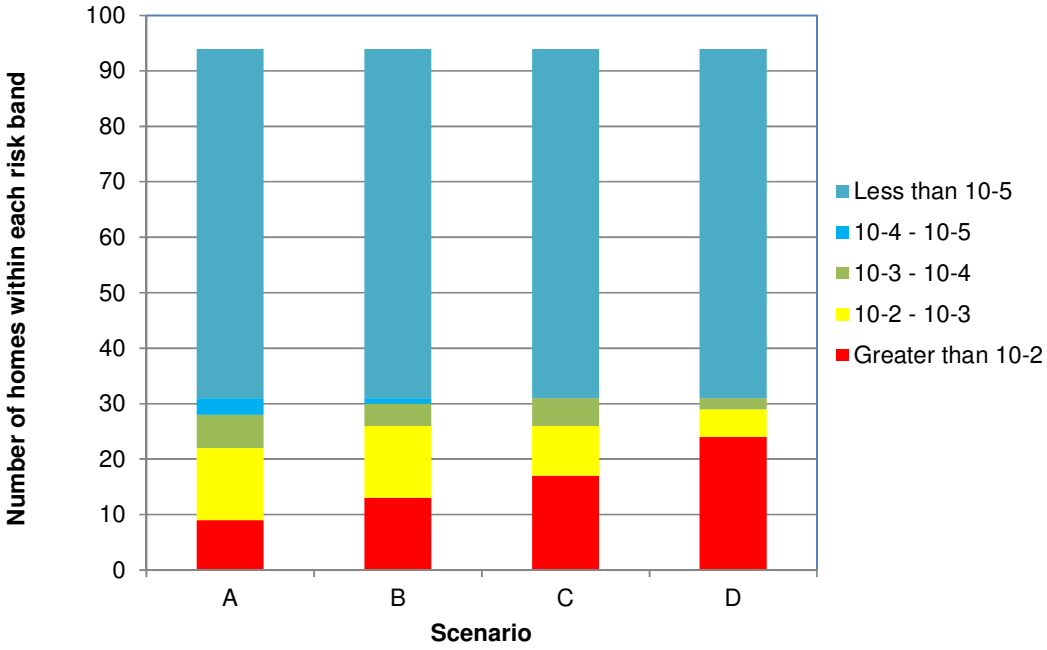

Figure 43 Numbers of dwellings estimated by band of annual individual fatality risk (AIFR) for each assessment scenario – debris avalanches only. The total number of homes in the areas analysed is 91 (between the toe of the cliff and the 20° Fahrboeschung angle).

The results in Figure 43 show that the number of dwellings within the annual individual fatality risk $>10^{-3}$ zone are similar for all scenarios, and that between the scenarios the number of dwellings in the annual individual fatality risk $>10^{-4}$ zone are almost identical, about 30 dwellings. These results indicate that the number of properties exposed to levels of risk $\geq 10^{-3}$ do not change significantly between the risk scenarios, therefore the choice of risk-scenario parameters used have little impact on the numbers of homes within each risk zone.

For debris avalanches the annual individual fatality risk for those dwellings within Fahrboeschung angles >33° are $>10^{-4}$. These risks are a function of the volume of debris leaving the slopes for each representative event. Unlike boulder rolls that involve individual boulders, debris avalanches involve many thousands of boulders and therefore the probability of being hit by debris while occupying a Fahrboeschung zones >33° is 100% for the representative earthquakes in the 1 – 2 g and >2 g peak ground acceleration bands. Therefore at Fahrboeschung angles of <33° the annual individual fatality risk is assessed as 10^{-5} or less).

For cliff top recession the annual individual fatality risk estimated for the various scenarios also have little impact on the number of dwellings at the cliff edge that are within the different fatality risk zones (Figure 44). This is because these zones are relatively narrow with respect to the width of the dwelling. To assess the number of dwellings at risk from cliff top regression the annual individual fatality risk zones and the earthquake event lines were projected back from the current cliff top location, as derived from the 2011c LiDAR survey. Using risk Scenario C there are about 35 dwellings within the annual individual fatality risk $>10^{-3}$ risk zone, and a further about 40 dwellings within the areas affected by earthquake event lines 2 and 3 (for all areas assessed) (Table 43).

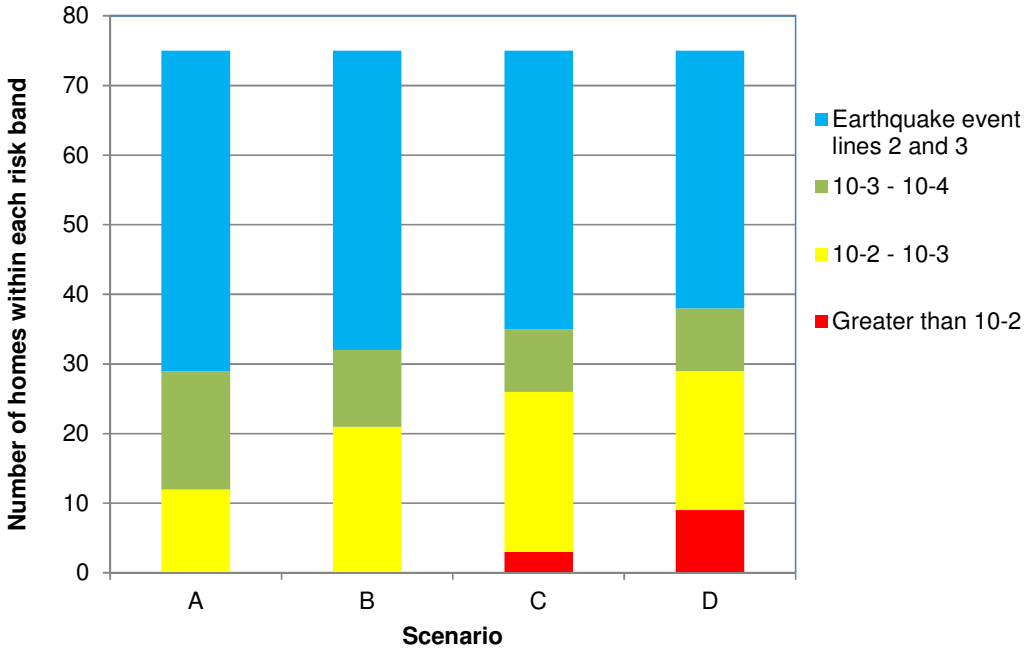

Figure 44 Numbers of homes estimated by band of annual individual fatality risk (AIFR) for each assessment scenario – cliff top recession only. Total number of homes in the areas analysed = 75.

Table 43 Width of the annual individual fatality risk zones and earthquake event lines from the cliff edge generated using risk Scenario C.

Site	i) Width of risk zone $>10^{-3}$ (m)	ii) Width of risk zone 10^{-3} to 10^{-4} (m)	iii) Width of earthquake event line 1 from the edge of ii) (m)	Combined width of i) + ii) + iii) (m)
Redcliffs	5	2	7	14
Shag Rock Reserve	10	4	14	28
Nayland Street	4	1	5	10
Wakefield Avenue	6	1	7	14
Whitewash Head	14	3	17	34

Many properties have dwellings where parts of the dwelling may be within the annual individual fatality risk $>10^{-4}$ zone and other parts within the area affected by earthquake event line 1, where this is the case the dwelling is assessed as being in the annual individual fatality risk $>10^{-4}$ risk zone, to avoid double counting. These numbers (Figure 43) include those dwellings that have already fallen from the cliff tops as a result of the 2010/2011 Canterbury earthquakes.

Risk maps have been produced using the parameters for risk Scenario C; these are shown in Appendix D. Although the annual individual fatality risk zones are insensitive to the different parameters used in the risk scenarios, those used in Scenario C have been adopted as they

are consistent with those used in the pilot rockfall risk report (Massey et al., 2012).

8.2 Field verification of risk results

Consultants of the Port Hills Geotechnical Group, in collaboration with GNS Science, carried out 'ground truthing' of the risk zones generated using the adopted risk Scenario C, to either:

1) Confirm that they were correctly defined in relation to the known rockfall source areas; or

2) Recommend changes to the risk-zone boundaries on the basis of site-specific ground conditions that were not considered at the scale of the assessments.

The field verification methodology and pro forma are contained in Appendix E. The cliff collapse annual individual fatality risk maps (in Appendix D) incorporate these changes.

8.3 Numbers of residential homes in each risk category

Using the revised "field verified" risk maps there are about 42 dwellings (including those classified as "unknown") located in the debris avalanche annual individual fatality risk zones. On the final field verified maps (shown in Appendix D), 22 dwellings expose people to annual individual fatality risks estimated to be greater than 10^{-2}/year, 12 expose people to risks between 10^{-2} to 10^{-3}/year, 3 expose people to risks between 10^{-3} to 10^{-4}/year, 1 exposes people to risks between 10^{-4} to 10^{-5}/year and 4 expose people to risks less than 10^{-5}/year.

Using the revised "field verified" risk maps there are 33 dwellings (including those classified as "unknown") located in the cliff recession annual individual fatality risk zones. On the final field verified maps (shown in Appendix D), 25 dwellings expose people to annual individual fatality risks estimated to be greater than 10^{-3}/year and 8 expose people to risks between 10^{-3} to 10^{-4}/year. There are 15 dwellings located between earthquake event lines 1 and 2, and 25 dwellings between earthquake event lines 2 and 3.

8.4 Re-evaluating the analysed risks

Given the time-varying nature of the seismic hazard it would be useful to re-evaluate the analysed risks after a period of about 10 years, to incorporate a seismic hazard model appropriate to the knowledge of that time. This would also allow data collected on the stability of the now seismically disturbed cliffs of the Port Hills to be taken into account.

8.5 Tolerability of risk

Tolerable risk criteria are discussed in Taig et al. (2012). Taig et al. (2012) provides guidance on life-risk criteria that could be applied to evaluate slope instability hazards in the Port Hills suburbs of Christchurch.

8.6 Societal risk

Societal risk is a measure of the combined risk associated with all individuals who may be exposed to the risk, and it reflects the number of people exposed. The simplest measure of societal risk is the potential total loss of lives, which is the predicted number of fatalities per

year and it is usually presented as the expected number of people killed in an event of a given frequency of occurrence (GEO, 1998).

The number of people killed as a result of the different representative earthquakes in each of the considered bands in any scenario can be estimated (Table 44). To do this, the 2006 census data (from Statistics NZ) have been used to populate the homes in the Port Hills. Using these data the mean number of people per residential dwelling in the Port Hills areas covered by this report is about 2.5, assuming night-time occupancy, and 0.4 people per dwelling assuming daytime occupancy. The numbers of residential homes in each risk category are estimated using the Christchuch City Council building footprint data.

Table 44 Estimates of societal risk from rockfalls from earthquakes in the assessed Port Hills suburban areas.

Earthquake	Earthquake frequency (assuming the median 1-year seismic model)	Average expected number of fatalities*
22nd February 2011 earthquake day-time (equivalent to the representative earthquake in the 1.0 – 2.0 g PGA band)	0.016 or 1/63 years	2 day-time
22nd February 2011 earthquake night-time (equivalent to the representative earthquake in the 1.0 – 2.0 g PGA band)	0.016 or 1/63 years	10 night-time
Representative earthquake in the >2.0 g PGA band (night-time)	0.0008 or 1/1,250 years	39 night-time
Representative earthquake in the 0.4 – 1.0 g PGA band	0.17 or 1/6 years	1 night-time

*Assumes no homes have been evacuated

In the light of the 2010/2011 Canterbury earthquakes, the greatest contributions to societal risk are from larger earthquakes of longer return periods, which have the potential to cause multiple fatalities in a single event.

9.0 CONCLUSIONS

1) Following the 4th September 2010 Darfield Earthquake, seismic activity in the Christchurch region has been considerably higher than the previous, and the expected future, long-term average, and is likely to remain higher for several decades. A seismicity model that takes into account the recent data indicates that the long- term estimates now are about an order of magnitude higher than they were before 4th September 2010. As a result, cliff-collapse fatality risk in the Port Hills is considerably higher now than it was before 4th September 2010. However, this fatality risk is expected to decrease over decades in direct proportion to any decrease in the seismic hazard.

2) The risks presented in this pilot study relate to the annual individual fatality risk from debris avalanches and cliff-top recession triggered by earthquakes or by any other causes.

3) Structurally controlled deformation of the cliffs within and between geological layers and defects and other large landslides at the cliff tops have been recognised and mapped. Any annual individual fatality risk from these features remains to be estimated when they are more fully investigated. They are not believed to pose an immediate fatality risk at their current rates and amounts of movement.

4) Precise measurements made of seismic shaking and associated volumes of cliff collapse in the assessment area resulting from aftershocks in 2011 provide very high quality data for calibration of the risk model.

5) The number of dwellings where the individual fatality risk exceeds 10^{-4} per year is similar for each of the scenarios considered. This means that the numbers are insensitive to model uncertainty and the choice of risk scenario.

6) The annual individual fatality risk decreases rapidly with distance back from the cliff edge, or distance outward from the bottom of the cliff, so that the overall numbers of dwellings affected are smaller than the numbers of dwellings at risk from boulder fall (falls of individual boulders).

7) The time-varying nature of the seismic hazard has been considered by comparing the differences in risk associated with the next 1- and 50-year composite seismic hazard model results (50-years being consistent with the design life used in typical seismic hazard analysis for residential building construction).

8) Over the next 10 years, the annual individual fatality risk of a person residing in at-risk dwelling is significantly higher (by a factor of about 3 to 5) when compared with the average over the next 50-years.

9) Using the revised “field verified” risk maps there are about 42 dwellings (including those classified as “unknown”) located in the debris avalanche annual individual fatality risk zones. On the final field verified maps (shown in Appendix D), 22 dwellings expose people to annual individual fatality risks estimated to be greater than 10^{-2}/year, 12 expose people to risks between 10^{-2} and 10^{-3}/year, three expose people to risks between 10^{-3} and 10^{-4}/year, one exposes people to risks between 10^{-4} and 10^{-5}/year and four expose people to risks less than 10^{-5}/year.

10) The risk outside of the 31° fly rock angle are assessed as being less than 10^{-6}/year.

11) Using the revised “field verified” risk maps there are 33 dwellings (including those classified as “unknown”) located in the cliff recession annual individual fatality risk zones. On the final field verified maps (shown in Appendix D), 25 dwellings expose people to annual individual fatality risks estimated to be greater than 10^{-3}/year and eight expose people to risks between 10^{-3} and 10^{-4}/year. There are 15 dwellings located between earthquake event lines 1 and 2, and 25 dwellings between earthquake event lines 2 and

3.

12) Within the analysed cliff-top recession areas, annual individual fatality risks are greater than 10^{-4}/year.

13) Cliff-top recession mainly occurs during earthquakes as witnessed during the 2010/2011 Canterbury earthquakes. It is likely that in the next decade further recession of the cliff edge will also occur during earthquakes. Each time the cliff top moves so too will the risk zones by an equal amount.

14) To take account of cliff-top recession and to make the risk assessment robust to further large earthquakes, "earthquake event" lines have been included on the maps. These lines represent the likely maximum loss of the cliff edge in future earthquakes with associated peak ground accelerations of about twice the gravitational acceleration (2 g), which is similar to those in the 22nd February and 13th June 2011 earthquakes.

15) These earthquake event lines do not mean that the entire cliff between that line and the cliff edge will recede in a single event; they mean that any given part of the cliff in this area could recede back to this line in another event of this magnitude. The distance between each earthquake event line is set equal to the width of the maximum cliff-top recession measured at each cliff after the 2010/2011 Canterbury earthquakes.

16) An additional 40 properties are, in part, within areas that could be affected in the next three earthquakes that are associated with peak ground accelerations of about two times the gravitational acceleration (2 g).

17) The annual individual fatality risk from falling into a crack near the cliff edge has been assessed using a similar analysis method to that adopted for cliff-top recession.

18) The annual individual fatality risk from falling into a crack formed in an earthquake with peak ground acceleration between one and two times gravity is about 10^{-7}. This is significantly lower than the nearby annual individual fatality risk from falling over the cliff as the cliff edge falls away, or from being hit by a debris avalanche triggered in a comparable event, both of which are higher than 10^{-4}. The estimation of individual fatality risk from falling into a crack does not take into account that differential movement across a crack could possibly cause a building to collapse. Building damage, and risk to people from collapsing buildings are not addressed in the report.

19) The report recognises that the cracks at the cliff top might evolve into cliff collapses at a later date, and that associated landslides might become more mobile. If these were to occur in some locations, such cracking could lead to failure of large areas of the cliff top and cause large debris avalanches to fall. It is not possible at present to determine the likelihood of such failures, or indeed that they can occur.

10.0 RECOMMENDATIONS

1) Christchurch City Council decide what levels of life risk will be regarded as tolerable and how Council will manage risk on land where life risk is assessed to be at various levels of

intolerability.

2) Christchurch City Council adopts the next 1-year seismicity model used in the analysis, as the number of dwellings exposing residents to particular levels of annual individual fatality risk are not expected to change significantly as the seismic hazard declines over time.

3) Given the time-varying nature of the seismic hazard, the assessed individual fatality risks should be re-evaluated after a period of about 10 years to incorporate a seismic hazard model appropriate to the knowledge of that time. This also would allow data collected on the stability of the now seismically disturbed cliffs of the Port Hills to be considered in the risk.

4) It is recommended that dwellings within areas showing evidences of large-scale rock-mass deformation and/or deep-seated landsliding not be occupied before these areas have been more rigorously investigated and the annual individual fatality risk within them determined.

5) Christchurch City Council, in the short term (over the next few years), should continue to monitor the movement of the land in the deformation areas and set in place emergency management plans that take account of any potentially life-threatening changes in the displacement patterns.

6) The areas of ongoing ground deformation and their surroundings need further subsurface investigation and in-situ deformation monitoring before analysis of the annual individual fatality risk from these features can be undertaken.

11.0 ACKNOWLEDGEMENTS

This work was funded by the New Zealand Public Good Science Fund via the New Zealand Natural Hazards Research Platform and by Christchurch City Council. The authors acknowledge the advice and comments on this work provided by the Port Hills Geotechnical Group. This work would not have been possible without the data collected by them. The team comprises the following consultants: URS, OPUS, Geotechnical Consulting, Aurecon, GHD. The authors wish to acknowledge: M. Gerstenberger and G. McVerry for providing the peak ground acceleration probabilities; D. Rhoades for carrying out the cliff collapse ground-acceleration analysis; Richard Jongens for geological mapping; Eileen McSaveney for historical literature searches and editing; and N. Litchfield and G. Dellow for internal reviews. The report has been considerably enhanced by comments made by the independent peer reviewers. These were T. Taig regarding risk assessment methods and risk management criteria and F.J. Baynes as the independent reviewer appointed by Christchurch City Council.

12.0 REFERENCES

Aoi, S.; Kunugi, T.; Fujiwara., H. 2008. Trampoline effect in extreme ground motion. Science 322: 727–730.

Australian Geomechanics Society 2007. Practice Note Guidelines for Landslide Risk Management. Journal and News of the Australian Geomechanics Society 42(1): 63–114.

Bell, D. 1992. Rockfall protection measures for 44 Raekura Place. University of Canterbury, Canterprise Report. 1st November 2011.

Berryman, K. 2011. A tale of two earthquakes: the Canterbury, New Zealand, sequence of 2010-2011. Abstract for the International Union of Geodesy and Geophysics 2011 Conference.

Brown, L.J.; Weeber, J.H. 1992. Geology of the Christchurch Urban Area. Scale 1:25,000. Institute of Geological and Nuclear Sciences map 1.

Corominas J. 1996. The angle of reach as a mobility index for small and large landslides. Canadian Geotechechnical Journal 33: 260-271.

Cowan, H.A. 1991. The North Canterbury earthquake of September 1, 1888. Journal of the Royal Society of New Zealand 21: 1-12.

Cruden, D.M.; Varnes, D.J. 1996. Landslide types and processes. Landslide: investigation and mitigation. Turner, K.A.; Schuster, R.L. (eds.). Special report, Transportation Research Board, National Research Council, 247. Chapter 3, 36–75.

Dorren, L.K.A. 2003. A review of rockfall mechanics and modelling approaches. Progress in Physical Geography 27(1): 69–87.

Evans, S.G.; Hungr, O. 1993. The assessment of rockfall hazard at the base of talus slopes. Canadian Geotechnical Journal 30: 620–636.

Finlay, P.J.; Mostyn, G.R.; Fell, R. 1999. Landslides: Prediction of Travel Distance and Guidelines for Vulnerability of Persons. Proceedings of the 8th Australia New Zealand Conference on Geomechanics, Hobart. Australian Geomechanics Society 1: 105–113.

Forsyth, P.J.; Barrell, D.J.A.; Jongens, R. (compilers) 2008. Geology of the Christchurch area. Institute of Geological & Nuclear Sciences 1:250,000 geological map 16.

Fry, B.; Benites, R.; Kaiser, A. 2011. The character of accelerations in the Christchurch Mw 6.3 earthquake. Seismological Research Letters 82: 846-852.

GEO Report No. 75 1999. Landslides and boulder falls from natural terrain: interim risk guidelines. Report written by ERM – Hong Kong Ltd, for the Geotechnical Engineering Office, Civil Engineering Department, Hong Kong, SAR. Consultancy agreement number GEO 4/97.

Gerstenberger, M.C. 2011. Update of the Z-factor for Christchurch considering earthquake clustering following the Darfield Earthquake. GNS Science Report 2011/29.

Hampton, S.J. 2010. Growth, structure and evolution of the Lyttelton volcanic complex, Banks Peninsula, New Zealand. Ph.D. thesis, University of Canterbury.

Hancox, G.T.; Perrin, N.D.; Dellow, G.D. 2002 Recent studies of historical earthquake-induced landsliding, ground damage, and MM intensity in New Zealand. Bulletin of the New Zealand Society for Earthquake Engineering 35(2): 59–95

Hancox, G.; Massey, C.; Perrin, N. 2011. Landslides and related ground damage caused by the M_w6.3 Christchurch Earthquake of 22 February 2011. New Zealand Geomechanics News 81: 53–67.

Harp, E.L.; Wilson, R.C. 1995. Shaking intensity threshold for rock falls and slides: Evidence from 1987 Whittier Narrows and Superstition Hills earthquake strong records. Bulletin of the Seismological Society of America 85(6): 1739–1757.

Harp, E.L.; Jibson, R.W. 2002. Anomalous concentrations of seismically triggered rock falls in Pacoima Canyon: Are they caused by highly susceptible slopes or local amplification of seismic shaking? Bulletin of the Seismological Society of America 92(8): 3180–3189.

Hunt, M.; Somaiya, K.; Taig, T. 2010. Risk assessment of corrosion leakage of LPG from domestic underground service pipework. A report produced for the Health and Safety Executive, UK. http://www.hse.gov.uk/gas/lpg/ttac-corrosion-leak-lpg.pdf

Hoek, E. 1999. Putting Numbers to Geology – an Engineer's Viewpoint. The Second Glossop Lecture. Quarterly Journal of Engineering Geology 32(1): 1-19.

Hough, S.E.; Altidor, J.R.; Anglade, D.; Given, D.; Janvier, M.G.; Maharrey, J.Z.; Meremonte, M.; Mildor, B.S.; Prepetit, C.; Yong, A., 2010. Localized damage caused by topographic amplification during the 2010 M7.0 Haiti earthquake. Nature Geoscience, 3(11): 778-782.

Jacomb, C. 2008. The chronology of Moncks Cave, Canterbury, New Zealand. Records of the Canterbury Museum 2008 22: 45 – 56.

Kaiser, A.E.; Benites, R.A.; Chung, A.I.; Haines, J.A.; Cochran, E.; Fry, B. 2011. Estimating seismic site response in Christchurch City (New Zealand) from dense low-cost aftershock arrays. Proceedings of ESG4 Symposium 2011; Cochran et al., Annals of Geophysics.

Kanari, M. 2008. Evaluation of rockfall hazard to Qiryat Shemona - possible correlation to earthquakes. M.Sc. Thesis, Department of Geophysics and Planetary Sciences, Tel Aviv University.

Keefer, D.K. 1984. Landslides caused by earthquakes. Geological Society of America Bulletin 95(4): 406–421.

Keylock, D.; Domaas, U. 1999. Evaluation of topographic models of rockfall travel distance for use in hazard applications. Antarctic and Alpine Research 31(3): 312–320.

Kramer, S.L. 1996. Geotechnical earthquake engineering. In: Prentice-Hall Civil engineering and engineering mechanics series.

Marinos, P., Hoek, E. GSI 2000. A geologically friendly tool for rock mass strength estimation. In: GeoEng 2000, 19 – 24 November 2000, Melbourne Australia. Volume 1: Invited papers. Pp. 1422 – 1440.

Massey, C.I.; McSaveney, M.J.; Heron, D.; Lukovic, B. 2012. Canterbury Earthquakes 2010/11 Port Hills Slope Stability: Pilot study for assessing life-safety risk from rockfalls (boulder rolls). GNS Science Consultancy Report 2011/311.

McFadgen, B.G.; Goff, J.R. 2005. An earth systems approach to understanding the tectonic and cultural landscapes of linked marine embayments: Avon-Heathcote Estury (Ihutai) and Lake Ellesmere (Waihora), New Zealand. Journal of Quaternary Science 20(3): 227-237.

McSaveney, E. 2009. Historic earthquakes - The 1888 North Canterbury earthquake, Te Ara - the Encyclopedia of New Zealand, updated 2-Mar-09. URL: http://www.TeAra.govt.nz/en/historic-earthquakes/4

Moon, A.T.; Wilson, R.A.; Flentje, P. 2005. Developing and using landslide size frequency models. http://ro.uow.edu.au/engpapers/384.

Muhammad, S.; van der Meijde., M.; Kerle, N.; van der Meer, F. 2011. Impact of DEM source resoliutiom on topographic seismic amplification. International Journal of Applied Earth Observation and Geoinformation 13: 420 – 427.

New Zealand Geotechnical Society 2005. Field description of soil and rock. Guideline for the field classification and description of soil and rock for engineering purposes.

Reyners, M. 2011. Lessons from the destructive Mw6.3 Christchurch, New Zealand, Earthquake. Seismological Research Letters 82(3): 371–372.

Sepulveda, S.A.; Murphy, W.; Jibson, R.W.; Petley, D.N. 2005. Seismically induced rock slope failures resulting from topographic amplification of strong ground motions: The case of Pacoima Canyon, California. Engineering Geology 80: 336–348.

Sewell, R.J. 1988. Late Miocene volcanic stratigraphy of central Banks Peninisula, Canterbury, New Zealnd. New Zealand Journal of Geology and Geophysics 31: 41 – 64

Sewell, R.J.; Weaver, S.D.; Reay, M.B. 1992. Geology of Banks Peninsular. Scale: 1:100,000. Institute of Geological and Nuclear Sciences Geological Map Sheet 3.

Standards New Zealand 2004. Structural Design Actions – Part 5 Earthquake Actions – New Zealand. New Zealand Standard NZS 1170.5:2004.

Stirling, M.; McVerry, G.; Gerstenberger, M.; Litchfield, N.; Van Dissen, R.; Berryman, K.; Barnes, P.; Wallace, L.; Bradley, B.; Villamor, P.; Langridge, R.; Lamarche, G.; Nodder, S.; Reyners, M.; Rhoades, D.; Smith, W.; Nicol, A.; Pettinga, J.; Clark, K.; Jacobs, K. In press. National Seismic Hazard Model for New Zealand: 2010 Update. Bulletin of the Seismological Society of America.

Trotter, M.M. 1975. Archaeological investigations at Redcliffs, Canterbury, New Zealand. Records of the Canterbury Museum 9(3): 189–220.

Taig, T.; Massey, C., Webb, T. 2012. Decisions about life risk in the Port Hills. GNS Science Consultancy Report 2011/319.

Webb, T.H. (compiler); Bannister, S.; Beavan, J.; Berryman, K.; Brackley, H.; Fry, B.; Gerstenberger, M.; Holden, C; Kaiser, A; McVerry, G.; McSaveney, E.; Pettinga, J.; Reyners, M.; Rhoades, D; Somerville, P; Stirling, M; Van Dissen, R.; Villamor, P.; Wallace, L.; Zhao, J., 2011. The Canterbury Earthquake Sequence and Implications for Seismic Design Levels. GNS Science Consultancy Report 2011/183.

Wieczorek, G.F.; Jager, S. 1996. Triggering mechanisms and depositional rates of postglacial slope-movement processes in the Yosemite Valley, California. Geomorphology 15: 17–31.

Yamada, M.; Mori, J.; Heaton, T. 2009. The slapdown phase in high-acceleration records of large earthquakes. Seismological Research Letters 80: 559-564.

APPENDIX A CLIFF COLLAPSE RISK FIELD DATA - LOCATION MAP

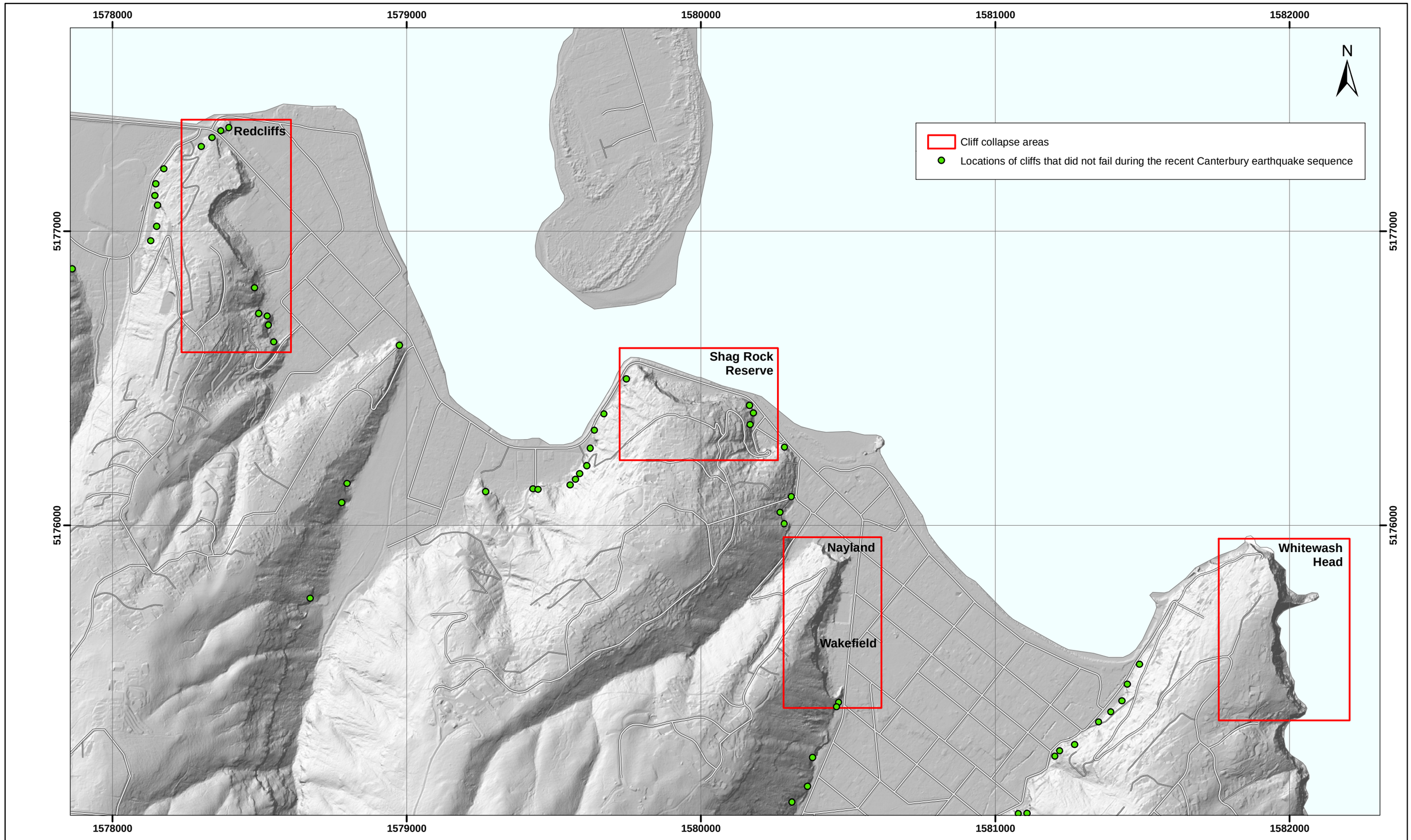

SCALE BAR: 0 0.5 1 km

EXPLANATION:

Background shade model derived from NZAM post earthquake 2011c (July 2011) LiDAR survey resampled to a 1m ground resolution.

Roads provided by Christchurch City Council.

DRW: BL

CHK: CM

GNS SCIENCE TE PŪ AO

CLIFF COLLAPSE FIELD DATA - SITE MAPS

Location Map

APPENDIX A

FINAL

PROJECTION: New Zealand Transverse Mercator 2000

REPORT: CR2012/57

DATE: Mar 2012

APPENDIX B CLIFF COLLAPSE RISK FIELD DATA - SITE MAPS

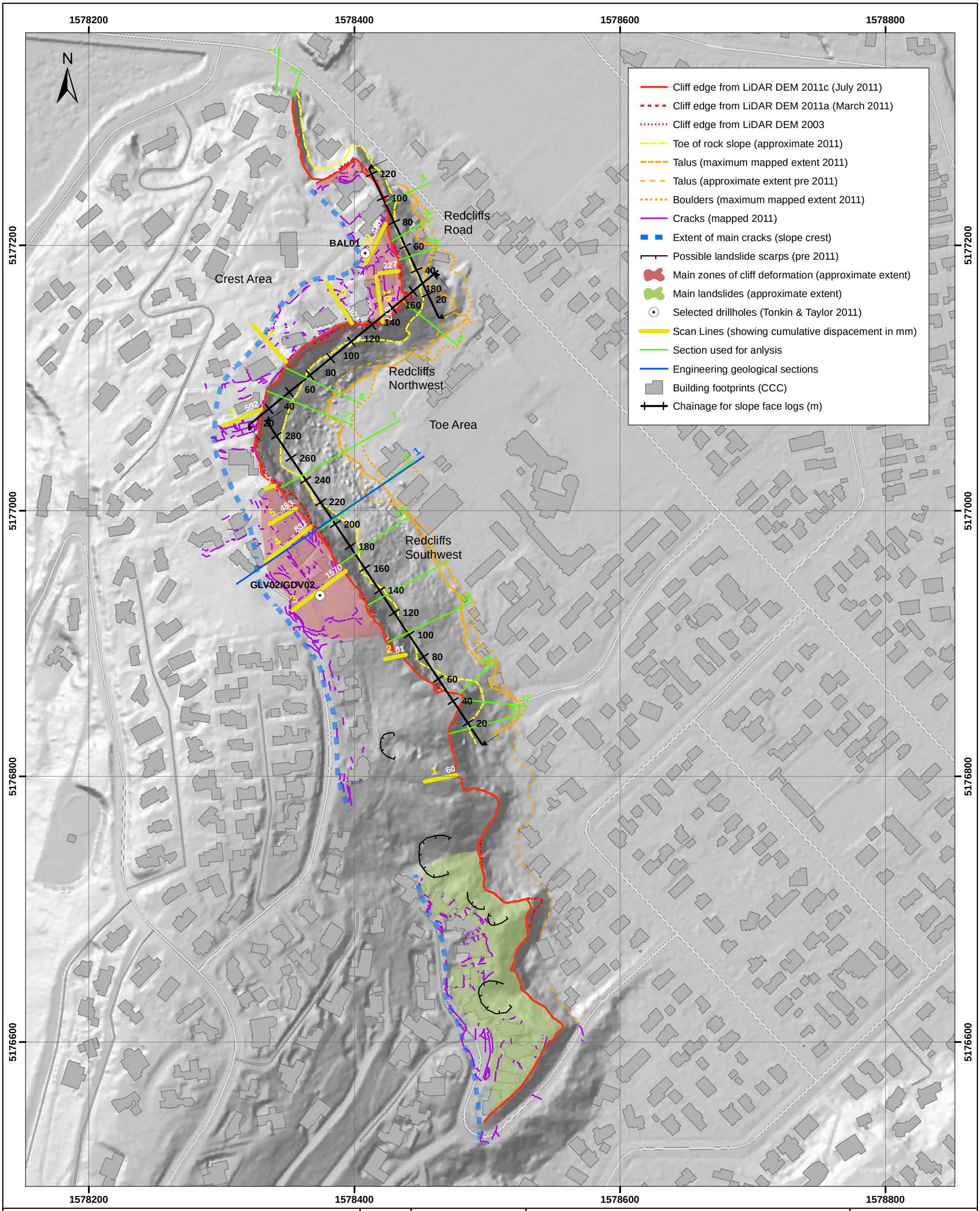

SCALE BAR: 0 50 100 m

EXPLANATION:

Background shade model derived from NZAM post earthquake 2011c (July 2011) LiDAR survey resampled to a 1m ground resolution.

Roads and building footprints provided by Christchurch City Council (20/02/2012).

DRW: BL, DWH

CHK: CM

CLIFF COLLAPSE FIELD DATA - SITE MAPS

Redcliffs Christchurch

APPENDIX B

FINAL

PROJECTION: New Zealand Transverse Mercator 2000

REPORT: CR2012/57

DATE: Mar 2012

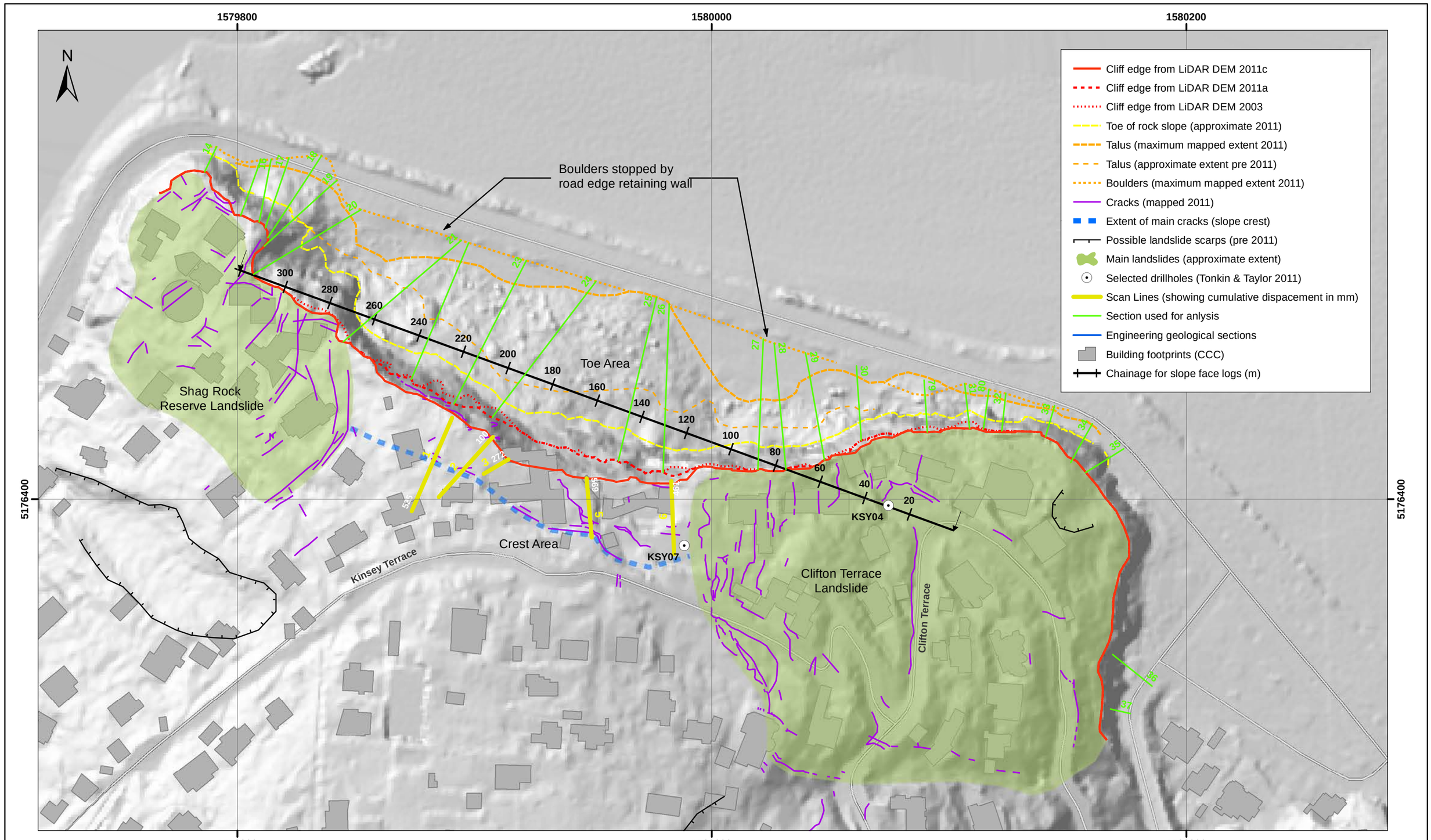

SCALE BAR: 0 50 100 m

EXPLANATION:

Background shade model derived from NZAM post earthquake 2011c (July 2011) LiDAR survey resampled to a 1m ground resolution.

Roads and building footprints provided by Christchurch City Council (20/02/2012).

DRW: BL, DWH

CHK: CM

CLIFF COLLAPSE
FIELD DATA - SITE MAPS

Shag Rock Reserve, Sumner
Christchurch

APPENDIX B

FINAL

PROJECTION: New Zealand Transverse Mercator 2000

REPORT: CR2012/57

DATE: Mar 2012

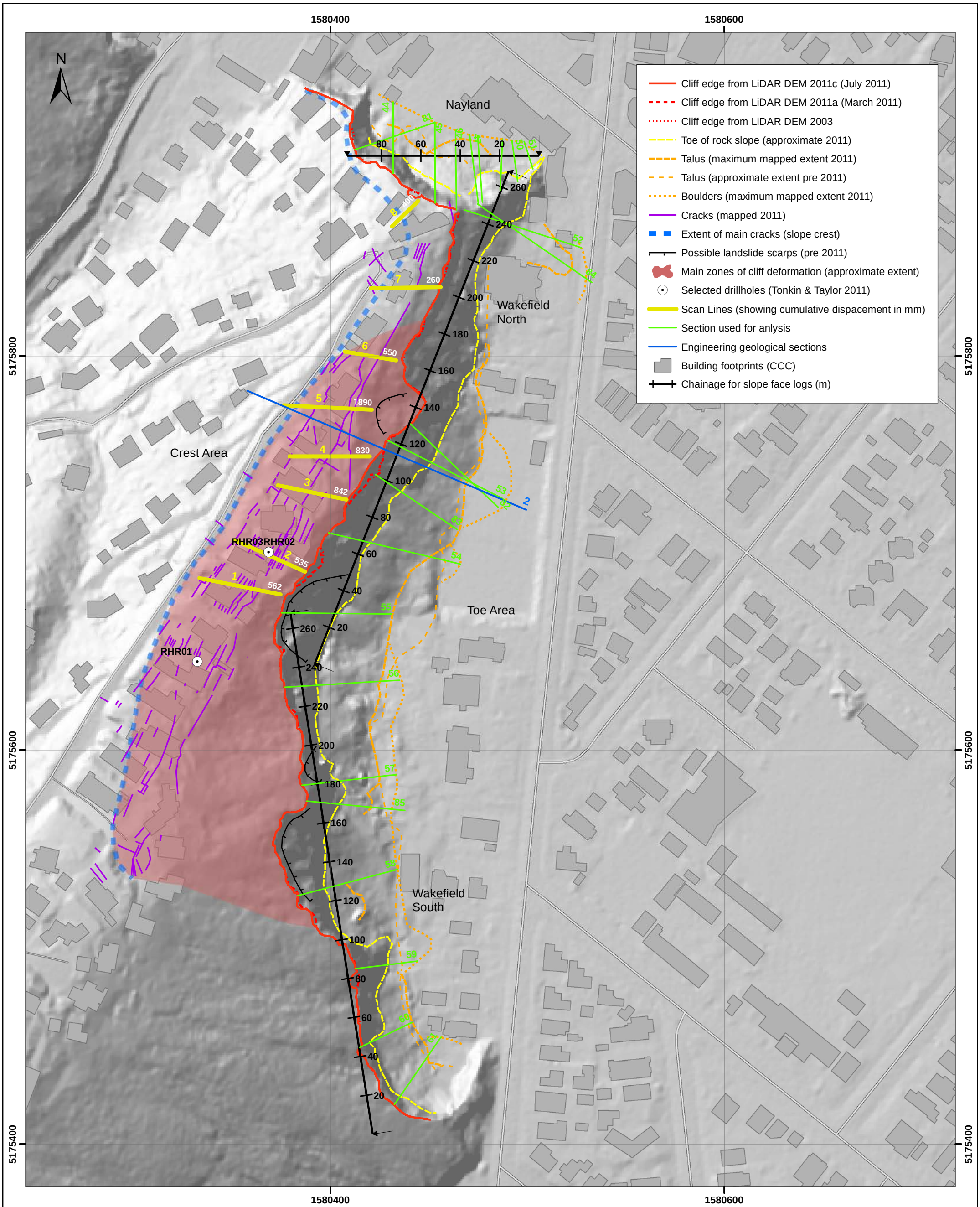

SCALE BAR: 0 50 100 m

EXPLANATION:

Background shade model derived from NZAM post earthquake 2011c (July 2011) LiDAR survey resampled to a 1m ground resolution.

Roads and building footprints provided by Christchurch City Council (20/02/2012).

DRW: BL, DWH

CHK: CM

CLIFF COLLAPSE FIELD DATA - SITE MAPS

Wakefield Avenue and Nayland Street, Sumner Christchurch

APPENDIX B

FINAL

PROJECTION: New Zealand Transverse Mercator 2000

REPORT: CR2012/57

DATE: Mar 2012

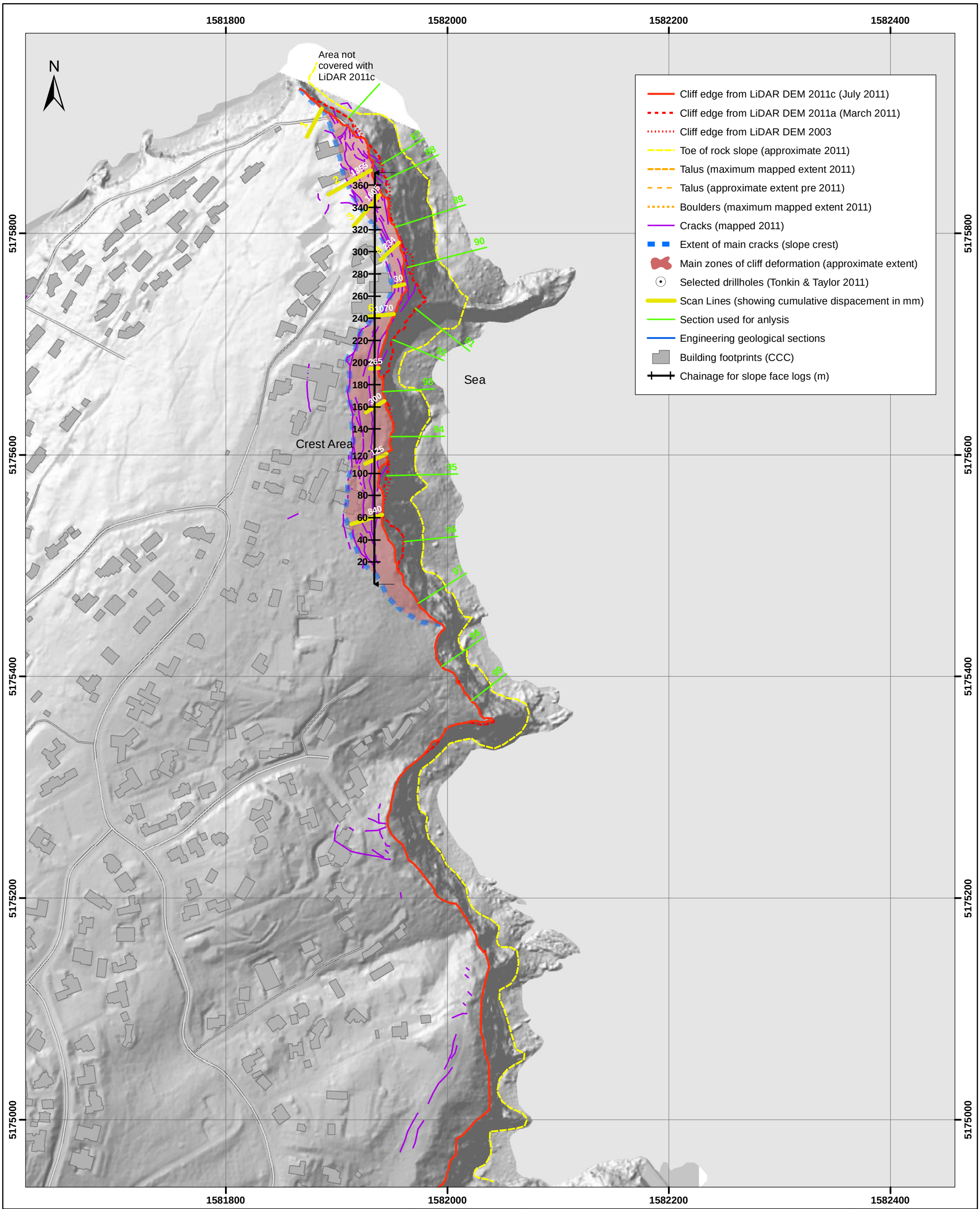

SCALE BAR: 0 50 100 m

EXPLANATION:

Background shade model derived from NZAM post earthquake 2011c (July 2011) LiDAR survey resampled to a 1m ground resolution.

Roads and building footprints provided by Christchurch City Council (20/02/2012).

DRW: BL, DWH

CHK: CM

CLIFF COLLAPSE FIELD DATA - SITE MAPS

Whitewash Head Christchurch

APPENDIX B

FINAL

PROJECTION: New Zealand Transverse Mercator 2000

REPORT: CR2012/57

DATE: Mar 2012

APPENDIX C CLIFF FRONTAL ELEVATION, GEOLOGY MAP AND SURFACE CHANGE MODELS

A)

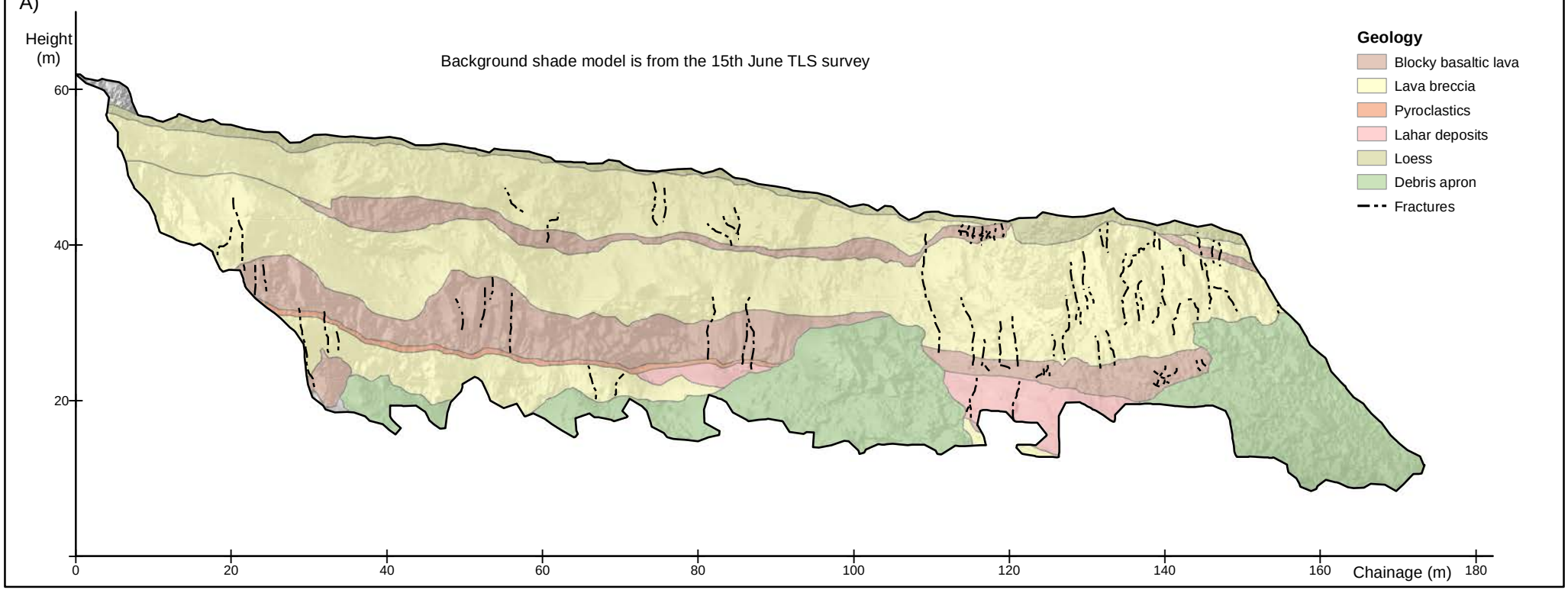

B)

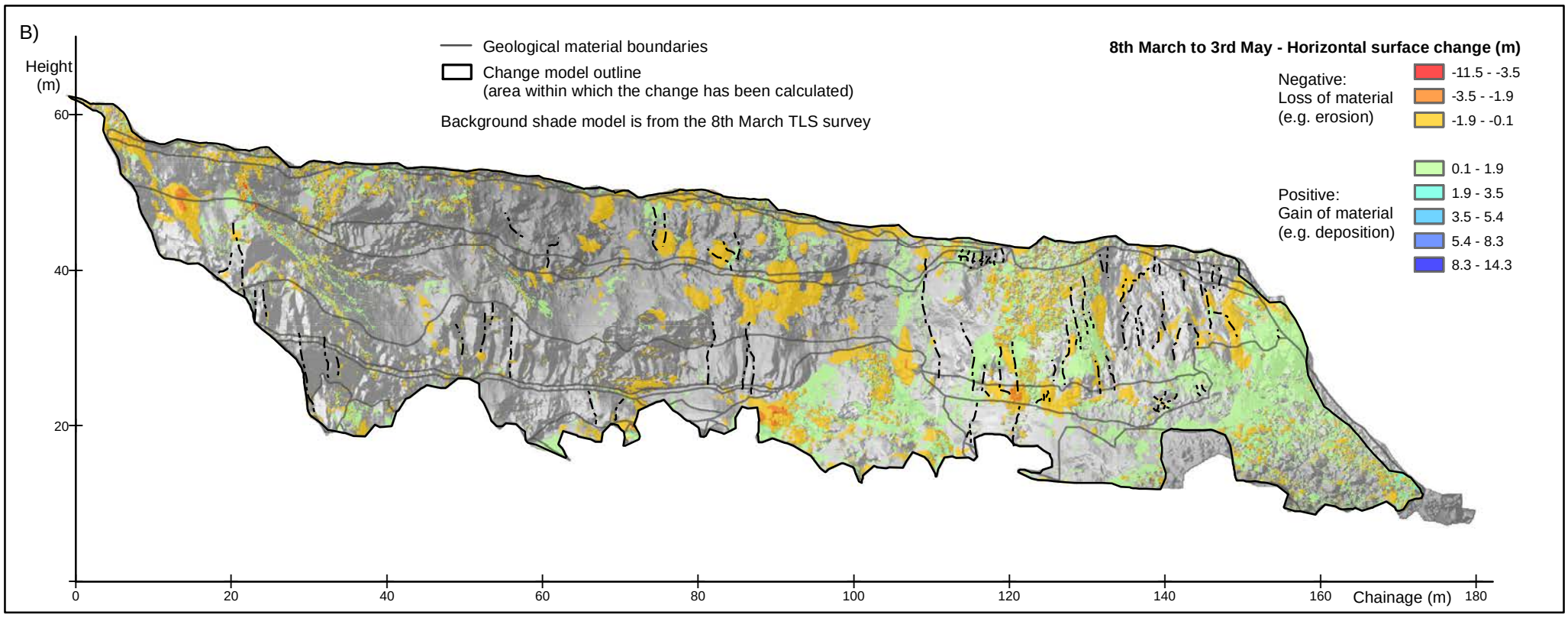

C)

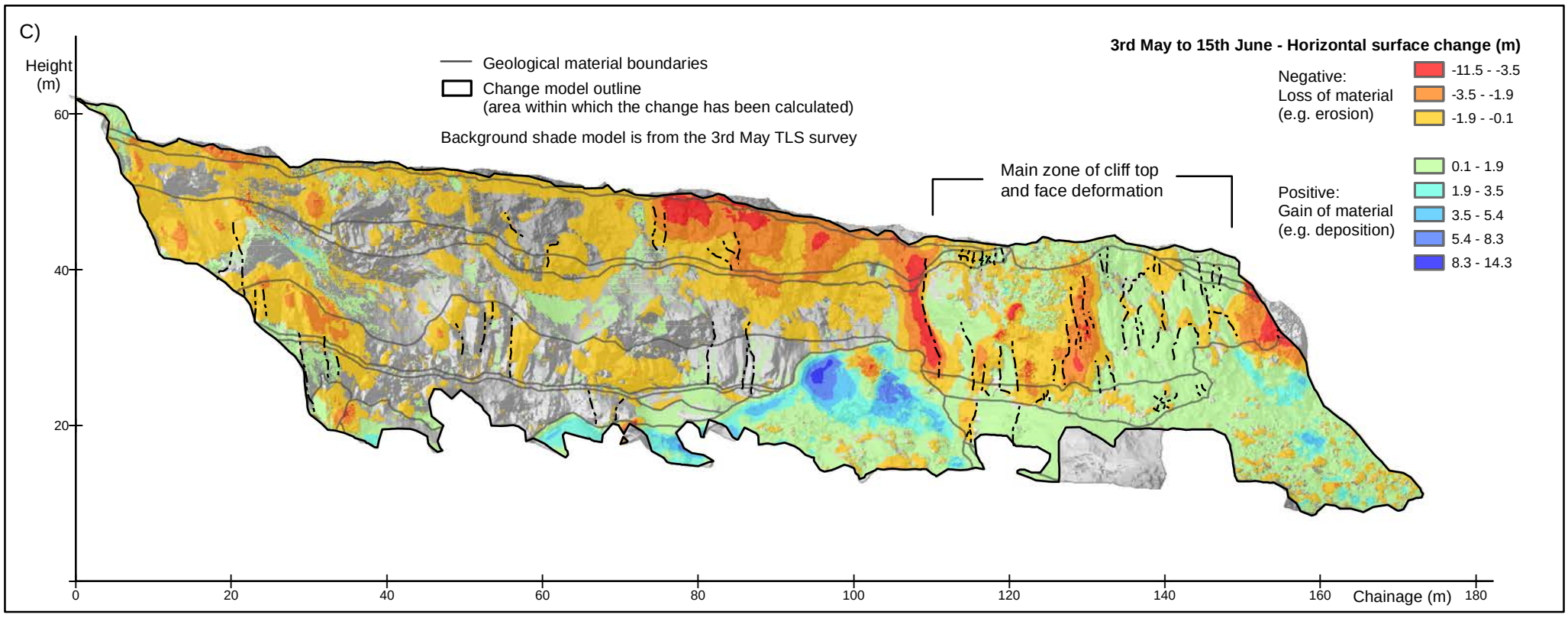

EXPLANATION:
A) Geology map of the cliff face
B) and C) surface change models - these show the horizontal changes of the cliff-face surface between given survey dates. Changes in the order of +/- 0.1 m are assumed to be error and are not shown in the change models. The surveys were carried out using a RIEGL LMSZ420i terrestrial laser scanner (TLS) in 2011.
The views are all frontal elevation i.e. as if standing at the bottom of the cliff looking towards it, with the data projected onto the chainage line.

DRW: BL

CHK: ZB, CM

GNS SCIENCE TE PŪ AO

CLIFF FRONTAL ELEVATION, GEOLOGY MAP AND SURFACE CHANGE MODELS

Redcliffs Northwest Christchurch

APPENDIX C

FINAL

REPORT: CR2012/57

DATE: Mar 2012

A)

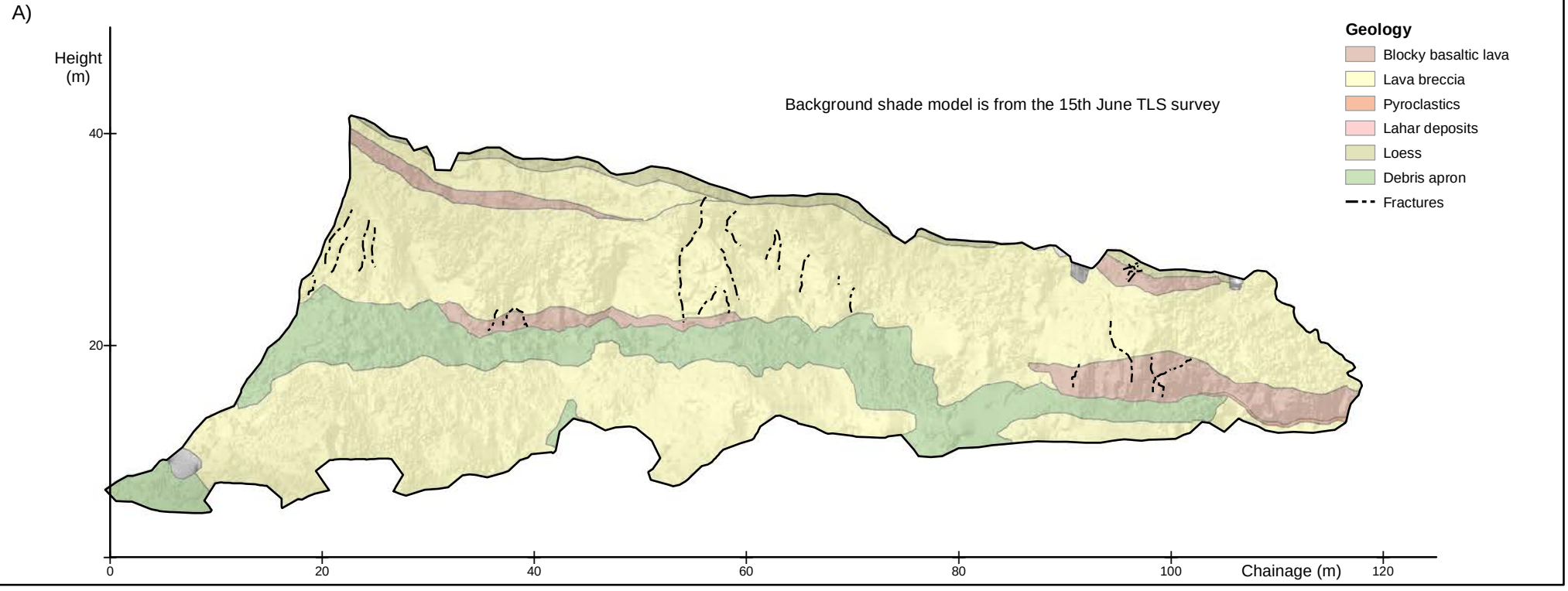

B)

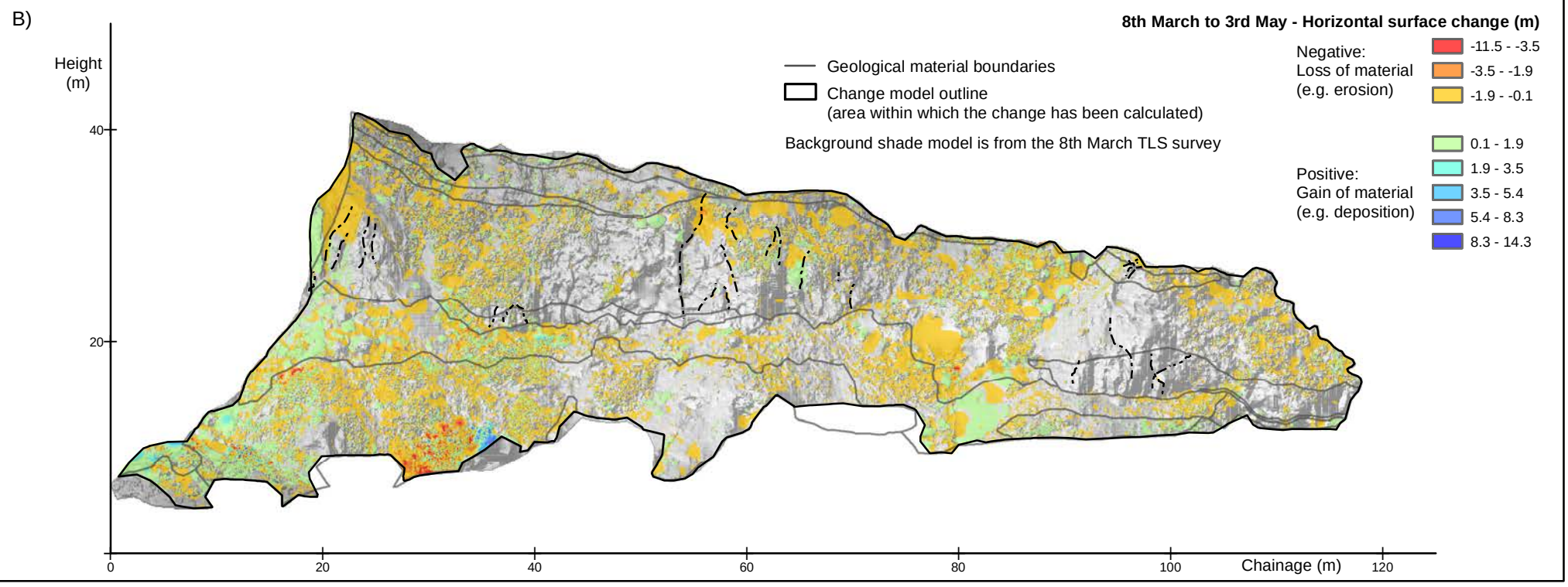

C)

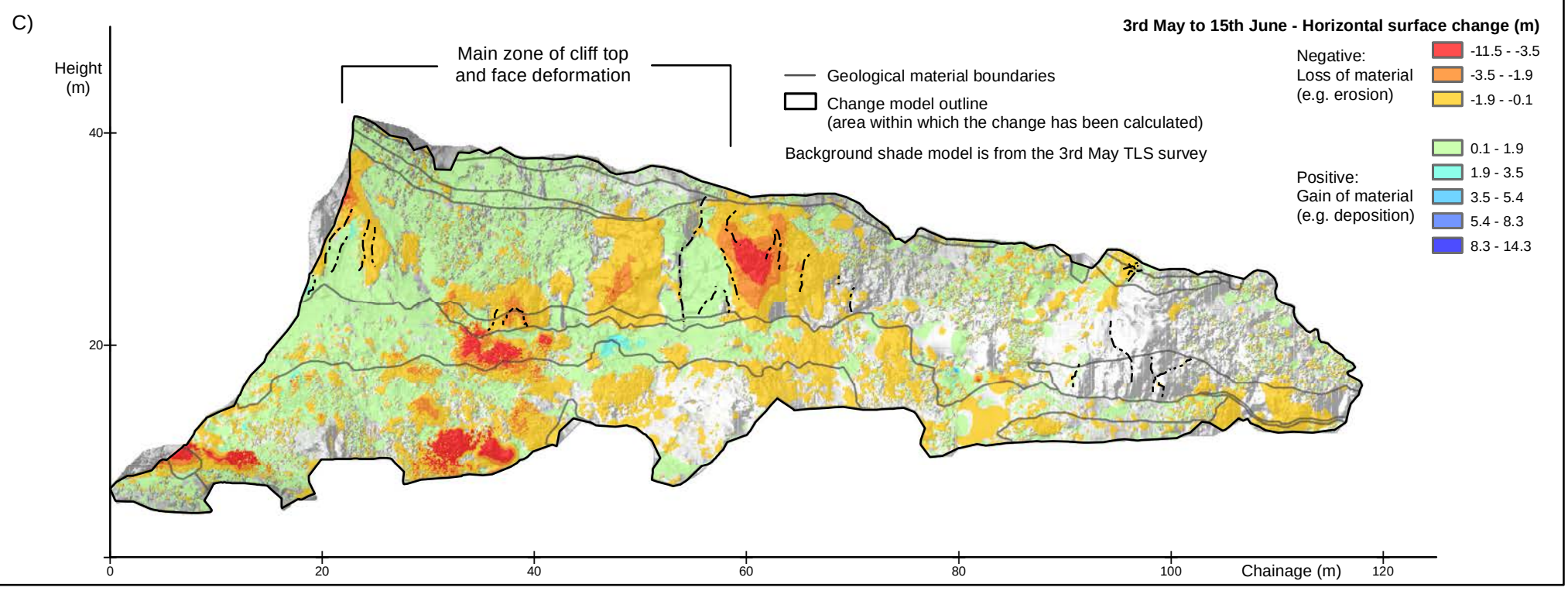

EXPLANATION:

A) Geology map of the cliff face

B) and C) surface change models - these show the horizontal changes of the cliff-face surface between given survey dates. Changes in the order of +/- 0.1 m are assumed to be error and are not shown in the change models. The surveys were carried out using a RIEGL LMSZ420i terrestrial laser scanner (TLS) in 2011.

The views are all frontal elevation i.e. as if standing at the bottom of the cliff looking towards it, with the data projected onto the chainage line.

DRW: BL

CHK: ZB, CM

GNS SCIENCE TE PŪ AO

CLIFF FRONTAL ELEVATION, GEOLOGY MAP AND SURFACE CHANGE MODELS

Redcliffs Main Road Christchurch

APPENDIX C

FINAL

REPORT: CR2012/57

DATE: Mar 2012

A)

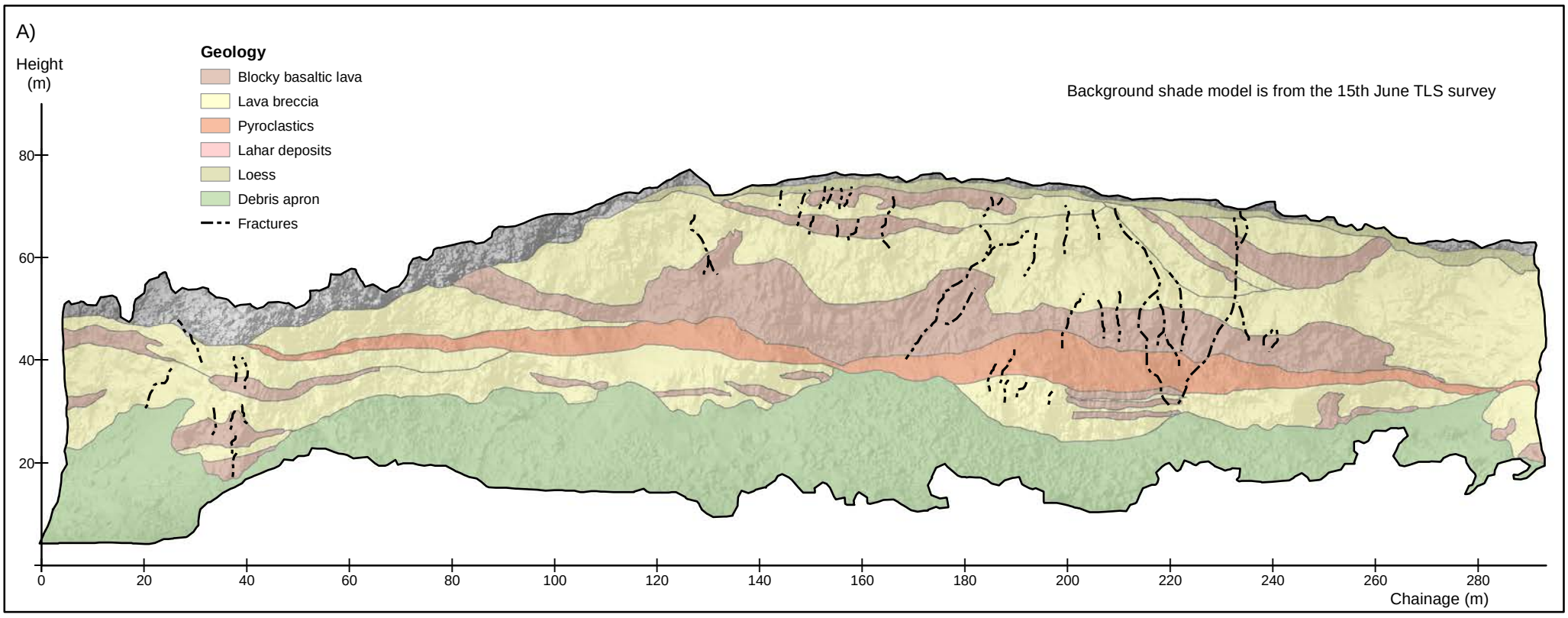

B)

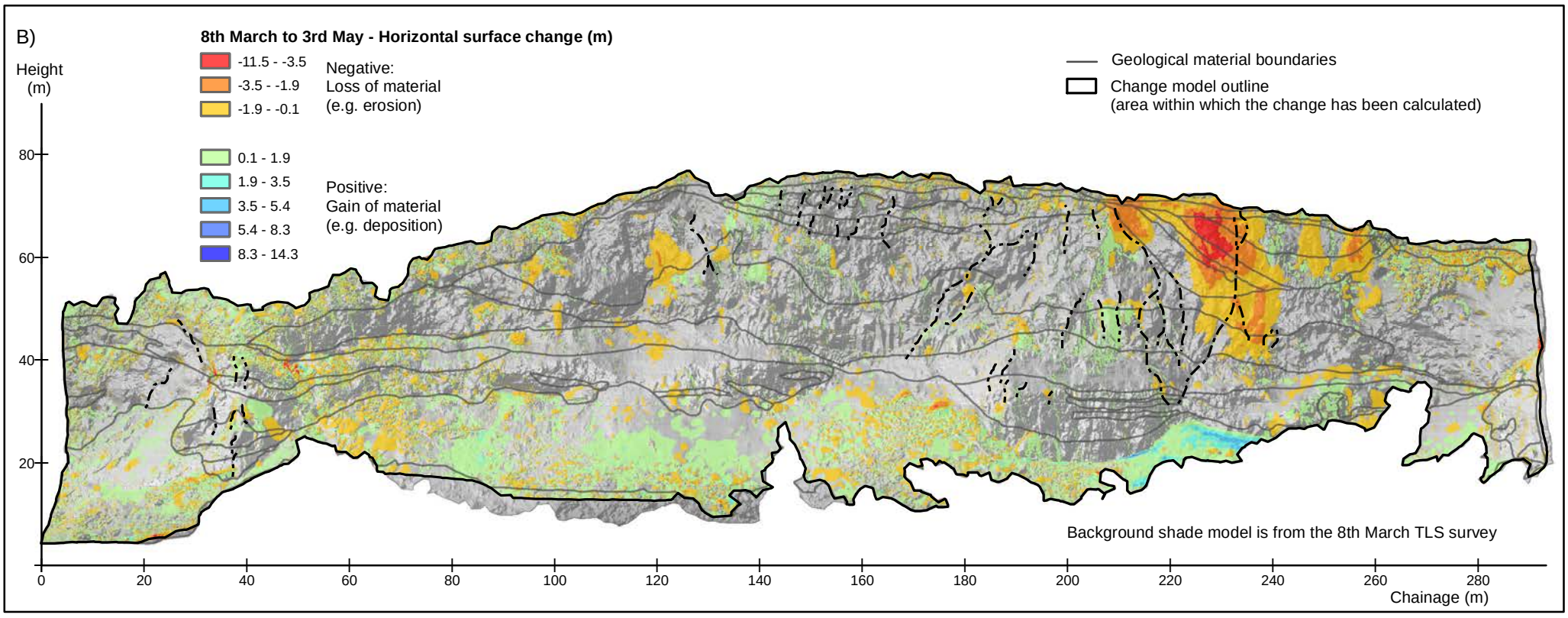

C)

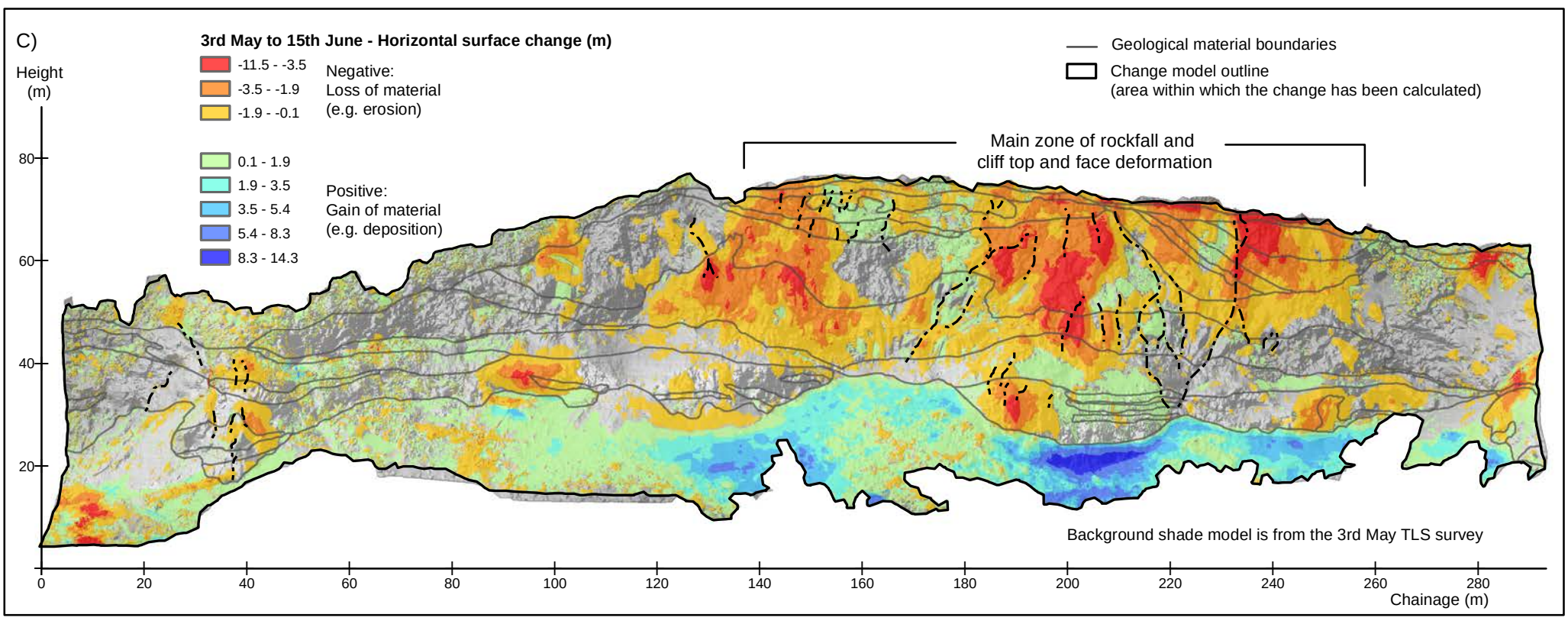

EXPLANATION:

A) Geology map of the cliff face

B) and C) surface change models - these show the horizontal changes of the cliff-face surface between given survey dates. Changes in the order of +/- 0.1 m are assumed to be error and are not shown in the change models. The surveys were carried out using a RIEGL LMSZ420i terrestrial laser scanner (TLS) in 2011.

The views are all frontal elevation i.e. as if standing at the bottom of the cliff looking towards it, with the data projected onto the chainage line.

DRW: BL

CHK: ZB, CM

GNS SCIENCE TE PŪ AO

CLIFF FRONTAL ELEVATION, GEOLOGY MAP AND SURFACE CHANGE MODELS

Redcliffs Southwest Christchurch

APPENDIX C

FINAL

REPORT: CR2012/57

DATE: Mar 2012

A)

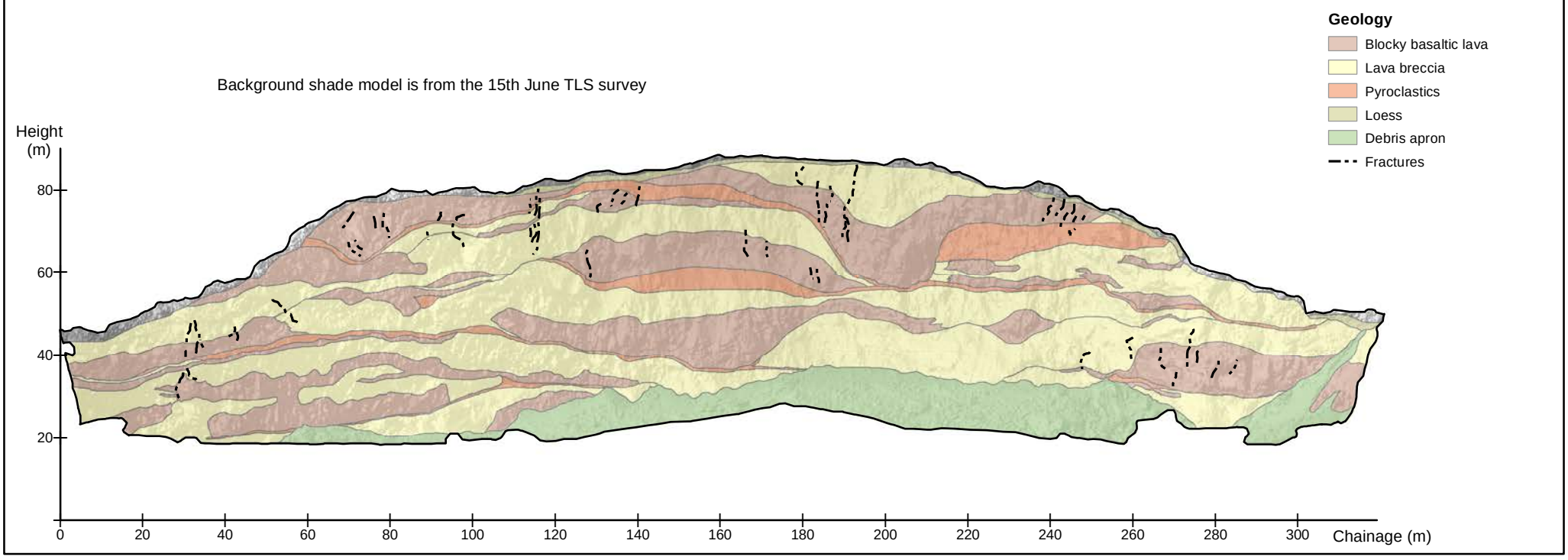

B)

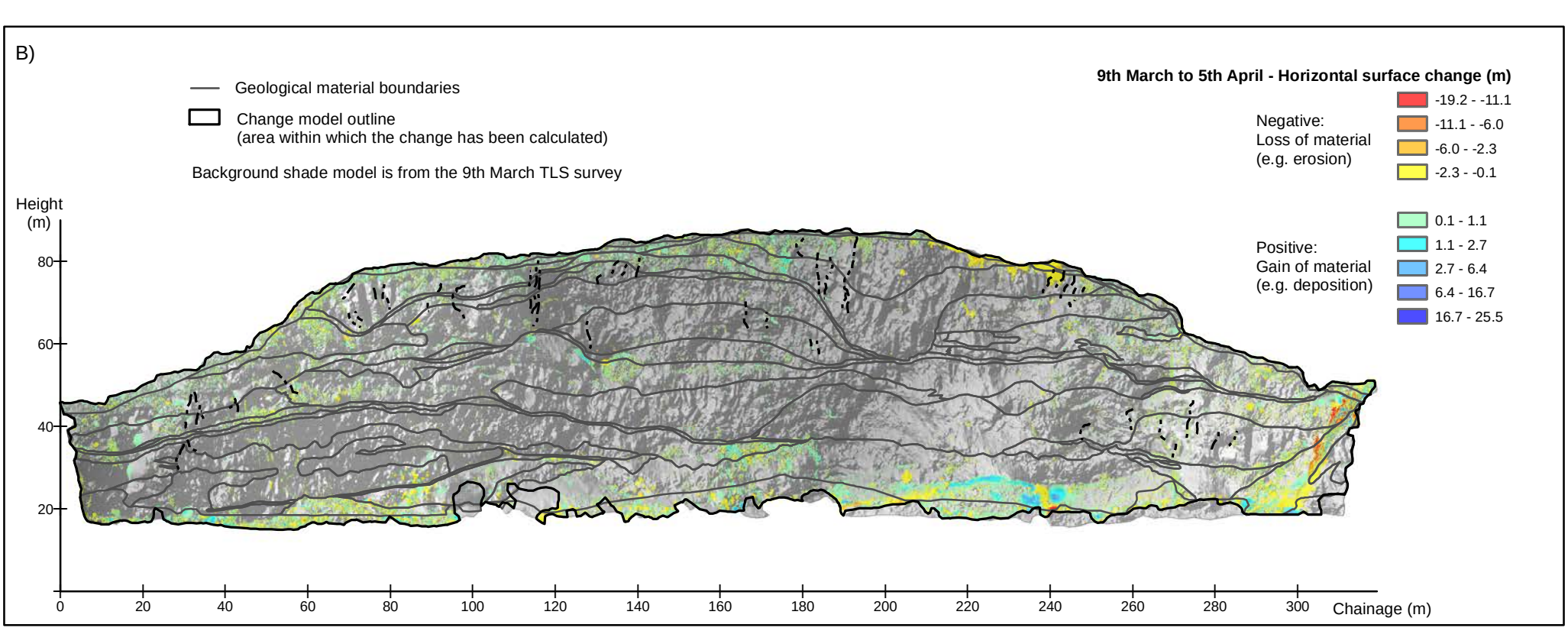

C)

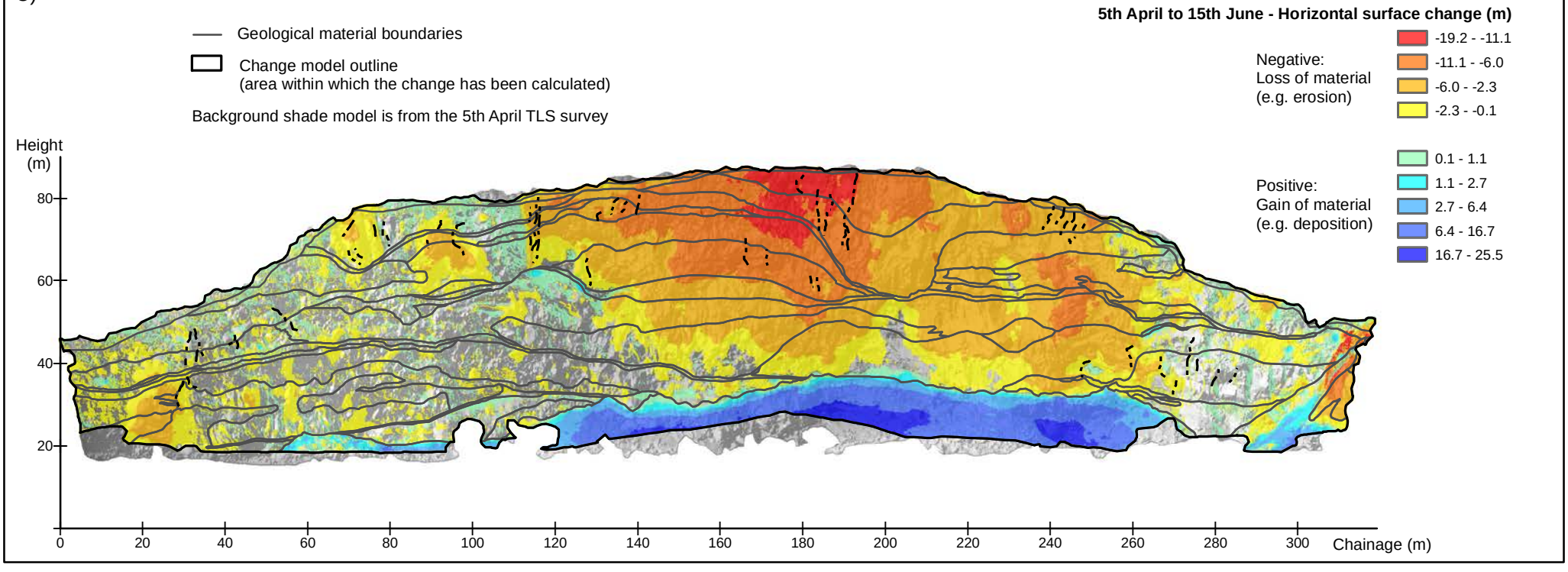

EXPLANATION:
A) Geology map of the cliff face
B) and C) surface change models - these show the horizontal changes of the cliff-face surface between given survey dates. Changes in the order of +/- 0.1 m are assumed to be error and are not shown in the change models. The surveys were carried out using a RIEGL LMSZ420i terrestrial laser scanner (TLS) in 2011.
The views are all frontal elevation i.e. as if standing at the bottom of the cliff looking towards it, with the data projected onto the chainage line.

DRW: BL

CHK: ZB, CM

GNS SCIENCE TE PŪ AO

CLIFF FRONTAL ELEVATION, GEOLOGY MAP AND SURFACE CHANGE MODELS

Shag Rock Reserve, Sumner Christchurch

APPENDIX C
FINAL

REPORT: CR2012/57

DATE: Mar 2012

A)

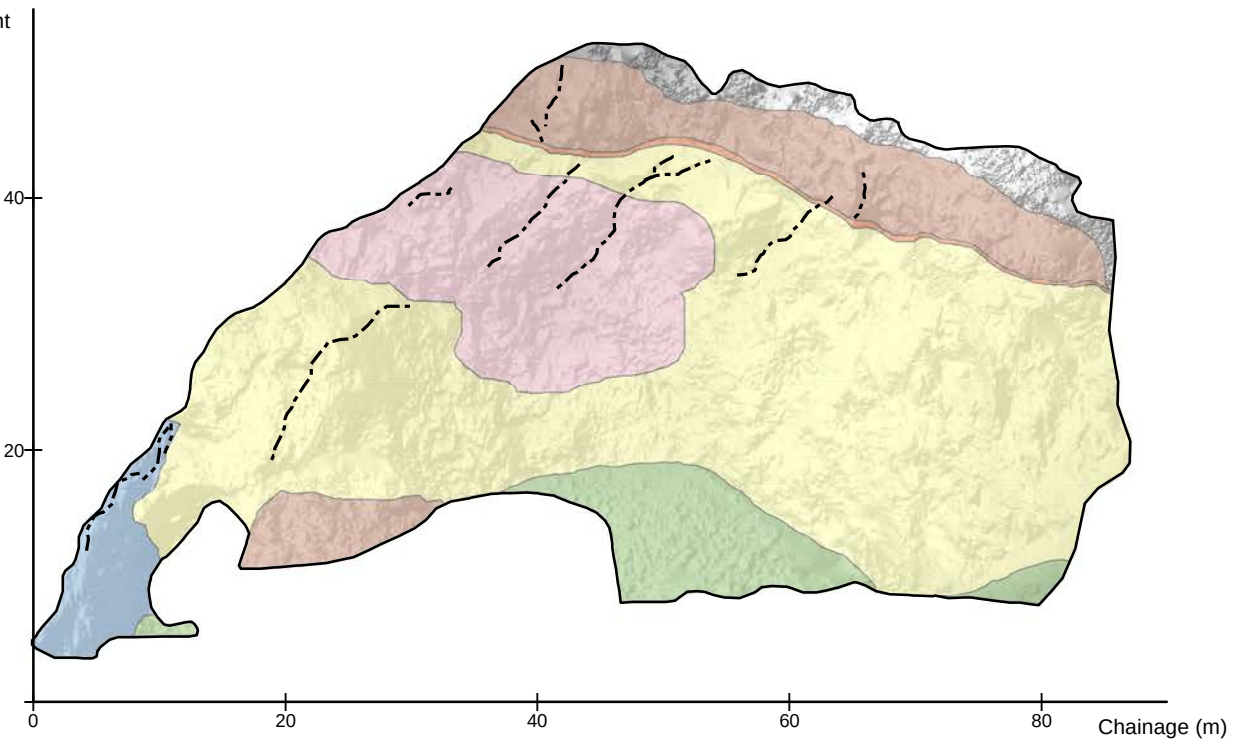

Geology

- Blocky basaltic lava
- Flaggy trachytic lava
- Trachytic lava breccia
- Pyroclastics
- Nayland St dike
- Debris apron
- Fractures

Background shade model is from the 16th June TLS survey

B)

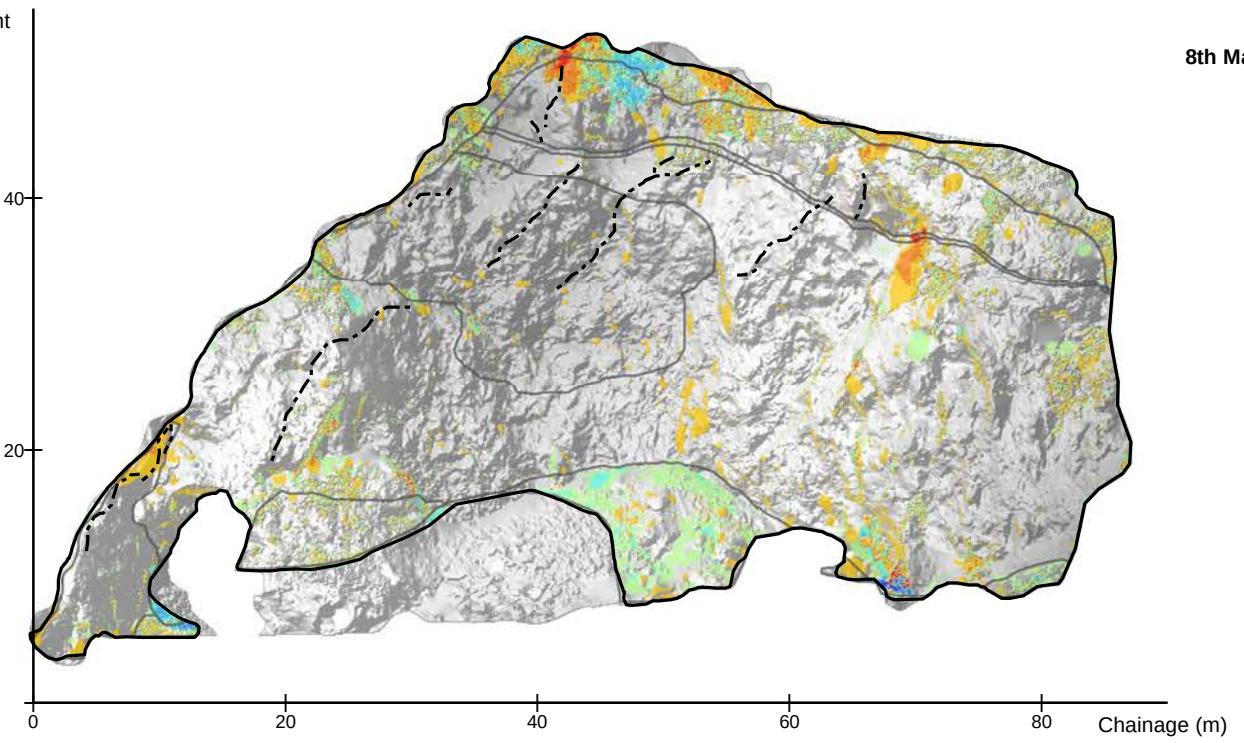

8th March to 6th May - Horizontal surface change (m)

Negative: Loss of material (e.g. erosion)
- -9.5 - -2.2
- -2.2 - -0.9
- -0.9 - -0.1

Positive: Gain of material (e.g. deposition)
- 0.1 - 0.5
- 0.5 - 1.4
- 1.4 - 3.5
- 3.5 - 7.0
- 7.0 - 12.3

Geological material boundaries

Change model outline (area within which the change has been calculated)

Background shade model is from the 8th March TLS survey

C)

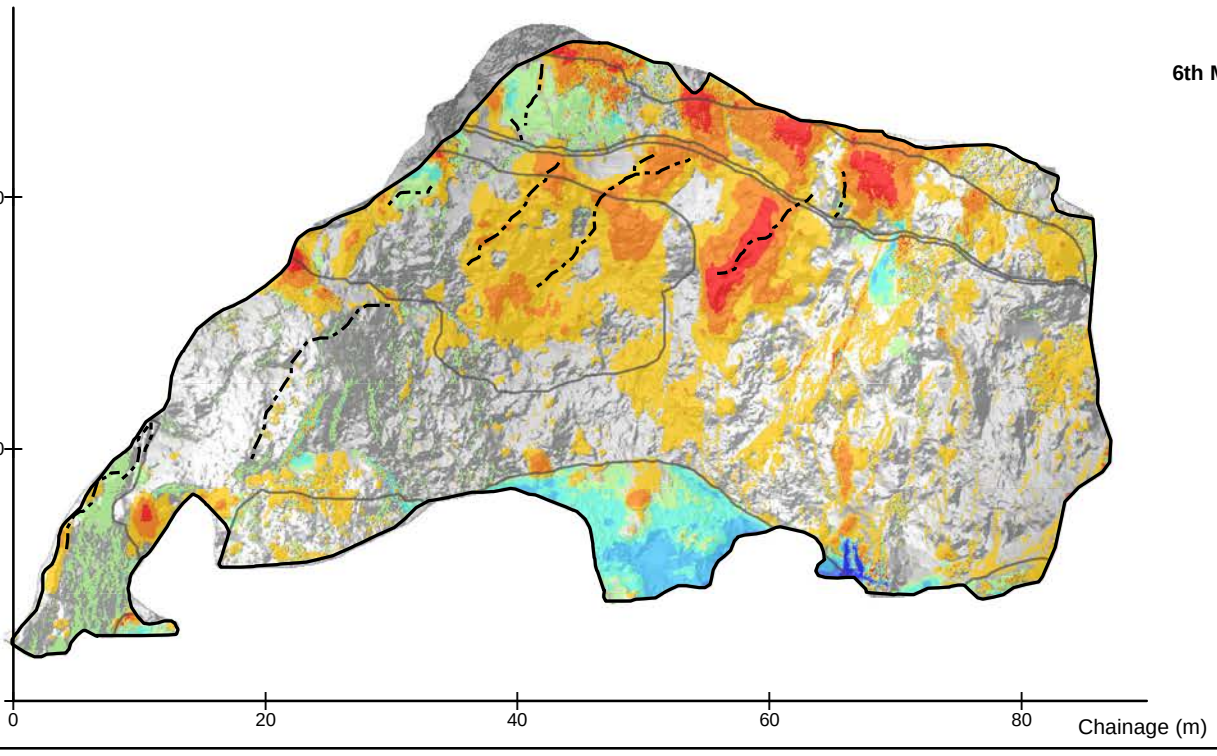

6th May to 16th June- Horizontal surface change (m)

Negative: Loss of material (e.g. erosion)
- -9.5 - -2.2
- -2.2 - -0.9
- -0.9 - -0.1

Positive: Gain of material (e.g. deposition)
- 0.1 - 0.5
- 0.5 - 1.4
- 1.4 - 3.5
- 3.5 - 7.0
- 7.0 - 12.3

Geological material boundaries

Change model outline (area within which the change has been calculated)

Background shade model is from the 6th May TLS survey

EXPLANATION:

A) Geology map of the cliff face

B) and C) surface change models - these show the horizontal changes of the cliff-face surface between given survey dates. Changes in the order of +/- 0.1 m are assumed to be error and are not shown in the change models. The surveys were carried out using a RIEGL LMSZ420i terrestrial laser scanner (TLS) in 2011.

The views are all frontal elevation i.e. as if standing at the bottom of the cliff looking towards it, with the data projected onto the chainage line.

DRW: BL

CHK: ZB, CM

GNS SCIENCE TE PŪ AO

CLIFF FRONTAL ELEVATION, GEOLOGY MAP AND SURFACE CHANGE MODELS

Nayland Street, Sumner Christchurch

APPENDIX C

FINAL

REPORT: CR2012/57

DATE: Mar 2012

A)

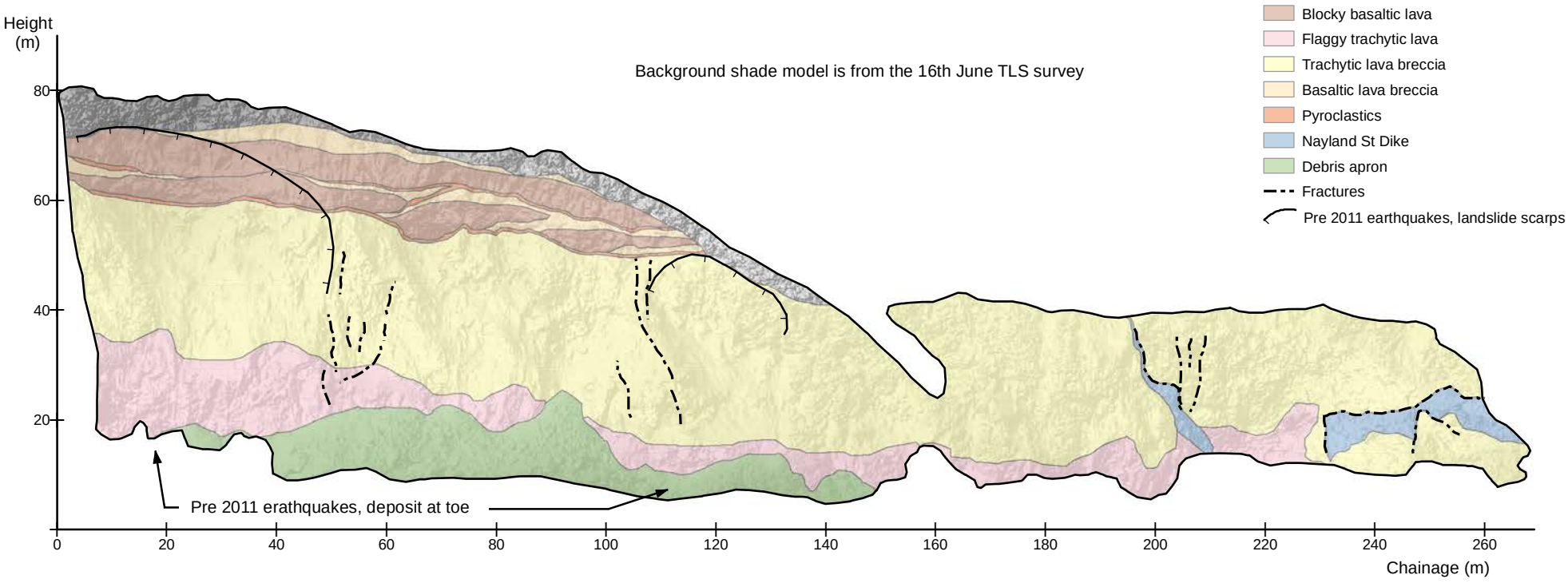

B)

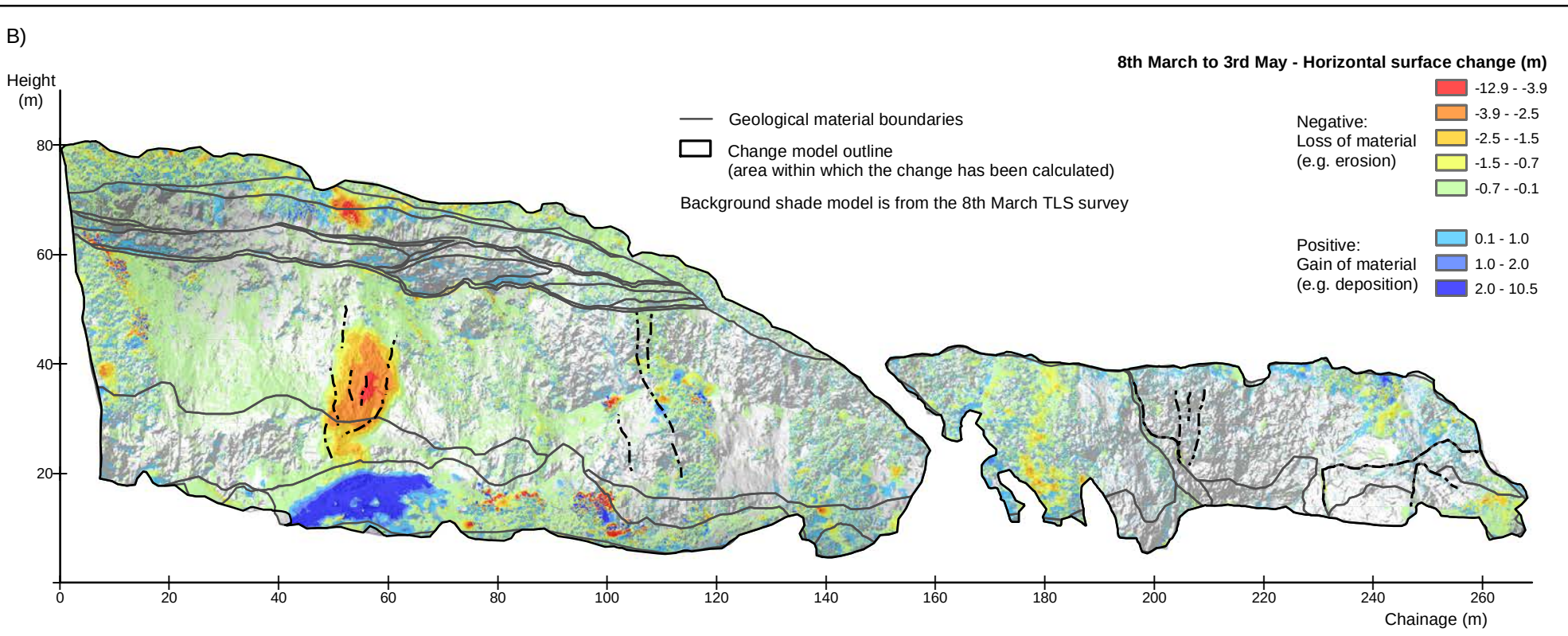

C)

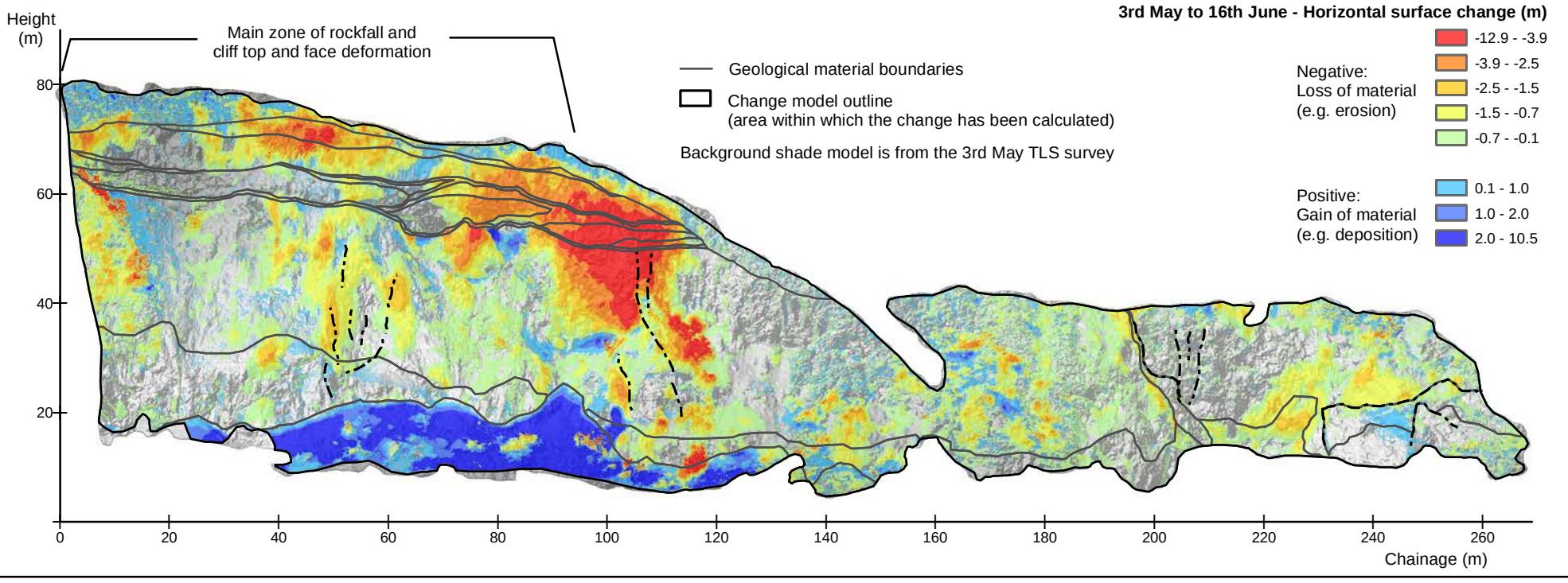

EXPLANATION:

A) Geology map of the cliff face

B) and C) surface change models - these show the horizontal changes of the cliff-face surface between given survey dates. Changes in the order of +/- 0.1 m are assumed to be error and are not shown in the change models. The surveys were carried out using a RIEGL LMSZ420i terrestrial laser scanner (TLS) in 2011.

The views are all frontal elevation i.e. as if standing at the bottom of the cliff looking towards it, with the data projected onto the chainage line.

DRW: BL

CHK: ZB, CM

GNS SCIENCE TE PŪ AO

CLIFF FRONTAL ELEVATION, GEOLOGY MAP AND SURFACE CHANGE MODELS

Wakefield Avenue North Christchurch

APPENDIX C

FINAL

REPORT: CR2012/57

DATE: Mar 2012

A)

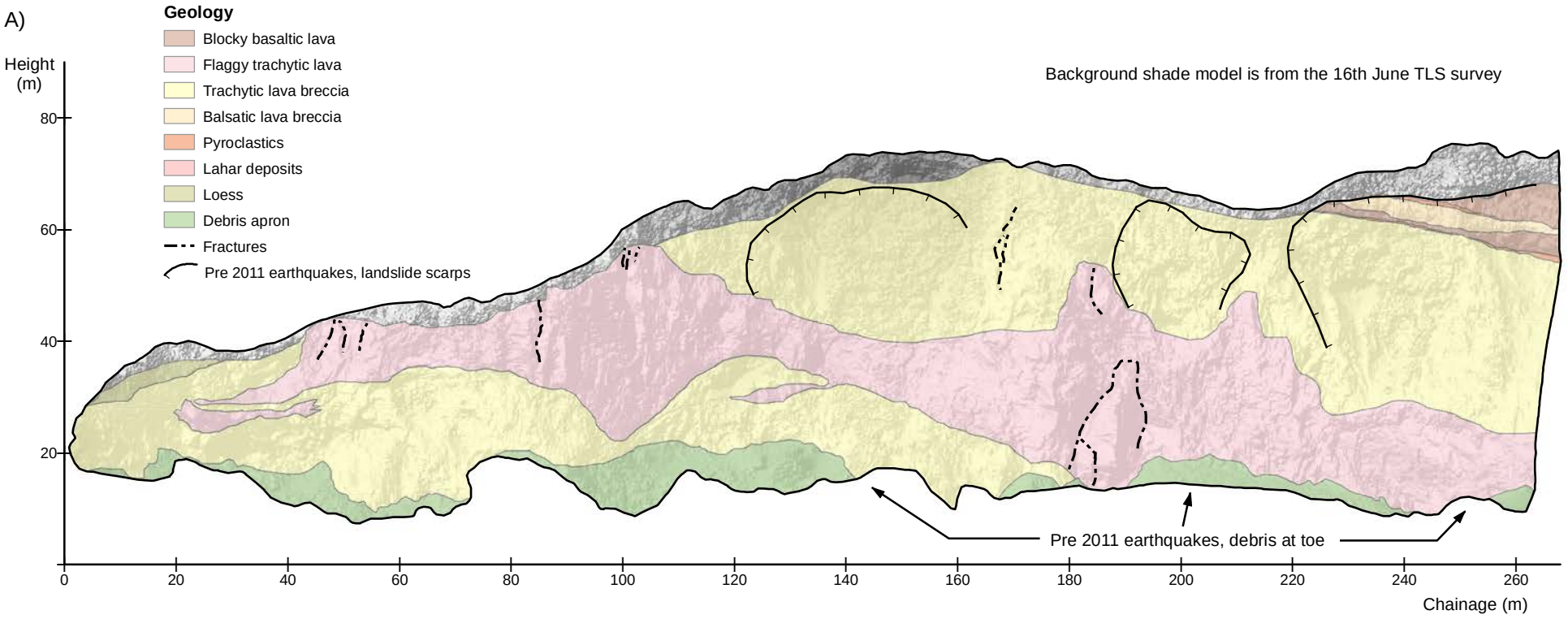

B)

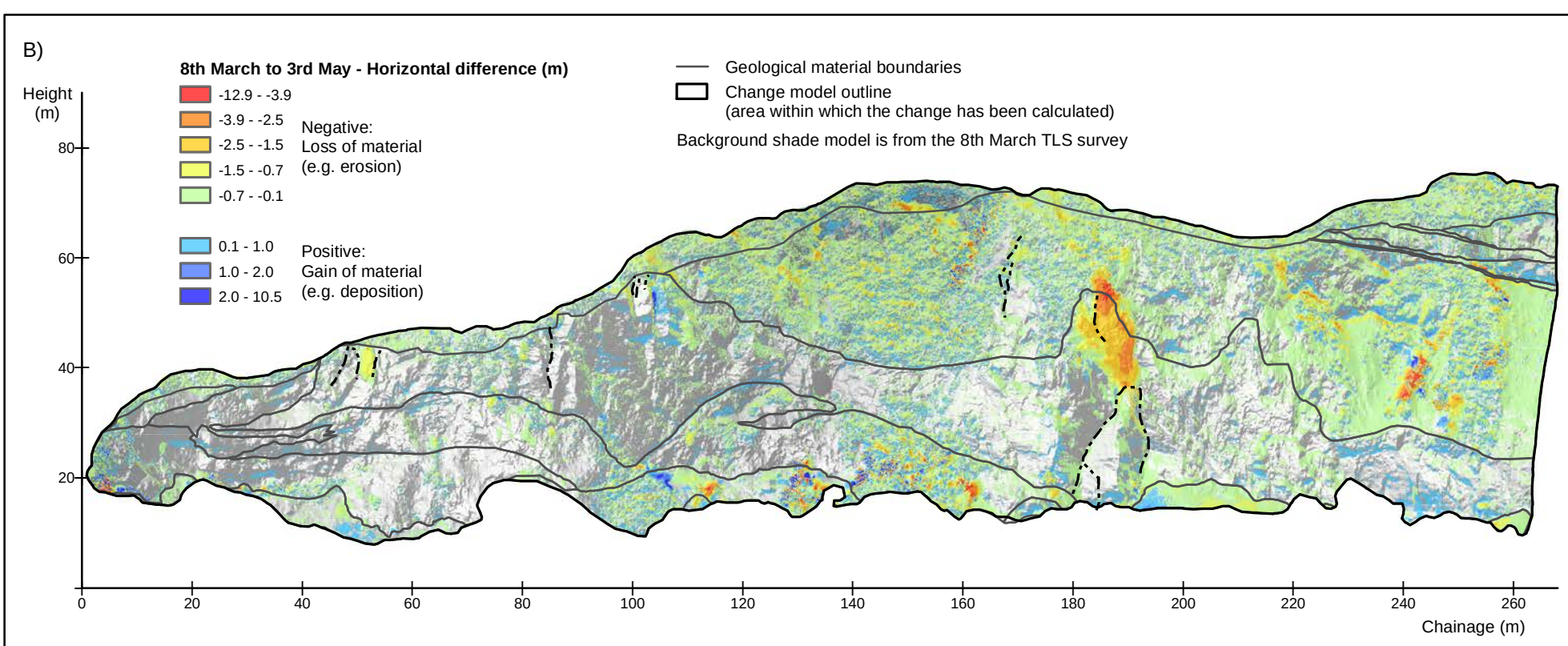

C)

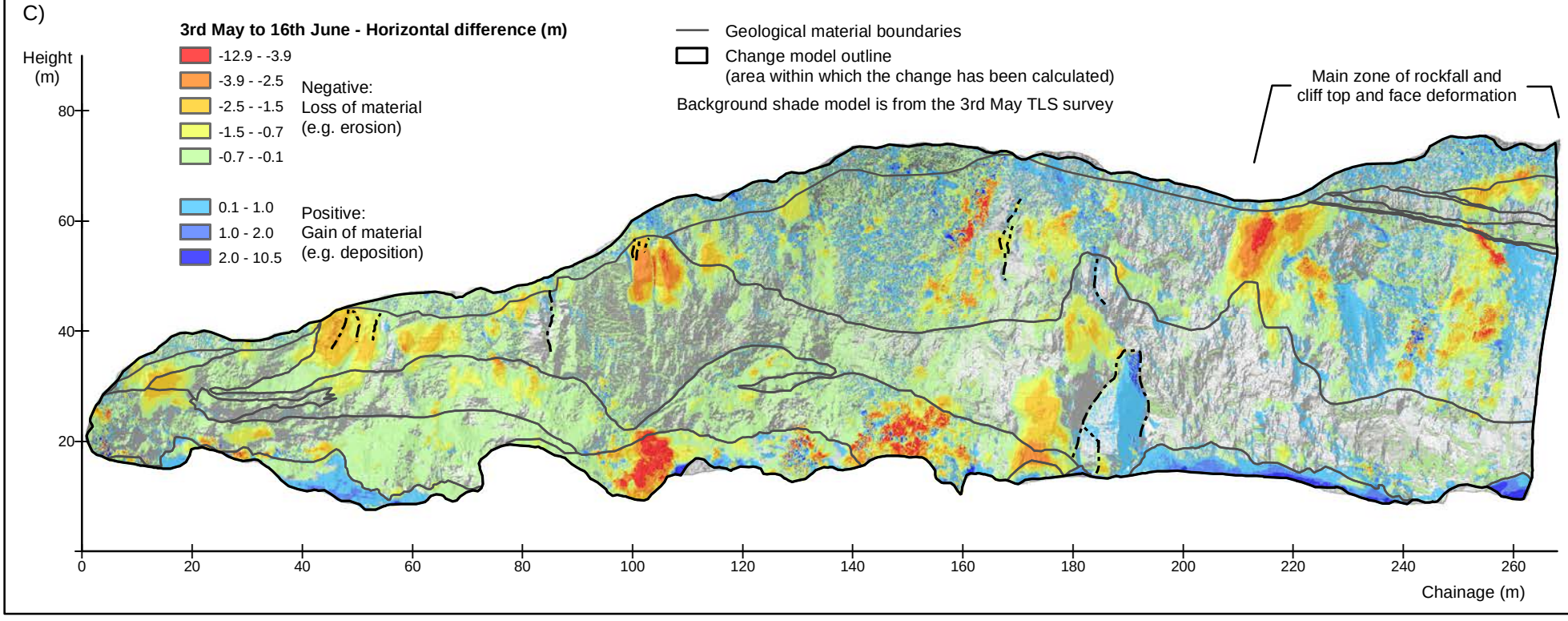

EXPLANATION:
A) Geology map of the cliff face
B) and C) surface change models - these show the horizontal changes of the cliff-face surface between given survey dates. Changes in the order of +/- 0.1 m are assumed to be error and are not shown in the change models. The surveys were carried out using a RIEGL LMSZ420i terrestrial laser scanner (TLS) in 2011.
The views are all frontal elevation i.e. as if standing at the bottom of the cliff looking towards it, with the data projected onto the chainage line.

DRW: BL

CHK: ZB, CM

CLIFF FRONTAL ELEVATION, GEOLOGY MAP AND SURFACE CHANGE MODELS

Wakefield Avenue South Christchurch

APPENDIX C
FINAL

REPORT: CR2012/57

DATE: Mar 2012

A)

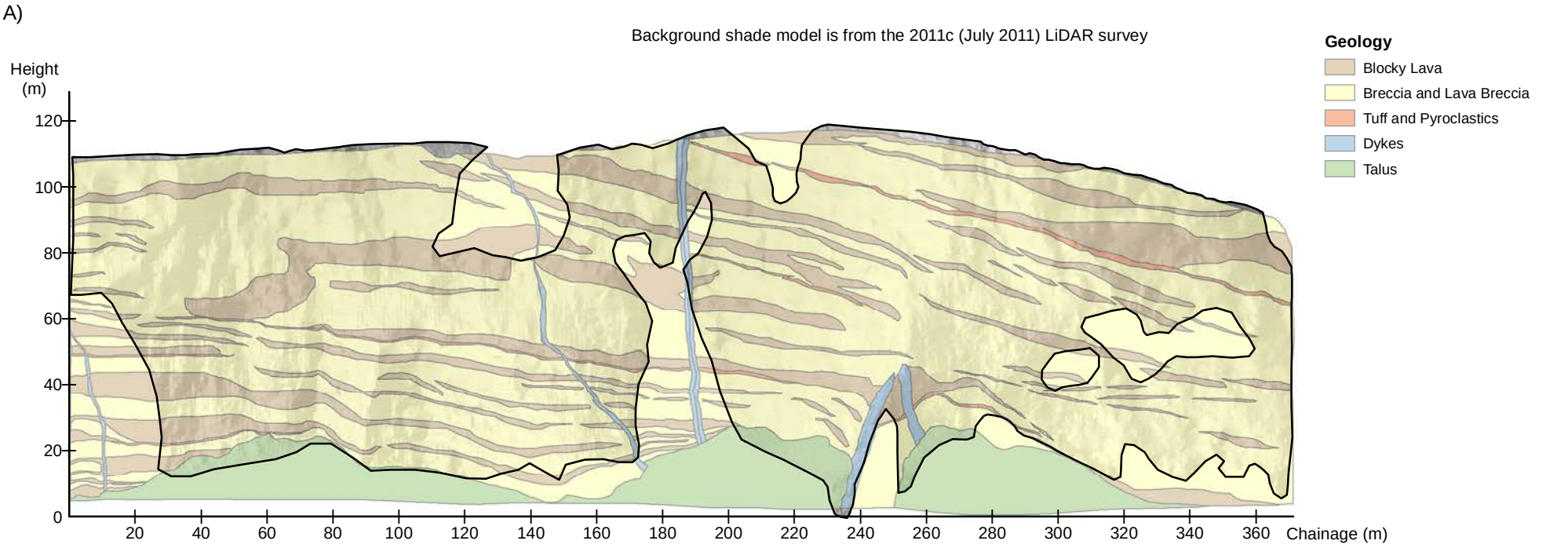

B)

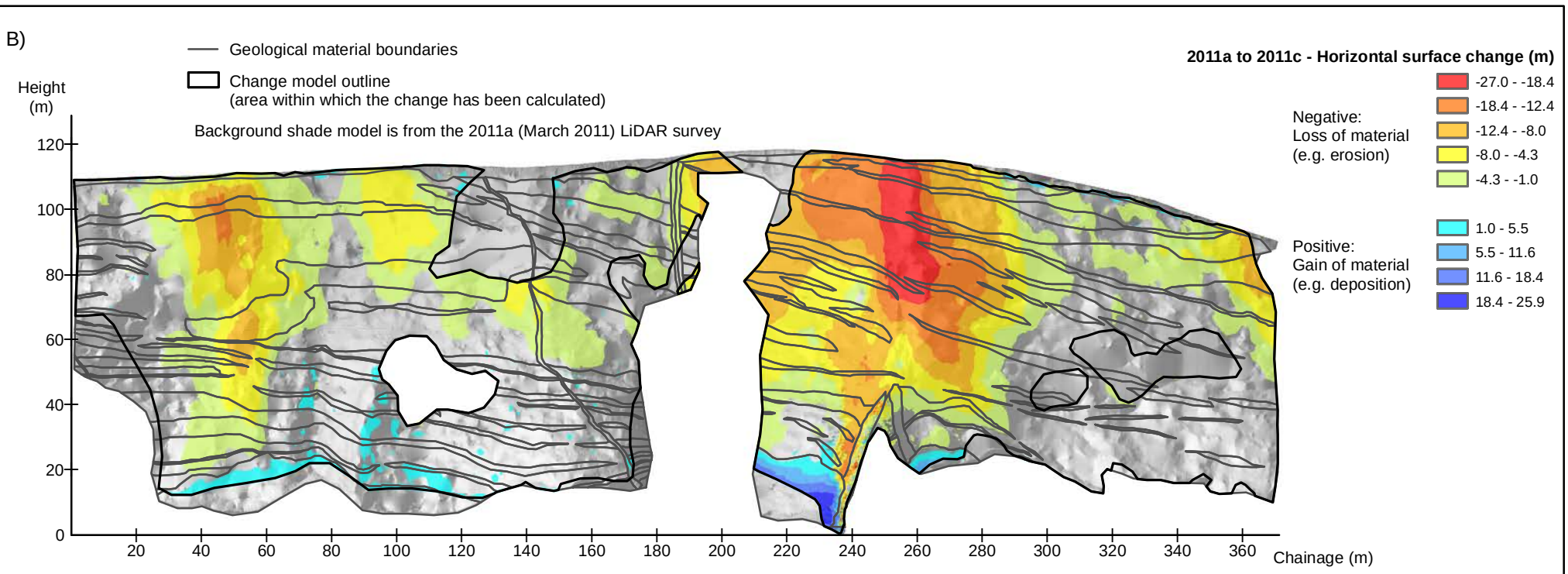

EXPLANATION:

A) Geology map of the cliff face
B) Surface change model - this shows the horizontal changes of the cliff-face surface between given survey dates. Changes in the order of +/- 1.0 m are assumed to be error and are not shown in the change models.

The views are all frontal elevation i.e. as if standing at the bottom of the cliff looking towards it, with the data projected onto the chainage line.

DRW: BL

CHK: ZB, CM

GNS SCIENCE TE PŪ AO

CLIFF FRONTAL ELEVATION, GEOLOGY MAP AND SURFACE CHANGE MODELS

Whitewash Head
Christchurch

APPENDIX C
FINAL

REPORT: CR2012/57

DATE: Mar 2012

APPENDIX D ANNUAL INDIVIDUAL FATALITY RISK FROM CLIFF COLLAPSE MAPS

1578500

5177000

N

Risk not evaluated

Earthquake Event Line 1
Earthquake Event Line 2
Earthquake Event Line 3

Main Rd

Glenstrae Rd

Glendevere Tce

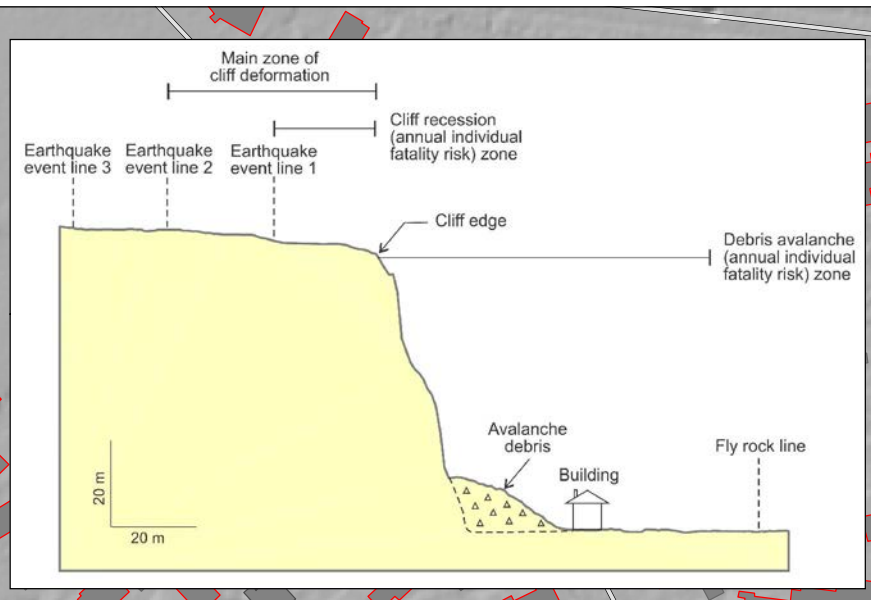

Annual individual fatality risk bands (e.g. 10^{-3} to 10^{-4}) - The risk of being killed in any one year is expressed as a number such as 10^{-4} ("ten to the minus four"). 10^{-4} can also be approximately represented as one chance in 10,000 years.

Debris avalanche - A type of landslide comprising many boulders falling simultaneously from a slope. The rocks start by sliding, toppling or falling before descending the slope rapidly (greater than 5 metres per second) by any combination of falling, bouncing and rolling.

Cliff edge – This is the position of the cliff edge defined using the 2011c airborne LiDAR survey. The cliff edge is defined as the line of intersection between the steeper slope (greater than 45 degree slope angle), forming the cliff face and the shallower slope above the cliff face.

Cliff recession – Is the result of parts of the cliff top collapsing, causing the cliff edge to move back up the slope.

Earthquake event lines - These lines represent the possible maximum recession position of the cliff edge given future earthquakes with associated peak ground accelerations in the 2.0 g range, similar to the 22 February 2011 and 13 June 2011 earthquakes. These lines do not mean that the cliff will fail along its entire length, but that any place along the cliff could fail back to this line given a future event of this magnitude.

Fly rock line – Is the mapped limit of fly rock. Fly rock is broken rock released as high-velocity projectiles created in impacts between rocks and other hard objects.

Debris Avalanche (annual individual fatality risk)
- 10^{-1} to 10^{-2}
- 10^{-2} to 10^{-3}
- 10^{-3} to 10^{-4}
- 10^{-4} to 10^{-5}
- Less than 10^{-5}

Cliff edge (2011c (July 2011) LiDAR survey)

Cliff Recession (annual individual fatality risk)
- Greater than 10^{-3}
- 10^{-3} to 10^{-4}

Earthquake event line
Fly-rock line
Limit of risk analysis
Main zones of cliff deformation (mechanism to be determined)
Main zones of land instability (mechanism to be determined)

Buildings (20/02/2012)
- Dwelling
- Commercial-Industrial
- Accessory building
- Unknown

Earthquake Event Line 3
Earthquake Event Line 2
Earthquake Event Line 1

Risk not evaluated

1578500

SCALE BAR: 0 50 100 m

EXPLANATION:

Background shade model derived from NZAM post earthquake 2011c (July 2011) LiDAR survey resampled to a 1m ground resolution.

Roads and building footprints and types provided by Christchurch City Council (20/02/2012).

DRW: DWH, BL

CHK: CM

GNS SCIENCE TE PŪ AO

CLIFF COLLAPSE ANNUAL INDIVIDUAL FATALITY RISK

Redcliffs Christchurch

APPENDIX D

FINAL

PROJECTION: New Zealand Transverse Mercator 2000

REPORT: CR2012/57

DATE: Mar 2012

1580000

5176500

N

Earthquake Event Line 1
Earthquake Event Line 2
Earthquake Event Line 3
Risk not evaluated
Main Rd
Kinsey Tce
Clifton Tce
Earthquake Event Line 1
Earthquake Event Line 2
Earthquake Event Line 3
Risk not evaluated

Debris Avalanche (annual individual fatality risk)
- 10^{-1} to 10^{-2}
- 10^{-2} to 10^{-3}
- 10^{-3} to 10^{-4}
- 10^{-4} to 10^{-5}
- Less than 10^{-5}
- **Cliff edge (2011c (July 2011) LiDAR survey)**

Cliff Recession (annual individual fatality risk)
- Greater than 10^{-3}
- 10^{-3} to 10^{-4}
- Earthquake event line
- Fly-rock line
- Limit of risk analysis
- Main zones of land instability (mechanism to be determined)

Buildings (20/02/2012)
- Dwelling
- Commercial-Industrial
- Accessory building
- Unknown

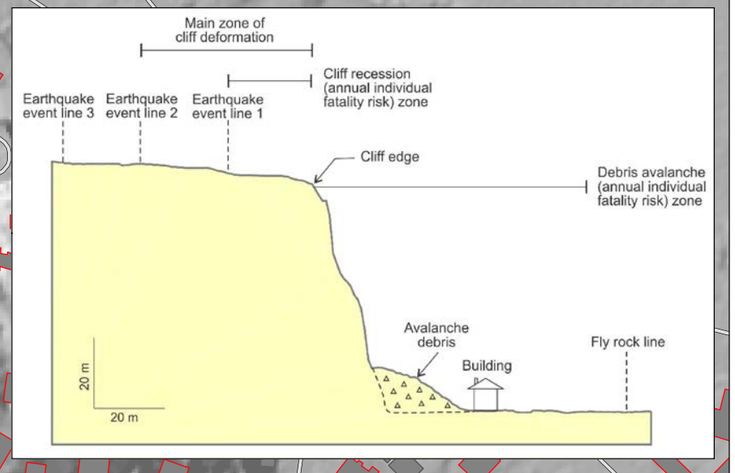

Annual individual fatality risk bands (e.g. 10^{-3} to 10^{-4}) - The risk of being killed in any one year is expressed as a number such as 10^{-4} ("ten to the minus four"). 10^{-4} can also be approximately represented as one chance in 10,000 years.

Debris avalanche - A type of landslide comprising many boulders falling simultaneously from a slope. The rocks start by sliding, toppling or falling before descending the slope rapidly (greater than 5 metres per second) by any combination of falling, bouncing and rolling.

Cliff edge – This is the position of the cliff edge defined using the 2011c airborne LiDAR survey. The cliff edge is defined as the line of intersection between the steeper slope (greater than 45 degree slope angle), forming the cliff face and the shallower slope above the cliff face.

Cliff recession – Is the result of parts of the cliff top collapsing, causing the cliff edge to move back up the slope.

Earthquake event lines - These lines represent the possible maximum recession position of the cliff edge given future earthquakes with associated peak ground accelerations in the 2.0 g range, similar to the 22 February 2011 and 13 June 2011 earthquakes. These lines do not mean that the cliff will fail along its entire length, but that any place along the cliff could fail back to this line given a future event of this magnitude.

Fly rock line – Is the mapped limit of fly rock. Fly rock is broken rock released as high-velocity projectiles created in impacts between rocks and other hard objects.

1580000

SCALE BAR: 0 50 100 m

EXPLANATION:

Background shade model derived from NZAM post earthquake 2011c (July 2011) LiDAR survey resampled to a 1m ground resolution.

Roads and building footprints and types provided by Christchurch City Council (20/02/2012).

DRW: DWH, BL

CHK: CM

GNS SCIENCE TE PŪ AO

CLIFF COLLAPSE
ANNUAL INDIVIDUAL FATALITY RISK

Shag Rock Reserve, Sumner
Christchurch

APPENDIX D

FINAL

PROJECTION: New Zealand Transverse Mercator 2000

REPORT: CR2012/57

DATE: Mar 2012

1580500

Annual individual fatality risk bands (e.g. 10^{-3} to 10^{-4}) - The risk of being killed in any one year is expressed as a number such as 10^{-4} ("ten to the minus four"). 10^{-4} can also be approximately represented as one chance in 10,000 years.

Debris avalanche - A type of landslide comprising many boulders falling simultaneously from a slope. The rocks start by sliding, toppling or falling before descending the slope rapidly (greater than 5 metres per second) by any combination of falling, bouncing and rolling.

Cliff edge – This is the position of the cliff edge defined using the 2011c airborne LiDAR survey. The cliff edge is defined as the line of intersection between the steeper slope (greater than 45 degree slope angle), forming the cliff face and the shallower slope above the cliff face.

Cliff recession – Is the result of parts of the cliff top collapsing, causing the cliff edge to move back up the slope.

Earthquake event lines - These lines represent the possible maximum recession position of the cliff edge given future earthquakes with associated peak ground accelerations in the 2.0 g range, similar to the 22 February 2011 and 13 June 2011 earthquakes. These lines do not mean that the cliff will fail along its entire length, but that any place along the cliff could fail back to this line given a future event of this magnitude.

Fly rock line – Is the mapped limit of fly rock. Fly rock is broken rock released as high-velocity projectiles created in impacts between rocks and other hard objects.

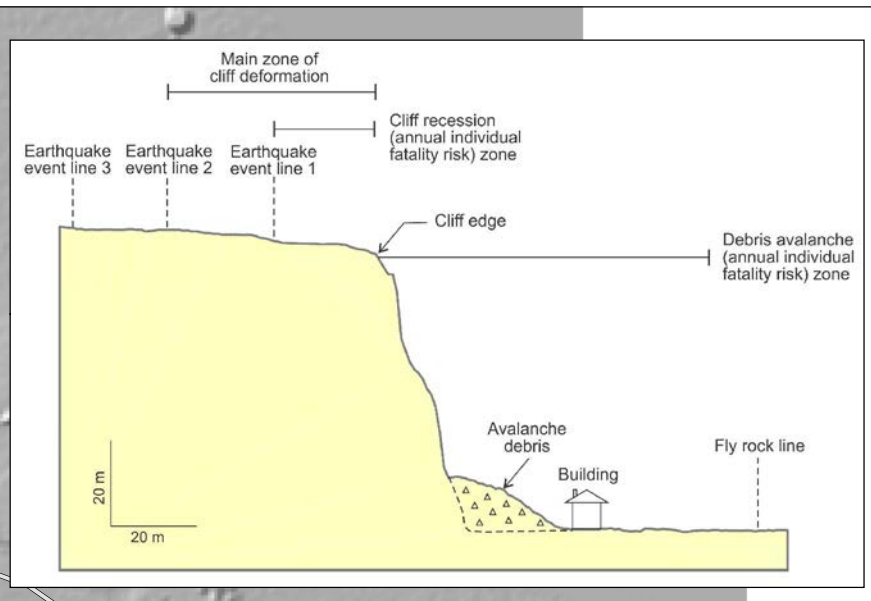

5176000

Nayland St

Wakefield Ave

Risk not evaluated

Earthquake Event Line 1
Earthquake Event Line 2
Earthquake Event Line 3

Debris Avalanche (annual individual fatality risk)

- 10^{-1} to 10^{-2}
- 10^{-2} to 10^{-3}
- 10^{-3} to 10^{-4}
- 10^{-4} to 10^{-5}
- Less than 10^{-5}

Cliff edge (2011c (July 2011) LiDAR survey)

Cliff Recession (annual individual fatality risk)

- Greater than 10^{-3}
- 10^{-3} to 10^{-4}

Earthquake event line
Fly-rock line
Limit of risk analysis
Main zones of cliff deformation (mechanism to be determined)

Buildings (20/02/2012)

- Dwelling
- Commercial-Industrial
- Accessory building
- Unknown

1580500

SCALE BAR: 0 50 m

EXPLANATION:

Background shade model derived from NZAM post earthquake 2011c (July 2011) LiDAR survey resampled to a 1m ground resolution.

Roads and building footprints and types provided by Christchurch City Council (20/02/2012).

DRW: DWH, BL

CHK: CM

GNS SCIENCE TE PŪ AO

CLIFF COLLAPSE ANNUAL INDIVIDUAL FATALITY RISK

Nayland Street, Sumner Christchurch

APPENDIX D

FINAL

PROJECTION: New Zealand Transverse Mercator 2000

REPORT: CR2012/57

DATE: Mar 2012

1580500

5176000

5175500

N

Nayland St

Wakefield Ave

Risk not evaluated

Earthquake Event Line 1
Earthquake Event Line 2
Earthquake Event Line 3

Risk not evaluated

Earthquake Event Line 1
Earthquake Event Line 2
Earthquake Event Line 3

Annual individual fatality risk bands (e.g. 10^{-3} to 10^{-4}) - The risk of being killed in any one year is expressed as a number such as 10^{-4} ("ten to the minus four"). 10^{-4} can also be approximately represented as one chance in 10,000 years.

Debris avalanche - A type of landslide comprising many boulders falling simultaneously from a slope. The rocks start by sliding, toppling or falling before descending the slope rapidly (greater than 5 metres per second) by any combination of falling, bouncing and rolling.

Cliff edge – This is the position of the cliff edge defined using the 2011c airborne LiDAR survey. The cliff edge is defined as the line of intersection between the steeper slope (greater than 45 degree slope angle), forming the cliff face and the shallower slope above the cliff face.

Cliff recession – Is the result of parts of the cliff top collapsing, causing the cliff edge to move back up the slope.

Earthquake event lines - These lines represent the possible maximum recession position of the cliff edge given future earthquakes with associated peak ground accelerations in the 2.0 g range, similar to the 22 February 2011 and 13 June 2011 earthquakes. These lines do not mean that the cliff will fail along its entire length, but that any place along the cliff could fail back to this line given a future event of this magnitude.

Fly rock line – Is the mapped limit of fly rock. Fly rock is broken rock released as high-velocity projectiles created in impacts between rocks and other hard objects.

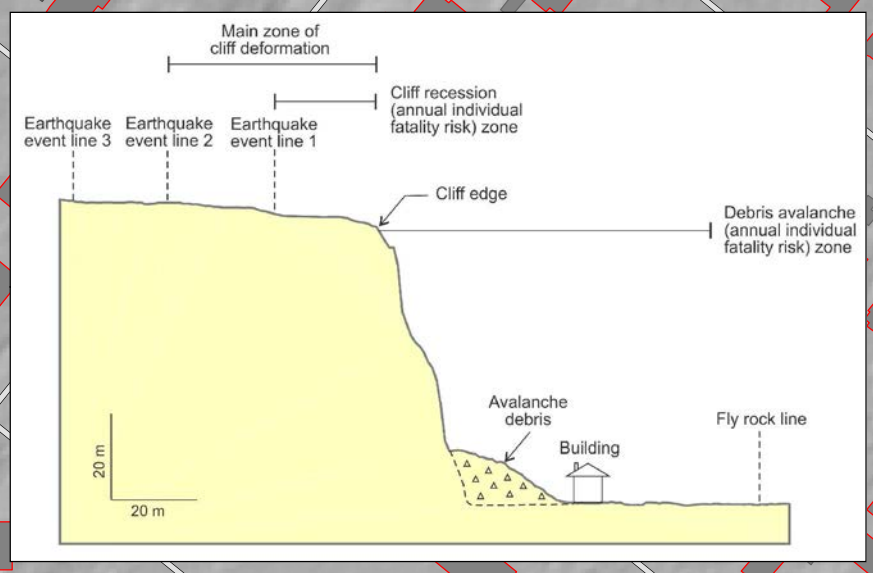

Debris Avalanche (annual individual fatality risk)

- 10^{-1} to 10^{-2}
- 10^{-2} to 10^{-3}
- 10^{-3} to 10^{-4}
- 10^{-4} to 10^{-5}
- Less than 10^{-5}

Cliff edge (2011c (July 2011) LiDAR survey)

Cliff Recession (annual individual fatality risk)

- Greater than 10^{-3}
- 10^{-3} to 10^{-4}

Earthquake event line
Fly-rock line
Limit of risk analysis
Main zones of cliff deformation (mechanism to be determined)

Buildings (20/02/2012)

- Dwelling
- Commercial-Industrial
- Accessory building
- Unknown

SCALE BAR: 0 50 100 m

EXPLANATION:

Background shade model derived from NZAM post earthquake 2011c (July 2011) LiDAR survey resampled to a 1m ground resolution.

Roads and building footprints and types provided by Christchurch City Council (20/02/2012).

DRW: DWH, BL

CHK: CM

GNS SCIENCE TE PŪ AO

CLIFF COLLAPSE ANNUAL INDIVIDUAL FATALITY RISK

Wakefield Avenue, Sumner Christchurch

APPENDIX D

FINAL

PROJECTION: New Zealand Transverse Mercator 2000

REPORT: CR2012/57

DATE: Mar 2012

1582000

1582500

5175500

5175000

N

Risk not evaluated

Earthquake Event Line 1

Earthquake Event Line 2

Earthquake Event Line 3

Taylors Mistake Rd

Smugglers Cove

Earthquake Event Line 3

Earthquake Event Line 1

Earthquake Event Line 2

Risk not evaluated

Annual individual fatality risk bands (e.g. 10^{-3} to 10^{-4}) - The risk of being killed in any one year is expressed as a number such as 10^{-4} ("ten to the minus four"). 10^{-4} can also be approximately represented as one chance in 10,000 years.

Debris avalanche - A type of landslide comprising many boulders falling simultaneously from a slope. The rocks start by sliding, toppling or falling before descending the slope rapidly (greater than 5 metres per second) by any combination of falling, bouncing and rolling.

Cliff edge – This is the position of the cliff edge defined using the 2011c airborne LiDAR survey. The cliff edge is defined as the line of intersection between the steeper slope (greater than 45 degree slope angle), forming the cliff face and the shallower slope above the cliff face.

Cliff recession – Is the result of parts of the cliff top collapsing, causing the cliff edge to move back up the slope.

Earthquake event lines - These lines represent the possible maximum recession position of the cliff edge given future earthquakes with associated peak ground accelerations in the 2.0 g range, similar to the 22 February 2011 and 13 June 2011 earthquakes. These lines do not mean that the cliff will fail along its entire length, but that any place along the cliff could fail back to this line given a future event of this magnitude.

Fly rock line – Is the mapped limit of fly rock. Fly rock is broken rock released as high-velocity projectiles created in impacts between rocks and other hard objects.

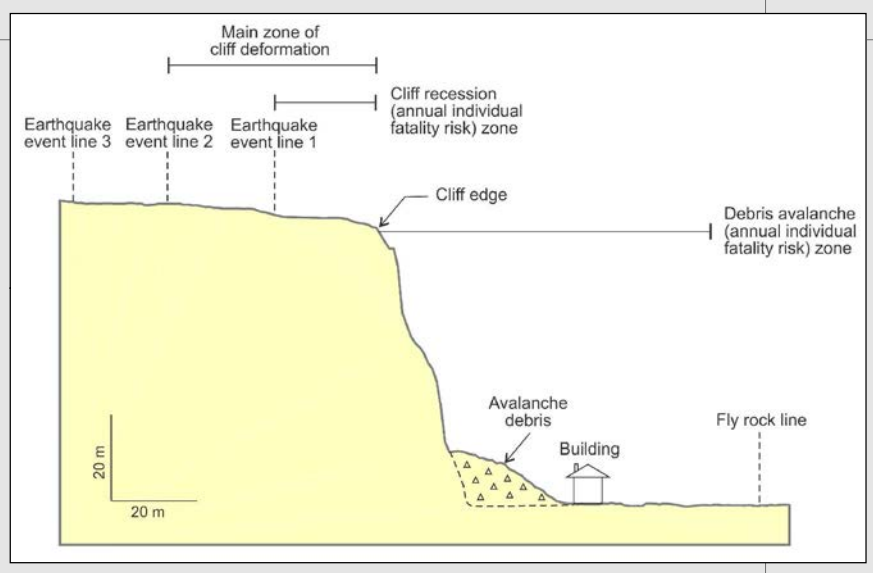

Cliff edge (2011c (July 2011) LiDAR survey)

Cliff Recession (annual individual fatality risk)

- Greater than 10^{-3}
- 10^{-3} to 10^{-4}
- Earthquake event line
- Limit of risk analysis
- Main zones of cliff deformation (mechanism to be determined)

Buildings (20/02/2012)

- Dwelling
- Commercial-Industrial
- Accessory building
- Unknown

SCALE BAR: 0 50 100 150 m

EXPLANATION:

Background shade model derived from NZAM post earthquake 2011c (July 2011) LiDAR survey resampled to a 1m ground resolution.

Roads and building footprints and types provided by Christchurch City Council (20/02/2012).

DRW: DWH, BL

CHK: CM

GNS SCIENCE TE PŪ AO

CLIFF COLLAPSE ANNUAL INDIVIDUAL FATALITY RISK

Whitewash Head Christchurch

APPENDIX D

FINAL

PROJECTION: New Zealand Transverse Mercator 2000

REPORT: CR2012/57

DATE: Mar 2012

APPENDIX E FIELD VERIFICATION METHODOLOGY

2 March 2012

Methodology for Ground-truthing Cliff Collapse Zones

Introduction

Preliminary Life Risk maps prepared by GNS Science for the Cliff Collapse Pilot Study have identified a series of Annualised Risk Zones (for individual loss of life) in areas subject to cliff collapse or debris inundation (including fly rock damage) following cliff collapse. About 60 homes and some key lifeline roads are located within the risk zones defined by the GNS study. All are currently within the 'white zone' as defined by CERA, meaning that they are subject to further evaluation to determine whether the houses cannot be occupied or can be occupied with conditions.

The Risk Zones are defined on the basis of a number of criteria and assumptions. PHGG, in collaboration with GNS Science, has been tasked with 'ground truthing' the risk zones to

1. Confirm that the potential cliff collapse areas are correctly defined in relation to the known ground cracking and reasonable setback from the current cliff edge, and
2. Confirm that the potential debris inundation and fly rock risk zones are correctly defined on the prepared maps, or
3. Recommend changes to the risk zone boundaries on the basis of site-specific ground conditions where and if applicable.

It is planned to complete the ground truthing of the known cliff collapse areas around the Port Hills suburbs by mid March 2012, following which GNS Science will review the field data and may revise the risk maps then issue a set of FINAL, field verified maps.

Proposed methodology and documentation

The PHGG assessment will consist of

1. an initial office assessment. This will include:
    a. generating base maps for field use by plotting the shape files onto air photo base plans (1:2000 scale) that also show topographic details, ground cracking, cliff collapse debris areas, property boundaries, street numbers and properties with s124 notices
    b. identifying all properties and key lifeline elements within the GNS risk zones
    c. reviewing all available relevant information including:
        i. geomorphic mapping (completed by GNS)
        ii. mapped debris limits (beneath cliffs, where accessible and relevant – eg. not relevant if no houses or lifelines)
        iii. ground cracking records (top of cliffs)
        iv. known or potential areas of cliff instability
2. office review and/or field checking of properties within the pilot study risk zones (but excluding adjacent 'negligible risk' areas) to determine whether the risk at each is judged to be consistent with the assessment by GNS
3. regular review of progress and results with GNS Science personnel

Properties within the 31° Fahrboeschung Angle line:

GNS have indicated that the 31° Fahrboeschung (F) Angle represents the maximum observed runout distance for flyrock associated with debris below a collapsed cliff. This represents the "negligible rockfall risk line". The indicated position of this line will be 'ground truthed' by PHGG. For Health and safety reasons, properties within the risk zone will NOT be individually visited as part of the assessment.

Cliff Top Properties

GNS have indicated potential risk zones and a suggested setback area behind the edge of each collapsed cliff assessed. All properties within the areas defined by the risk zones are assessed to be at risk of ground loss or cracking in a future cliff collapse event and the setback area is intended to provide an additional buffer zone.

Methodology

The attached check sheet "Assessment of GNS Model Applicability for Cliff Collapse" will be used to determine whether the site-specific life-safety risk is consistent with the level of risk shown on the relevant drawings provided by GNS Science.

The assessment is to be completed for EVERY property within the life safety risk zones defined by the GNS report (ie. between the rear limit of the setback zone at the top of the cliff and the 31° F angle line at the base of the cliff). As much as possible of the review will be undertaken in the office. Only those properties that can be safely accessed will be physically inspected as part of the field review.

Field Maps

Maps for validation and ground checking will be generated at a scale of 1:2000 (approx) and will include at least the following:

- GNS risk zone limits (top of cliff setback line and flyrock limit line at base of cliffs - from GNS draft report dated February 2012)
- PHGG mapped ground cracking and known unstable cliff top areas
- Air photo map showing areas of debris due to cliff collapse
- Edge of cliff (from latest Lidar data)
- Street names
- Property boundaries and numbers
- House footprints
- S124 properties

Quality Assurance

To ensure consistency in all procedures so far as possible, we will

1. Provide a dedicated Team Leader (Adam Broadbent, after training by Mark Yetton) to oversee and manage the field aspects of the ground truthing
2. Undertake weekly reviews of progress with GNS Science and CCC

Deliverables

Regular reporting

- A Friday pm operational debrief will be held with GNS and CCC personnel each week
- Weekly updates will be provided to CCC in a spreadsheet each Friday listing the cliff top and/or cliff bottom properties inspected in each Sector and the outcome
- Copies of the completed check sheets and marked up field maps will be provided to GNS at an agreed frequency, but no later than the following Friday.
- Additional supporting documentation (as below) will be provided as finalised.

Documentation to be provided for each property:

- Completed check sheet including explanatory notes (where applicable)
- Photos of the house including F angle measurements where these can be measured to illustrate the context of the property and hazard source(s).

Final Report (per Pilot Study area)

Brief (1-2 page) summary including

- when and where the inspections were carried out
- by whom
- summary of methodology [standard text]
- key outcomes
- GIS formatted digital copy of the "negligible risk line"
- Air photo base plan showing properties, ground cracking and cliff collapse debris area(s), annotated as appropriate. It is expected that these will be generated directly from the project GIS database and will clearly indicate the properties assessed.

Plus Appendices

A. Table listing properties inspected and summarising key information and inspection outcomes (see attached example). This will be the final version of the weekly update.
B. Geocoded GIS version of the summary table
C. Property-specific package for each property inspected that includes the following information:
    i. Completed proforma
    ii. Photograph(s) of house showing setting (ground cracking or debris as appropriate)
    iii. Photograph(s) documenting Fahrboeschung angle at property at risk of debris inundation (where possible)
    iv. Photograph(s) of ground cracking or cliff collapse debris in the vicinity of the house
D. Copy of annotated A3 field maps
E. Ipad calibration photographs

Field data will be given to GNS once each area within each sector has been completed.

Prioritisation

At this stage it proposed that the first priority is to test the process by assessing the Sector 3 cliff areas (Redcliffs/Moa Bone cave), using this as a training area.

It is proposed to commence this work in the week beginning 5 March 2012. This will allow us to determine the time frame required for each property to be assessed and will provide a basis for developing a forward programme and assessing resource requirements.

It is expected that the Sector 2 cliff collapse areas (Wakefield Avenue/Richmond Hill Road and Kinsey Terrace/Peacocks Gallop) will be the next areas assessed.

Programme and Timeline

The following table summarises our proposed programme. This will be reviewed weekly and revised if necessary to reflect actual progress or changes in priority.

The programme outlined does not include all cliff areas that may affect residential or commercial properties. It is limited to the major cliffs within the GNS pilot study.

Week	Commencing	Planned Activities
1	27 Feb	Finalise ground truthing methodology for CCC signoff.
2	5 Mar	Commence ground truthing in Sector 3 (Redcliffs/Moa Bone Cave) Adjust methodology as appropriate.
2	5 Mar	Move to Sector 2 (Wakefield Av/Richmond Hill/Nayland St)
3	12 Mar	Complete Sector 2 (Kinsey Terrace/Peacocks Gallop) Sector 1 (Whitewash Head)

Assessment Teams

Each assessment team will consist of two appropriately trained geotechnical personnel, one of whom will have good knowledge of the sector. Those undertaking evaluations will undergo an appropriate training session, including field calibration.

GNS will provide support personnel in Christchurch for the duration of the ground-truthing exercise. GNS will not fully participate in the ground truthing but will provide advice as required and will undertake consistency checks by reviewing the field data. It is anticipated that GNS will participate in weekly field reviews (Friday pm).

Port Hills Geotechnical Group
Assessment of GNS Model Applicability for Cliff Collapse Risk

Sector: ____ Address: _____

Pilot Study Area: _____ **Current S124 Notice? □ yes □ no**

Cliff Type: ☐ *Natural* or ☐ *Man-made* Cliff Height: ☐ >15m or ☐ <15m

In LH column below, complete EITHER grey or yellow boxes, then blue box:

CLIFF BOTTOM PROPERTIES

From existing records, did debris land within 10m of dwelling?

☐ Yes ☐ No

If Yes, ☐ *House hit* ☐ *Not hit* ☐ *Fly rock Passed*

Previously mapped? ☐ Yes ☐ No

Is dwelling within 31 deg "F" angle line?

☐ Yes ☐ No ☐

CLIFF TOP PROPERTIES

Does previously mapped ground cracking pass within 10m of the dwelling?

☐ Yes ☐ No

If Yes, does the cracked area include the dwelling?

☐ Yes ☐ No

Does the recommended risk/setback zone intrude onto the property?

☐ Yes ☐ No

Are there any other known mass movement issues that could increase risk to dwelling?

☐ Yes ☐ No

☐ Debris flow ☐ Landslide

Based on observations of the site, is it possible to determine whether the site risk is consistent with the GNS assessment?

☐ **Yes** → **RISK IS** *consistent with* **GNS Assessment**

☐ **No** → **SITE REQUIRES MORE DETAILED EVALUATION**

Is an S124 Notice Required?

☐ Yes ☐ No

☐ *Cannot make this assessment from available information*

Comments:

Assessed *for CCC/Port Hills Geotechnical Group* by: _____ Date: _____

www.gns.cri.nz

Principal Location

1 Fairway Drive
Avalon
PO Box 30368
Lower Hutt
New Zealand
T +64-4-570 1444
F +64-4-570 4600

Other Locations

Dunedin Research Centre
764 Cumberland Street
Private Bag 1930
Dunedin
New Zealand
T +64-3-477 4050
F +64-3-477 5232

Wairakei Research Centre
114 Karetoto Road
Wairakei
Private Bag 2000, Taupo
New Zealand
T +64-7-374 8211
F +64-7-374 8199

National Isotope Centre
30 Gracefield Road
PO Box 31312
Lower Hutt
New Zealand
T +64-4-570 1444
F +64-4-570 4657